Long Distance Dispersion Managed Soliton Transmission Experiments

Paul Harper

Doctor of Philosophy

The University of Aston in Birmingham

October 1997

The University of Aston in Birmingham

Long Distance Dispersion Managed Soliton Transmission Experiments

Paul Harper

Doctor of Philosophy

October 1997

This thesis presents results of transmission experiments using optical solitons in a dispersion managed optical fibre recirculating loop. The basic concepts of pulse propagation in optical fibre are introduced before optical solitons and their use in optically amplified fibre systems are discussed. The role of dispersion management in such systems is then considered.The design, operation and limitations of the recirculating loop and soliton sources which were used and the experimental techniques are described before the experimental work is presented.

The experimental work covers a number of areas all of which used dispersion management of the transmission line. A novel ultra-long distance propagation scheme which achieved low timing jitter by suppression of the amplifier noise and by working close to the zero dispersion wavelength has been discovered. The use of fibre Bragg gratings as wavelength filters to suppress noise and reduce timing jitter has been investigated. The performance of the fibre grating compared favourably with that of a bulk device and was in good agreement with theoretical predictions.

The upgrade of existing standard fibre systems to higher bit rates is currently an important issue. The possibility of using solitons with dispersion compensation to allow an increase in data rate of existing standard fibre systems to 10Gbit/s over 5000km has been demonstrated. The applicability of this technique to longer distances, higher bit rates or longer amplifier spans is also investigated by optimisation of the dispersion management scheme. The use of fibre Bragg gratings as the dispersion compensating elements in such standard fibre transmission experiments has been examined and the main problem that these devices currently have, high polarisation mode dispersion, is discussed. The likely future direction of optical communications and what part solitons and dispersion management will play in this development is discussed in the thesis conclusions

Additional key words and phrases

Nonlinear optics, optical networks and systems, optic fibres, dispersion management, optical solitons.

Acknowledgements

I would like to take this opportunity to acknowledge and thank several people who have helped during the work for this thesis. Firstly, my supervisor Nick Doran who has guided me throughout my 3 years at Aston and has always been on hand with useful advice. A much appreciated Case studentship was provided by Alcatel Submarine Networks and I would like to thank Steve Desbrulais, my external supervisor, for the interest he has shown in this project and for numerous useful discussions. All members, both past and present, of the Photonics Research Group at Aston University have given valuable assistance at one point or another. I must especially thank Allister Pattison, Ian Phillips and Andrew Gloag (who all helped in general lab matters) and Bert Biggs who provided excellent technical support throughout. I am particularly indebted to thank Peter Kean and Finlay Knox, with whom I worked most closely, for their constant encouragement and support.

The experimental work was done in collaboration with Finlay Knox and Peter Kean. The original recirculating loop was constructed by Finlay Knox who has been closely involved with all subsequent development. The figure of eight laser described in Section 4.3 was the idea of Peter Kean and it was developed with his and Finlay Knox's help. The phase locked loop controllers used in that laser, the fibre ring laser and the clock recovery circuit were all designed by Peter Kean. Finlay Knox also built the ring laser described in Section 4.4 and was closely involved in the experimental work for Chapter 5. The Mach-Zehnder inter-leaver was based on a design by Peter Kean, Finlay Knox and myself but was built by Ian Phillips. The fibre Bragg gratings used were fabricated "in-house" by Lin Zhang, Lorna Everall, Kate Sugden and John Williams. John Williams also devised the dispersion measurement technique described in Section 3.4.2 and has been a great help with the many computer problems I have had the misfortune of encountering. The numerical simulation which appear in this thesis were performed with the help of Donald Govan.

Contents

List of Figures

List of Tables

Chapter 1

Introduction to optical fibre communications

The rapidly increasing global demand for telecommunications products has induced a great deal of research into high speed, long distance optical communication systems. Until recently the only services which were required were traditional telephony and facsimile services but with the development and introduction of new services such as Internet access and quality audio and video transmission, increases in system capacities are required. In order to transmit a telephone conversation of reasonable quality a data rate of 64kbit/s is required (i.e. 64 000 "bits" of information must be transmitted per second) [1]. A telecommunications link with a capacity of 1Gbit/s is therefore capable of transmitting approximately 15,000 telephone calls simultaneously. If sound is to be transmitted with a quality comparable with that of a compact disc the required bit rate is increased tenfold, whilst colour video requires a data rate of ~44Mbit/s which would allow only 22 simultaneous broadcasts on a 1Gbit/s system. It is therefore clear how these new broadband services can put a severe strain on existing systems which were not designed for such bandwidth intensive use. There has also been a great deal of research into high speed sources, detectors and other components as well as new ways of increasing the data rate which can be achieved in optical systems. The global nature of modern telecommunications requires that these new high bit rate optical systems are capable of spanning trans-oceanic distances.

Since the first proposal of glass fibre as a possible transmission medium for optical telecommunication [2] and the subsequent development of low loss glass fibres [3] it has become clear that the potential capacity of glass fibre based optical systems is far higher than traditional coaxial cable electrical systems. In addition to the enormous potential

bandwidth, fibre has an low loss and unlike coaxial cable the attenuation of the signal being propagated does not increase as the data rate is increased [4] pp5. Fibre can now be routinely manufactured with a loss as low as 0.18dB/km at a wavelength of $1.55\mu m$ which is close to the fundamental limit set by Rayleigh scattering. This low loss allows propagation of optical signals over large distances (~400km) [5] before amplification is required and also allows nonlinear phenomena to be observed at moderate power levels due to the long interaction lengths which can be achieved [6].

Using all optical systems has allowed the bit rate of trans-oceanic systems to reach 5Gbit/s [7] and this data rate is likely to keep increasing with the demand for new broadband services either through direct increase to the data rate or by using multiple wavelength channels.

1.1 Optical fibre

The most common type of fibre which is used in optical communications systems, step index fibre (SIF) is shown schematically in Figure 1.1. The central "core" area of the fibre is a length of transparent silica glass with a cylindrical geometry. This core is surrounded by a cladding made of a similar material but with a lower refractive index to allow waveguiding. Other types of fibre include graded index fibre where there is a gradual change in the refractive index from the core to the cladding, and multiple cladding fibre where more than one cladding layer is used.

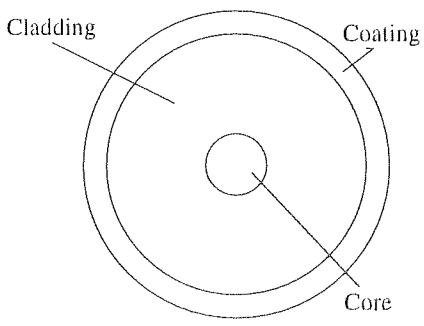

Figure 1.1: Schematic representation of a step index fibre

In step index fibre the number of propagation modes which can be supported in a fibre is determined by the refractive indices of the core and the cladding, the diameter of the core and the wavelength of the light. Two useful parameters in the characterisation of optical fibre are the relative core-cladding refractive index difference Δ and the V number

defined by

$$\Delta = \frac{n_1 - n_2}{n_1} \tag{1.1}$$

$$V = \frac{2\pi}{\lambda} a (n_1^2 - n_2^2)^{\frac{1}{2}} \tag{1.2}$$

where a is the core radius, n_1 and n_2 are the refractive indices of the core and cladding respectively

This thesis concentrates on systems which use single mode fibre (i.e. fibre for which a single propagation mode is supported) which has $V < 2.405$ [6] pp32. The main practical difference between multi-mode and single mode fibre is the core diameter although the number of modes which are supported also depends on the wavelength of the light. In this thesis when fibre is referred to as being single mode it is understood that the wavelength of the signal is $\sim 1.55 \mu m$, this wavelength was used for reasons which will be explained below. For standard telecommunications fibre Δ is $\sim 3\text{x}10^{-3}$, the fibre fibre core diameter is $\sim 8 \mu m$ and the cladding diameter is $\sim 125 \mu m$.

Before proceeding further it is necessary to consider some of the basic characteristics of optical fibre.

1.1.1 Fibre loss

One of the most important fibre characteristics is the loss which a signal propagating along the fibre experiences. The loss of a fibre, α is defined by

$$\alpha = -\frac{1}{L} ln \frac{P_o}{P_i} \tag{1.3}$$

where P_o is the power at the fibre output, P_i is the input power and L is the fibre length. The fibre loss is commonly expressed in dB/km using the relation

$$\alpha_{dB} = -\frac{10}{L} log \frac{P_o}{P_i} \tag{1.4}$$

where L is in km.

There are several mechanisms which contribute to the loss of a fibre. The main intrinsic loss is due to Rayleigh scattering which is proportional to λ^{-4} and therefore dominates at short wavelengths but there are further intrinsic losses due to absorption in the glass (material absorption) and electron absorption. The tails of these absorption peaks can lead to additional losses above $1.6 \mu m$ and below $1 \mu m$ respectively. The main extrinsic

loss is due to absorption by OH^- impurities in the fibre. The fundamental absorption peak of these ions is at $2.7\mu m$ but there are also strong overtones at 1400nm 950nm and 725nm all of which are important in relation to optical communications. Figure 1.2 shows the loss of silica glass versus wavelength with the three above effects annotated. This loss profile determines the possible regions of operation of optical systems. The earliest systems operated in the $\sim$ 850nm region where the loss is $\sim$ 10dB/km due to the availability of sources and detectors at this wavelength. There are further minima at $1.3\mu m$ and $1.5\mu m$ and it is at the latter of these regions which modern systems use due to the lower loss $\sim 0.2dB$ and availability of suitable optical amplifiers at this wavelength.

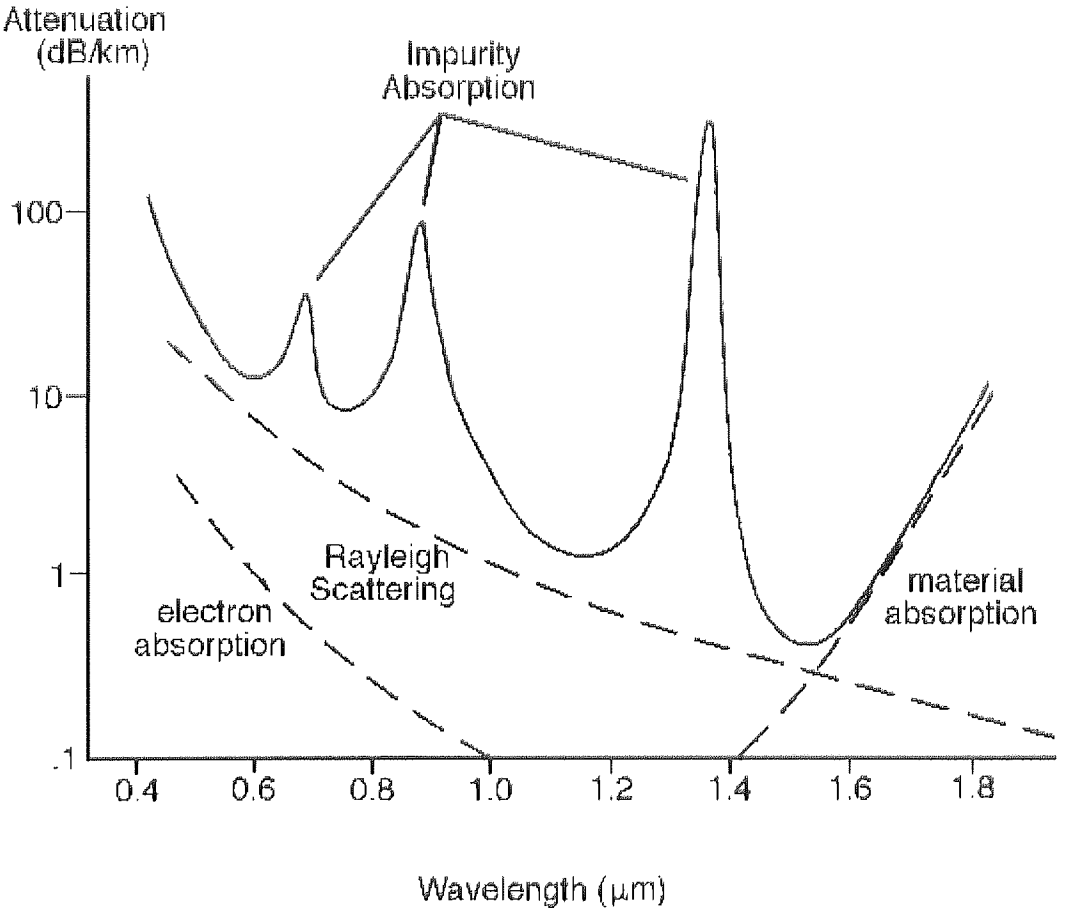

Figure 1.2: Typical loss characteristics of silicone glass - after [1] pp67.

1.1.2 Chromatic dispersion

As a result of the frequency dependent response of the bound electrons when an electromagnetic wave is propagated through the glass fibre different wavelengths of light travel at different speeds. This effect is known as chromatic dispersion and since no source is

truly monochromatic, it can lead to appreciable spreading of an optical pulse after long propagation distances in optical fibre as shall be seen in Section 2.3. This can seriously affect the performance of high speed optical communications systems where closely spaced light pulses are used to represent data "ones" and any spreading of the pulses can lead to corruption of the data signal. A measure of the difference in propagation speeds of different wavelengths is given by the group delay dispersion parameter D_2 which is the second derivative of the refractive index with respect to time and is measured in ps/(nm km). In addition to the intrinsic dispersion of the fibre material (which can be altered by the inclusion of dopants) there is also a contribution which depends on the structure of the fibre known as the waveguide dispersion. This waveguide dispersion can deliberately be altered to adjust the dispersion characteristics of a fibre by changing the refractive indices and dimensions of the core and cladding.

The vast majority of fibre which has been installed in optical systems is what is known as standard telecommunications fibre which has a low dispersion in the second optical window at $1.3\mu m$ which was the wavelength at which early electrically regenerated optical systems operated. The main contribution to the dispersion of standard fibre comes from the dispersion of the fibre material and the dispersion profile of a typical single mode standard fibre is shown in Figure 1.3. The dispersion zero wavelength, λ_0 is at $\sim$

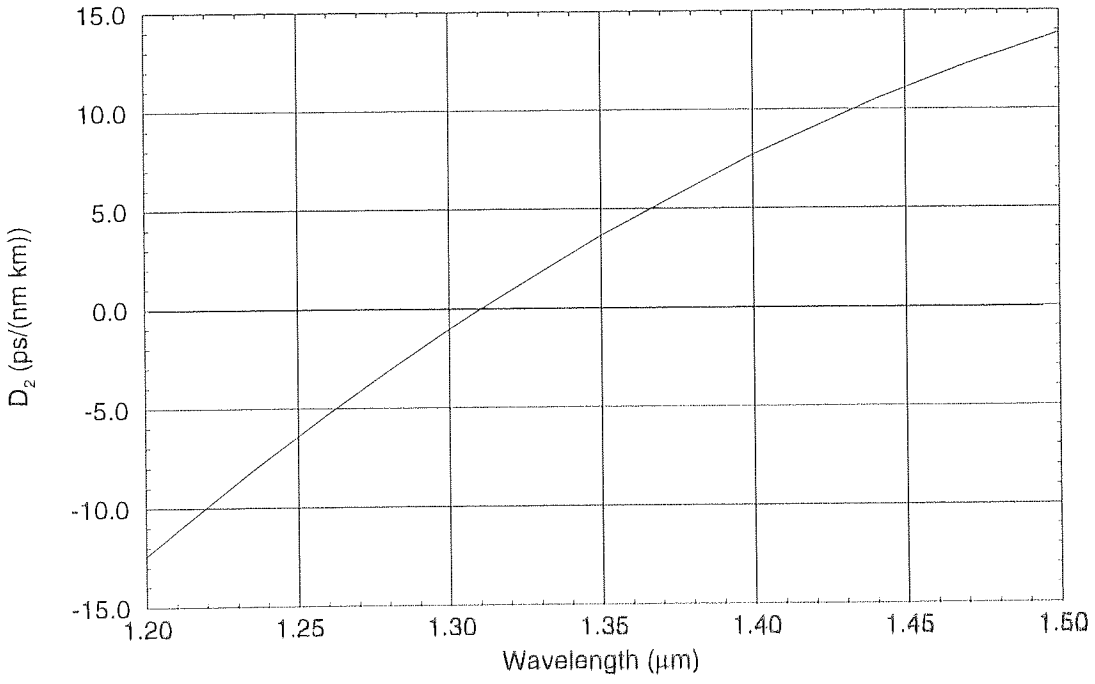

Figure 1.3: Dispersion parameter D_2 of standard fibre versus wavelength.

$1.31\mu m$ and the dispersion becomes positive at higher wavelengths and negative for lower

wavelengths. This sign change of the dispersion gives rise to two distinct regimes, the normal dispersion regime where D_2 is negative and the anomalous dispersion regime where D_2 is positive. In the anomalous dispersion regime short wavelengths travel faster than long wavelengths and so light propagated through a fibre with anomalous dispersion will emerge with the blue end of the spectrum leading the red end. In the normal dispersion regime the opposite is true. Reference to Figure 1.3 shows that in the low loss region at $\sim 1.5\mu m$ standard fibre has a high positive dispersion of $\sim$ +17ps/(nm km). This makes the fibre unsuitable for use in optical systems operating at this wavelength as the high dispersion can cause significant pulse broadening of $1.5\mu m$. Dispersion shifted fibres (DSFs), which rely on the waveguide dispersion to shift λ_0 into the $1.5\mu m$ region, have therefore been developed for use at this wavelength. While DSF can be used in new systems which are being deployed there is a desire to use existing installed fibre systems at higher data rates than they currently use because this offers an economical way of increasing capacity. In order to achieve this it is necessary to reduce the average dispersion of the system which can be done by including a length of dispersion compensating fibre (DCF) which is designed to have a dispersion zero wavelength beyond $1.6\mu m$. This is a subject area which is currently receiving a great deal of interest and will be studied in Chapter 7.

1.1.3 Fibre nonlinearity

Although the nonlinear coefficient (the factor which determines to what extent nonlinear effects can be observed in a dielectric medium) is relatively low for silica glass, the long propagation distances which can be achieved in optical fibre means that nonlinear effects can be observed at relatively low power levels. They can therefore be important in telecommunications systems and the main nonlinear process which is of interest here is nonlinear refraction. Nonlinear refraction leads to a dependence of the net refractive index of the fibre on the intensities of the wave or waves propagating along the fibre. It is a near instantaneous effect and gives rise to several effects including self phase modulation, which can lead to the generation of stable optical pulses known as solitons, and cross phase modulation which causes an interaction between two waves propagating along the same fibre.

1.1.4 Fibre Birefringence

In a fibre which has a perfect cylindrical geometry there is no polarisation dependence. However it is not possible to manufacture fibre which is perfect and small random variations in the fibre structure or composition can lead to different propagation velocities for different polarisation states. This is known as birefringence and is generally undesirable because it leads to dispersion between different polarisation states and causes a linearly polarised input signal to quickly reach some arbitrary polarisation state after propagating due to mixing of the polarisation modes of the fibre. Polarisation maintaining fibre, which has a strong but constant birefringence and allows a signal to propagate without variation of the polarisation state, can be manufactured by deliberately changing the structure of the fibre core to make it elliptical or by introducing stressing elements into the fibre. A possible application of this fibre is to allow the capacity of systems to be doubled by using different polarisation states to carry different data channels [8].

1.2 All optical systems

Currently, optical systems use the linear, binary non - return - to - zero (NRZ) scheme [1] pp189 to encode the required data pattern on the source. In the NRZ scheme the data pattern consists of a series of time slots, the length of which is determined by the data rate of the system – in a 1Gbit/s system each time slot is 1ns wide. A "one" in the data pattern is represented by a square pulse of a fixed intensity which entirely fills a time slot and a data "zero" is represented by an empty time slot. The intensity of the pulses is kept sufficiently low that nonlinear effects are not significant over the transmission path. As the name suggests the signal intensity does not return to zero in-between consecutive ones in the data stream, thus the 1Gbit/s (bit interval = 1ns) data stream representing the binary code 11100101 would be as as shown schematically in Figure 1.4 (a).

An alternative data format is the return-to-zero (RZ) scheme which uses an individual pulse positioned at the centre of the timing slot to represent a data one and an empty time slot to represent a zero. The temporal width of an RZ pulse is less than that of the time slot and so the optical intensity returns to zero between adjacent data ones. A representation of the RZ data pattern 11100101 is shown in Figure 1.4 (b).

In order for an error free data pattern to be recorded at the end of an optical system it is essential that the optical data pattern is not degraded along the length of the system. A photo-diode is used to detect the optical data stream at the end of a system and the

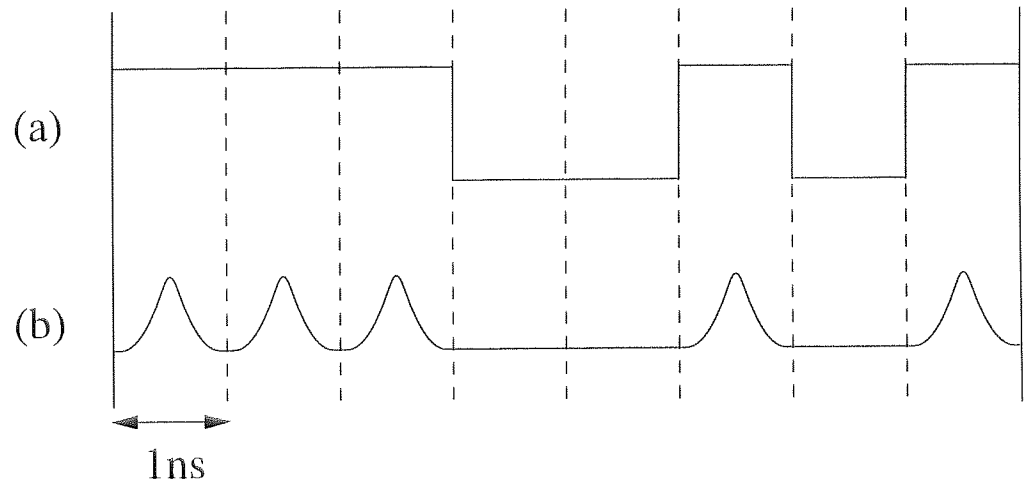

Figure 1.4: Schematic representation of the pattern 11100101 for (a) NRZ encoding and (b) RZ encoding

energy in each time slot is measured. A threshold energy is set above which a data one is recorded and below which a zero is recorded. There are therefore a number of ways that errors can be detected at the end of the system: the temporal position of an RZ data pulse can change so that the pulse energy is recorded in an adjacent time slot; the noise level can increase leading to a one being recorded instead of a zero; the energy of a pulse energy can be attenuated below the threshold value or the pulse energy can be transfered from the original wavelength. It is inevitable that there will always be some errors and so a level has to be set for how many errors can be accepted. This level is generally taken as being less than one error in every 10^9 data bits (i.e. less than one error per 1000 million bits).

Although the NRZ pulse format is currently used universally RZ pulses appear to perform better at high ($\geq$ 10Gbit/s) bit rates [9]–[12] and have the advantages of being compatible with optical time division multiplexed systems where low base rate pulses are interleaved to increase the system data rate [13, 14, 15] and are required for optical switching [16]–[19]. New techniques such as dispersion management and bit-synchronous amplitude and/or phase modulation [20, 21] may allow increases to NRZ data rates but it is likely that RZ pulses will be used in the near future. One major problem with RZ pulses is that they require a larger spectral bandwidth than NRZ pulses due to the narrower temporal width which makes them more susceptible to dispersive broadening.

First generation optical fibre based systems rely on electronic re-generator stages to amplify the data signal and maintain the signal integrity – the optical fibre is simply used as the transmission medium between the regenerators. The length of the optical fibre spans is typically 30-50km, the exact length depending on degradations to the data signal

due to the loss of the fibre and on other effects such as dispersion and nonlinearity. At the electrical re-generator the optical signal is converted into an electronic signal by a semiconductor detector and re-timed, re-shaped and amplified electronically to recover the original data pattern. The signal is then converted back into an optical signal and propagated through the next fibre span. This continues along the system until the destination is reached. It is therefore only necessary to control the perturbations to the data stream over a ~50km length scale with electronically regenerated systems.

The need to convert between the optical to electrical domains and the electronic processing required in an electrically regenerated system leads to a limitation in the speed of the system. There was therefore a great deal of interest in developing all optical systems and with the discovery and development of the erbium doped fibre amplifier (EDFA) [22, 23] all optical systems became a reality. The major advantages of all optical systems are that they are fast (the data passes through the entire system at the speed of light) and the amplifiers are not data rate dependent as is the case with electronic repeaters. The upgrade of an all optical system to higher data rates can therefore be achieved by replacing only the source and the detector provided the fibre is suitable for the new data rate. The all optical system does not however re-time or re-shape the data pulses at any point along the system and so the perturbations to the pulses must not be significant over the entire system length (10 000km for a trans oceanic system) as opposed to over a single amplifier span (typically 40km). The effects of fibre dispersion and nonlinearity therefore have a more significant effect on the performance of the system.

For this reason there has been a great deal of interest in the use of optical solitons as the data pulses in RZ all optical systems. Optical solitons are nonlinear pulses which can propagate along ideal lossless fibre with no alteration to their pulse width or spectrum due to a balance between the otherwise problematic effects of dispersion and nonlinearity in the fibre. In real fibre which has a loss, soliton-like pulses can still propagate but the signal power must be amplified along the system length. This thesis concentrates on the use of soliton and soliton-like pulses in high bit rate long distance experiments and investigates their potential for use in future all optical systems.

1.3 Thesis overview

It is first of all necessary to briefly review the theory of pulse propagation in optical fibre and study the main effects which can limit the performance of soliton telecommunication

systems. This is done in Chapter 2 which also introduces the concept of dispersion management, a technique whereby different types of optical fibre are combined to give the desired average system dispersion.

Chapter 3 describes the operation and design of the recirculating loop which was used to conduct the soliton propagation experiments. The experimental measurement techniques which were used are also explained. The characteristics, principles of operation, advantages and limitations of the various soliton pulse sources which were used in these experiments are described in Chapter 4.

The actual experimental work is covered in Chapters 5-8. Chapter 5 describes a novel pulse propagation scheme which allowed pulse propagation over ultra long distances (greater than 1 million kilometres) without any active control. Chapter 6 investigates the practicality of using fibre Bragg gratings to provide spectral filtering in soliton systems. These devices can be written in the core of optical fibres and can be used for a number of additional telecommunications applications. Chapter 7 looks at many aspects of soliton propagation in non dispersion shifted, standard optical fibre using dispersion compensating fibre to reduce the average dispersion and Chapter 8 presents preliminary results of a similar standard fibre system which used a fibre Bragg grating to provide the dispersion compensation. Finally, the findings of the thesis will be summarised in Chapter 9 and the future of soliton based systems will be considered.

Chapter 2

Solitons: Principles and system considerations

2.1 Introduction

To study the propagation of pulses in an optical fibre system, a mathematical model is required. This section outlines the derivation, from Maxwell's equations, of the nonlinear Schrödinger equation (NLSE) which describes pulse propagation in a dispersive medium and will be used to investigate two important effects, group velocity dispersion (GVD) and self phase modulation (SPM) which will be introduced and investigated separately before their combined effect, which can lead to the formation of optical solitons, is studied. Other effects which can have a bearing on soliton system performance are also discussed and dispersion managed systems which use more than one type of fibre will be introduced. Although the NLSE will be derived from Maxwell's equations, a rigourous derivation will not be presented as this is not relevant to an experimental thesis. Such a complete derivation can be found in suitable textbooks [6, 24].

2.2 Derivation of the nonlinear Schrödinger equation

In deriving the NLSE, the basic wave equation

$$\nabla^2\mathbf{E} - \frac{1}{c^2}\frac{\partial^2\mathbf{E}}{\partial t^2} = \mu_0\frac{\partial^2\mathbf{P}_L}{\partial t^2} + \mu_0\frac{\partial^2\mathbf{P}_{NL}}{\partial t^2} \tag{2.1}$$

is used. $\mathbf{E}(\mathbf{r},t)$ is the electric field, c is the speed of light, μ_0 is permeability of free space and $\mathbf{P}_L$, $\mathbf{P}_{NL}$ are the linear and nonlinear parts of the induced polarisation $\mathbf{P}(\mathbf{r},t) =$

$\mathbf{P}_L(\mathbf{r},t) + \mathbf{P}_{NL}(\mathbf{r},t)$. The linear and nonlinear induced polarisation fields are related to $\mathbf{E}(\mathbf{r},t)$ through the dielectric tensors $\chi^{(1)}$ and $\chi^{(3)}$ respectively [6],pp28.

In order to solve Equation 2.1 three approximations are required to simplify the problem: the nonlinear polarisation $\mathbf{P}_{NL}$ is taken as only a small perturbation to the linear polarisation $\mathbf{P}_L$; it is assumed that the polarisation of the optical field does not change as it propagates along the fibre – thus a scalar approach is valid and finally, it is assumed that the optical field is quasi-monochromatic, i.e $\Delta\omega/\omega_0 \ll 1$ where $\Delta\omega$ is the spectral width and ω_0 is the central frequency.

$\mathbf{E}(\mathbf{r},t)$ can then be written as

$$\mathbf{E}(\mathbf{r},t) = \frac{1}{2}\hat{x}[\bar{E}(\mathbf{r},t)exp(-i\omega_0 t) + c.c.] \tag{2.2}$$

where c.c denotes the complex conjugate, $\hat{x}$ is the polarisation unit vector of the propagating light and $\bar{E}(\mathbf{r},t)$ is a slowly varying function of time compared to the optical period. $\mathbf{P}_L$ and $\mathbf{P}_{NL}$ can be represented in a similar way.

In order to proceed it is necessary to assuming that the nonlinear response is instantaneous which means neglecting the dispersion of $\chi^{(3)}$. This is valid for pulses longer than $\sim$ 0.1ps since the electronic contribution to $\chi^{(3)}$ is at a 1-10fs time scale. For pulses shorter than 100fs the effect of Raman gain must be included [25] pp46. Taking ϵ_{NL}, the nonlinear contribution to the dielectric constant, as a constant (valid in the slowly-varying-envelope approximation), the Fourier transform of $\mathbf{E}(\mathbf{r},t)$, defined by

$$\tilde{E}(\mathbf{r},\omega-\omega_0) = \int_{-\infty}^{\infty} \bar{E}(\mathbf{r},t)exp([i(\omega-\omega_0)t]dt. \tag{2.3}$$

satisfies the equation

$$\nabla^2\tilde{E} + \epsilon(\omega)k_0^2\tilde{E} = 0 \tag{2.4}$$

where $k_0 = 2\pi/\lambda$ is the propagation constant and $\epsilon(\omega)$ is the dielectric constant. $\epsilon(\omega)$ is related to the dielectric tensor and can be used to define the refractive index $\bar{n}$, with the nonlinear contribution to $\epsilon(\omega)$ leading to an intensity dependence of the refractive index. $\bar{n}$ is generally defined as

$$\bar{n}(\omega) = n(\omega) + n_2|\bar{E}|^2 \tag{2.5}$$

with $n(\omega)$ being the linear refractive index and n_2 being the coefficient of nonlinearity, given by

$$n_2 = \frac{3}{8n}\chi^{(3)}_{xxxx}. \tag{2.6}$$

In order to solve Equation 2.4, the method of separation of variables is used. A solution of the form

$$\tilde{E}(\mathbf{r}, \omega - \omega_0) = F(x, y)\tilde{A}(Z, \omega - \omega_0)exp(i\beta_0 Z) \tag{2.7}$$

is assumed, where $F(x, y)$ gives the transverse fibre mode distribution, $\tilde{A}(Z, \omega - \omega_0)$ is a slowly varying function of Z and β_0 is the propagation constant. For single mode fibre $F(x, y)$ is a Bessel function within the fibre core and decays exponentially outside the core. As this function has a complicated form and is difficult to use it is often approximated by a Gaussian. In the first approximation perturbation theory $F(x, y)$ is not changed by nonlinear variations in the refractive index and so it is ignored below. Substitution of Equation 2.7 in Equation 2.4 then gives

$$\frac{\partial \tilde{A}}{\partial Z} = i[\beta(\omega) + \Delta\beta - \beta_0]\tilde{A} \tag{2.8}$$

where $\Delta\beta$ is evaluated from the modal distribution $F(x, y)$ and Δn [6] pp38. The inverse Fourier transform of Equation 2.8 then gives the propagation equation for the slowly varying amplitude $A(z, t)$. In taking the inverse Fourier transform it is useful to expand $\beta(\omega)$ in a Taylor series about the central frequency ω_0 to give

$$\beta(\omega) = \beta_0 + (\omega - \omega_0)\beta_1 + \frac{1}{2}(\omega - \omega_0)^2\beta_2 + \frac{1}{6}(\omega - \omega_0)^3\beta_3 + \cdots \tag{2.9}$$

where

$$\beta_n = \left[\frac{\partial^n \beta}{\partial \omega^n}\right]_{\omega=\omega_0}. \tag{2.10}$$

In this expansion β_0 represents the propagation constant, β_1 is the inverse group velocity, β_2 is the group velocity dispersion and β_3 is third order dispersion. In general, the cubic and higher order terms in this expansion can be neglected if the quasi-monochromatic assumption that the spectral width $\Delta\omega \ll \omega_0$ holds, which is true for pulse widths greater than ~ 0.1ps. It may however be necessary to include the effect of third order dispersion when considering propagation close to λ_0, the zero-dispersion wavelength where $\beta_2 = 0$.

Making this substitution for $\beta(\omega)$, taking the inverse Fourier transform and evaluating $\Delta\beta$ to give explicit terms for fibre loss (α) and nonlinearity (n_2) gives the propagation equation [6] pp40

$$\frac{\partial A}{\partial Z} + \beta_1\frac{\partial A}{\partial t} + \frac{i}{2}\beta_2\frac{\partial^2 A}{\partial t^2} + \frac{\alpha}{2}A = i\gamma|A|^2 A \tag{2.11}$$

where the nonlinear coefficient γ is defined as

$$\gamma = \frac{n_2 \omega_0}{c A_{eff}} \left[W^{-1} km^{-1} \right]. \tag{2.12}$$

A_{eff} is the effective core area of the fibre determined from the the modal distribution $F(x, y)$. A_{eff} therefore depends on fibre parameters such as the core radius and the difference in the refractive index between the core and cladding as well as the wavelength of the propagating light. In the 1.5μm region which is of interest here, the value of A_{eff} is generally taken to be 50-80 μm^2. Precise values of A_{eff} are difficult to obtain as the exact modal distribution in the fibre is difficult to determine and there will also be some fluctuation in the value along the length of a given fibre due to small random changes in the fibre structure. In this thesis a value of $70\mu m^2$ is used for SIF and $50\mu m^2$ is used for DSF unless otherwise stated.There is also some uncertainty in the actual value of n_2 which varies depending on the exact composition of the fibre core. Measurements of n_2 have found the value to vary between 2.2 and 3.4 x $10^{-20} m^2 W^{-1}$ and in this thesis the value is taken to be 2.5 x $10^{-20} m^2 W^{-1}$. Using this value with the above values of A_{eff} gives $\gamma \sim 1.5 W^{-1} km^{-1}$ for SIF and $\gamma \sim 2 W^{-1} km^{-1}$ for DSF.

In order to further simplify Equation 2.11 it is helpful to use a frame of reference moving with the pulse at the group velocity v_g, by making the transform

$$T = t - \frac{Z}{v_g} = t - \beta_1 Z. \tag{2.13}$$

Equation 2.11 then becomes

$$i \frac{\partial A}{\partial Z} = -\frac{i}{2} \alpha A + \frac{1}{2} \beta_2 \frac{\partial^2 A}{\partial T^2} - \gamma |A|^2 A. \tag{2.14}$$

This propagation equation, known as the generalised nonlinear Schrödinger equation (GNLSE), is the starting point for further study. The three terms on the right hand side of this equation determine the effects of loss, group velocity dispersion and nonlinearity respectively. In the case where the loss of the fibre is neglected ($\alpha = 0$) it is known as the nonlinear Schrödinger equation (NLSE).

Depending on the initial pulse width and power either dispersive or nonlinear effects can dominate and it is useful to define two length scales, the dispersion length, L_D and the nonlinear length, L_{NL} which can be used to categorise the pulse evolution into four distinct regimes depending on the relative lengths of L_D, L_{NL} and L, the fibre length.

L_D and L_{NL} are defined as

$$L_D = \frac{\tau_0^2}{|\beta_2|} \qquad L_{NL} = \frac{1}{\gamma P_0} \tag{2.15}$$

where τ_0 is the half width of the pulse, P_0 is the peak pulse power and γ is the nonlinear coefficient. τ_0 is related to the more commonly used full pulse width at the half intensity points (τ_{fwhm}) and the exact relation between these two measurements of pulse width depends on the pulse shape. Unless otherwise stated the pulse widths quoted in the following will be the FWHM value.

The four propagation regimes are then as follows

i) $L \ll L_D$, $L \ll L_{NL}$: neither dispersive nor nonlinear effects play a significant part in the pulse evolution.

ii) $L \ll L_{NL}$, $L \geq L_D$: the pulse evolution is dominated by GVD with the nonlinearity playing only a minor part.

iii) $L \ll L_D$, $L \geq L_{NL}$: the evolution is governed by the nonlinearity with dispersion being negligible.

iv) $L \geq L_D$, $L \geq L_{NL}$: both dispersion and nonlinearity have a significant effect on the pulse propagation.

In the analysis that follows " much less than" is taken as meaning roughly a factor of 10 and the emphasis will be on the implications for long distance ($\geq$ 1000km) high bit rate ($\geq$ 1Gbit/s) systems. In such systems the FWHM pulse widths are typically 10s of ps and so the assumptions that the optical signal is quasi-monochromatic and that the nonlinear response of the medium is instantaneous, which were made in the derivation of the GNLSE, are valid. In relation to high speed telecommunications systems only the final three scenarios are of interest, the first is of little interest as it requires long pulses ($\tau_0^2 \sim$ 100ps) with low dispersion and low peak powers ($P_0 \sim$ 0.05mW) for propagation over 500km. The three cases (ii) - (iv) will be considered in turn to investigate the effects of GVD and SPM alone before their combined effect is studied.

2.3 Group Velocity Dispersion

The first propagating regime which is considered is case (ii) where GVD dominates. This requires that $L \ll L_{NL}$, $L \geq L_D$ or equivalently,

$$\frac{L_D}{L_{NL}} = \frac{\gamma P_0 \tau_0^2}{|\beta_2|} \ll 1 \tag{2.16}$$

Taking typical values of γ and $|\beta_2|$ for SIF at a wavelength of 1.55μm of $1.5W^{-1}km^{-1}$ and -$20ps^2/km$ respectively means that for a 1000km system P_0 must be $< 70\mu W$, indicating that in a high speed telecommunications system this regime is only important at low pulse powers.

To study the effect of GVD alone, γ is set to zero in Equation 2.14. The effect of loss is included but as it has no effect on the dispersive behaviour it is removed by introducing the normalised amplitude U(Z, T) defined by

$$A(Z,T) = \sqrt{P_0} exp\,(-\alpha Z/2)\, U(Z,T). \tag{2.17}$$

U(Z, T) then satisfies the partial differential equation

$$i\frac{\partial U}{\partial Z} = \frac{1}{2}\beta_2 \frac{\partial^2 U}{\partial T^2} \tag{2.18}$$

This equation can be solved using the Fourier method. If $\tilde{U}(Z,\omega)$ is the Fourier transform of U(Z, T) defined by

$$U(Z,T) = \frac{1}{2\pi}\int_{-\infty}^{\infty} \tilde{U}(Z,\omega) exp(-i\omega T) d\omega \tag{2.19}$$

then it satisfies the ordinary differential equation

$$i\frac{\partial \tilde{U}}{\partial Z} = -\frac{1}{2}\beta_2 \omega^2 \tilde{U}. \tag{2.20}$$

This equation is easily solvable and has the solution

$$\tilde{U}(Z,\omega) = \tilde{U}(0,\omega) exp\left(\frac{i}{2}\beta_2 \omega^2 Z\right) \tag{2.21}$$

where $\tilde{U}(0,\omega)$, the Fourier transform of the pulse at $Z = 0$ is given by

$$\tilde{U}(0,\omega) = \int_{-\infty}^{\infty} U(0,T) exp(i\omega T) dT. \tag{2.22}$$

Equation 2.21 shows that there is no change to the pulse spectrum as it propagates along the fibre but each of the spectral components of the pulse receives a phase change proportional to the distance travelled along the fibre and proportional to the square of the frequency of the spectral component. These phase changes can lead to an alteration of the pulse shape as the pulse propagates. The phase change is also proportional to β_2

indicating that the behaviour is different in the anomalous and normal dispersion regions as the sign of β_2 is different in these two regions.

The general solution of Equation 2.18 is found by substituting Equn 2.21 in Equn 2.19 to give

$$U(Z,T) = \frac{1}{2\pi}\int_{-\infty}^{\infty} \tilde{U}(0,\omega) exp\left[\frac{i}{2}\beta_2\omega^2 Z - i\omega T\right] d\omega. \tag{2.23}$$

In order to study the effect of GVD on a pulse as it propagates along a fibre it is useful to consider as an example the case of a Gaussian input pulse. A Gaussian is used as it makes the integrations involved simpler than they would be with a more complicated pulse shape. The Gaussian input pulse is given by

$$U(0,T) = exp\left(-\frac{T^2}{2\tau_0^2}\right). \tag{2.24}$$

For a Gaussian pulse τ_0 is related to the FWHM pulse width by $\tau_{fwhm} = 2\sqrt{ln2}\tau_0 \simeq 1.665\tau_0$. Using this input pulse and carrying out the substitutions and integrations required in Equations 2.22 and 2.23 gives [6] pp56

$$U(Z,T) = \left(\frac{\tau_0^2}{\tau_0^2 - i\beta_2 Z}\right)^{1/2} exp\left(-\frac{T^2}{2(\tau_0^2 - i\beta_2 Z)}\right) \tag{2.25}$$

By taking the real and complex parts of this equation it is found that on propagation the Gaussian pulse maintains a Gaussian profile but the pulse width increases becoming

$$\tau_1 = \tau_0\sqrt{1 + \left(\frac{Z}{L_D}\right)^2}. \tag{2.26}$$

This equation shows that for a given fibre length, the shorter the pulse the more rapid the dispersive broadening as the rate of broadening is inversely proportional to L_D.

Further insight into the dependence of dispersive pulse broadening on pulse width can be obtained by recalling that the different frequency components of a pulse travel at different speeds on propagation through a fibre (red travelling faster than blue in the normal dispersion regime where $\beta_2 > 0$ and vice-versa in the anomalous dispersion regime where $\beta_2 < 0$). Thus after propagation along a fibre in the anomalous dispersion regime, the blue components of the pulse will arrive ahead of the red components. In relation to pulse width, a shorter pulse requires more spectral components to maintain the pulse shape and hence there will be a greater difference in arrival time of the spectral components compared to a longer pulse leading to an increase in the rate of temporal broadening.

Similarly, when different pulse shapes are considered, pulses with steeper leading and trailing edges experience a greater rate of dispersive broadening due to their broader spectra. Spectral broadening also highlights the physical significance of the dispersion length L_D - at $Z = L_D$ the Gaussian pulse width has increased by a factor of $\sqrt{2}$.

In addition to the effect of spectral broadening the pulse also acquires an instantaneous frequency shift on propagation. This can be seen by separating Equation 2.25 into an amplitude and a phase term to give

$$U(Z,T) = |U(Z,T)|exp(i\phi(Z,T)) \tag{2.27}$$

where the phase term $\phi(Z,T)$ is given by [6] pp56

$$\phi(Z,T) = -\frac{sgn(\beta_2)(Z/L_D)}{1+(Z/L_D)^2}\frac{T^2}{\tau_0^2} + tan^{-1}\left(\frac{Z}{L_D}\right) \tag{2.28}$$

The time dependence of $\phi(Z,T)$ indicates that at any point along the fibre there is an instantaneous frequency difference across the pulse give by

$$\delta\omega = -\frac{\partial\phi}{\partial T} = 2\frac{sgn(\beta_2)(Z/L_D)}{1+(Z/L_D)^2}\frac{T}{\tau_0^2}. \tag{2.29}$$

At $Z = 0$ which corresponds to the fibre input $\phi(Z,T)$ is zero and the input pulse is recovered. The linear frequency change or linear frequency chirp across the pulse, $\delta\omega$, depends on the sign of β_2. In the anomalous dispersion regime (where $\beta_2 < 0$) $\delta\omega$ is positive when $T < 0$ at the leading edge of the pulse and decreases across the temporal profile of the pulse. The reverse is true in the normal dispersion regime where $\beta_2 > 0$ but Equation 2.26 shows that for an unchirped input pulse the *amount* of spectral broadening is independent of the sign of β_2 and for a given value of L_D the pulse broadens by the same amount in the normal and anomalous dispersion regimes.

Thus far the discussion has been restricted to unchirped Gaussian input pulses. When a $sech^2(t)$ input pulse is used (which is of particular interest as this is the temporal profile of the optical soliton) the qualitative features of the dispersive broadening are very similar to those of Gaussian pulses but when a steeper edged pulse shape such as a super Gaussian is used, oscillations can develop in the trailing edges of the pulse. This more complex dispersive broadening is due to the wider spectrum of such pulses [6] pp62. When a chirped input pulse is used the effect of dispersive broadening depends on the sign of β_2 and the input chirp. If these two are of the same sign then the rate of broadening

increases but more interestingly if they are of the opposite signs, the initial chirp of the pulses is reduced as the pulse is propagated along the fibre and there is a corresponding reduction in the pulse width. This pulse compression continues until the initial chirp is completely cancelled by the dispersion induced chirp to give a transform limited pulse. As the propagation distance is increased further the pulse begins to broaden, with the broadening being similar qualitatively to that of an unchirped input pulse. This dispersive pulse compression has a practical use in that down chirped pulses emitted by a gain switched, distributed feedback semiconductor laser can be compressed by propagation through a length of normal dispersion fibre [26]. This application will be discussed in Section 4.5.

By referring back to Equation 2.26 it is seen that when β_2 is equal to zero i.e. at λ_0, there is no dispersive broadening. However, in deriving this equation, cubic and higher order terms in the Taylor series of Equation 2.9 were neglected. When operating close to λ_0 it is necessary to include third order dispersion, β_3, which leads to an additional term in Equation 2.18 . The influence of this term is to lead to an asymmetric and oscillatory temporal pulse profile [6] pp. 64.

Although the group velocity parameter β_2 has been used throughout this section, a second parameter, the group delay dispersion D_2 is more commonly quoted as it has the more useful units of ps/(nm km). The difference between β_2 and D_2 is that the latter is proportional to the second derivative of the refractive index with respect to wavelength as opposed to frequency. The two are thus related by

$$D_2 = \frac{-2\pi c}{\lambda^2}\beta_2. \tag{2.30}$$

As an experimental example of GVD, 2.5GHz pulses from the fibre laser described in Section 4.4 which was operated at 1550nm, were propagated through various lengths of standard fibre. The pulse width of the laser pulses was measured using the autocorrelation technique described in Section 3.3.1. From the autocorrelation width the actual pulse width could be inferred by assuming a particular pulse shape. Figure 2.1 (a) shows the autocorrelation trace of the input pulses which has been scaled to show the actual pulse width assuming a $sech^2(t)$ pulse shape. The $sech^2(t)$ curve fit shown as a solid line in this graph indicates that this assumption was not unreasonable. The FWHM pulse width of the pulses was then 18ps. For $sech^2(t)$ pulses the relationship between τ_0 and τ_{fwhm} is

[6] pp60

$$\tau_{fwhm} = 2ln(1+\sqrt{2})\tau_0 \sim 1.763\tau_0 \tag{2.31}$$

giving $\tau_0 = 10.2$ps. Using this value and taking D_2 ~16.5ps/nm/km gives a dispersion length $L_D \sim$ 5km. The fact that $D_2 \gg 0$ indicates that third order effects could be neglected. In order for GVD effects to be dominant the propagation distance must be greater or comparable with the dispersion length of 5km and Equation 2.16 shows that for this case the peak power P_0 must be much less than ~130mW (this calculation assumed $\gamma = 1.5W^{-1}km^{-1}$). These conditions were met by having a minimum propagation distance of 6km and a peak power of ~2mW. Figure 2.1 (b) - (d) show the pulse widths, again

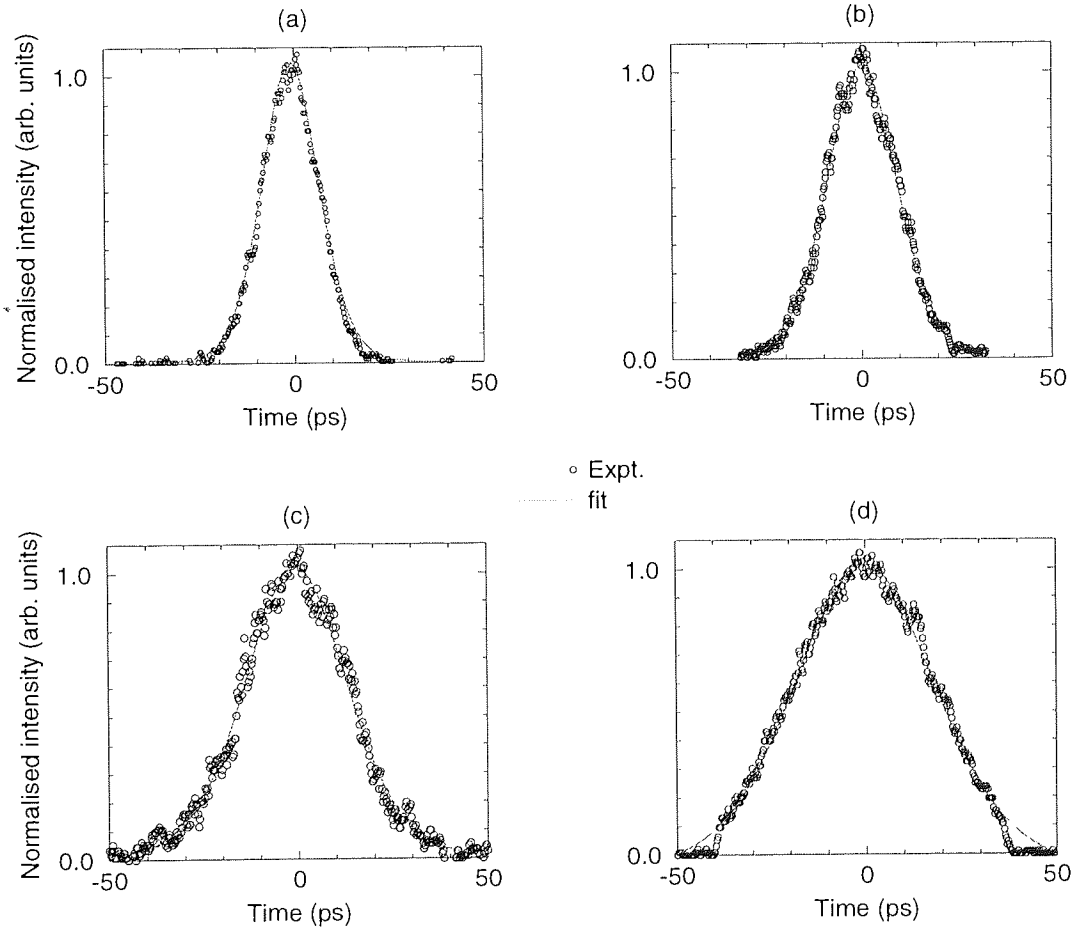

Figure 2.1: Experimentally measured Pulse widths (circles) and $sech^2(t)$ fits (solid lines) for (a) input pulses and pulses after propagation through (b) 6km, (c) 13km and (d) 19km of standard fibre.

found by taking autocorrelations, of the pulses after propagating through 6, 13 and 19km of standard fibre respectively. These results show that as predicted by theory the effect of GVD is to broaden the pulses. After propagating 6km the pulse width had increased to ~23ps and with further increases to the propagation distance the pulses continued to broaden, the pulse widths being ~33ps and ~45ps after propagation distances of 13 and

19km respectively. A $sech^2(t)$ fit to the experimental data is also shown for each case, indicating that there was little change to the temporal profile of the pulses (the mismatch between the wings of the measured pulse width and the fit for (d) is due to the pulse width exceeding the measurement window of the autocorrelator). Measurement of the spectra of the input and propagated pulses showed that there was no variation in the spectral width, it remained constant at 0.17nm throughout. This spectral width gave a time bandwidth product, $\Delta\nu\Delta\tau$, of 0.36 for the input pulses showing that they were slightly chirped (transform limited $sech^2(t)$ pulses have $\Delta\nu\Delta\tau$ =0.32). The rate of dispersive broadening in this experiment was roughly 1.5 times higher than that predicted by Equation 2.26, the difference being due to the experimental input pulses being chirped $sech^2(t)$ pulses as opposed to unchirped Gaussian pulses which this equation assumes. The peak power in this experiment was too low to observe any nonlinear effect which would have caused a reduction in the pulse broadening and a slight increase in the spectral bandwidth of the pulses.

2.4 Self Phase Modulation

The next propagating regime which is considered is case (iii) where $L \ll L_D$ but $L \geq L_{NL}$ and the pulse evolution is dominated by nonlinear effects with the GVD being negligible. This condition can be re-stated as

$$\frac{L_D}{L_{NL}} = \frac{\gamma P_0 \tau_0^2}{|\beta_2|} \gg 1 \tag{2.32}$$

and for this to hold for a high bit rate system with a pulse width τ_0= 50ps requires a peak pulse power of 50mW in standard fibre and the SPM dominates for a few 10s of km. If τ_0 is reduced to 10ps the required peak power increases to $\sim$ 1W and the length scale reduces to only a few hundred meters. In dispersion shifted fibre which is taken to have a dispersion of 1ps/(nm km) the peak power required is reduced to ~60mW for τ_0 =10ps.

In order to investigate the effect of SPM mathematically, the normalisation of Equation 2.17 must be applied to Equation 2.14 with β_2 set to zero to give

$$\frac{\partial U}{\partial Z} = \frac{i}{L_{NL}} exp(-\alpha Z)|U|^2 U, \tag{2.33}$$

where α determines the fibre loss, which plays an important part in the pulse propagation.

This equation can be solved to give the solution

$$U(Z,T) = U(0,T)exp\left(i\phi_{NL}(Z,T)\right), \tag{2.34}$$

where U(0, T) is the input pulse amplitude and ϕ_{NL} is the nonlinear phase shift given by

$$\phi_{NL}(Z,T) = |U(0,T)|^2 \frac{Z_{eff}}{L_{NL}} \tag{2.35}$$

with

$$Z_{eff} = \frac{1}{\alpha}[1 - exp(-\alpha Z)] \tag{2.36}$$

being an effective length scale which is smaller than Z and takes into account the effect of the fibre loss (when fibre loss is disregarded $\alpha = 0$ and $Z_{eff} = Z$).

Equations 2.34 and 2.35 show that SPM induces a phase shift on the pulse which is proportional to the intensity $|U(0,T)|^2$ and that this phase shift increases with propagation distance.

Similarly to Equation 2.29 the chirp induced by SPM is given by

$$\delta\omega = -\frac{\partial\phi_{NL}}{\partial T} = -\frac{\partial|U(0,T)|^2}{\partial T}\frac{Z_{eff}}{L_{NL}}. \tag{2.37}$$

This shows that the chirp increases in magnitude as propagation distance increases, with new frequencies being self-generated as the pulse propagates along the fibre. These SPM-generated frequencies lead to the pulse having a broader frequency spectrum after propagation that at the fibre input, with the rate of the spectral broadening being determined by the rate of change of the intensity, due to the $\frac{\partial|U(0,T)|^2}{\partial T}$ term. This means that different input pulse shapes suffer different degrees of spectral broadening.

From Equation 2.35 it is seen that the maximum phase shift ϕ_{max} occurs at the centre of the pulse (T = 0) as this is the point where the intensity is greatest. In addition, since U is normalised such that $|U(0,0)| = 1$, it is given by

$$\phi_{max} = Z_{eff}/L_{NL} = \gamma P_0 Z_{eff}. \tag{2.38}$$

This shows the physical significance of L_{NL}: it is the effective propagation distance at which the phase shift is unity.

As an experimental example of SPM, 24ps (FWHM) fibre laser pulses were passed through a 25km length of dispersion shifted fibre (DSF). The operating wavelength (which

like all optical spectrum measurements quoted in this thesis, was measured using an optical spectrum analyser with a 0.1nm resolution) was 1551nm and the dispersion was $\sim$ 0.1ps/(nm km) giving a dispersion length, $L_D \sim$ 1500km showing that by using DSF the condition $L \ll L_D$ was met. The actual value of L_{NL} was not well known because of uncertainty in A_{eff} and n_2 but taking, as an estimate $\gamma = 2\ W^{-1}km^{-1}$ gives $L_{NL} \sim$ 25km for a peak power $P_0 = 0.02$W which was the minimum power used in this experiment. This shows that the condition that $\frac{L_D}{L_{NL}} \gg 1$ held and so nonlinear effects were expected to be dominant. Due to the long length of fibre which was used the effect of loss could not be neglected. As the signal propagated along the fibre the exponential decay in the pulse power would have led to a decrease in the SPM effect. In calculating the nonlinear phase shift it was therefore necessary to use the effective length scale which takes account of this loss. The fibre had an approximate loss of 0.2dB/km giving a value of α=0.046 and so the effective length given by Equation 2.36 was $\sim$ 15km.

Equations 2.37 and 2.38 show that for a fixed fibre length, ϕ_{max} and $\delta\omega(T)$ depend on the peak power P_0 and so the spectral evolution of the pulses could be observed by increasing the peak power of the launched pulses. Figure 2.2 shows the spectra of the input pulses and the pulses after propagation through the fibre for various peak powers. As (b)

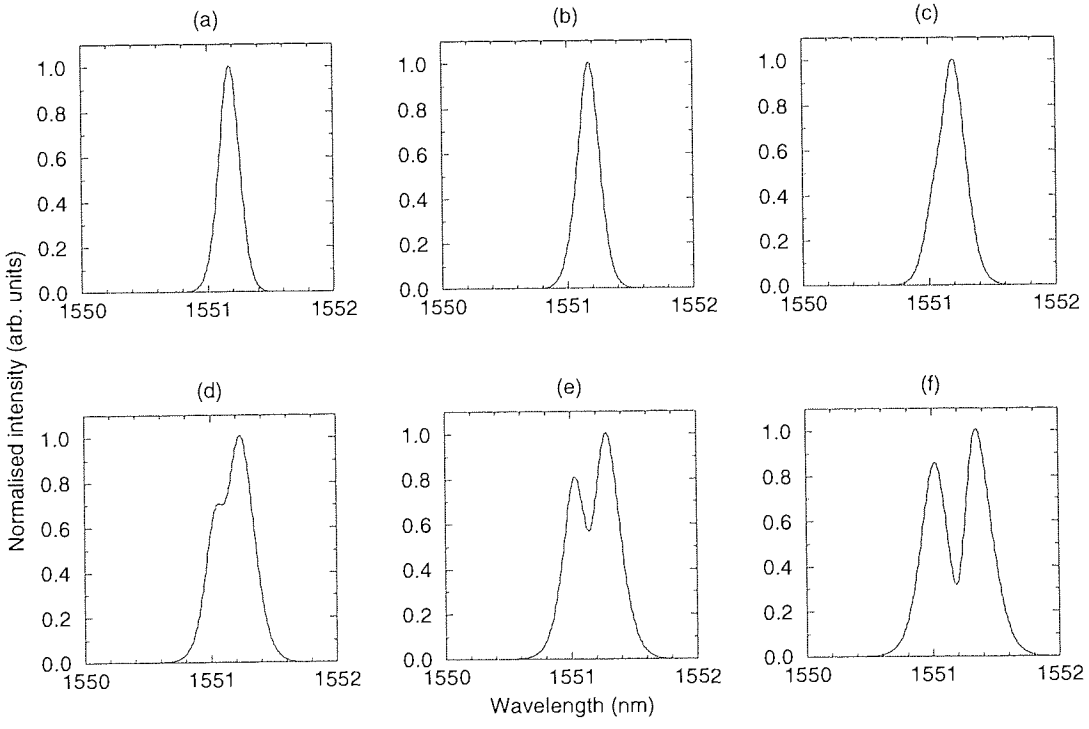

Figure 2.2: Optical spectra of (a) the input pulses and pulses after propagation through 25km of DSF for peak pulse powers of (b) 0.02W (c) 0.05W (d) 0.08W (e) 0.1W and (f) 0.15W

shows there was little change in the spectrum of the pulses at low input power but as the

power was increased there was first a broadening of the spectrum and at the highest input powers (e) and (f) show the oscillatory nature of the spectrum which is typical of SPM. The asymmetry which was seen in these spectra was probably due to slight asymmetry in the input pulses. The number of peaks expected in the SPM broadened optical spectrum can be found approximately from the expression

$$\phi_{max} \sim (M - 1/2)\pi \tag{2.39}$$

where M is the number of peaks in the spectrum and ϕ_{max} is the nonlinear phase shift. In the above experiment two peaks were seen in the optical spectrum and so ϕ_{max} should be $\sim \frac{3\pi}{2} \sim 4.7$. From Equation 2.38 the value of ϕ_{max} was calculated to be ~5.4 taking a fibre loss of 0.2dB/km and a value of $\gamma = 2W^{-1}km^{-1}$. These two values for ϕ_{max} are in reasonable agreement considering the approximations made.

The oscillations in the pulse spectrum can be understood by considering the chirp across the pulse as shown in Figure 2.3 (b) for the $sech^2(t)$, Gaussian and super Gaussian (of third order) pulse profiles shown in Figure 2.3 (a). The chirps, which were calculated

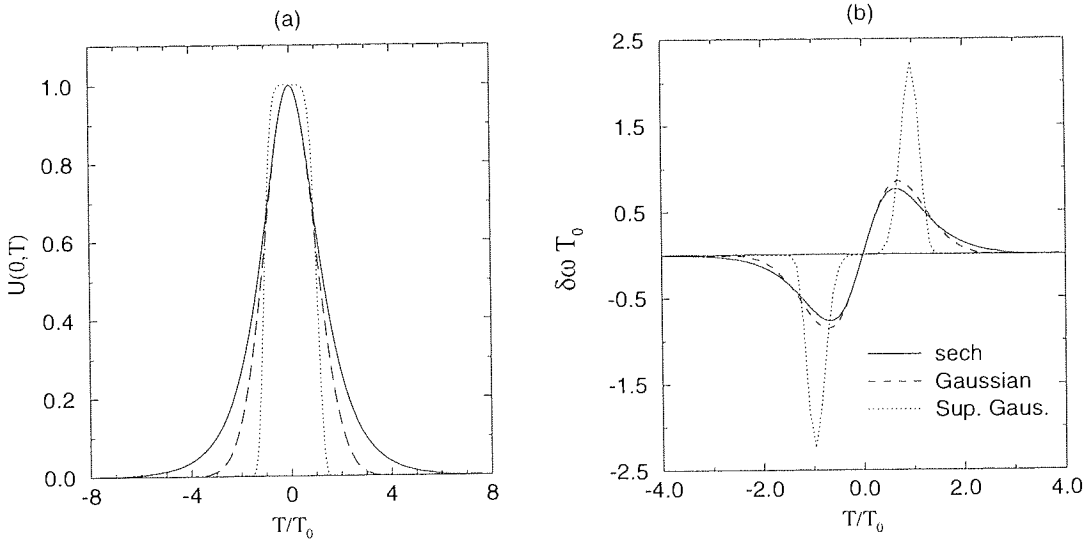

Figure 2.3: (a) Pulse shapes and (b) chirps for $sech^2$, Gaussian and super Gaussian (of third order) pulses.

at $Z_{eff} = L_{NL}$, show that there are two points in the temporal profile of the pulse which have the same instantaneous frequency. These two points represent two waves which have the same frequency but different phases, which can interfere constructively of destructively depending on their relative phase difference. It is the interference between these two waves which leads to the oscillations in the optical spectrum of the pulses.

Figure 2.3 also shows how the chirp varies for different pulse shapes. There is little difference between the $sech(t)$ and Gaussian amplitude profiles over the central region of the pulses leading to a similar chirp over this region with the chirp being linear and positive (the frequency increases with T) over this region. Away from the pulse peak there is a greater variation between these two pulse shapes which is reflected in their slightly different chirps. The Gaussian pulse has a slightly higher chirp due to the steeper wings and as the pulse shape is changed to give a super Gaussian shape which, as is shown in Figure 2.3 (a) is much squarer, with steeper leading and trailing edges, the chirp increases greatly in magnitude. There is also a qualitative change with the chirp only occuring in the wings of the pulse as there is little intensity change over the central region. Although SPM still leads to spectral broadening for these pulses the majority of the energy remains within the central peak and there is therefore an advantage in using flat square NRZ type pulses to reduce the effect of SPM. A further feature of the chirp is that there is a change of sign with the chirp being negative (corresponding to a red shift) at the leading edge of the pulse where $T < 0$ and becomes positive (blue shift) at the trailing edge. If the input pulse is chirped there are also changes to the effect of SPM. For a Gaussian pulse a positive chirp adds to the SPM induced chirp over the central region of the pulse leading to an increase in the number of peaks seen in the optical spectrum of the pulse whilst the opposite is true when the input pulse has a negative chirp [6] pp84.

2.5 The soliton solution

The final regime which is considered corresponds to case (iv) where $L \geq L_D$, $L \geq L_{NL}$ and both GVD and SPM have a significant effect on the propagation. In this case, the behaviour depends on the sign of the β_2: in the normal dispersion regime, where $\beta_2 > 0$, there is a stable c.w. solution but when the dispersion is anomalous ($\beta_2 < 0$) any small perturbation to the c.w. or quasi c.w. power level leads to the spontaneous formation of an ultrashort pulse train through a phenomenon known as modulation instability [6] pp105. Modulation instability can be a problem in NRZ systems where a long series of data "ones" gives a quasi c.w. power level. For this reason NRZ systems operate in the normal dispersion regime. When a pulsed source is used there is again a difference in the evolution depending on whether the dispersion is normal or anomalous. The case which is of interest here is that of anomalous dispersion where the combined effect of GVD and SPM can lead to the formation of optical solitons.

The lossless case, where α is set to zero in Equation 2.14, is considered first of all. The equation governing the evolution is then the nonlinear Schrödinger equation

$$i\frac{\partial A}{\partial Z} = \frac{1}{2}\beta_2\frac{\partial^2 A}{\partial T^2} - \gamma|A|^2 A. \tag{2.40}$$

This equation can be normalised using

$$u = N\frac{A}{\sqrt{P_0}},\ z = \frac{Z}{L_D},\ \tau = \frac{T}{\tau_0}, \tag{2.41}$$

where N is defined as

$$N^2 = \frac{L_D}{L_{NL}} = \frac{\gamma P_0 \tau_0^2}{|\beta_2|}, \tag{2.42}$$

to give

$$i\frac{\partial u}{\partial z} + \frac{1}{2}\frac{\partial^2 u}{\partial \tau^2} + |u|^2 u = 0 \tag{2.43}$$

where $sgn(\beta_2)$ has been set to -1 corresponding to the anomalous dispersion regime. When the normal dispersion is being considered the second term (which dictates the dispersive behaviour) is negative.

Although the NLSE cannot be solved directly, it can be exactly solved using the inverse scattering method which was devised by Gardener *et al.* [27] and was used to solve the NLSE by Zakharov and Shabat [28]. The inverse scattering method will not be discussed here but is similar to the inverse Fourier transform method used to solve linear partial differential equations [6] pp111. Using this method gives a series of solutions the most simple of which corresponds to the fundamental or N=1 soliton and is given by

$$u(z,\tau) = 2\zeta sech(2\zeta\tau)exp(2i\zeta^2 z), \tag{2.44}$$

where the eigenvalue ζ determines the soliton amplitude. Normalising such that $2\zeta = 1$ gives the canonical form of the fundamental soliton

$$u(z,\tau) = sech(\tau)exp(iz/2). \tag{2.45}$$

This equation shows that if a hyperbolic secant pulse with a peak power and pulse width chosen such that N=1 or equivalently such that

$$P_0 = \frac{|\beta_2|}{\gamma\tau_0^2}, \tag{2.46}$$

is launched into an ideal lossless optical fibre, it will propagate undistorted indefinitely with no change to the pulse shape or width. The pulse does however acquire a phase which increases linearly with propagation but this phase has no temporal dependence and so the pulse does not become chirped as it propagates. There is therefore no change to the pulse spectrum. Obviously, pulses which can propagate along optical fibre without any distortion are of enormous interest in optical communications.

Equation 2.46 shows that the peak pulse power and the pulse width of the fundamental soliton are related, with the peak power being inversely proportional to the square of the pulse width, and so narrower pulses have higher peak powers. For standard fibre at $1.55\mu m$, with $\gamma = 1.5W^{-1}km^{-1}$ and $|\beta| = 20ps^2/km$ the peak pulse power is $\sim$ 4mW for a 100ps FWHM pulse width and increases to $\sim$ 400mW for a 10ps soliton. If DSF is used, which has values of D_2 $\sim$1ps/(nm km) and $\gamma \sim 2W^{-1}km^{-1}$, the peak power required for a 10ps soliton is reduced to $\sim$ 20mW.

There are further solutions to the NLSE and of particular interest are the higher order solitons which have the initial form

$$u(0,\tau) = Nsech(\tau), \tag{2.47}$$

where N is an integer which denotes the soliton order. These higher order soliton require a peak power N^2 times that of a fundamental soliton for the same pulse width. Unlike fundamental solitons, the higher order soliton undergoes a complicated evolution, with the pulse splitting as it propagates but the evolution is periodic and the soliton returns to the original form at $z = m\pi/2$ where m is an integer [6] pp115. Thus the soliton period is defined in physical units (using the normalisation of Equation 2.41) as

$$Z_0 = \frac{\pi}{2}L_D = \frac{\pi}{2}\frac{\tau_0^2}{|\beta_2|}. \tag{2.48}$$

For a 10ps (FWHM) pulse the soliton period is $\sim$2.5km in standard fibre and $\sim$25km in DSF.

In order to gain further insight into the evolution of higher order solitons and the lack of evolution of fundamental solitons it is useful to consider the chirps induced on the pulse by SPM and GVD. The sign of the GVD induced chirp depends on the sign of the β_2 whilst that of the SPM induced chirp is invariant. In the normal dispersion regime, the two chirps have the same sign and combine leading to unstable pulses, whilst in the anomalous dispersion regime the chirps have the opposite signs and if the pulse width

and pulse peak power are chosen such that N =1, the two chirps cancel exactly leading to the formation of an optical soliton. In the case of the higher order solitons the two chirps cancel in such a way that the original pulse shape is recovered after an integral number of soliton periods.

As an experimental example 25ps pulses from a fibre ring laser were propagated along a 25km length of standard fibre and the input power of the pulses was varied. The spectral width of the pulses was 0.12nm giving a time bandwidth product of 0.37 showing that these were close to transform limited $sech^2(t)$ pulses. The peak power required to generate a fundamental soliton of this pulse width was estimated to be ~60mW using Equation 2.46 and assuming β_2 = -20ps/(nm km) and $\gamma = 1.5W^{-1}km^{-1}$. This calculation neglected the effect of loss but the 25km length of fibre used had a loss of ~5dB. As will be seen in Section 2.5.1 the fibre loss leads to a higher power being required to launch a stable pulse and in this experiment a peak power of ~ 90mW was estimated for stable pulses.

Autocorrelations were taken of the pulses at the fibre output for various input powers and the pulse width was calculated from the autocorrelation width. Figure 2.4 shows these autocorrelations scaled to give the actual pulse widths and $sech^2(t)$ fits to the experimental results for (a) the input pulses and the output pulses for peak powers of (b) 100mW, (c) 80mW, (d) 30mW, (e) 5mW, (f) 0.4mW. The experimental results show that when the peak power was 100mW (Figure 2.4 (b)) there was no significant pulse broadening after propagation through the 25km of fibre. The pulse width of the output pulses was 26ps compared to 25ps for the input pulses. There was little change to the pulse spectrum either, the spectral width remaining at ~ 0.12nm. However when the peak power of the input pulses was reduced pulse broadening was observed (see Figure 2.4 (c) - (f)) because the SPM effect was not strong enough to counteract the dispersion and the pulse spread in the time domain but there was no spectral broadening. The amount of spectral broadening increased as the input power was decreased. At an input power of 80mW the temporal width of the output pulses had increased to only 32ps but with a further reduction of the power to 30mW the pulse width increased to 41ps. At a peak powers of 5mW and 0.4mW a large degree of pulse broadening occurred which is hardly surprising as for these peak powers the propagation distance $L \ll L_{NL}, L \geq L_D$ and so the propagation was dominated by GVD with nonlinearity being insignificant (see Section 2.3). There was reasonable agreement, when the effect of loss was taken into account, between the experimental peak power for a stable pulses (~ 100mW) and

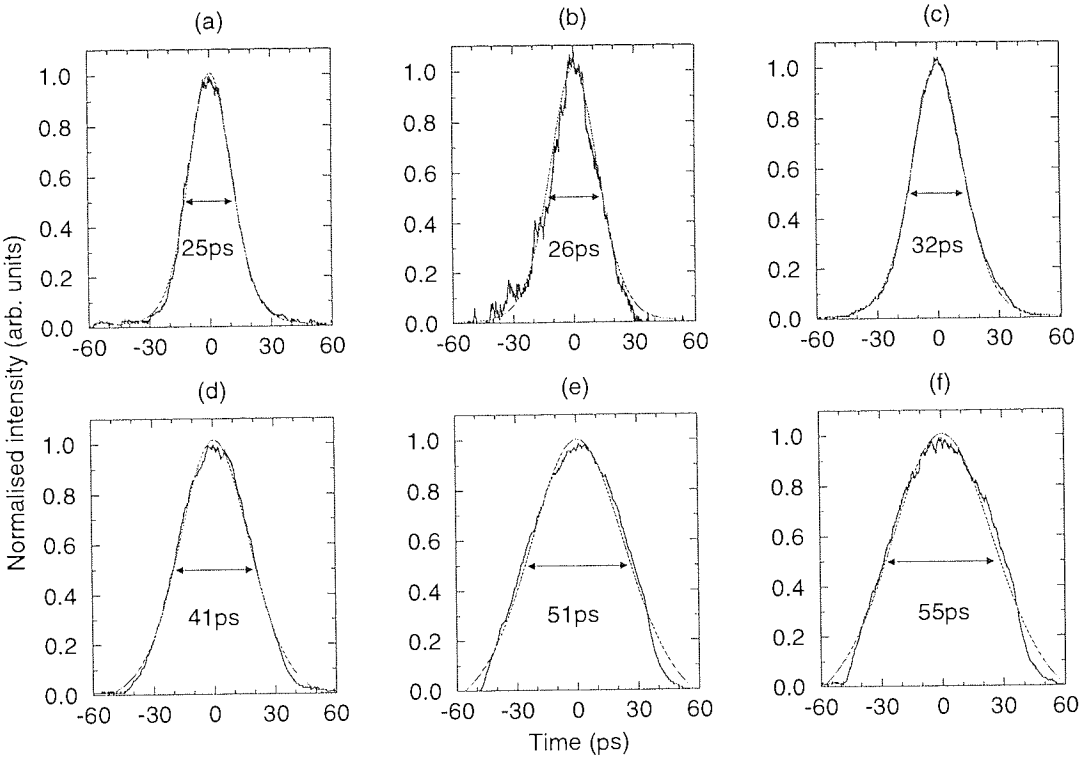

Figure 2.4: Pulse widths obtained from autocorrelation and $sech^2(t)$ fits for (a) the input pulses and pulses after propagation through 25km of SIF for peak pulse powers of (b) 100mW (c) 80mW (d) 30mW (e) 5mW and (f) 0.4mW

the calculated value of 90mW. The small discrepancy between these two values can be attributed to the approximate values of γ, β_2 and α used in the calculation.

Another remarkable property of solitons is that they are resilient to small perturbations. If the soliton width or spectrum is slightly changed the soliton will try to adjust itself so as to remain soliton-like. This does however often result in a change in the temporal position of the pulse in its own frame of reference. As shall be seen in Section 2.7.1 this has a serious implication for soliton based communication systems. It is also possible to excite a soliton even if the pulse launched into the fibre is not of the exact shape, power or chirp required for a soliton. The pulse will eventually evolve into a soliton after propagation with the excess energy being shed as dispersive radiation[29]–[32]. In a soliton communication system this shedding of radiation has to be avoided as much as possible since the dispersive radiation would add to the background noise degrading the signal to noise ratio. It is therefore necessary to use the correct pulse shape and power in soliton systems.

This simple analysis has shown that optical solitons have many of the attributes of the ideal pulses for optical communications systems: they are stable against perturbation; have a stable pulse width and spectrum on propagation and owe their existence to an

interplay between the otherwise troublesome effects of GVD and SPM. There are also disadvantages of using solitons which will be discussed below but first the implications of a serious omission of the above analysis must be considered.

2.5.1 The effect of loss - The average soliton

In the previous analysis the fibre was assumed to be ideal and lossless. However loss cannot be disregarded in practice and it has a major effect on soliton propagation since any decrease in the pulse power leads to a decrease in nonlinear effects and the balance between GVD and SPM is destroyed. As was seen in the previous experiment this can lead to pulse broadening as the pulse propagates because GVD begins to dominate the pulse evolution. A second implication of fibre loss is that the signal power in a communications system must be boosted in order to compensate for the loss in the fibre. In contemporary systems this amplification is usually done all optically by "lumped" erbium doped fibre amplifiers (EDFAs) although some work has also been done using distributed EDFAs [33, 34, 35]. Here only lumped amplifiers are considered. The exponential decay of the soliton power led to the proposal of the average (or guiding centre) soliton as the stable pulse in a periodically amplified system [36, 37].

When considering an amplified all optical system each EDFA can be taken as being a discrete amplifier as the amplifier length is much less than the span between amplifiers. The loss between each amplifier is however, distributed along the whole of the span with the signal power decreasing exponentially between the amplifiers before being restored to the initial power by the amplifier. The starting point for the mathematical analysis is the GNLSE re-written as

$$i\frac{\partial u}{\partial z} + \frac{1}{2}\frac{\partial^2 u}{\partial \tau^2} + |u|^2 u = -i\Gamma u \tag{2.49}$$

using the normalisation of 2.41 and where

$$\Gamma = \frac{\alpha}{2} L_D \tag{2.50}$$

is the normalised loss.

In order to compensate for the loss of the preceding fibre span, the fields u_1 and u_2 before and after the m^{th} amplifier must be related by

$$u_2(mz_a) = G^{1/2} u_1(mz_a) \tag{2.51}$$

where $z_a = L_a/L_D$ is the amplifier span, L_a, normalised to the dispersion length L_D and $G = e^{2\Gamma z_a}$ is the power amplification required to compensate for the loss in the preceding fibre span. Using the transformation $u(z,\tau) = \Lambda(z)R(z,\tau)$ in Equation 2.49 gives

$$i\frac{\partial R}{\partial z} + \frac{1}{2}\frac{\partial^2 R}{\partial \tau^2} + \Lambda^2(z)|R|^2 R = 0 \tag{2.52}$$

where

$$\Lambda(z) = \Lambda(0)e^{-\Gamma(z-mz_a)} \tag{2.53}$$

gives an exponentially decreasing nonlinear coefficient in the NLSE (c.f. Equation 2.40). If the amplifier span is short compared to the soliton period then the variations in $\Lambda(z)$ between amplifiers are rapid on the scale of the dispersion distance and $\Lambda(z)$ can be approximated by an average value [37]. Taking the average of $\Lambda(z)$ over one amplifier span and normalising, i.e. setting

$$< \Lambda^2(z) >= \frac{1}{z_a}\int_0^{z_a} \Lambda^2(z)dz = 1, \tag{2.54}$$

gives

$$\Lambda^2(0) = \Lambda_0^2 = \frac{2\Gamma z_a}{1 - e^{-2\Gamma z_a}} = \frac{GlnG}{G-1}. \tag{2.55}$$

Λ_0 is then the peak amplitude of the so-called *average* or *guiding centre* soliton given by $R(z,\tau)$ which is the soliton solution of the averaged NLSE, Equation 2.52 [36, 37, 38]. The peak power of the average soliton is then given by

$$P_0 = \Lambda_0^2 \frac{|\beta_2|}{\gamma \tau_0^2} \tag{2.56}$$

which is a factor Λ_0^2 higher than the peak power for a fundamental lossless soliton. By analogy with the equation for the peak power of higher order solitons, Λ_0^2 is often written as N^2 but for an average soliton N is not necessarily an integer as is the case for lossless higher order solitons. As an example consider a 40km span of fibre with a loss of 0.2dB/km. α is then $0.046km^{-1}$ and so G = exp(0.046 x 40) = 6.3. This gives $\Lambda_0^2 \sim 1.8$ and so the power of the average soliton is, in this case, 1.8 times that of the fundamental soliton.

Average solitons can propagate along real systems, which have distributed loss and periodic amplification, with little distortion provided that the amplification period is much shorter than the soliton period, the input amplitude is set correctly and the amplifiers compensate exactly for the total loss of the preceding span (this total loss comprising the

fibre loss and losses due to other components).

In physical terms, average solitons can be understood by referring to Figure 2.5, which shows the intensities of an average soliton propagating in a fibre with a loss of 0.2dB/km (solid line) and a fundamental soliton propagating in a lossless fibre (dashed line). The

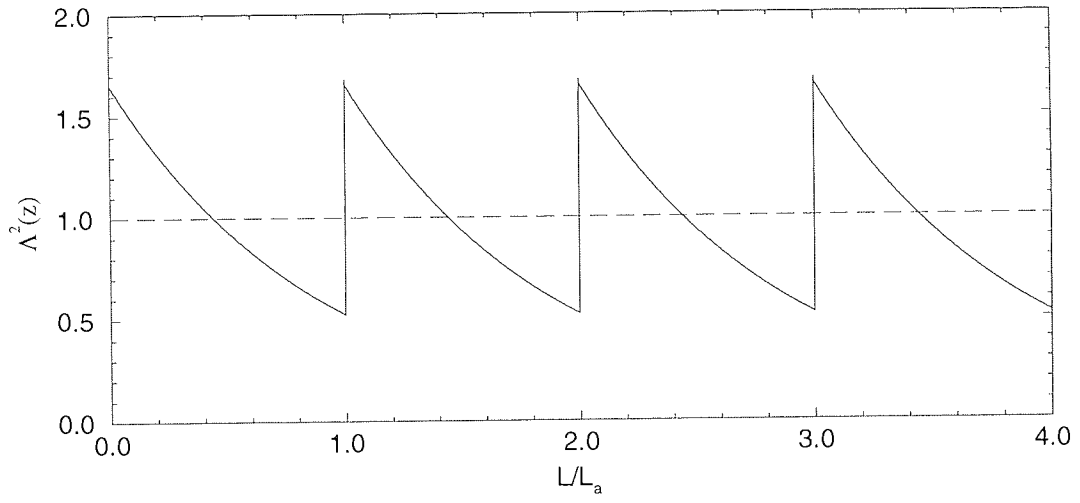

Figure 2.5: Variation of the soliton energy with propagation distance over 4 amplifier spans. Due to loss in the fibre the energy decreases exponentially before being restored at each amplifier. The average energy is equal to 1 which is the energy of a fundamental soliton in a lossless fibre.

amplifier spacing is set to 25km giving a total loss of 5dB per amplifier span and propagation distance is normalised to the amplifier span. In the lossless case Γ is set to zero in Equations 2.55 and 2.49 giving an initial intensity of 1 which is unchanged on propagation i.e. the fundamental (N=1) lossless soliton result is recovered. However when loss is included, there is an exponential decay of the average soliton intensity as the pulse propagates along the fibre before the intensity is restored to the initial value by amplification. Equation 2.53 shows that the higher the fibre loss is, the faster is this rate of decay while Equation 2.55 shows that the higher the fibre loss or the amplifier span then the higher the average soliton input amplitude must be.

Considering the first amplifier span shown in Figure 2.5, the initial average soliton intensity is in excess of the N=1 lossless soliton intensity and in the initial part of the propagation the SPM chirp dominates over the GVD chirp. However as the average soliton intensity falls so does the SPM until a point is reached where the intensity is equal to that of the lossless soliton and SPM and GVD are matched. With a further increase in the propagation distance the GVD chirp is greater than the SPM chirp. In order to launch a stable average soliton the excess SPM chirp from the initial, high intensity part of the propagation must be balanced by that from the excess GVD chirp from the final

part of the propagation. This is equivalent to matching the areas above and below the $\Lambda^2(z) = 1$ line in Figure 2.5.

Although loss is the most significant perturbation, there are other periodic effects, such as manufacturing defects, which can affect the soliton propagation. Similarly to the average soliton, the period of such perturbations must be smaller than the soliton period if they are to be neglected.

2.6 Birefringence and Cross Phase Modulation

A second important assumption which has been made thus far is that the optical fibre is homogeneous and so has no polarisation dependence. However, in reality the fibre fabrication process introduces imperfections to the cylindrical geometry of the fibre which causes a local birefringence. This birefringence leads to two orthogonal polarisation modes of the fibre which will have slightly different refractive indices. The random nature of the birefringence causes mixing of the two polarisation modes so that linearly polarised light which is launched into the fibre will develop an arbitrary polarisation on propagation. This can be a problem because a difference between the refractive indices of the two polarisation modes will lead to different different group velocities, thus causing a polarisation dependent dispersion known as polarisation mode dispersion (PMD) which can lead to the splitting of a randomly polarised input pulse into two orthogonally polarised parts [39]. Although modern fibre manufacturing processes allow fibre to be made with low PMD values, older systems may suffer from high enough PMD to cause serious problems when upgrading NRZ systems to higher data rates [40, 41, 42]. It can also be a problem in polarisation division multiplexed experiments which try to double the capacity by using orthogonal polarisation states to carry different data channels [8, 43].

In addition to the dispersive effect of PMD, data can also be corrupted through a nonlinear effect known as cross-phase modulation (XPM). XPM is an interaction between two or more waves which co-propagate along a fibre and originates from the fact that the effective refractive index of a wave propagating in a fibre depends not only on its own intensity (which leads to SPM) but also on the intensities of other co-propagating waves. XPM is therefore especially important in WDM systems where there can be several channels, all assigned to a different wavelength, propagating in a single fibre but there can also be an effect in single channel systems as two waves with the same frequency but different polarisation states also interact.

The case of XPM between two different signal frequencies will be considered first. To determine the effect of the XPM in the case of two waves with different frequencies, the input field of Equation 2.2 is replaced by

$$\mathbf{E}(\mathbf{r},t) = \frac{1}{2}\hat{x}[E_1 exp(-i\omega_1 t) + E_2 exp(-i\omega_2 t)] + c.c. \tag{2.57}$$

where ω_1 and ω_2 are the central frequencies of the two pulses. Following a similar derivation to that for a single wave leads to a change in refractive index given by

$$\Delta n_j \simeq n_2(|E_j|^2 + 2|E_{3-j}|^2) \tag{2.58}$$

where j=1,2 for the two pulses and it is assumed that $n_1 \simeq n_2$ [6] pp175.

This equation shows that the refractive index of the optical wave depends on both the intensity of the wave itself and on the intensity of the co-propagating wave. This refractive index change leads to a nonlinear phase shift as the signal propagates along the fibre, given by

$$\phi_j^{NL} = \frac{\omega_j z}{c}\Delta n_j = \frac{\omega_j z n_2}{c}\left[|E_j|^2 + 2|E_{3-j}|^2\right]. \tag{2.59}$$

The first term is responsible for SPM (c.f. Equation 2.35) whilst the second represents the phase change of one wave due to the other and is responsible for XPM. It is immediately obvious that for waves of the same intensity the XPM term is twice that of the SPM term.

For two waves which have the same frequency but different polarisations the XPM process can be studied by using an elliptically polarised input wave given by

$$\mathbf{E}(\mathbf{r},t) = \frac{1}{2}(\hat{x}E_x + \hat{y}E_y)exp(-i\omega_0 t) + c.c. \tag{2.60}$$

where E_x and E_y are the complex amplitudes of the two orthogonal polarisation states and ω_0 is the central frequency. The effect on one of the polarisation states due to the presence of the other is again a change in the refractive index [6] pp178 and the nonlinear birefringence is given by

$$\Delta n_x = n_2\left(|E_x|^2 + \frac{2}{3}|E_y|^2\right) \tag{2.61}$$

$$\Delta n_y = n_2\left(|E_y|^2 + \frac{2}{3}|E_x|^2\right). \tag{2.62}$$

This is qualitatively the same as the XPM effect between two waves of different frequencies but quantitatively the effect is weaker due to the 1/3 term.

The effect of this nonlinear birefringence is to change the state of polarisation of the input elliptically polarised light. A consequence of this polarisation variation is a nonlinear polarisation rotation (NPR) which causes a larger self-induced change in the polarisation of the high intensity pulse peak than in the low intensity wings of the pulse [44]. NPR can lead to pulse shaping through a saturable absorption mechanism if a polarising element is used to discriminate between polarisation states. This effect has been used to passively mode lock lasers [45] and is discussed in Chapter 5 in relation to a pulse propagation experiment.

As XPM only affects co-propagating signals it has a limited effect on pulse propagation due to the group velocity mismatch between waves of different central frequencies and of different polarisation states – as the two pulses propagate along the fibre at different speeds they will walk-off, with one pulse passing through the other which restricts the interaction length.

The previous soliton evolution equations assumed that the launched pulses were linearly polarised into an isotropic fibre. In reality, even weak birefringence can lead to polarisation instability which can affect the propagation [6] pp190 but for the ~10ps solitons used in high bit rate experiments, there is little effect because the soliton power is below the threshold power for polarisation instability. In strongly birefringent fibre but where the birefringence is below $\sim 0.3D_2$, the lower intensity polarisation component of an elliptically polarised input pulse is "trapped" by the higher intensity component and so the pulse splitting expected for a linear pulse is avoided but at the expense of a timing jitter [6] pp192, [46]. This resilience of solitons to the effect of PMD may be of use when upgrading existing fibre links which are more likely to be hampered by high PMD than newly installed systems. At higher birefringences ($> 0.3D_2$), the nonlinear effects can no longer balance the dispersion and pulse splitting occurs as for linear pulses.

2.7 Soliton system design considerations

In designing a soliton transmission system there are several effects which must be taken into consideration. The design of the system depends not only on the system length but also on the data rate and amplifier span which are required and as shall be seen below, there must be compromises made in the system design brought about by the requirements of low timing jitter on arrival at the detector, high signal to noise ratio and an acceptable average power. Of particular interest in the context of this thesis is the case of long-haul

systems of trans-oceanic distances (~10 000km) with Gbit/s data rates and such systems are emphasised here but without loss of generality to all systems.

2.7.1 Gordon-Haus Jitter

One of the most serious problems which must be overcome if long-haul soliton transmission systems are to become viable is a consequence of the amplification of the signal along the transmission line. Amplifiers must be included in order to compensate for the loss of the optical fibre and any other components which are included in the system. In all optical systems EDFAs are used to provide this amplification but like all amplifiers they introduce some noise into the system as well as amplifying the signal. In a linear system this noise is undesirable as it degrades the signal to noise ration (SNR) but in a nonlinear soliton system the effect is more drastic and the ability of the soliton to re-adjust to accommodate small changes leads to a random timing jitter, known as Gordon-Haus jitter, as the solitons propagate [47].

Noise which originates from the spontaneous emission of the EDFA, known as amplified spontaneous emission noise (ASE), leads to a small change in the soliton parameters as a soliton passes through an EDFA. The most serious perturbation is that to the soliton frequency. The soliton will absorb the random noise spectrum of the EDFA whilst maintaining a soliton nature, leading to a random frequency shift at each amplification stage. Whilst the interaction between the soliton and the noise is small, the combined effect of many amplifiers can lead to a significant frequency shift by the end of the system. Through the effect of GVD, which causes different frequencies to travel at different speeds along the fibre, this random frequency shift is translated into a random timing shift of the soliton from the centre of the allotted timing slot in the data stream. It is this random time shift which is known as Gordon-Haus jitter.

After a single amplifier span of length L_a, the change of the group delay caused by a frequency change of $\Delta\omega$ is given by $\Delta t_g = \beta_2 L_a \Delta\omega$. By considering an ensemble of pulses, taking the variance of the group delay (to take account of the random nature of the frequency shift) and assuming that the time delay due to each amplifier is independent of the time delays introduced by all the other amplifiers, the total variance is given by [48]

$$\left\langle t_N^2 \right\rangle = \frac{2\pi n_2 N_{sp} |\beta_2| hc(G-1)L^3}{9\tau_0 \lambda^2 A_{eff} L_a \Lambda_0^2} \tag{2.63}$$

where N_{sp} is the spontaneous emission noise factor of the amplifier, h is Planck's con-

stant, c is the speed of light, G is the amplifier gain, Λ_0 is the average soliton amplitude enhancement factor defined by Equation 2.55 and $L = NL_a$ is the system length. The r.m.s. jitter after N amplifiers is then taken as the root of $\langle t_N^2 \rangle$ showing that Gordon-Haus jitter has a larger effect on long-haul systems than short haul, due to the L^3 term which puts a limit on the maximum distance which can be achieved in a soliton system.

In order to determine this limit an acceptance window must firstly be defined for the detector at the end of the system – if the soliton arrives outside this time window then an error will be recorder at the detector. In order to achieve an acceptable bit-error ratio (BER) of 10^{-9} or less then requires

$$\left\langle t_N^2 \right\rangle \leq \left(\frac{t_w}{6.1} \right)^2, \tag{2.64}$$

where $2t_w$ is the temporal width of the time window and Gaussian statistics are assumed [49, 48].

Substituting from Equation 2.63 and using physical parameters, the maximum propagation distance can then be determined using

$$L_{max}^3 = 0.1372 \frac{\tau_{fwhm} t_w^2 A_{eff} L_a \Lambda_0^2}{N_{SP} n_2 D_2 h (G-1)}. \tag{2.65}$$

Although this equation does not have an explicit term dependent on the data rate of a system, both the pulse width τ_{fwhm} and the width of the timing window of the detector t_w are dependent to the data rate, R. Introducing $\kappa_F = R\tau_{fwhm}$, which is the inverse of the mark to space ratio (the ratio of the space between the centre of adjacent timing slots in the data stream to the data pulse width) and $\kappa_w = Rt_w$, which determines the fraction of the bit period to which the detector time window is set, and writing G explicitly as $G = exp(\alpha L_a)$ where α is the effective loss coefficient, which takes into account fibre loss and any additional losses, the maximum possible system length is then given by

$$L_{max} = \frac{0.5158}{R} \left[\frac{\kappa_F \kappa_w^2 A_{eff} L_a \Lambda_0^2}{N_{SP} n_2 D_2 h (exp(\alpha L_a) - 1)} \right]^{1/3}. \tag{2.66}$$

This equation shows that the maximum system length is inversely proportional to the data rate. The dependence on the amplifier span is more complicated as L_a appears on both the numerator (explicitly and also in Λ_0^2) and the denominator. The dispersion D_2 can be reduced to increase L_{max} by changing the operating wavelength, using dispersion shifted fibre or dispersion management (see Section 2.8). However reducing the dispersion

also reduces the peak power of the solitons according to Equation 2.46, which reduces the signal to noise ratio of the system. When working at low dispersion higher order dispersive effects also become important. Figure 2.6 shows the effect on $L_{max}R$, which is

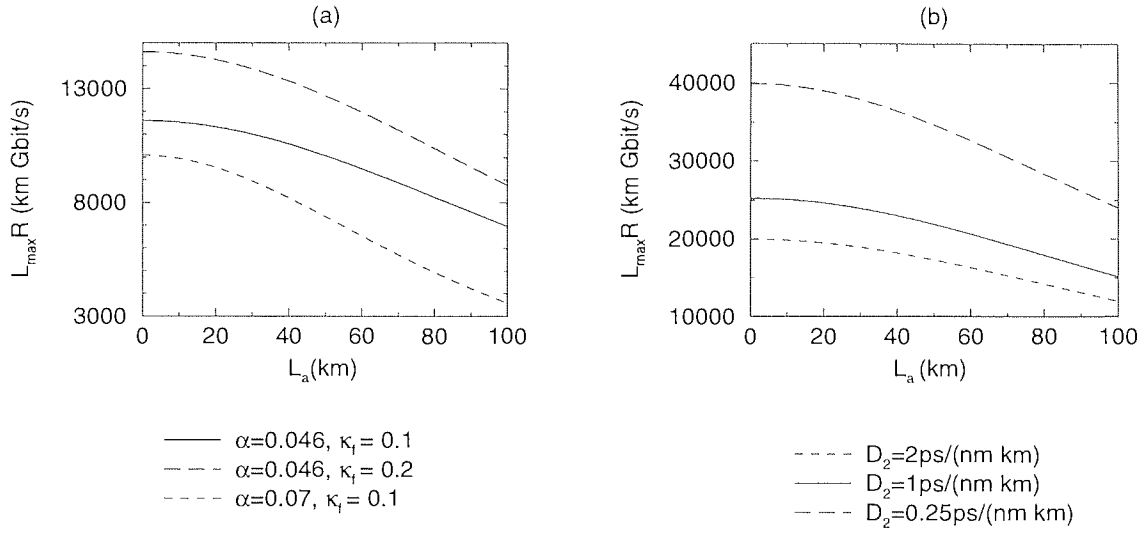

Figure 2.6: Variation of the product L_{max}R as L_a is changed for: (a) SIF systems with 0.2dB/km loss and 1:10 mark to space ratio (solid line), 0.3dB/km loss and 1:10 mark to space ratio (dotted lone) and 0.2dB/km loss and 1:5 mark to space ratio (dashed line); (b) DSF systems with dispersions of 2ps/(nm km) (dotted line), 1ps/(nm km) (solid line) and 0.25ps/(nm km) (dashed line

the product of the bit rate (in Gbit/s) and the maximum propagation distance (in km), as the amplifier span is varied, for SIF systems and DCF systems. In Figure 2.6 (a) three standard fibre systems are shown with $A_{eff} = 70\mu m^2$, $\kappa_w = 1/3$ (detector time window = 1/3 bit interval), $N_{SP} = 1.5$, $n_2 = 1.5$ x $10^{-20}m^2W^{-1}$ and $D_2 = 17$ ps/(nm km). The solid line is for a system with a mark to space ratio of 1:10 ($\kappa_F = 0.1$) and with a loss of 0.2dB/km ($\alpha = 0.046$). The dotted line is for the same system but with the loss increased to 0.3dB/km ($\alpha = 0.07$) and as expected the Gordon-Haus limit is reduced by including more loss. The dashed line is for a system with 0.2dB/km but with a mark to space ratio of 1:5 ($\kappa_F = 0.2$) which shows that by increasing the pulse width the Gordon-Haus limit can be increased. Figure 2.6 (b) shows curves for three different dispersion shifted fibre systems with $A_{eff} = 50\mu m^2$, $\kappa_w = 1/3$, $N_{SP} = 1.5$ and $n_2 = 2.5$ x $10^{-20}m^2W^{-1}$. In this diagram the dotted line is for $D_2 = 2$ ps/(nm km), the solid line is for $D_2 = 1$ ps/(nm km) and the dashed line is for $D_2 = 0.25$ ps/(nm km). The mark to space ratio was kept fixed at 1:10 ($\kappa_F = 0.1$) and α was 0.046, corresponding to a loss of 0.2dB/km, throughout. These calculations show clearly that if the dispersion is decreased the Gordon-Haus limit increases dramatically. Considering a 10Gbit/s system with a 1:10 mark to space ratio, a loss of 0.2dB/km and an amplifier span of 40km shows that with standard fibre which

has $D_2 \sim 16.5$ps/(nm km),the Gordon-Haus limit is 1000km (solid line in Figure 2.6 (a)). If dispersion shifted fibre with $D_2 = 1$ ps/(nm km) is used the limit more than doubles to 2300km and with a further reduction in the dispersion to 0.25 ps/(nm km) (which can be achieved using dispersion management as discussed in Section 2.8) a system length of 3600km is possible. In order to allow propagation over the trans pacific distance of 10 000km the dispersion must be kept low and the data rate must be reduced below 5Gbit/s to allow a realistic amplifier span of $>$ 30km to be used.

Since the Gordon-Haus effect puts such a serious constraint on system design several jitter reduction methods, known collectively as soliton control, have been proposed and demonstrated. One scheme involves the inclusion of optical bandpass filters in the transmission line [50, 51] or using an amplifier with frequency dependent gain [52, 53] to control the soliton frequency although the latter is more applicable to the sub-picosecond regime-where a soliton self frequency shift can occur through the Raman effect [54, 55]. When filters are included in the transmission line the mean square jitter given by Equation 2.63 is reduced by the factor $f(4\delta Z)$, where δ is the excess gain required to compensate for the additional loss of the filter and where

$$f(x) = \frac{3}{2x^3}\left[2x - 3 + 4exp(-x) - exp(-2x)\right]. \tag{2.67}$$

This shows that for x$\gg$1 $f(x) \sim 3x^{-2}$ and hence at large propagation distances $\langle t_N^2 \rangle$ is proportional to L as opposed to L^3 in the unfiltered case. This leads to an increase of the Gordon-Haus limit when filters are used and system length or data rate can be increased.

Physically, the bandwidth of the individual filters is large compared to the soliton bandwidth (typically 5-10 times) and the soliton is largely unaffected by the filtering since the filtered spectral wings can be recovered between filters due to the nonlinear nature of the pulse. The linear bandwidth of the cascaded filters is however, much narrower than the soliton bandwidth and the noise is largely filtered out. As there is less noise incorporated into the soliton spectrum the resultant frequency shift reaches a steady level and the timing jitter increases only linearly thereafter. Using this technique propagation over 15 000km has been demonstrated at 5Gbit/s [56] in a recirculating loop experiment with a 25km amplifier spacing. The soliton guiding filter used in this experiment was a bulk air gap Fabry-Perot device and was included every 80km round trip of the three span loop. This is far in excess of the 10 000km Gordon-Haus limit for the unfiltered case and shows that a transoceanic 5Gbit/s soliton system is feasible.

One problem which is introduced by the inclusion of filters is that the loss of the system is increased through both the insertion loss of the filter and the loss due to the filtering effect. These losses must be compensated for by increasing the the amplifier gain. This additional gain increases the Gordon-Haus jitter (see Equation 2.63 and Figure 2.6 (a)) and effectively limits the strength of filter which can be used – the stronger the filter the more it will attenuate the pulses and the higher the amplifier gain must be to compensate.

The Gordon-Haus limit can be further increased using the "sliding-guiding" scheme where there is a gradual change (typically 5-20GHz/Mm) in the central frequency of the filters along the transmission line [57]–[61]. Solitons have the ability to regenerate their spectral components and they can propagate largely unperturbed by changing their central frequency as the filter central frequency changes. The linear amplifier ASE cannot follow the frequency change and as a result the soliton and the noise separate in the frequency domain. Using this technique transmission at 10s of Gbit/s rates over transoceanic distances have been achieved in several experiments [62]–[66]. As a modification to this technique the signal frequency can be changed while keeping the filter frequency fixed [67, 68].

Although there is a marked increase in system performance, the inclusion of filters in a real long haul system is an additional complication and as systems are designed to have a lifetime of at least 25 years, all elements in the system have to meet this requirement. The inclusion of bulk filters, which requires the signal to be coupled out of the fibre before being passed through the filter and re-coupled into fibre, is therefore a risk which must be carefully evaluated by the system designers. Rigid device tolerance specifications may also dissuade systems designers from including bulk filters, particularly in the harsh environment of submarine systems. Fibre Bragg grating filters offer an alternative method of performing the soliton guiding [69] and their use is investigated in Chapter 6. Implementing a sliding-guiding scheme poses further problems; a set of filters, each with a specific central frequency and bandwidth, would have to be made and put into the system in a particular order. Although it may be possible to take advantage of statistical fluctuations in the filter production process by specifying a particular central wavelength and passband characteristics to a filter manufacturer and ordering a large number of filters. The filters produced would have a spread in central wavelengths depending on how well the production process could be controlled and the filters could be characterised and put into the order required for the system. This method may give the required set of filters but it is rather haphazard and wasteful as a large number of filters would undoubtedly have to

be rejected leading to additional expense.

Other methods which have been used to increase the Gordon-Haus limit include: the use of phase sensitive or nonlinear amplifiers to amplify the signal preferentially[70]–[76]; using a saturable absorber to distinguish between the signal and noise [77]–[80] and using an in-line amplitude modulator operating in synchronisation with the bit rate [81]–[84] to re-time the solitons so that they remain in their timing slots. Using the latter method soliton propagation has been achieved at 10Gbit/s over an effectively limitless distance [81] but it requires active control and so is undesirable for use in a real system where entirely passive effects are desirable. The inclusion of a single phase modulator at the mid-point of a 5Gbit/s, 9000km propagation simulation has also shown a reduction in Gordon-Haus jitter comparable to that achieved by spectrally filtering at each amplifier [85].

Recent years have seen a great deal of interest in the use of dispersion management [86]–[98], where more than one type of fibre is used in the transmission line, to control solitons. This has an associated reduction in the Gordon-Haus limit and this is discussed in Section 2.8.

2.7.2 Electrostriction

Electrostriction provides another source of timing jitter in soliton systems [99, 100, 101]. As the solitons propagate along the fibre they excite acoustic shock waves which travel transverse to the fibre axis resulting in a self-frequency shift of the soliton [99] and also an interaction with the following solitons [101] as the acoustic wave is partially reflected from the outer cladding with a round trip time of $\sim$ 20ns for fibre with an outer diameter of $125\mu m$. While the self frequency shift causes a uniform shift for all the pulses the interaction between pulses in a data stream causes a random timing jitter which is proportional to the square of the propagation distance but can be reduced to linear by the use of filters [102]. The strength of the acoustic interaction is proportional to the square of the dispersion and hence this effect can be reduced by using a low dispersion but can be significant in standard fibre systems where the average dispersion is high [103].

2.7.3 Soliton-soliton interactions

In addition to the interaction due to electrostriction there is another interaction force which exists between solitons[104, 105]. This interaction is nonlinear in origin and the

qualitative effect depends on the relative phases and amplitudes of the interacting solitons while the strength of the interaction depends on the temporal separation of the solitons. The result on the design of a soliton system is that this interaction restricts the maximum possible system length or alternatively restricts the mark to space ratio and hence the data rate which can be used in a system of a given length. The initial chirp of the solitons[106], higher order dispersion[107], and higher order nonlinear effects [105, 108] can also affect the soliton interactions but for simplicity these effects are neglected here.

A soliton pair launched into a transmission fibre can be described by the equation

$$u(0,\tau) = sech(\tau - \frac{T_R/2}{\tau_0}) + rsech\left(r(\tau + \frac{T_R/2}{\tau_0})\right)e^{i\theta}, \tag{2.68}$$

where $T_R = 1/R$ is the initial separation (R is the data rate), r is the relative amplitude and θ is the relative phase of the two input pulses. The soliton interaction can then be studied by using this as the input pulse in Equation 2.40 and solving numerically but the inverse scattering method and perturbation theory give insight into the nature of the interaction [6] pp132.

In the case of in-phase solitons ($\theta = 0$) which have equal amplitude ($r = 1$) and have an initial separation which is large compared to the pulse width ($T_R \gg 2\tau_0$), the soliton interaction is attractive and the solitons undergo a periodic collapse and separation with a period

$$Z_p = Z_0 exp\left(\frac{T_R/2}{\tau_0}\right) = Z_0 exp\left(\frac{1}{2R\tau_0}\right). \tag{2.69}$$

In the lossless case the first collapse occurs at the midpoint of this period and so in order to avoid problems associated with the soliton collapse, the system length must be less than $Z_p/2$. Alternatively, the mark to space ratio can be set so that the collapse length is greater than the system length. As an example consider the collapse length for a 10GHz systems with mark to space ratios of 1:10 (which is achieved by using a pulse width of 10ps) and 1:5 (which is achieved by using a pulse width of 20ps). For dispersion shifted fibre with a dispersion of 1ps/(nm km) and using a mark to space ratio of 1:10, the collapse length is ~140 000km, which is much longer than any global system but is reduced to ~7000km (which is less than the length of a trans-oceanic system) for a mark to space ratio of 1:5. In standard fibre the collapse lengths are reduced to ~ 8800km and ~ 400km due to the higher dispersion of the fibre. This strong dependence of the collapse length on the mark to space ratio, which is a manifestation of the exponential dependence of Z_p on the initial soliton separation, indicates that the soliton interaction is strongly

dependent on the overlap of the fields of the solitons and leads to the soliton collapse and subsequent separation being a rapid process, with the onset of the collapse occuring over a short distance, as the numerical simulation in Figure 2.7 shows. This simulation was done for a lossless 10Gbit/s system with 20ps pulses (mark to space ratio =1:5) and a dispersion of 1ps/(nm km). As stated above the collapse took place at ~7000km. In this simulation a 10% change in the position of the soliton (in the time domain) took 60% of the collapse length. If the mark to space ratio was increased to 1:10 a 10% change in the position of the solitons tails ~ 80 % of the collapse length.

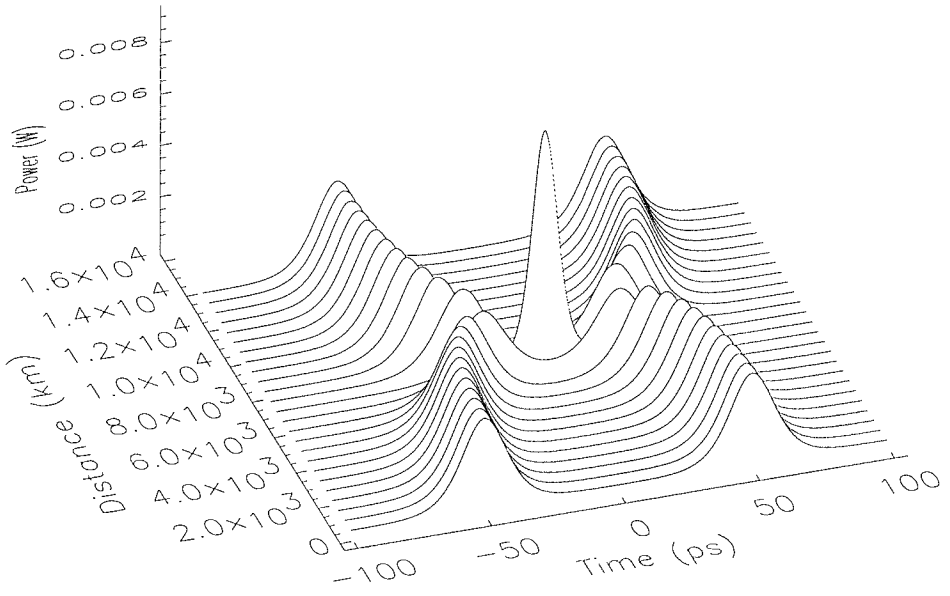

Figure 2.7: Numerical simulation of a soliton interaction for 20ps pulses at 10Gbit/s in lossless fibre with a dispersion of 1ps/(nm km). The solitons are in phase and of equal amplitudes leading to collapse after 7000km

For a given mark to space ratio the collapse length is proportional to the soliton period. Referring to Equation 2.48 shows that this means that the collapse length is proportional to the square of the pulse width and inversely proportional to the dispersion. Thus, as was the case for the Gordon-Haus effect, low dispersion of the system is desirable. The fact that the collapse length is proportional to the soliton period which is itself inversely proportional to the soliton peak power is an consequence of the soliton-soliton interaction being nonlinear in origin.

When the pulses are initially out of phase ($\theta \neq 0$) the interaction becomes repulsive

even for small values of θ and the solitons separate [6] pp132. This can also be disastrous for a soliton system as the pulses can move from their timing slots into those of their neighbours. Whilst it is true that in a real system there may be some cancellation of the interaction forces as there will be a data stream and not simply a pair of pulses as in the above investigation, there will not however be a complete cancellation since there will be empty bit slots in the data stream representing zeros leading to uneven forces on some of the solitons. When $\theta = \pi/2$ there is no interaction between the solitons but this point is unstable and so cannot be used in real systems.

So far only solitons of the same amplitude have been considered. In the case where adjacent solitons have the same phase but unequal amplitudes the problem of soliton interactions is greatly reduced [109, 110, 111] as the intensity difference leads to a difference in the phase evolution rates for the two pulses and so the attractive and repulsive forces are largely cancelled and although there is still a periodic interaction it does not lead to a collapse of the solitons. This is clearly a simple method of avoiding problems associated with soliton interactions and is not restricted to the ideal lossless case studied above [106] and it has been used in soliton propagation experiments at 20Gbit/s over 11500km [110] (collapse length with equal amplitudes $\sim$16 000km) and over 500km at 80Gbit/s [111](collapse length $\sim$ 770km).

In the case of WDM systems where solitons in different channels have different frequencies the process is more complicated as the different channels will travel along the fibre at different speeds due to GVD. This leads to a periodic interaction as the pulses of different channels pass through each other. After such a collision, pulses from different channels emerge intact but there is a modification to the relative temporal positions of the pulses due to a temporary change in the refractive index[49, 112]. As only single channel propagation is considered here, interactions between solitons of different frequencies will not be studied.

2.7.4 Signal to noise ratio requirements

For error free operation of an optical system, a high signal to noise ratio (SNR) must be maintained along the system length and at the receiver. The SNR is a measure of the mean-square current due to the signal divided by the mean-square current due to the

noise detected at the receiver, i.e.

$$SNR = \frac{< i_{sig}^2 >}{< i_{noise}^2 >} \tag{2.70}$$

where i_{sig} and i_{noise} are the detector currents due to the signal and noise. There are several sources of noise which can contribute to the degradation of the SNR in an optically amplified system, including Shot noise and thermal noise of the detector but the most dominant noise source is due to beating of the signal and ASE frequencies [113]. The value of the SNR due to this effect is given by

$$SNR = \frac{(eS_0/(h\nu))^2}{(2e/(h\nu))^2 S_0 N_a F_0} = \frac{S_0}{4N_a F_0} \tag{2.71}$$

where S_0 is the signal power out of the amplifiers, h is Planck's constant, ν is the signal frequency, e is the electronic charge, N_a is the number of amplifiers and F_0 is the ASE noise power of the amplifier within a bandwidth, B. F_0 is given by

$$F_0 = (G-1)\mu h\nu B \tag{2.72}$$

where μ is the inversion factor of the amplifiers ($\mu = 1$ for a perfect amplifier) and G is the amplifier gain. Substituting this into Equation 2.71 gives

$$SNR = \frac{S_0}{4N_a(G-1)\mu h\nu B}. \tag{2.73}$$

This shows that the SNR increases as G decreases i.e. a small amplifier spacing is better despite the fact that decreasing the amplifier span means increasing N_a, the number of amplifiers – the exponential variation of amplifier gain with propagation distance overshadows the increase in N_a. An obvious dependence of the SNR is that it is proportional to the signal power S_0, however in a soliton system, the power cannot simply be increased as it can when using linear pulse formats because the peak pulse power is determined by the soliton width through Equation 2.46 (the SNR can however be increased by using narrower pulses). The soliton power is also proportional to the fibre dispersion and so the SNR requirement puts a limit on how low a fibre dispersion can be used. In practice a SNR of 23dB gives a BER less than 10^{-9} within a bandwidth, B, equal to half the data rate of the system.

2.7.5 Average power limit

Whereas the SNR requires a high power level, there are reasons for keeping the signal power low. Firstly, low signal power means low output power from the laser pulse sources. Semiconductor lasers are now used universally in telecommunications systems and at high output powers these devices become more unreliable and device lifetime is reduced. This is one reason that there has been prejudice against soliton systems – it is assumed that because solitons are nonlinear pulses, they must have a much higher power than linear NRZ pulses. To investigate whether this is the case it is first necessary to derive an expression for the average power for a soliton pulse stream. This can be done by integrating the power over a single bit period, T_R, and multiplying by the data rate R (= $1/T_R$). Hence

$$P_{av} = R\int_{-T_R/2}^{T_R/2} P_0 sech^2(t/\tau_0)dt = \left[P_0\tau_0 R tanh\frac{t}{\tau_0}\right]_{t=-T_R/2}^{t=T_R/2} \simeq 2P_0\tau_0 R, \tag{2.74}$$

since $tanh \pm \frac{T_R/2}{\tau_0} \sim 1$ for $\frac{T_R/2}{\tau_0} > 1$ as is the case in soliton systems. When data is imposed on the pulse stream this average power is divided by 2 assuming the data stream contains half ones and half zeros on average. Substituting from Equations 2.42 and 2.30 then gives the average power of a soliton system to be

$$P_{av(sol)} = \frac{N^2\lambda^2 D_2 R}{2\pi c\gamma\tau_0}. \tag{2.75}$$

This shows that for a fixed mark to space ratio, the average power scales as the dispersion and is proportional to the square of the data rate – not linear as it seems at first glance since for a fixed mark to space ratio the pulse width is inversely proportional to the data rate. A bonus of the high (typically $\geq$ 1:6) mark to space ratio of a soliton system is that despite the high peak power, the average power is reduced. In NRZ systems, the mark to space ratio is essentially 1:1 and so the average power is simply half the peak power for a data stream containing half ones and half zeros.

The minimum acceptable average power for an NRZ system is determined by the required SNR and can be evaluated from Equation 2.73. For a data stream with half ones and half zeros the minimum average power is given by

$$P_{av(NRZ)} = 2(SNR)\mu h\nu B(G-1)\frac{L}{L_a}, \tag{2.76}$$

where L is the system length given by $L = N_a L_a$. Thus, the minimum average power for an NRZ system is proportional to the system length and is also proportional to the data rate (through the dependence on B) assuming that the energy per unit time is constant. Unlike the case for the solitons, the average power is independent of the fibre dispersion. It should be pointed out that this minimum acceptable average power constraint must also be met by soliton systems in addition to the soliton average power constraint derived above.

The average power constraints of the two data formats can now be compared. For both the soliton and the NRZ cases, the average power is dependent on the amplifier spacing (for the soliton case this dependence is through the N^2 term which is given by Equation 2.42) while for the NRZ case there is an explicit term in L_a and also a dependence of the gain G on L_a) and so the average powers can be compared graphically for a range of amplifier spans.

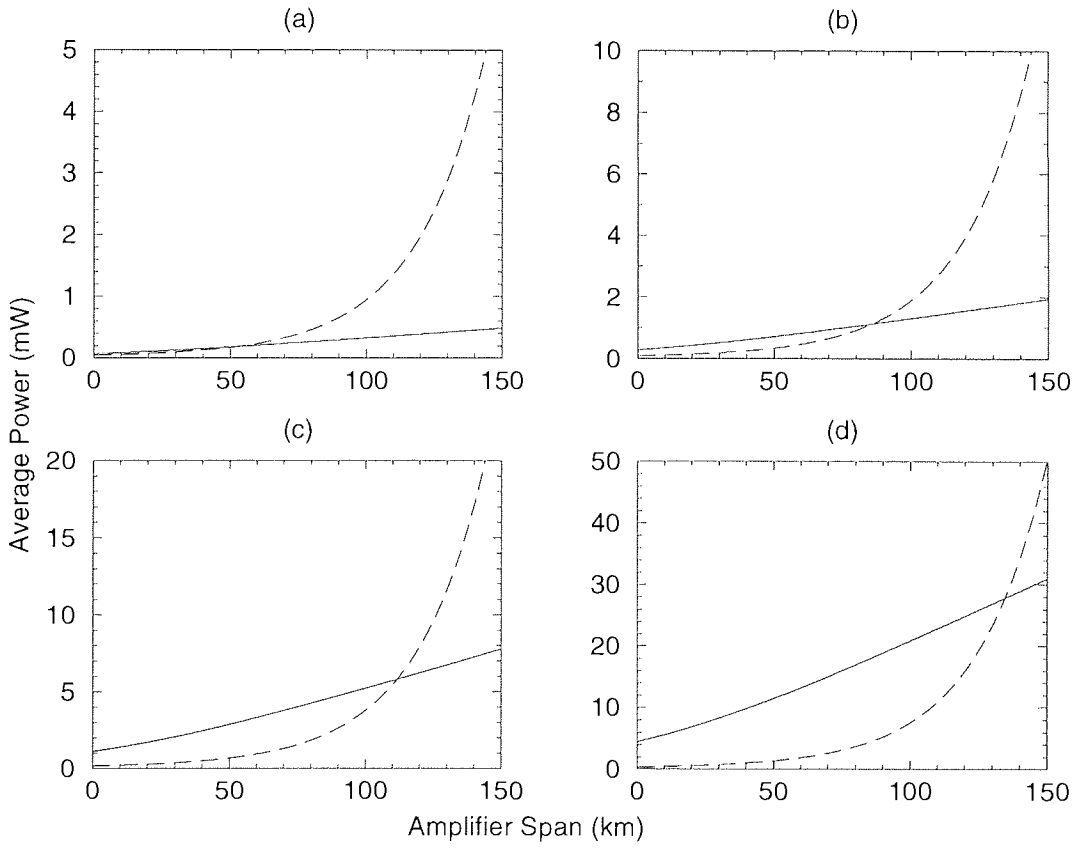

Figure 2.8: Average power constraints for soliton and NRZ systems with varying amplifier spans. The system length was 10 000km and the data rates were (a) 2.5Gbit/s, (b) 5Gbit/s, (c) 10Gbit/s and (d) 20Gbit/s. The solid line is the soliton power constraint and the dashed line is the SNR power constraint.

Figure 2.8 gives such a comparison for a 10 000km fibre length which corresponds to a trans-oceanic system. The four graphs correspond to data rates of (a) 2.5Gbit/s

(b) 5Gbit/s, (c) 10Gbit/s, (d) 20Gbit/s, where the curves have been calculated using Equations 2.75 and 2.76, with the solid line being the average soliton power constraint and the dashed line being the SNR constraint. In the soliton case the mark to space ratio was set to 1:10, the dispersion was 1ps/(nm km) and γ was taken to be $2W^{-1}km^{-1}$. For the NRZ case μ was 1.5, B was half the data rate and the SNR ratio was 23dB. In both cases the loss was 0.2dB/km. These graphs show that at low data rates and short amplifier spans there was very little difference between the average powers of soliton and NRZ systems. However as the data rate was increased the difference between the two also increased and for a data rate of 10Gbit/s with a 40km amplifier span the soliton average power was ~2mW which was ~5 times higher than that for the NRZ system. The significance of the intersection of the two curves is that at longer amplifier spans than this value the average power of the soliton system was too low to give the required SNR and so soliton systems were not feasible. Thus at 10Gbit/s soliton systems cannot operate with an amplifier span greater than 110km and at 2.5Gbit/s the maximum amplifier span is reduced to ~50km.

Another constraint which must be taken into consideration is that the average power must be kept below the maximum safe power which is currently set at 50mW in the U.K. Whilst this is still far below the average soliton power required for 10Gbit/s in DSF it is an important consideration when upgrading standard fibre systems which have high dispersion and so require high power for solitons.

2.7.6 Soliton system design

In designing a possible soliton system the main considerations are the required system length and the operating data rate. System parameters such as pulse width, dispersion and amplifier span must then be chosen such that error free operation of the system is possible with a built in safety margin to take account of system aging. This is a difficult process since many of the physical effects have different requirements and a balance must be found between them. For example, Gordon-Haus jitter and the average soliton constraint require a large pulse width whilst the SNR and soliton-soliton interaction requirements need a short pulse width.

In addition to the physical effects there is one further very important constraint – system cost. As telecommunications systems are commercial ventures, the cost of development and deployment of the system must be carefully controlled. One implication of this is that the number of amplifier stages (which are expensive) must be kept low and

so a long amplifier span is desirable. In order to find a compromise between all the requirements it is useful to construct a system design diagram which plots the pulse width requirement for each of the various effects versus amplifier span with the dispersion held fixed [114]. Possible windows of operation can then be determined.

2.8 Dispersion management

So far, the theory and some of the problems of soliton propagation in optical fibre have been considered and the details of the fibre itself have been assumed, with typical values for parameters such as effective core area, nonlinearity coefficient and dispersion being used in calculations. Whilst this approach causes no problem in rough calculations it does have limitations, in particular it assumes that the fibre is the same throughout the system. Increasingly this is not the case and there is currently a great deal of work being done with dispersion managed systems [12],[86]-[98],[115, 116, 117] which use a combination of different types of fibres to give the required average dispersion. This technique has uses in NRZ systems [86, 118, 119, 120] but is becoming increasingly popular in RZ systems as a means of compensating for the high dispersion of standard fibre [121, 122, 123]. Before considering this important application of dispersion management, stepwise dispersion profiling will be considered.

2.8.1 Dispersion profiling

As discussed in Section 2.5.1, the balance between SPM and GVD required for the stability of optical solitons is upset due to the effect of loss. The average soliton model takes account of this fact by ensuring that over one amplifier span SPM and GVD balance each other with SPM dominating in the initial high power section of the fibre and GVD dominating in the latter low power section of the fibre. An alternative method of keeping the soliton balanced is to reduce the dispersion of the fibre exponentially along the length of the system such that the decrease in the SPM due to the exponential power loss is matched by a decrease in GVD [76, 124, 125]. Although there has been some experimental evidence that such systems may be feasible, the careful design and manufacture of the fibres required limits the practicality of this scheme. By approximating the exponential decay of the fibre dispersion by a step wise decrease in the fibre the mismatch between SPM and GVD can be reduced leading to propagation regimes which are forbidden to uniform dispersion systems becoming accessible [126]. Using a dispersion profile with n

steps of fibre leads to an n-fold decrease in the perturbations to the solitons and data rates and/or propagation length can be increased accordingly.

2.8.2 Dispersion compensation

One of the main problems encountered in long haul soliton systems is Gordon-Haus timing jitter which is a consequence of the dispersion of the fibre and Equation 2.63 shows that the jitter is proportional to the dispersion. It has been shown that by including a dispersion compensating element, which has the opposite sign of dispersion to that of the transmission fibre, at the end of the transmission fibre the jitter can be reduced since the average dispersion is reduced [127]. Since this discovery, dispersion management on a shorter length scale has led to further improvements in soliton propagation[121, 122, 123],[128]–[134] and it has been discovered that by periodically alternating the sign of the dispersion along the transmission line it is possible to propagate stable pulses but the nature of the pulse propagation is significantly different from soliton propagation[95, 98, 129], with the pulse dynamics being closely related to stretched pulse mode-locking in fibre laser cavities[135]. By using dispersion management it is possible to achieve stable soliton-like pulse propagation over systems which have a high local dispersion (and even over systems which are of predominantly normal dispersion[131]) as long as the average dispersion is low and anomalous. The immediate implication of this is that by the periodic inclusion of normally dispersive elements to compensate for the high anomalous dispersion of standard fibre, it may be possible to upgrade existing standard fibre links to 10s of Gbit/s data rates[122, 123, 134]. This use of dispersion compensation is studied extensively in Chapter 7 and the use of fibre Bragg grating filters for dispersion compensation is discussed in Chapter 8.

Studies of the dynamics of pulse propagation in dispersion managed systems, using numerical simulations have produced some startling results. It has been shown that for a simple dispersion map consisting of two fibres of equal length and with negligible loss, the stable pulse shape changes from the $sech^2(t)$ profile of the fundamental soliton towards a Gaussian profile as the strength of the map (i.e. the difference between the dispersions of the two fibres)is increased [98, 92]. There is also an increase of the energy of the stable pulses compared to that of the average solitons of a uniform dispersion system with the same average dispersion [98]. The energy of the stable pulses of the dispersion managed system being F times greater than the uniform dispersion average solitons with F given

by

$$F = 1 + \alpha \left[\frac{(\beta_{2(1)} - \beta_{2(av)})l_1 - (\beta_{2(2)} - \beta_{2(av)}l_2)}{\tau^2_{fwhm}} \right]^2 . \tag{2.77}$$

The value of α has been found empirically to be ~ 0.7 with the effect of loss neglected. It is not yet certain how loss affects this energy enhancement but there is some evidence that F is reduced when loss is included [117].

In the stable state the pulses returns to the same profile, peak power and width after each span of the dispersion map but there still remains a complex pulse evolution within the map [95]. Figure 2.9 (b), (c), and (d) show numerical simulations of the spectrum, pulse width and time-bandwidth product fluctuations within the dispersion map shown in Figure 2.9 (a). The dispersion map consisted of two 100km long lossless fibres shown

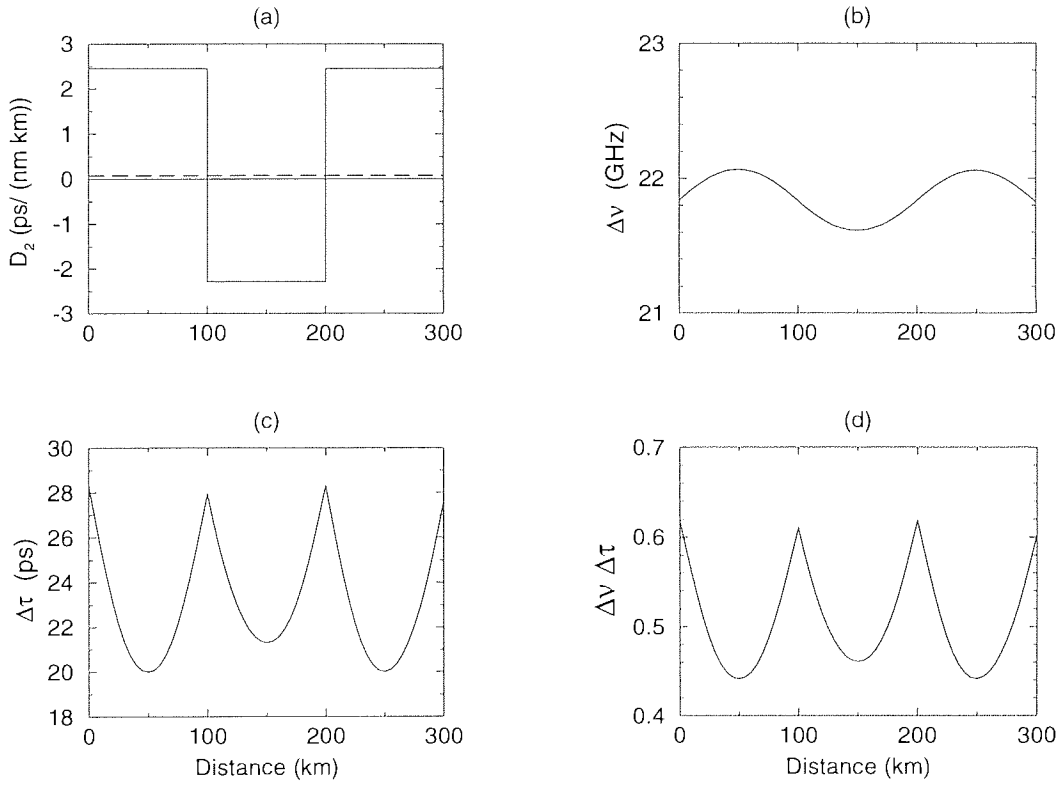

Figure 2.9: Evolution of (b) the spectral width, (c) the temporal width and (d) the time-bandwidth product of the stable pulses of the dispersion map shown in (a). In (a) the solid line indicates the local dispersion and the dashed line is the average dispersion of the system.

as solid line in Figure 2.9 (a). One of the fibres was anomalous with a dispersion of 2.46ps/(nm km) and the other was normal with a dispersion of -2.3ps/(nm km) giving an average anomalous dispersion of +0.08ps/(nm km). The spectral variations shown in Figure 2.9 (b) are due to the fibre nonlinearity acting on the chirped pulse. The variations of the pulse width are shown in Figure 2.9 (c). At the input of the anomalous fibre the

pulses were chirped but were compressed due to the effect of dispersion as they propagated along the fibre. At the mid-point of the fibre the pulse width was at the minimum value and the pulses were unchirped. With further propagation, the pulse width increased and the pulses become chirped again but with the sign of the chirp reversed. On propagation through the normal fibre the pulses were re-compressed (since the sign of the dispersion was reversed) with the pulses becoming transform limited again at the mid-point of the fibre. After this point the pulses again increased in width and became chirped. Although the pulses width was at a minimum at the mid-point of the two fibres the values of these two minima were different with the minimum in the anomalous fibre being lower than that in the normal fibre. In addition, the pulse shapes at these two transform limited positions were different as indicated by the two minimum values of the time bandwidth product $\Delta\nu\Delta\tau$ shown in Figure 2.9 (d). These time-bandwidth product variations were dominated by the pulse width variations since the spectral variation was only a small effect (the spectral width only changed by $\sim$1% whereas the pulse width varied by $\sim$30%). At the centre of the anomalous fibre the time-bandwidth product of the transform limited pulses was $\sim$0.44 showing that the pulses were Gaussian in profile. When loss is included, the complex pulse evolution within the dispersion map still remains but there is less variation from the $sech^2(t)$ pulse profile and the position at which the pulses become transform limited is no longer at the midpoint of the fibres [117]. There is also a reduction of the power enhancement factor of the stable pulses.

The results of these numerical simulations indicate that, if a transform limited pulse is launched at the start of the standard fibre it must undergo a complex evolution before reaching the stable pulse shape and width which is unchirped at the appropriate points in the fibres. Thus, the optimum launch position into the dispersion map for a transform limited source is not at the start of the standard fibre but at the point where the stable pulses are transform limited. When a chirped source is used the optimum launch position is altered to match both the magnitude and the sign of the chirp of the source. The effect of varying the launch position of the source is investigated in Section 7.4. An alternative way of optimising the match between the source and the dispersion map is to pre-chirp the pulses to give the required sign and magnitude before launching into the dispersion map [136].

In a real system the lengths of the anomalous and normal dispersion fibres are unlikely to be the same and will also likely have different losses. A further issue which must be considered in an amplified system is the positioning of the dispersion compensating fibre

in relation to the amplifier [94]. Consider the power of the pulses: at the amplifier output the power is at the highest value and nonlinearity will dominate GVD. As the pulses propagate along the transmission fibre the power is reduced due to the attenuation of the fibre and as in the average soliton model there will come a point where GVD dominates [36]. For a standard fibre system the compensating fibre will have normal dispersion and so will not be soliton supporting. The characteristics of the pulse evolution will therefore depend on what point this normal fibre is included relative to the amplifier. The effect of altering the position of the dispersion compensating fibre is studied in Section 7.5.

In relation to soliton propagation systems, there are other advantages of using dispersion management. In addition to an alteration in the pulse profile the energy of the stable pulses is higher than the average soliton power [98]. This has two effects: the signal to noise ratio is improved since the signal power is higher and the Gordon-Haus jitter is reduced since the noise injected at each amplifier presents a smaller perturbation to the pulse [96, 97]. The fact that the stable pulse shape changes from $sech^2(t)$ towards Gaussian in profile means that soliton-soliton interactions are reduced as the overlap of adjacent solitons is reduced due to the steepening of the wings of the pulses. In WDM systems dispersion management can help to reduce the efficiency of the four wave mixing process [137] and decrease the collision induced frequency shift between different channels [138]. These advantages and the simplicity of implementing dispersion compensated standard fibre soliton systems has lead to a rapid growth in interest in such systems.

2.9 Summary

The derivation of the NLSE, which governs pulse propagation in optical fibre has been outlined and the effects of GVD and SPM have been investigated separately before studying how their combined effect leads to optical solitons being supported in the anomalous dispersion regime of an ideal lossless fibre. The average soliton model, which takes into account the loss of real fibre, has also been outlined. The major problems which are encountered in soliton systems and the constraints that they put on system design have been introduced and methods of system improvement have been discussed. Dispersion management, which is being used increasingly in both NRZ and RZ systems has also been introduced. The basic ideas which have been put forward in this chapter will be expanded on as required throughout this thesis.

Chapter 3

The recirculating loop and experimental techniques

3.1 Introduction

The propagation experiments which are described in the following chapters were performed using a recirculating loop. A recirculating loop is a simplified transmission system which consists of one or a few amplifiers and a corresponding number of fibre spans. Recirculating loops can be used to perform long distance (1000s of km) propagation experiments by propagating a signal many times around the loop until the required propagation distance has been achieved and results can be taken. Reconfiguration of a loop is extremely easy compared to a full in-line system due to the reduction in the number of components and fibre spans used and this flexibility is a major advantage when several experiments are to be done which require comparison of fibres or components. The other major advantage of using a recirculating loop is that the cost is a very small fraction of that for a full system. Recirculating loops were first used in electronically repeated systems [139] and were first used in all optical experiments using Raman amplification to compensate for the fibre loss [140]. With the development of the EDFA [22, 23] loop experiments became common [81],[141]–[145] because EDFAs were not widely available and recirculating loops offered a way of testing system performance without requiring a large number of EDFAs. Today, recirculating loops are used extensively and a loop is the obvious choice when new ideas and configurations are to be tried for the first time as loop experiments can give a good indication of system performance [43, 64, 109, 110, 121, 131, 133, 134],[146]–[158].

The recirculating loop can however, only give an indication of what would happen in a real system; the maximum error free distances (usually defined as the maximum

distance which a data signal can be propagated with fewer than one error per 10^9 bits) for a loop and an in-line experiment may differ significantly. The reason for this is that in a recirculating loop experiment, there is little variation in parameters such as amplifier span, component characteristics, average dispersion and loss per span. The problem is particularly pronounced when a single span loop is used where there is only one fibre span, amplifier and set of components. Whilst these factors could be expected to give a falsely high propagation distance there are other effects associated with the use of a loop which have a detrimental effect and may lead to loop experiments giving a pessimistic impression of system performance. When a loop is used the loss per amplifier span is in general higher than for an in-line experiment as components such as isolators and filters have to be included more frequently - the maximum spacing of components is determined by the number of spans of the loop and so a single span loop fares particularly badly as all of the components to be used must be contained within a single amplifier span. An addition loss is encountered as a portion of the signal must be coupled out of the loop to allow measurements to be taken. All these losses must be compensated for by the optical amplifiers and as described in Section 2.7.1, increasing amplifier gain leads to system degradation as more noise is introduced into the system. To give a good indication of system performance state of the art recirculating loops now contain up to twenty fibre spans [158] but even in the simplest form a recirculating loop is an indispensable tool in the initial stage of long haul system development. If necessary a larger loop or full length system can be constructed to fully test a configuration once there is sufficient confidence in the preliminary results. This chapter will discuss the operation and design of the single span recirculating loop used for the experiments undertaken for this thesis. The loop operation and other experimental techniques used will also be described.

3.2 Design considerations and principle of operation

A single span recirculating loop which consists of only one amplifier, one fibre span and one set of components has obvious economic advantages but it does bring restrictions as all the optical components must be included every amplifier span. Thus, experiments such as investigating the effect of filtering or dispersion compensating every X^{th} amplifier can not be done with a single span loop. As the following chapters will show there is still an enormous variety of experiments which can be done and the results are a good indication of real system performance.

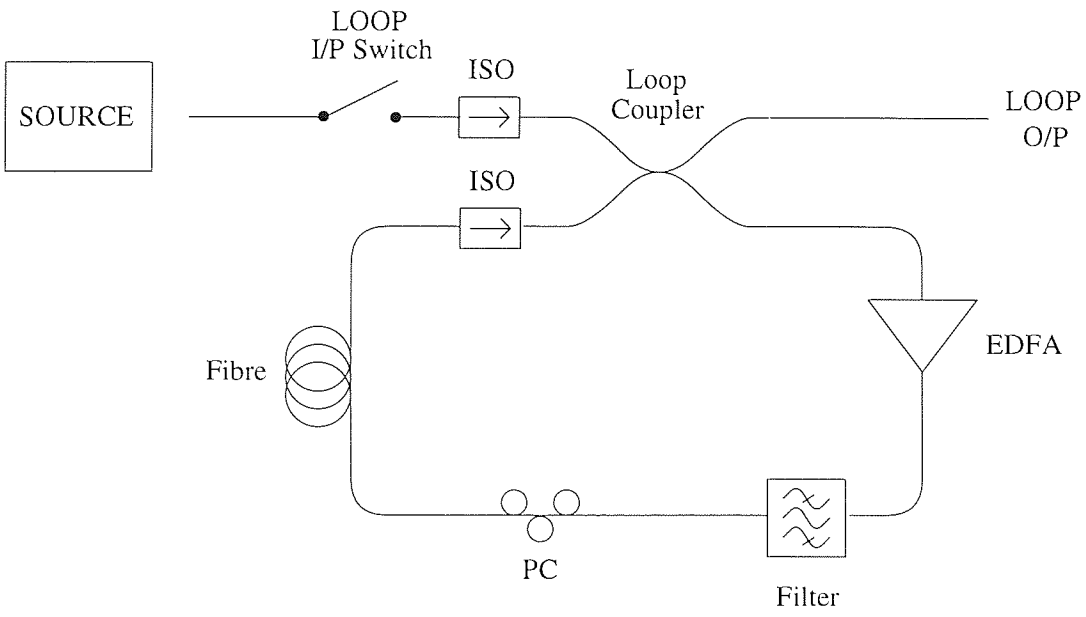

Figure 3.1: Schematic diagram of the recirculating loop. ISO: isolator, EDFA: Erbium Doped Fibre Amplifier, PC Polarisation Controller

A schematic diagram of a typical single span recirculating loop is shown in Figure 3.1. Before it can be propagated in the loop, the signal from the source must be gated into the loop using a switch and a fibre coupler. To compensate for the losses of these devices it is usually necessary to amplify the source to give the required power level in the loop. The purpose of the switch is to allow a burst of signal to pass into the loop as required. The length of this signal burst must be exactly equal to the round trip time, or fill time, of the loop. For a loop length of 40km the fill time is $\sim 195\mu$s which corresponds to 1.9 million bits at 10Gbit/s which is roughly $1/1100^{th}$ of a 2^{31}-1 pseudo-random-bit-sequence (PRBS) data pattern. If the loop is not completely filled the ASE noise level from the amplifier can build up in the unfilled section but if the switch is left open for too long and the loop is overfilled, pulses which have already propagated once round the loop will arrive back at the coupler whilst signal is still being coupled into the loop. This can obviously lead to degradation of the signal as the two sets of pulses will interfere. The switch must also have a relatively fast switching time, as pulses which are incident on the switch during the transitions will be partially transmitted. A high extinction ratio is required so that when the switch is opened to stop signal passing into the loop, there is no leak-through - any leakage into the loop would appear as additional noise in the system, which is obviously undesirable. In addition to these specific requirements, low insertion loss and low polarisation dependence are also desirable. An acousto-optic modulator (AOM) is the most commonly used switching device as it encompasses many of the device requirements and in particular has a very high extinction ratio (60-70dB). An

AOM works by splitting the input beam into a straight through and a deflected beam by passing it through a standing wave pattern which is set up inside the device using acoustic waves. This standing wave pattern acts as a grating leading to the diffraction of the input beam. By switching the power to the device so that the diffraction only occurs at the required time the input to the loop can be switched by ensuring that only the diffracted beam is coupled into the loop input coupler (the straight through signal is *always* present and must not be coupled into the loop). As the diffraction process is not 100% efficient there is always loss when using an AOM. In addition to the loss in the device it is also necessary to couple the signal out of fibre before passing it through the AOM and then back into fibre which increases the insertion loss. The device which was used here had a total insertion loss of $\sim$ 6dB, which was compensated for by pre-amplification of the source. The switching speed was $\sim$200ns, which is $\sim$0.1% of the typical fill time of the loop, and the polarisation dependence below 0.1dB. An isolator positioned between the input switch and the input coupler gave an extra $\sim$ 0.5dB loss but avoided any problems associated with back reflections into the AOM.

The choice of loop coupler is also important, particularly so in the case of a single span loop because a portion of the signal is coupled out of the loop through this coupler after each round trip of the loop. Using a 50:50 coupler therefore leads to an additional 3dB loss per round trip. If too large a fraction of the signal is coupled out of the loop after each round trip the system performance will be compromised as a higher amplifier gain will be required whereas if too small a fraction is coupled out, the loop output signal requires high gain amplification before measurements can be done. There is also the problem that the same coupler must be used for both coupling into and out of the loop. This means that if the coupling ratio is chosen so that only a small fraction of the circulating signal is coupled out of the loop each round trip, then only a small fraction of the input signal is coupled into loop. Therefore a compromise must be reached and for different experiments different coupling ratios may be required.

Once the signal is coupled into the loop it is first of all amplified. This is the obvious position for the amplifier as the signal power coupled into the loop is generally low. The design of the amplifier is crucial to the loop performance and once again this is particularly important in a single span loop where there is only one amplifier and any imperfections will be magnified by the many recirculations involved in propagation experiments. The gain of the amplifier must be sufficient so as to exactly compensate for all the losses in the loop – the round trip gain of the loop must be unity so that the signal power and hence

pulse power remains the same after each amplification. In a soliton system the soliton power is fixed and any increase/decrease in the pulse energy will lead to pulse narrowing/ broadening. The pulse power can be stabilised by operating the amplifier in saturation so that any decrease/increase in the input power leads to a corresponding increase/decrease in amplifier gain and recovery of the required output power. A general requirement of all loop components is that there should be minimal polarisation dependence. In relation to the EDFA, this is important because the same amplifier will be used several times and any polarisation dependence of the EDFA will be accentuated by multiple passes. EDFAs can have polarisation dependent gain (PDG) with there effectively being two erbium populations prefering orthogonal polarisation states [159]–[162] and also exhibit polarisation hole burning [163, 164]. If the signal is polarised to coincide with one of the erbium populations, that population will become more saturated and the gain will be depleted. This leaves the orthogonal population undepleted and it will amplify the ASE which is polarised orthogonal to the signal leading to a more rapid build up of the noise. Although the PDG of EDFAs is low (typically 0.1dB) it can become significant in long distance propagation after many round trips of the loop [159]. As with all amplifiers, a low noise figure is also desirable so that the ASE noise level can be kept to a minimum.

In a typical configuration with a 40km amplifier span, the round trip loss of the loop would be ~14 dB and the amplifier output power would be ~ 0 dBm corresponding to an input power of ~-14dBm. Using the amplifier with the characteristics shown in Figure 3.2 these requirements could be met by operating ~ 4dB into saturation. This amplifier was backward pumped with a 980nm laser diode and had a noise figure of 4.1dB.

As discussed in Section 2.7.1, including a filter in the transmission line can reduce the rate of Gordon-Haus jitter build up in a soliton system but including a filter introduces an additional loss which is dependent on the strength of the filter and so a compromise between filter strength and jitter reduction must be reached. In practice, a filter with a 3dB bandwidth of 3nm and an insertion loss of ~2dB was used. The bandwidth of this filter was much greater than the ~ 0.1nm typical bandwidth of the solitons and so there was little soliton guiding. The main purpose of the filter was to suppress the ASE level outside the soliton bandwidth.

Including a polarisation controller (PC) allowed the polarisation state of the signal to be altered before launching into the transmission fibre. This gave a greater degree of controllability in loop experiments compared to a full length in-line system which is necessary because the same components and amplifier were being used repeatedly. A real

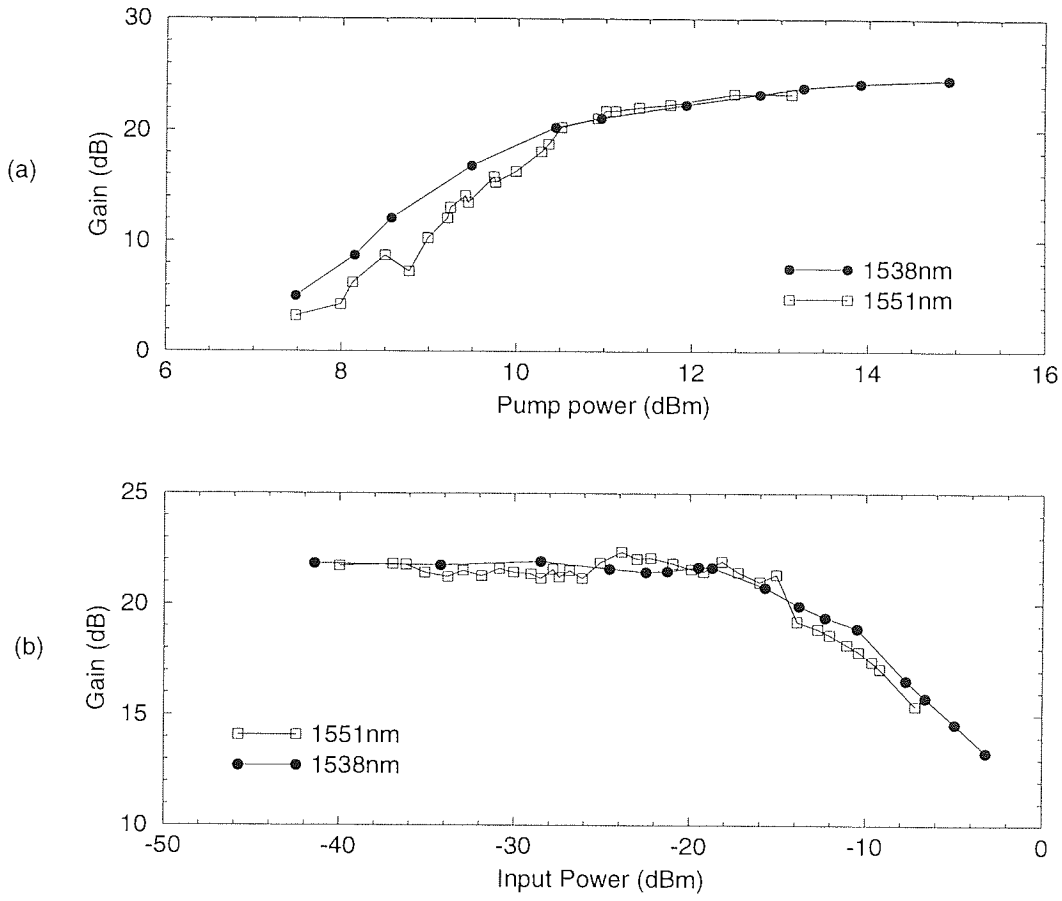

Figure 3.2: Characteristics of the loop EDFA at 1538nm and 1551nm: (a) Small signal gain for an input power of -40dBm and (b) gain saturation at a pump power of 16mW.

system could not use these PCs and due to variations in the polarisation characteristics of the amplifiers, would probably not be needed. This is another factor which can lead to discrepancies in the propagation distance achievable in loop experiments and in-line experiments. The PC does however impose an additional loss of ~0.5 dB. When an experiment was being performed the polarisation state of the signal would be altered as required using the PC before beginning and then left unaltered throughout the duration of the experiment in order to give consistent results.

The actual transmission fibre in the loop varied greatly from experiment to experiment with total fibre length typically being 30-40km. In any given soliton propagation experiment, the average power which must be launched into the fibre is determined by the average soliton power (given by Equation 2.56), the dispersion map [95, 98], the data pattern being used and the data rate. In order to fine tune the power launched into the transmission fibre, the EDFA gain and output power could be altered by adjusting the current of the pump diode. The inclusion of an optical isolator after the propagation fibre

stops any counter-propagating noise/signal from degrading the signal.

The loop was completed with a fibre coupler as described above. The portion of the signal which remains in the loop is re-amplified and continues to circulate in the loop until the required number of circulations (corresponding to the desired propagation distance) is reached. Thus, after the first circulation, there is a continuous output from the loop coupler. This output can be further split to give a continuous monitor as well as the main loop output.

Once the required propagation distance has been achieved the signal circulating in the loop must be removed before the loop can be re-started. A common way of doing this is to include a second AOM in the loop, which can be switched to either pass or block the circulating signal. A second technique, which was employed in all the experiments in this thesis, is to stop pumping the loop amplifier after the propagation distance has been reached. This attenuates the circulating signal and within a few round trips the amplifier can be re-pumped in preparation for the injection of the next signal burst. The length of time for which the loop EDFA must be unpumped and re-pumped are inter-dependent to some degree and were determined experimentally by trial and error. The reason for using this second technique was primarily that a second AOM was not available but it has other advantages: including an AOM increases the round trip loss of the loop and when an AOM is used the signal undergoes a small frequency shift (typically ~80MHz) each time it passes through the device[165]. This frequency shift is small compared to that of the sliding guiding scheme (see 2.7.1) but will still have an effect on the propagation.

In general, measurements were only taken when the required propagation distance had been achieved. This meant that switching was required to select a measurement window covering only the section of the continuous loop output which had propagated for the required distance i.e. the final circulation of the loop. The timing of this switching was controlled by one of two electronic delay generators which were used to control the entire loop cycle. The measurement window could be easily adjusted both in duration, to allow time for clock recovery to be performed (see Section 3.3.2), and position so that data at the beginning and end of the recirculation could be rejected.

The timing of the propagation and measurement cycle can be understood with reference to Figure 3.3. The loop cycle was begun by "opening" the AOM input switch to allow signal to pass into the loop. When the loop was filled the AOM was "closed". The signal then propagated for the required distance. When this distance was reached the measurement switch was opened and a burst measurement could be performed. The

circulating signal was then attenuated by stopping the pumping of the loop EDFA. When the signal level was sufficiently attenuated the amplifier was re-pumped, and after waiting for the amplifier gain characteristics to recover, the cycle could be repeated by re-opening the AOM input switch to allow another burst of signal to be admitted into the loop. The loop fill time, propagation time and measurement window were controlled by one delay generator with the second, which was triggered by the first, controlling the loop amplifier. These delay generators allowed precision control of the loop fill time, propagation time, measurement window position and length, amplifier kill time and re-pump time.

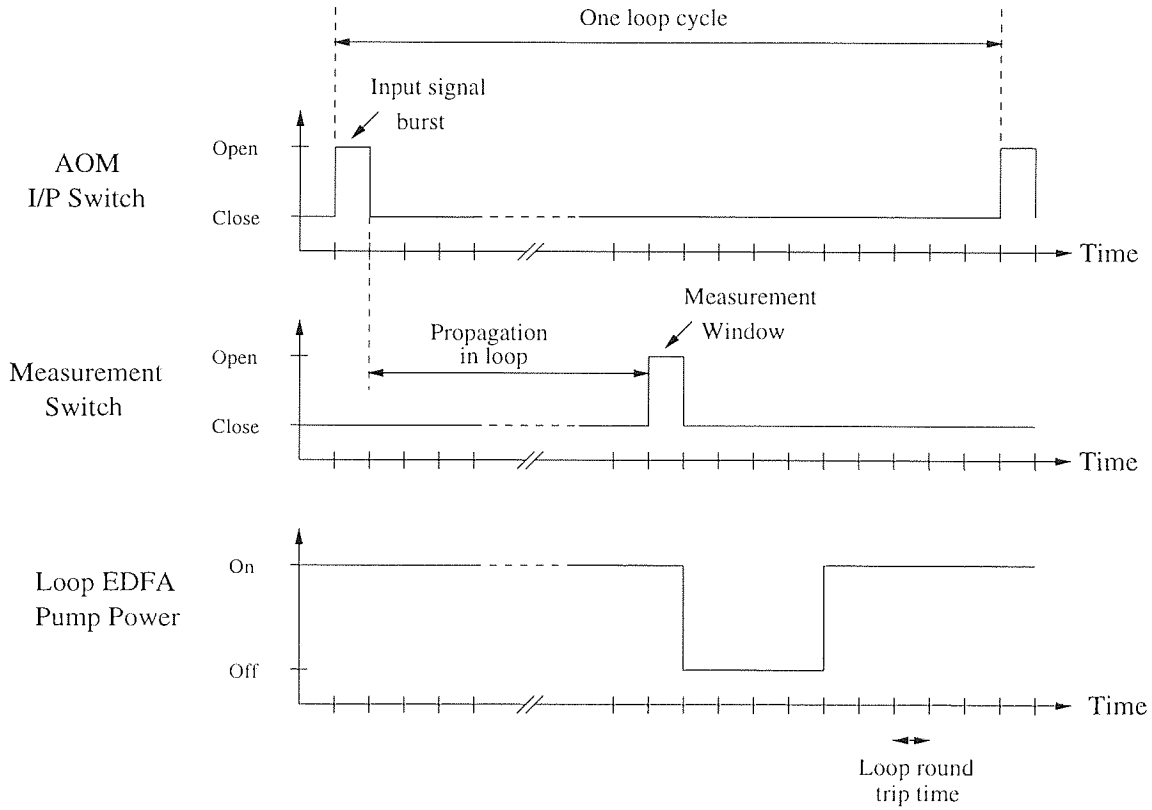

Figure 3.3: Representation of the loop cycle. The three figures show the states of the input and measurement switches and the state of the EDFA pump diode throughout the loop cycle. The unit of time is the round trip time of the loop.

3.3 Experimental measurement techniques

One of the main drawbacks of the recirculating loop is that the measurement time window is usually much shorter than the propagation time and so the time to perform experiments is considerably longer than for an in-line experiment. As mentioned previously, there is also the need to switch the loop output signal so that the burst measurement is made at the correct time. This section describes how burst measurements were performed, highlights

the limitations of these techniques and also describes how the system performance could be monitored.

3.3.1 Continuous monitoring

As described in Section 3.2, there was a continuous output from the loop when experiments were being performed. By splitting this signal with fibre couplers it was possible to obtain continuous monitor outputs which could be used to give an indication of the loop performance. Using a slow photo-diode and an oscilloscope, the average power and ASE noise level could be monitored as shown in Figure 3.4. The loop input signal burst appears at an artificially high voltage due to the positioning of the loop input coupler. There followed a relaxation oscillation as the power in the loop stabilises. These oscillations could be suppressed to some degree by adjusting the loop EDFA gain and the loop timings. As shown on this trace the ASE noise level (the lower line) build up could also be checked by reducing the fill time of the loop so that it was a few μs (typically 2) less than the round trip time. This meant that a section of the circulating signal was left free of data and so the only power detected in this section was due to the background noise. Within the $\sim 2\mu$s gap, the ASE level remains constant as the $\sim$10ms lifetime of the excited erbium state is relatively long and the ASE level is only changed on a millisecond time scale. Thus, the noise accumulation with propagation distance could be checked and minimised by alteration of the PC, amplifier gain and loop delays before an experiment was started. When a set of results was actually being taken the loop had to be completely filled and so the noise level could not be monitored. A second monitor output was often used so that the power of the fundamental component of the electrical spectrum of the propagating signal could be measured using an electrical spectrum analyser. This gave an indication of pulse width variations and timing jitter accumulation.

Before an experiment was begun, the source had to be checked to ensure that the quality of the pulses in the data stream was acceptable and that the back-to-back performance (i.e. the system performance with the data passed straight through to the receiver without any recirculation in the loop) of the system was optimised. A fixed propagation distance was then set and the EDFA gain, the loop delays, the filter and the polarisation controller were adjusted whilst checking the continuous monitors to ensure that the loop was performing as required. An experiment could then be commenced with the propagation distance being adjusted as required.

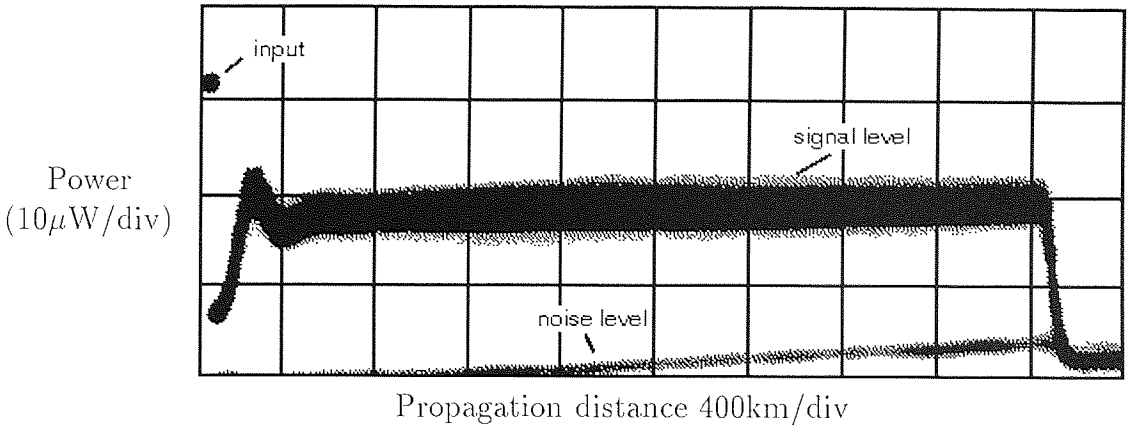

Figure 3.4: Oscilloscope trace showing the average power level (upper line) and the noise level (lower line) over one loop cycle.

Pulse width measurement

It was frequently necessary to have a measure of the pulse width being used so that parameters such as pulse power, soliton period and mark to space ratio could be determined. Generally the pulses which were being used were on the order of 10ps which is at the limit of the resolution achievable by *direct* measurement of the pulse width using a fast photodiode and sampling oscilloscope. An alternative method of pulse width measurement was therefore required and the common technique of using the second harmonic signal induced in a nonlinear crystal to determine the autocorrelation width of the input pulse profile was used. From the width of the autocorrelation function the pulse width could be deduced by assuming the form of pulse shape.

Second harmonic generation is a nonlinear process and the intensity of the second harmonic signal is

$$I_{2\omega}(t) \propto \int_{-\infty}^{\infty} I_{\omega}(t)^2 dt \tag{3.1}$$

where $I_{\omega}(t)$ is the input intensity and $I_{2\omega}(t)$ is the second harmonic intensity. In order to determine the pulse width the input pulse stream is first split into two parts. A relative time delay, T, is then introduced between the two signals before they are re-aligned and passed through the nonlinear crystal. Assuming the signal is split equally, Equation 3.1 becomes

$$I_{2\omega}(t) \propto \int_{-\infty}^{\infty} \left[\frac{1}{2} I_{\omega}(t) + \frac{1}{2} I_{\omega}(t-T)\right]^2 dt \tag{3.2}$$

$$\propto \int_{-\infty}^{\infty} I_{\omega}(t)^2 dt + 2\int_{-\infty}^{\infty} I_{\omega}(t) I_{\omega}(t-T) dt \tag{3.3}$$

The first term can be removed from this equation if a non-collinear arrangement is

Pulse Shape	k	$\Delta\nu\Delta t$
Gaussian	1.41	0.441
$Sech^2$	1.55	0.315

Table 3.1: Autocorrelation conversion factors and time bandwidth products for two common pulse shapes

used and in this case the autocorrelation function, $G(T)$, is given by the normalised second harmonic intensity i.e.

$$G(T) = \int_{-\infty}^{\infty} I_\omega(t) I_\omega(t-T) dt \tag{3.4}$$

In practice a plot of $G(T)$ versus the delay T can be obtained by measuring the intensity of the second harmonic signal as the delay between the two pulse trains is changed. The FWHM of $G(T)$ can then be found and from this value the pulse width can be found by dividing by an appropriate conversion factor k. The conversion factor and the time bandwidth product, $\Delta\nu\Delta t$, of a transform limited pulse depend on the pulse shape. Values for Gaussian and $sech^2$ pulse shapes are given in Table 3.1

Where pulse width measurements are quoted in the following chapters it is this method which has been used. After taking an autocorrelation a curve fit was performed to the experimental data to determine the pulse shape and hence the relevant conversion factor which had to be used to calculate the actual pulse width.

3.3.2 Burst measurement techniques

A disadvantage of using a recirculating loop is that burst measurements must be taken. Unlike an in-line experiment, where there is a continuous output which can be measured, measurements can only be made for a small fraction of the recirculating loop cycle – the majority of the loop cycle is taken up with the propagation and only the final recirculation can be measured. In addition to increasing the time scale of experiments there is also the problem that the loop output must be switched so that only the relevant part of the loop output is sampled. The switching method used in practice depended on the measurements which were being taken. For some a switched optical signal was sufficient but for others the electrical trigger had to be switched to initiate the measurement at the required time. Unfortunately, autocorrelations could not be taken as this required a continuous signal.

To give an indication of system performance the most frequently quoted parameter is

the bit-error ratio (BER). The BER is defined as the number of errors detected divided by the total number of bits received in the measurement period [166]. For a system to be defined as "error free" a BER of 10^{-9} or better is required. To measure BER, dedicated test equipment is required, consisting of a data pattern generator and an error detector. Unfortunately, a bit error test set (BERTS) was not available throughout the duration of the experimental work for this thesis and so other measures of system performance were required. This section describes these measurements and indicates their limitations. The validity of these measurements has been checked by using a BERTS when possible.

Timing Jitter measurement

Taking timing jitter measurements gives an indication of the variation of arrival times of pulses in a pulse/data stream relative to a fixed triggering point, and as such can give an indication of system performance. A serious limitation of this technique is that amplitude jitter, which can seriously affect system performance, has only a very minor effect on the timing jitter measurement. A further disadvantage of the technique is that the length of time required to acquire the data can be prohibitively long. This problem was exaggerated at low data rates and at long propagation distances.

Jitter measurements were performed using a high speed sampling oscilloscope and Figure 3.5 shows a typical jitter measurement. A voltage window of variable width was

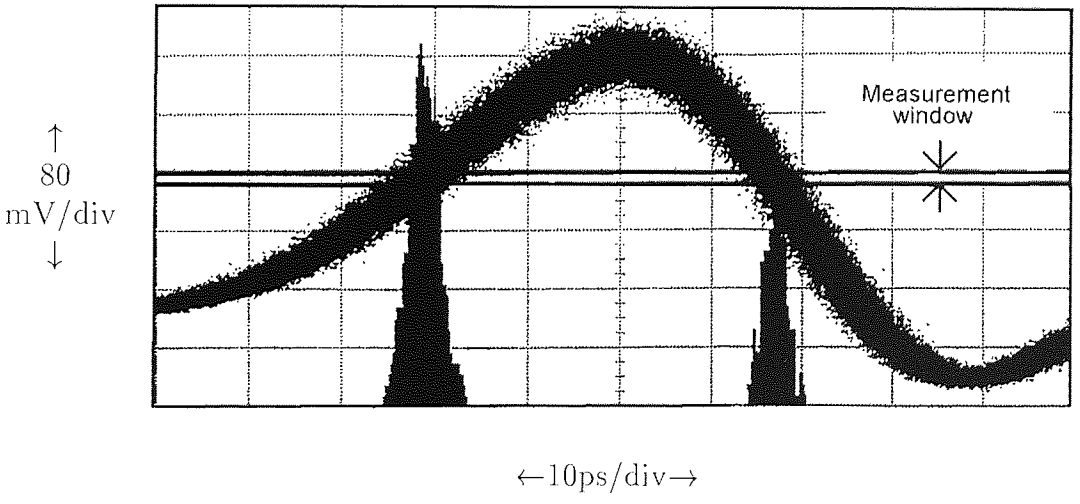

Figure 3.5: A typical jitter measurement. Data points within a pre-set voltage window were used to construct a time histogram from which the r.m.s. jitter could be calculated.

first positioned as required. The number of samples required was then set and the measurement could begin. The oscilloscope records all points which fall within the pre-set voltage window and measurement continues until the required number of samples have

been obtained. A time histogram is then constructed from the measured data with the height of the histogram at any position in time being directly proportional to the number of samples which occured at that time position. The mean and standard deviation of the histogram can then be determined assuming Gaussian statistics. The r.m.s timing jitter is then given by the standard deviation of the histogram.

The example shown in Figure 3.5 is typical of the experimental results. A 2.5mV voltage window was positioned roughly half way between the zero level (the baseline) and the one level (the pulse peak) of the signal pulses. The number of samples was 1000 which gave a good compromise between speed of acquisition and resolution of the histogram. Either the leading or trailing edge of the pulse could be used to give the jitter measurement but once either the trailing or leading edge was chosen this was used consistently throughout the duration of an experiment. In the example, which shows a jitter measurement of a 2.5GHz fibre laser, the r.m.s. jitter was 1.6ps. The maximum jitter which could be measured accurately using this method was 10ps since for jitter values above this the leading and trailing edges of the pulse began to merge with one another causing ambiguities in the statistics. This effectively limited the maximum transmission distance which could be measured using this method.

When taking jitter measurements it was not necessary to switch the trigger to the scope and an optical switch, such as a lithium niobate modulator, operated by the loop electronic timing controllers could be used to switch the loop output as required. Continuous triggering leads to an overemphasis of the baseline since there is no optical signal to the sampling scope except during the measurement burst, but because the sampling scope only records points falling within the pre-set voltage window this would not affect the measurements.

Jitter measurements were only used where the propagating signal was a continuous pulse stream as opposed to a data stream. When a data stream was used Q value measurements could be made which are quicker and give a more useful indication of system performance.

Q measurement

The Q value of a system is defined by [165, 167, 168]

$$Q = \frac{\mu_1 - \mu_0}{\sigma_1 + \sigma_0} \tag{3.5}$$

where $\mu_{1,0}$ represent the mean values of the ones and zeros in the data stream and $\sigma_{1,0}$ represents their standard deviations.

The Q value gives a measurement of system performance which is related to the bit error ratio (BER) by [169]

$$BER = \frac{1}{\sqrt{2\pi}} \frac{exp(-Q^2/2)}{Q} \tag{3.6}$$

but can only be measured when a data stream is being used as the propagating signal because it requires measurement of the ones and zeros in the data stream, when a pulse stream is being used all data slots are occupied by ones. A BER of 10^{-9} is generally accepted as representing "error free" system performance and the equivalent Q value is 6.

Whereas a voltage window was set to allow timing jitters to be measured, a time window had to be defined before a Q measurement could be made. Any sampled points within this time window were then used to build up a histogram as shown in Figure 3.6. From this histogram the mean and standard deviations of the one and zero levels could be determined using the statistics facilities of the sampling oscilloscope allowing the Q to be calculated using Equation 3.5. In measuring $\mu_{0,1}$ and $\sigma_{0,1}$ it was necessary to set a decision level with all sampled points above this decision level being taken as representing ones and points below the decision level representing zeros. This decision level was generally taken as being half way between μ_0 and μ_1 but in cases such as that depicted in Figure 3.6 where there was no overlap of the two histograms, the positioning of the decision level made little difference to the Q value but when the Q values were lower and there was more overlap of the two histograms the positioning of the decision level became more crucial and it was important that the decision level was consistent throughout the measurements. This lead to a greater error in the measurement of low Q values (~ 4) than high Q's and significantly, for a Q value of 6 (which corresponds to the minimum acceptable value), varying the decision level position led to a variation in Q of less than 0.1.

The eye diagram in Figure 3.6 shows that in a soliton system the one level is defined as the peak pulse height and the zero level corresponds to the baseline. From the definition of Q it is immediately obvious that any increase in the ASE noise level, timing jitter or amplitude jitter will degrade the system Q by increasing $\sigma_{0,1}$. Variations in the pulse height can also affect the Q as μ_1 will be altered. This has implications for soliton systems as the pulse power (and hence μ_1) depends on the pulse width and so broader pulses will have lower Qs given the same noise conditions. This implies that broader pulses will also give lower BER measurements through Equation 3.6. The reason for the BER being lower

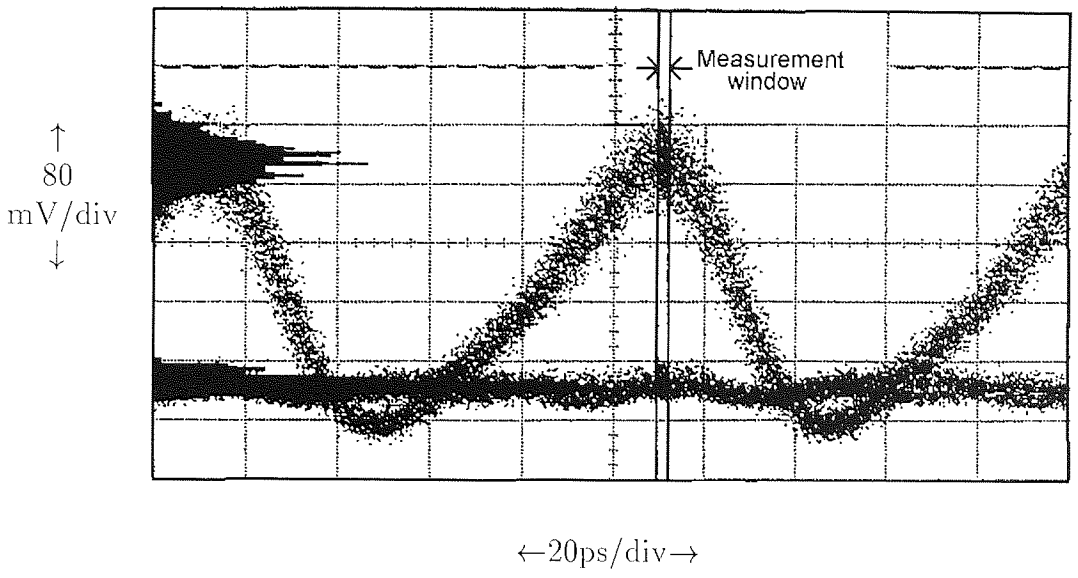

Figure 3.6: A typical Q value measurement. Mean and standard deviations of the one and zero levels are found and used in the calculation of the Q.

is that in taking a BER measurement a decision level must be set such that the energy detected in a given time interval must be above the decision level for a data one to be detected. As a pulse broadens the pulse energy is spread over a greater time interval and the integrated energy detected in the bit interval may fall below the decision level giving an error.

When Q measurements were to be taken, it was necessary to switch the trigger to the sampling scope as opposed to switching the optical signal. If a continuous trigger is used the baseline is overemphasised as described above, leading to inaccuracy in the true values of σ_0 and μ_0.

The main problem found experimentally with taking Q values was that even a small change in the position of the time window on the sampling oscilloscope could lead to a change in Q value. This could give inconsistencies in results as the time position of the pulses on the sampling scope could vary due to variations in trigger phase as propagation distance was changed and so it was necessary to reposition the time window when this occured. The optimum window position was generally with the window centred on the peak of the pulse but this position was often difficult to determine so before measurements were take the position of the time window was optimised by taking repeated measurements of the Q value with the position changed. Ideally the measurement window would be a delta function positioned at the peak of the pulse and an infinite number of samples would be taken but as for jitter measurements the width of the window and then number of samples recorded for the histograms had to be compromised to give a

reasonable measurement time.

Clock Recovery

When measurements were being taken on the sampling scope an electrical trigger signal was required. Two methods were used - the first, using a fast photo-diode to give a direct conversion of the optical signal, was used only for a low bit rate experiment with a continuous pulse stream and the second, using a clock recovery circuit, was used for the remaining experiments.

Using a clock recovery circuit, an electrical signal which is in synchronisation (and stays in synchronisation) with the optical signal can be obtained. The clock recovery set-up is shown schematically in Figure 3.7.

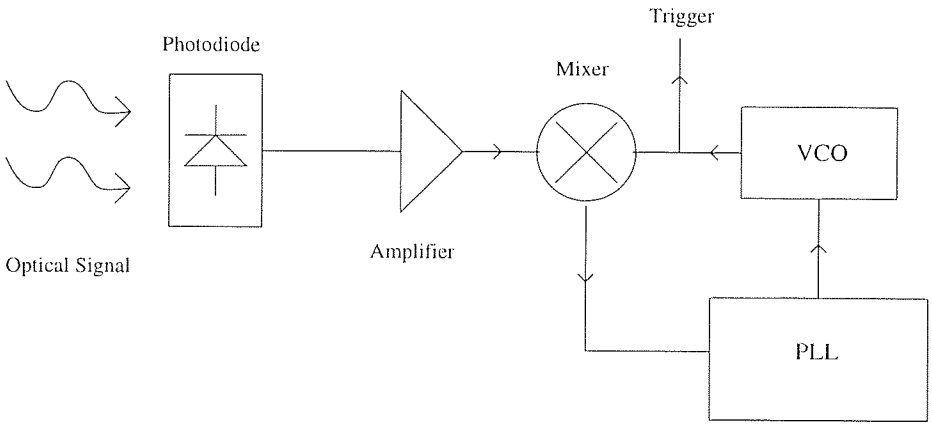

Figure 3.7: Clock Recovery Set-up. VCO: voltage controlled oscillator, PLL: phase locked loop

The optical pulse train was first converted into an electrical signal using a photo-diode before being electrically amplified and mixed with the signal from a voltage controlled oscillator (VCO) to generate an error signal which was fed into a control circuit. This feedback circuit adjusted the VCO frequency so as to minimise the frequency difference between the VCO output and the signal frequency from the photo-diode. Thus, by splitting the VCO output a continuous electrical trigger signal in synchronisation with the optical signal was obtained. This electrical signal would remain in synchronisation with the optical signal even if the optical frequency altered as long as the change in optical frequency was not greater than the locking range of the PLL. This locking range was typically $\sim$ 20MHz which allowed the clock recovery circuit to remain locked to the optical frequency for a period of hours. The performance of the clock recovery circuit had a bearing on the quality of the system performance and before beginning an experiment

the system performance was optimised by measuring the back-to-back Q of the system i.e. the Q value with the propagation distance being effectively zero.

3.4 Dispersion measurements

In soliton propagation experiments it is necessary to know the dispersion of the propagation fibre accurately as this has a major effect on the system performance as discussed in Section 2.7. Commercially available fibre is normally supplied with fibre parameters such as λ_0 and the average dispersion specified but it is prudent to measure these values as a double check before beginning time consuming experiments. This is particularly true when dispersion managed systems are being used which include more than one type of fibre. Two methods of dispersion measurement were used as described below.

3.4.1 Measurement of fibre in the recirculating loop

The first method which was used to measure dispersion had the advantage that the dispersion of the entire loop could be measured and not just that of the transmission fibre. Figure 3.8 shows the set-up used which was essentially just the recirculating loop with no

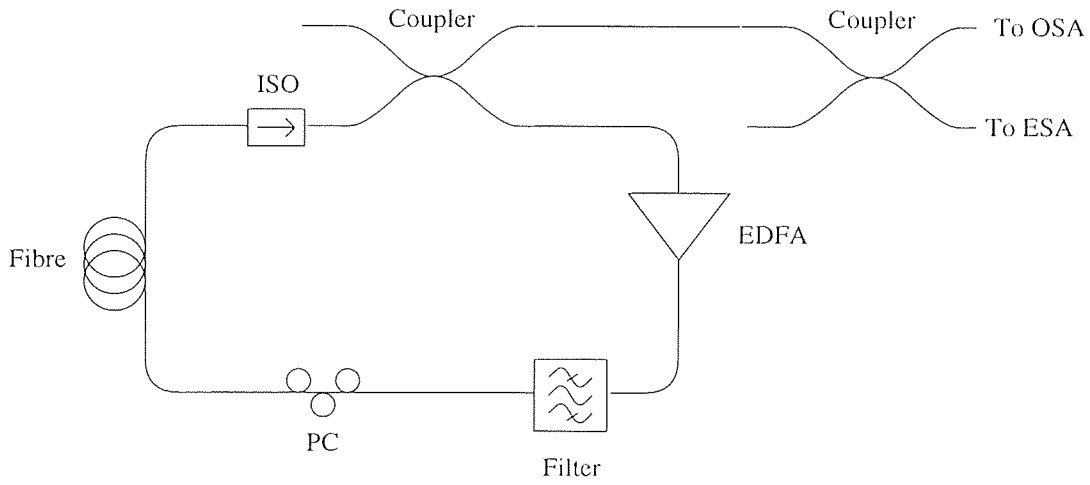

Figure 3.8: Schematic representation of the set-up used to measure the dispersion of the fibre in the recirculating loop.

input. The pump power of the amplifier in the loop was increased to the point where the loop would lase CW. The cavity mode spacing of this ring laser could then be measured using an electrical spectrum analyser (ESA) and the wavelength of operation could be measured using an optical spectrum analyser (OSA). The cavity length could be found using the equation $L = c/n\delta\nu$ where L is the cavity length, n is the refractive index

and $\delta\nu$ is the cavity mode spacing. The dispersion could be measured by changing the wavelength of the filter in the loop to alter the lasing wavelength. As the frequency of the laser was altered the round trip time was also altered due to the effect of dispersion and this time delay was seen as a change in the frequency of the harmonics in the electrical spectrum, with the time and frequency changes being related by $\Delta t = -m\Delta\nu/\nu^2$ where m is the mode number of the harmonic being observed, $\Delta\nu$ is the frequency change and ν is the frequency. The average dispersion D_2 is then found by dividing this time delay by the product of the wavelength change and the loop length. The dispersion of the fibre could be found for a range of wavelengths by taking a series of measurements at different wavelengths. This method assumes that the loop length remains fixed throughout the experiment and so for accurate results cavity expansion and contraction due to environmental effects must be minimised. This could be accomplished by placing the transmission fibre inside insulating containers to avoid thermal effects and by performing the measurements as quickly as possible. A further limitation of this technique was that it required a tunable filter to be included in the loop which was not always practical, for example when a fibre Bragg grating was being used in the loop which had a fixed pass-band (see Chapters 6 and 8). When using this technique the measurement could only be performed over the tuning range of the filter and over the erbium fluorescence spectrum, which meant that in practice the wavelength range from 1530-1560nm could be covered. This wavelength range was however suitable for all of the experiments undertaken for this thesis, where the operating wavelength was in the $1.5\mu m$ window. An advantage of this technique was that it offered a simple means of measuring the dispersion of the system with the transmission fibre in situ and a quick sweep of the lasing wavelength could give a rough idea of λ_0 and the average dispersion. The dispersion could not generally be measured more accurately than ± 0.1ps/(nm km), the main restriction being that the experiment had to be performed with a large wavelength step size to reduce the measurement time.

3.4.2 Dispersion measurement using optical delay

A second experimental set-up, which was used when increased accuracy was required or when a tunable filter could not be used in the loop, is shown schematically in Figure 3.9.

This was an adaptation of a set-up used to measure the dispersion and spectra of fibre Bragg gratings and so it was particularly useful for measuring combinations of fibres and

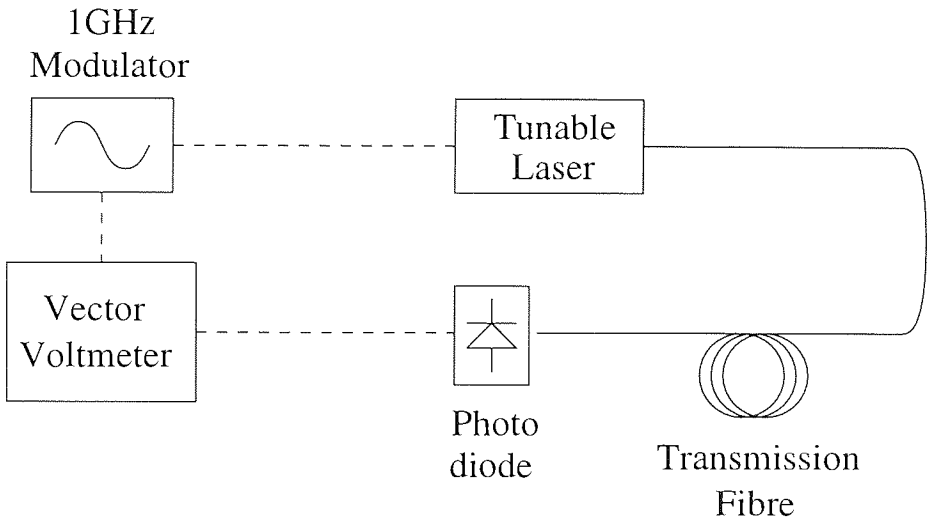

Figure 3.9: Schematic diagram of the experimental set-up used to determine the dispersion through measurement of the optical delay. Solid lines represent optical paths and dashed lines are electrical connections.

gratings where the bandwidth of the measurement was limited by the grating bandwidth but could be used equally well with lengths of fibre alone where the bandwidth was unconstrained. The source used was a tunable wavelength laser whose output signal was amplitude modulated by a 1GHz fixed frequency modulator. The optical signal from the laser was transmitted through the transmission fibre and converted into an electrical signal using a photo-diode. The phase of this electrical signal was then compared with the reference phase from the 1GHz modulator using a vector voltmeter. By measuring the change in this phase as the wavelength of the tunable source was changed, the time delay due to the dispersion could be calculated using $\Delta t = \delta\phi/2\pi\nu$ where $\delta\phi$ is the phase change and ν is the frequency (1GHz in this case). The dispersion could then be calculated by dividing the time delay by the product of the wavelength change and fibre length. An advantage of this technique was that the measurement process was computer controlled which made the set-up quick and easy to use. The speed of measurement was again important as fibre length changes due to environmental factors would lead to a phase change between the measured and reference electrical signals, indistinguishable from that caused by the dispersion leading to inaccuracies in the dispersion measurement. The wavelength range over which measurements could be performed using this technique were only limited by the tuning range of the source and again this range was sufficiently large to covered the entire $1.55\mu m$ window. Using a computer controlled tunable source gave a greater resolution with this technique. The wavelength step size typically being $\sim$0.1nm compared to $\sim$1nm with the previous method which allowed measurements to be made

over a smaller wavelength range with this technique. The main factor which determined the wavelength step size which was used was the wavelength range of the measurement or more precisely the time to perform the measurement– a measurement over 10nm with a 0.1nm step size required 100 data points each of which took $\sim$ 2sec to acquire. The stability against polarisation/length fluctuations of the set up therefore had to be assured for over 3 minutes to allow such an accurate measurement to be made.

The one major disadvantage of this technique was that in order to perform a dispersion measurement, the transmission fibre had to be removed from the loop and the dispersion of the entire loop could not be measured. The improved accuracy of this technique (the dispersion could be measured to $\sim \pm$ 0.01ps/(nm km)) made this worthwhile though time consuming. The two measurement techniques were often used in conjunction with this technique being used to give an accurate measure of the transmission fibre dispersion and the previous technique used as verification of the system dispersion once the transmission fibre was in position. Alternatively the dispersion could be measured roughly using the previous technique and the fibre length adjusted to give a good approximation to the required dispersion before fine tuning the fibre using this technique.

3.5 Summary

This chapter has introduced the operating principles of the recirculating loop and has highlighted the design considerations and the requirements of the various devices required to operate a recirculating loop. The limitations and problems associated with loop experiments in general and of using a single span loop in particular have been discussed. The methods used to monitor the loop's performance and to take propagation results have also been outlined. These techniques will be discussed in more detail where required.

Chapter 4

Soliton sources

4.1 Introduction

In the following chapters, which discuss various propagation experiments the pulse source is generally taken as being a "black box" which generates pulses as required. The purpose of this chapter is to describe in greater detail the characteristics of the various sources used. The basic operating principles are described and the advantages and disadvantages of each source are discussed.

In a commercial long haul propagation system it is obviously imperative that the pulse source is of the highest possible standard in terms of long term stability. Any decrease to the output power of the source as it ages will have a direct effect on the system performance and although it is easier to replace the source in a system than it is to replace an errant fibre section or an amplifier, the source should still be capable of operating continuously for 10s of years. Accelerated aging can predict how the performance of a source will degrade as time goes by and this information can be used when determining the system tolerance to effects such as decrease in average power. In a research environment these long lifetimes are not necessary but flexibility in terms of wavelength of operation and pulse width are desirable. It is also important that there is no change in the output power, pulse width, operating wavelength or repetition rate during the course of an experiment and so short term stability of the source is important. In order to allow repetition of experiments for verification of previous results and to allow different experiments to be performed with the same input pulses the source should not degrade over a period of weeks to months.

There are several additional factors which must be taken into consideration when assessing the performance of a source. The timing jitter of the source, the pulse width,

the wavelength tunability, the repetition rate and the chirp will have a bearing on the suitability of a source for a given experiment. The source requirements can also vary from one experiment to another. When working at high data rates (10's of Gbit/s) the source jitter becomes an important factor. At 10Gbit/s the maximum r.m.s. jitter which can be tolerated (given by Equation 2.64) is only ~5.5ps and a source jitter of 1ps can lead to a reduction in system length of ~13%. The output power of the source is also important. In soliton transmission experiments the peak power of the pulses which must be launched into the transmission is critical. The output power of the source must therefore be high enough to give this peak pulse power after the pulses have passed through all the optical components (which will all introduce losses) between the source and the transmission fibre. If the source power is too low then an amplifier must be used which will introduce additional noise to the source degrading the signal before transmission has even begun. As an example of the typical source power which is required consider a 10Gbit/s system using 10ps pulses and having a dispersion of 1ps/(nm km). For such a system the average soliton peak power would typically be 40mW which corresponds to an average power of ~4.5mW. Taking a loss of 6dB between the source and the transmission fibre implies that an average source power of 18mW would be required if no amplifier is used.

The data rate of experiments continues to increase with data rates of experiments now reaching 200Gbit/s [170] and so it is also necessary to increase the repetition rate of the source. It is however possible to increase the system data rate by optical time division multiplexing (OTDM) of the source. If soliton systems are to be used at such high data rates the pulse widths must be on the order of 1ps to ensure that soliton-soliton interactions do not limit the system length. The highest data rate which was used in the experiments performed for this thesis was 10Gbit/s and therefore pulse widths as high as ~20ps could be used. In order to be used as a research tool some flexibility in the source is a great asset – it is often desirable to perform the same experiment with different pulse widths, wavelengths or data rates and if a single source can be used without the need to carry out extensive reconfiguration then a great deal of time and trouble can be saved. This flexibility can be achieved by using a broadband source such as a fibre laser but the price which must be paid is that stability is compromised. As will be seen from the following sections, fibre lasers are far more difficult to operate than solid state devices such as a gain switched distributed feedback diode laser (DFB) from which a pulse stream can easily be obtained and maintained for extended periods of times. What advantages the gain switched DFB has in stability must be weighed up against the lack

of wavelength tunability that it gives and the fact that although it is capable of giving pulses with a few ps widths at 10s of Gbit/s data rates the pulses suffer from a severe chirp. Generally speaking a source which give transform limited pulses is preferable in a research environment. If chirped pulses are needed for a particular experiment then the chirp can be imposed on the source pulses as required.

The above discussion has shown that there are many things which must be considered when determining the ideal source parameters for a particular experiment. However even once the ideal source parameters have been determined the question of availability must be considered. The source for a required application may not be commercially available or may be too expensive to be considered and in such cases either compromise must be made in the choice of source or a source must be developed to suit. The four sources which were used in the experiments presented here all had their own specific advantages and limitation which will be discussed for each laser in turn.

4.2 FCL colour centre laser

In initial experiments a colour centre laser (shown schematically in Figure 4.1) was used as the pulse source. The laser gain medium was an F-colour centre NaCl:OH crystal. In

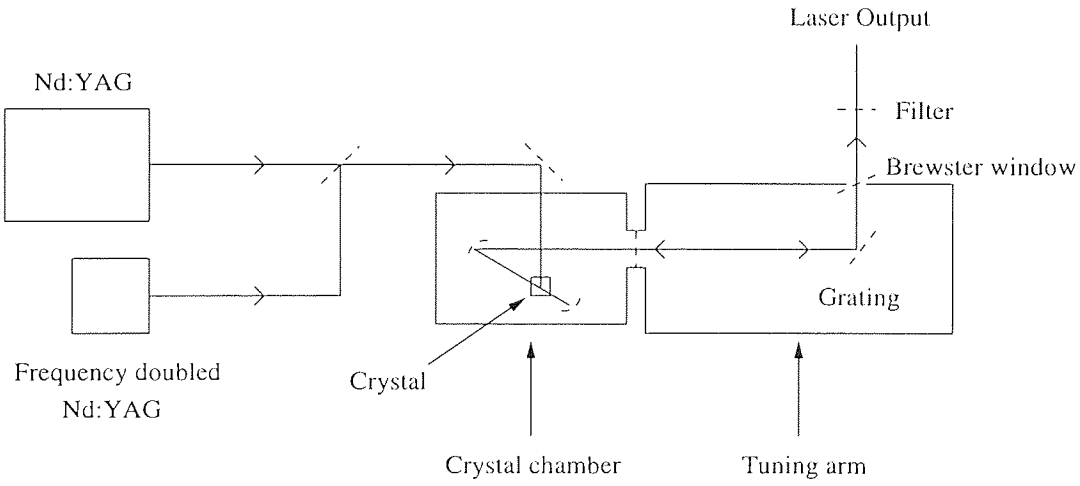

Figure 4.1: Schematic diagram of the F-centre laser. Co-linear Nd:YAG and frequency doubled Nd:YAG lasers were used to pump the laser crystal, which was kept at liquid nitrogen temperature in the crystal chamber. A grating in the tuning arm controlled the lasing wavelength. The laser output beam was filtered to remove the residual pump.

order for the colour centres to remain stable, the crystal had to be kept at low temperature and so the crystal chamber was liquid nitrogen cooled. The laser had an extended, folded cavity and was pumped by co-linear Nd:YAG and frequency doubled Nd:YAG laser beams. A pulsed output was obtained by mode-locking the Nd:YAG laser and altering the FCL

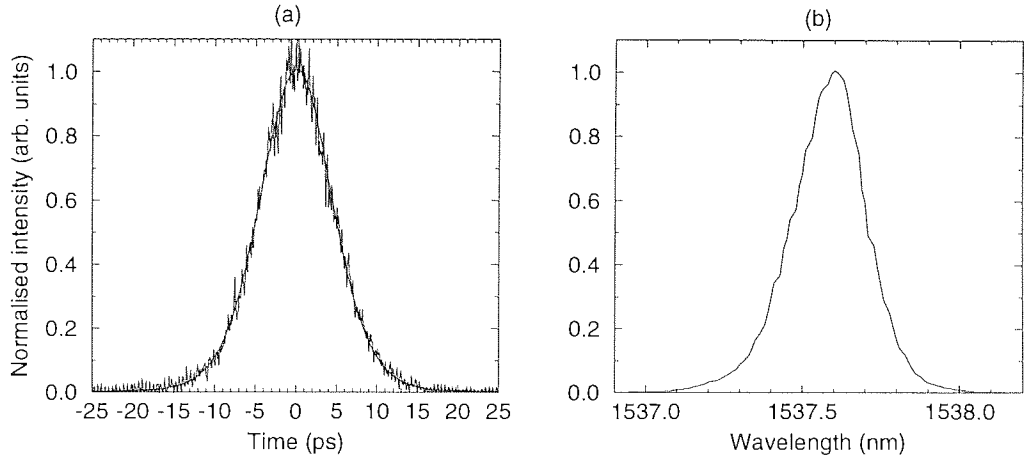

Figure 4.2: Measurements of (a) Pulse width (a $sech^2(t)$ fit is also shown) and (b) optical spectrum for the FCL laser. The pulse width was 10ps and the spectral width was 0.26nm.

laser cavity length to achieve synchronous mode-locking. To remove the residual pump beam from the laser output a filter was required after the laser output Brewster window.

Colour centre lasers have the advantages of being tunable, the tuning range depending on the type of colour centre crystal used. They also give a high output power near $sech^2(t)$ soliton output but they are notoriously temperamental - in order to achieve lasing the cavity mirrors, crystal orientation and pump beam orientations had to be carefully aligned and all optics cleaned, a process which could take several days. Once lasing was achieved it was still necessary to further fine tune the optics throughout the day as drifting of the mirror mounts due to thermal effects led to laser output power fluctuations. The output power also depended on the quality of the crystal being used but was typically greater then 100mW which was far in excess of that required for the soliton propagation experiments.

Figure 4.2 (a) shows an auto-correlation of the output pulses and a $sech^2(t)$ fit to the data. The pulse width was ~10.2ps and the pulses were a good approximation to $sech^2(t)$ in temporal profile. The optical spectrum of the FCL output with the laser tuned to 1537.5nm is shown in Figure 4.2 (b). The spectral width was 0.26nm giving a time bandwidth product $\delta\nu\delta t$ of 0.34 showing that the output pulses were close to transform limited $sech^2$ pulses. When mode-locked, the FCL operated at a repetition rate of 76MHz, the repetition rate being defined by that of the mode-locked Nd:YAG pump.

4.3 Figure of eight erbium fibre laser

The major problem which was encountered when using the FCL laser was the short term instability of the output power. The 76MHz repetition rate was also well below that required for propagation experiments and so a new laser was constructed. This laser was to operate at 1GHz and had greater stability than the FCL. A figure-of-eight configuration consisting of a main laser cavity and a nonlinear optical loop mirror (NOLM) as shown in Figure 4.3 was used.

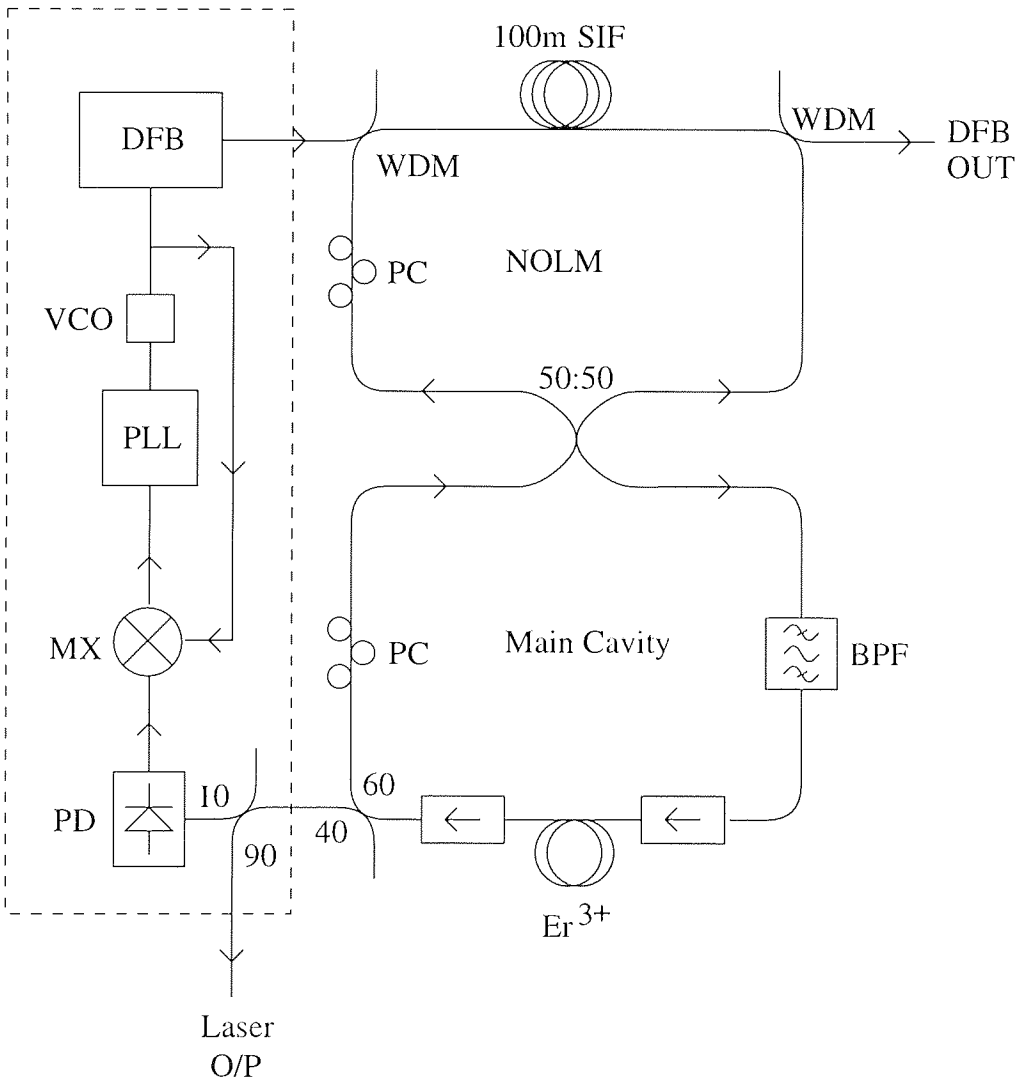

Figure 4.3: Schematic diagram of the figure of eight fibre laser. The laser consisted of two rings, the main laser cavity and a NOLM, connected by a 50:50 fibre coupler. The main cavity contained ~15m of $Er^{3}+$ doped fibre, a polarisation controller(PC) and a bandpass filter (BPF). The NOLM consisted of a PC and 100m of standard fibre (SIF). DFB control pulses were coupled in and out of the NOLM by WDMs. The control electronics for the DFB are shown within the dotted box.

The gain medium was a 15m length of Er^{3+} fibre which was pumped with a 980nm laser diode. The laser output was coupled from the main laser cavity into the NOLM using a 50:50 coupler to split the signal. Each of the two signals propagated in opposite directions round the NOLM and returned back at the coupler in coincidence. If these two

signals were in-phase, they were reflected by the NOLM but if they were out of phase they were transmitted [171]. This property of the NOLM allowed the laser to be mode-locked: by injecting a 1GHz gain switched DFB signal (see Section 4.5) at 1538nm into and out of the NOLM through a WDMs, the relative phases of the two counter propagating signals could be altered through the effect of XPM (see Section 2.6). The power of the DFB could then be adjusted to give full transmission of the fibre laser signal giving a synchronously mode-locked output. The DFB switching power required was ~40mW. The DFB itself was not used as a soliton source as the pulse width was 60ps which was longer than desired and also had a relatively high source jitter of ~8ps. A similar device which was used as a pulse source at 10GHz is described in Section 4.5.

Polarisation controllers were required in both the NOLM and the main cavity to optimise the mode-locking and isolators were required before and after the erbium doped fibre to increase stability. A tunable filter was included so that the laser wavelength could be controlled. This filter was positioned before the amplifier to give extra isolation from the 1538nm DFB signal. Although the laser could successfully be mode-locked by driving the DFB with a synthesiser at a fixed frequency, environmental factors caused long term instability – as room temperature changed the laser cavity and NOLM lengths changed and mode-locking drifted. It was therefore necessary to use active control to increase the laser stability. This was done using the electronics shown in Figure 4.3.

The DFB frequency was controlled using a voltage controlled oscillator (VCO). A VCO is a device which gives an output RF frequency which can be altered by changing the applied input voltage. The DFB frequency could therefore be altered to compensate for any drift of the laser cavity by adjusting the voltage to the VCO as required. When environmental effects caused the laser cavity length to change, the corresponding laser frequency change was detected by a photo-diode. The photo-diode output was then mixed with part of the VCO output to give an error signal which was a measure of the mismatch between these two frequencies. This error signal was then used as the input to a phase locked loop (PLL). The effect of the PLL was to adjust the VCO output so as to minimise the error signal i.e. it changed the voltage to the VCO such that the RF output frequency was kept equal to the laser frequency. Thus, the laser could be kept mode-locked for a period of hours and the stability was largely determined by the locking range of the PLL (~20MHz) and environmental conditions around the laser.

The laser was operated at ~1GHz and gave an output power of ~5mW. As Figure 4.4 (a) shows, the pulse width was 10ps and was a good approximation to $sech^2(t)$ in profile.

Since this was a soliton laser, the pulse width could be varied by altering the pump power as this varied the peak power of the soliton laser pulses. The pulse widths shown in Figure 4.4 correspond to the minimum pulse width.

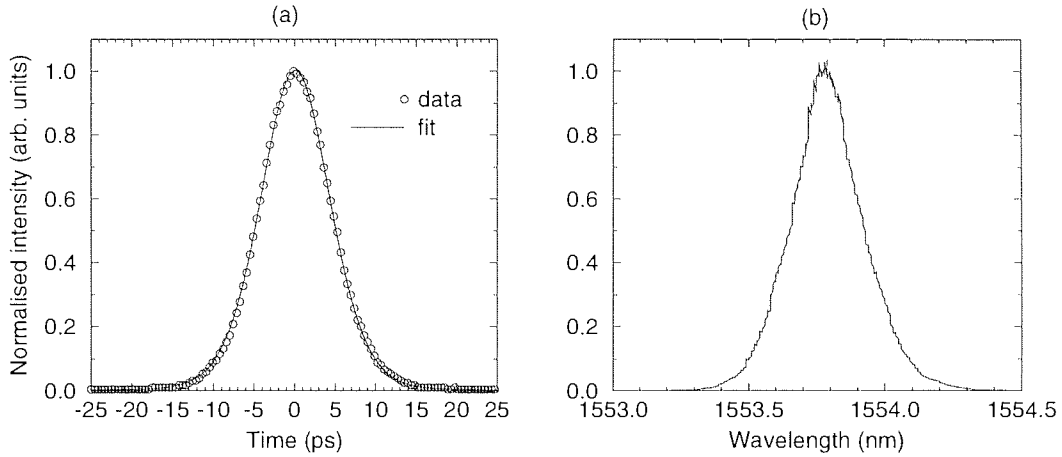

Figure 4.4: Measurements of (a) Pulse width (a $sech^2(t)$ fit is also shown) and (b) optical spectrum for the figure of eight laser. Pulse width was 10ps and the spectral width was 0.27nm.

Figure 4.4 (b) shows the optical spectrum of the laser, the spectral width was 0.27nm giving a time bandwidth product of 0.33 which indicates that as expected for this type of laser, the pulses were close to transform limited. The stability of this laser was much better than that of the FCL laser but it still required some degree of adjustment before a mode-locked output could be achieved with low jitter. When the laser was optimised the source jitter was typically 2ps which was a factor of 4 lower than the jitter of the DFB switching pulses. The repetition rate was liable to drift throughout the day but as long as a clock recovered trigger was used this did not have a great effect on experiments. The bit rate was also increased from 76MHz to a more useful value of 1GHz.

4.4 Fibre ring laser

Although the figure-of-eight laser was a far more reliable laser than the FCL, a further increase in stability and data rate was required. To achieve these aims a fibre ring laser which operated at 2.5GHz was developed. This laser was simpler than the figure-of-eight laser and had a smaller cavity which helped to increase the stability.

The laser is shown schematically in Figure 4.5. The gain medium was ~15m of Er^{3+} doped fibre which was reverse pumped by a 980nm diode laser diode. The pump light was coupled into the cavity through a WDM. After pumping the fibre the residual pump was coupled out of the cavity using a second WDM. Isolators were included before and after the

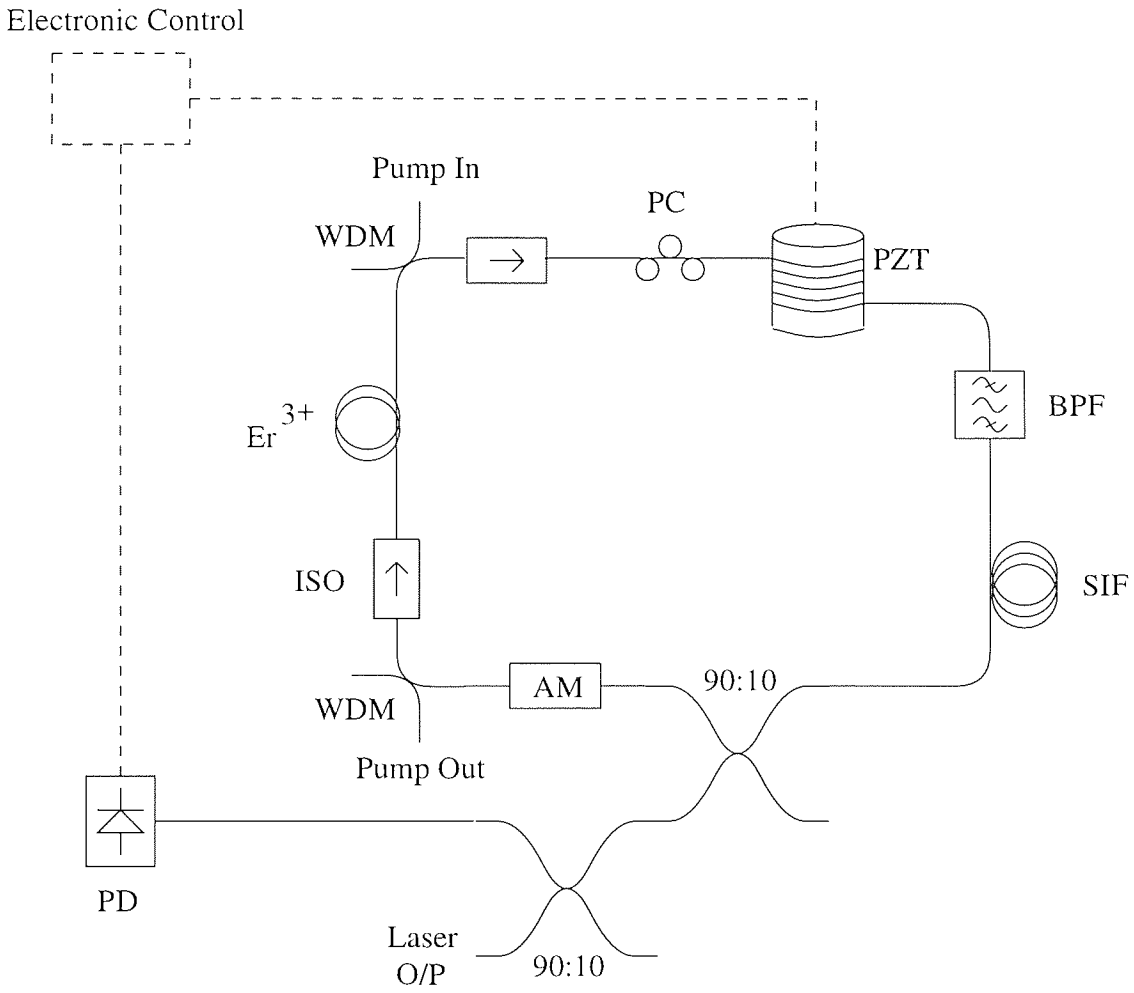

Figure 4.5: Schematic diagram of the fibre ring laser. The gain medium was ~15m of Er^3+ doped fibre. This fibre was reverse pumped by a 980nm pump diode. The cavity length was actively controlled using a piezo electric element (PZT) and control electronics. The laser was actively mode-locked using an amplitude modulator (AM) and could be wavelength tuned using a band-pass filter (BPF).

Er^{3+} fibre to increase the laser stability. A piezo-electric tube (PZT) was used to adjust the cavity length – a ~10m length of dispersion shifted fibre (DSF) was wrapped around the PZT (DSF was used as it has lower bend loss than standard fibre) and the diameter of the PZT could be altered to stretch the fibre by applying a voltage. Thus, the cavity length could be adjusted to counteract any thermal expansion or contraction by altering the voltage applied to the PZT as required. Cavity length changes led to corresponding changes in the laser output frequency and so by monitoring the laser output frequency using a photo-diode and minimising the difference between this frequency and the desired set-point frequency using an electronic feedback circuit to control the PZT voltage, the laser output frequency could be kept constant for a period of hours.

The laser was actively mode-locked at 2.5GHz using a lithium niobate amplitude modulator driven by a frequency synthesiser. A polarisation controller was required to optimise the mode-locked output and the wavelength could be altered using a tunable 3nm bandpass filter. When mode-locked, the output power of the laser was typically ~1mW.

The pulse width depended on the pump power and how well the laser mode-locking was optimised by altering the drive frequency and DC bias to the amplitude modulator and by altering the polarisation controller. The minimum pulse width was ~15ps and a typical value was 20ps. The output spectrum of the pulses was relatively invariant indicating that the chirp of the output pulses varied with pulse width. Typical laser outputs are shown in Figure 4.6. The auto-correlation shows a pulse width of 15ps and is again a

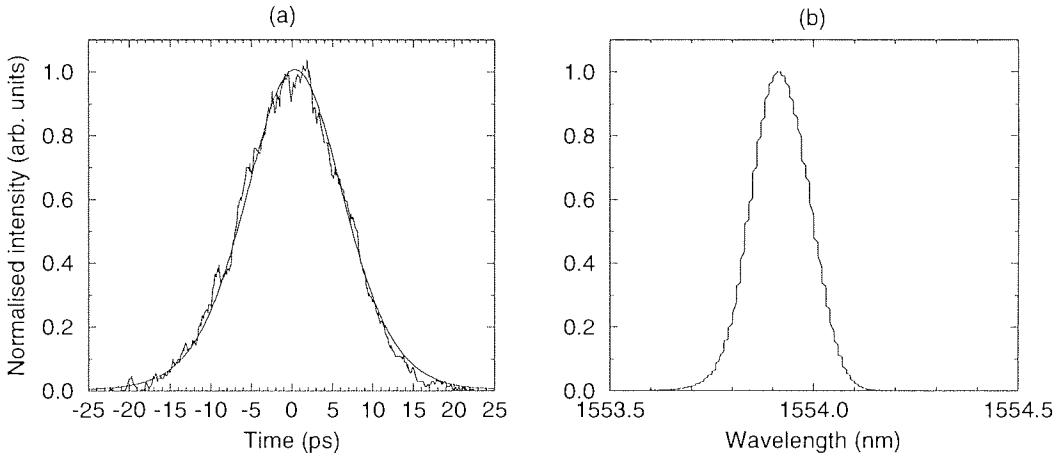

Figure 4.6: Measurements of (a) Pulse width (a $sech^2(t)$ fit is also shown) and (b) optical spectrum for the fibre ring laser laser. Pulse width was 15ps and the spectral width was 0.18nm.

good approximation to the $sech^2(t)$ fit. The spectral width was 0.18nm giving a time-bandwidth product of 0.33 showing that at this pulse width the pulses were very close to transform limited.

The operation of this laser was much more stable than the figure-8 laser due to the simpler configuration but the laser still required careful adjustments to initiate and optimise mode-locking and periodic readjustment throughout the day. Although the pulse width was greater than the figure of eight laser, the repetition rate was increased from 1GHz to 2.5GHz. A Mach Zehnder inter-leaver (described below) was also used with this laser in order to further increase the repetition rate to 10GHz.

4.4.1 Mach-Zehnder Inter-leaver

The technique of time division multiplexing narrow pulses to give a high data rate from a lower base rate is becoming common as the bit rate of experiments continues to increase. The design of the Mach-Zehnder inter-leaver which was used here to increase from the 2.5GHZ fibre laser repetition rate to 10GHz is shown schematically in Figure 4.7. The 2.5GHz pulse stream was first split by a 50:50 fibre coupler with one of the signals passing through a variable fibre stretcher (FS) which was used to give a variable optical delay. The

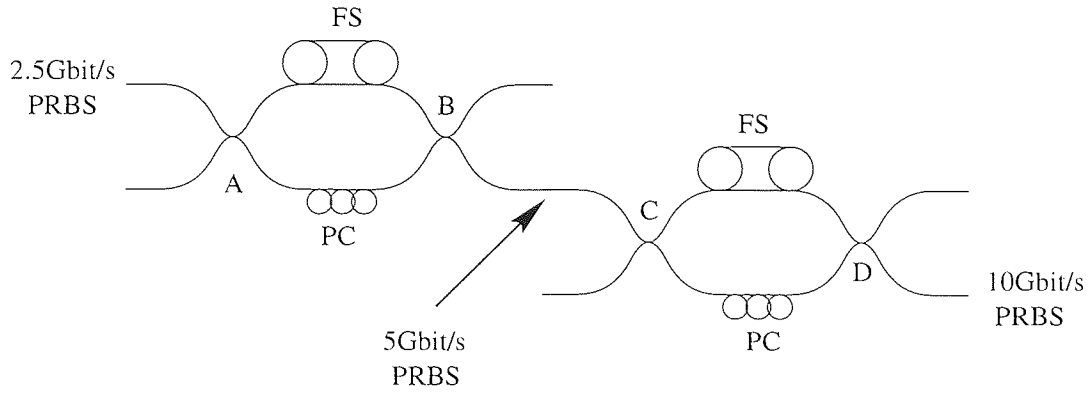

Figure 4.7: Schematic diagram of the double Mach-Zehnder inter-leaver. The 2.5Gbit/s PRBS was split at coupler A. One of the inter-leaver arms included an adjustable fibre stretcher (FS) to give the required delay, the other arm contained a polarisation controller (PC). Recombining at coupler B gave a 5Gbit/s which was then interleaved to 10Gbit/s. All couplers had a 50:50 splitting ratio.

other half of the signal was passed through a polarisation controller before the two data streams were re-combined. By adjusting the fibre stretcher to vary the optical delay to be a odd number of half bit periods, a 5GHz data stream was obtained at coupler B. The polarisation of the two interleaved data streams could be equalised using the polarisation controller. The process was then repeated to interleave from 5 to 10GHz. By passing this 10GHz pulse stream through a further polarisation controller followed by a fibre polariser, and with careful adjustment of the PCs, it was possible to achieve a 10GHz output at the fibre polariser output with equal amplitudes and polarisation of all the pulses, regardless of the path taken through the inter-leaver. In order that the inter-leaver could be used over a range of wavelengths, wavelength flattened couplers were used. Figure 4.8 shows the 2.5GHz fibre laser pulse stream and the inter-leaver output at 5GHz and 10GHz. The inter-leaver output was amplified to give the same intensity of pulses from the 2.5GHz, 5GHz and 10GHz outputs to make comparison easier. On the 2.5GHz and 5GHz outputs the ripple on the base line is due to ringing of the photo-diode used to convert the optical signal to an electrical signal. As shown it was possible to obtain a good 10GHz output with all pulse heights the same and with equal spacing between the interleaved pulses. Autocorrelations of the interleaved and fibre laser pulses showed that there was no change in the pulse width after interleaving. In this experiment the pulse width remained at 24ps throughout. Interleaving did however introduce an additional timing jitter due to small variations in the temporal position of the pulses in the interleaved stream relative to one another, these temporal shifts being due to small random path length changes in one or all paths through the inter-leaver. These jitters led to degradation of the Q value. From a typical Q of ~18 for the 2.5Gbit/s data stream the 10Gbit/s Q was reduced to ~14.

Typically, a 10Gbit/s data stream was required as the loop output. There were two

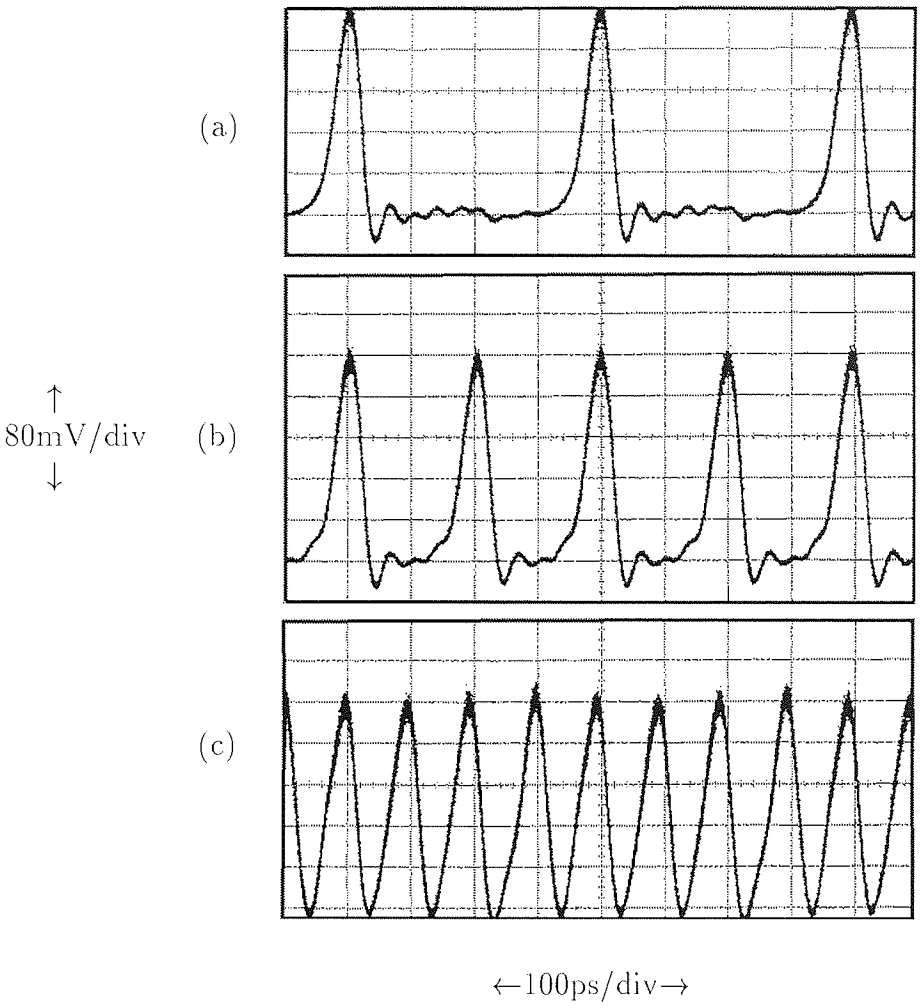

Figure 4.8: Sampling scope screen captures showing (a) the fibre laser 2.5GHz pulse stream, (b) the inter-leaver output at 5GHz and (c) the inter-leaver output at 10GHz

ways of deriving such a data stream, the data could either be imposed on the pulse stream at 2.5Gbit/s before interleaving or at 10Gbit/s after interleaving. This choice was dictated by the availability of equipment - a 10Gbit/s pattern generator was not permanently available and so the inter-leaver had, generally, to be used with a 2.5Gbit/s PRBS input. Indeed, had a 10Gbit/s pattern generator been available, there would have been little need for the inter-leaver, the laser itself would simply have been optimised for use at 10GHz and the data imposed on the laser output. A further practical consideration was the performance of the lithium niobate modulator used to impose the data pattern on the bit stream. This device performed considerably better at 2.5Gbit/s than at 10Gbit/s with the voltage driver available which indicated that operating at 2.5Gbit/s was preferable. The situation was however complicated by the fact that there was a degradation of the data stream on interleaving and there was not a great difference in the back to back system performances when the data was imposed on the pulse stream before and after

interleaving.

So that patterning effects associated with the interleaving did not cause problems or enhance the results when the data was imposed at 2.5Gbit/s, it was necessary to have a fairly large optical delay between the two signals before they were re-combined. This was achieved in practice by using a $\sim$ 10m length of fibre in the fibre stretcher stages which provided the variable optical delay. This length of fibre allowed a variation in the optical delay of $\sim$500ps which is 5 bit intervals at 10Gbit/s. After re-combination and equalisation of the polarisations the 10Gbit/s data stream was not a true but PRBS - all pulses were derived from the same PRBS and each fourth pulse was in PRBS order but adjacent pulses came from different sections of the 2.5Gbit/s PRBS. The inter-leaver output was however a random sequence of ones and zeros.

Apart from the obvious problem of the degradation of the data stream caused by the inter-leaver there was also a large insertion loss of 7dB. The majority of this loss was in the portion of the signal rejected at couplers B and D but there was also some loss in the polarisation controllers, fibre stretchers and in the PC/FC connectors used. This high loss meant that an additional amplifier was required before the recirculating loop input.

4.5 Gain switched DFB laser

In commercial telecommunication systems solid state semiconductor lasers are used as the pulse sources. Unlike fibre lasers which require active cavity length and polarisation control, solid state devices require only electrical drive and temperature control making them easy to use. In addition they are compact and are extremely reliable with long lifetimes if properly used. This section describes such a device, a DFB laser which was gain switched and used in propagation experiments.

In order to achieve a pulsed output from the DFB, a DC bias and an RF drive have to be applied. The DC current was such that the laser was kept just below the lasing threshold, then when an RF of the required power was applied the laser current was taken above the threshold current once within each period of the RF cycle leading to a pulsed laser output at the applied RF frequency. The DFB was generally operated at 10GHz, was simple to control and had an output extremely stable output power. There was however one major problem, which is inherent with gain switched DFB lasers - the output was severely chirped and so the output pulses were not time bandwidth limited solitons. Figure 4.9 shows an autocorrelation and spectrum of the DFB output when gain

switched at 10GHz and also for CW operation.

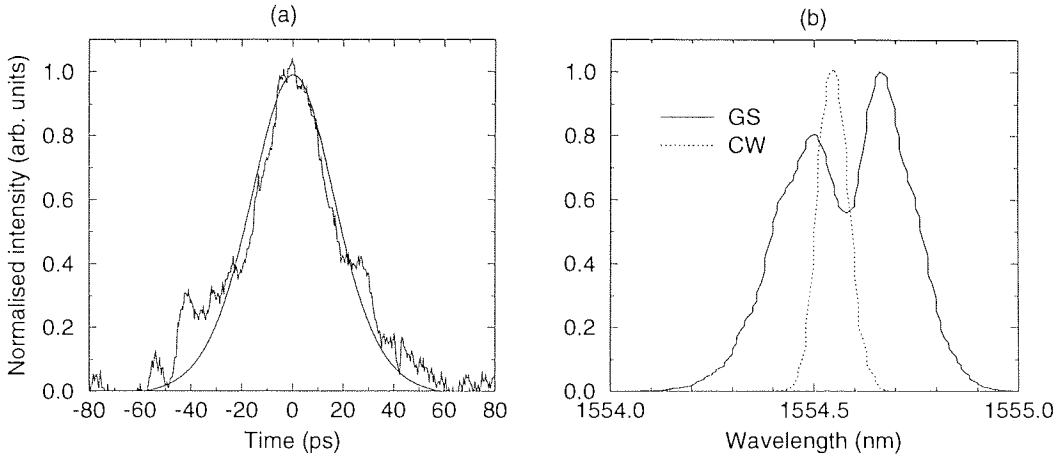

Figure 4.9: Measurements of (a) Pulse width (a $sech^2(t)$ fit is also shown) and (b) optical spectrum for the DFB laser. The spectrum is shown with the laser gain switched at 10GHz (GS) and for a CW output. When gain switched, the pulse width was 45ps and the spectrum showed double peaks. The spectral width was 0.1nm for a CW output

When gain switched, the pulse width was 45ps and as shown, the spectrum had two peaks at 1554.5nm and 1554.7nm. These two peaks are due to different modes of the device lasing. The 0.2nm wavelength spacing of the modes corresponds to a cavity length of $\sim$ 3mm. Changing the DC bias and RF power led to a slight change in the pulse width but the spectrum still retained the double peaked structure shown. The central wavelength of the laser could be altered over a $\sim$ 1nm range by temperature tuning and by altering the DC bias.

Taking the spectral width to be 0.37nm gives a time bandwidth product $\Delta\nu\Delta t$= 2 and the pulses were severely chirped. A common technique used to reduce the chirp of DFB lasers is to pass the DFB output pulses through a length of fibre or a grating which has the opposite sign of chirp and hence can compress the laser pulses. This was tried with various lengths of DCF in order to try and optimise the compression of the DFB pulses and using a 400m length of fibre with a dispersion of -92ps/(nm km) gave the pulse width and spectrum shown in Figure 4.10 The pulses were compressed from 45ps to 20ps but a pedestal remained which is typical of DFB outputs. There was no change to the spectrum of the laser pulses as the chirp was undone and the double peaked spectrum remained. This led to difficulty in measuring the spectral width. Taking the spectral width as being the width at half the maximum intensity of the full spectrum of both peaks – 0.36nm in this case, gave a time bandwidth product, $\delta\nu\delta t$, of 0.89. This is far in excess of the time bandwidth limited value of 0.32 for $sech^2(t)$ pulses and is mainly due to the double peaked nature of the spectrum of the gain switched DFB. The two peaks in the spectrum

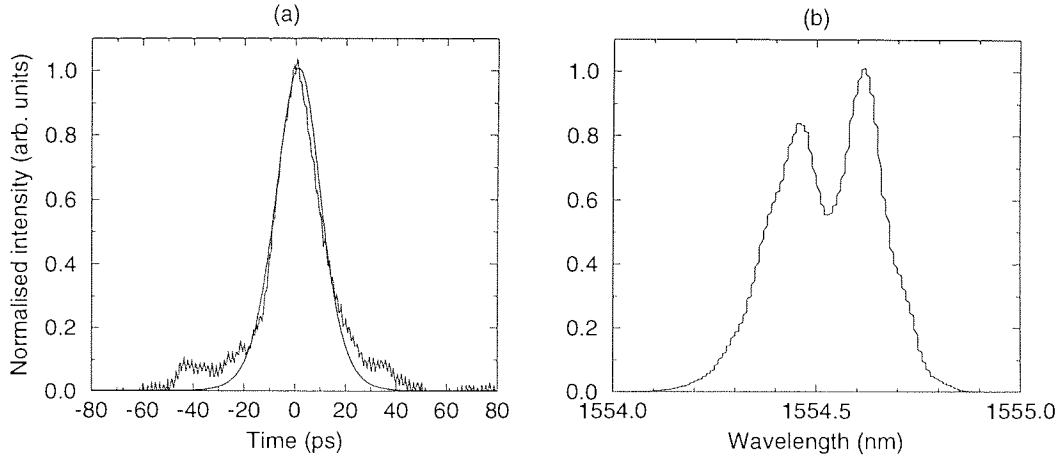

Figure 4.10: Measurements of (a) Pulse width (a $sech^2(t)$ fit is also shown) and (b) optical spectrum for the DFB laser with optimum DCF pulse compression. Pulse width was 20ps and again, the spectrum had two peaks.

present a significant problem if this source is to be used for propagation because dispersive broadening would lead to pulse break-up. The wavelength separation of the two peaks was 0.2nm and even at a low dispersion of 0.1ps/(nm km) the relative delay across the pulse would be equal to one 10Gbit/s bit interval after 5000km of propagation. This problem is magnified if a large dispersion is used. In standard fibre which has a dispersion of ~16.5ps/(nm km) a propagation of only 30km would be required to give a delay of 100ps. In a dispersion managed system where the local dispersion can be high despite having a low average dispersion, severe distortion of the pulses could occur. To show this effect the pulses from the DFB were passed through various fibre lengths and combinations. The DFB output was amplified and the power launched into the fibre was varied by adjusting the gain of the pre-amplifier so that the power at the fibre output was the same for all fibre lengths. The output power was chosen to be that of an average soliton launched into a system with an average dispersion of ~0.15ps/(nm km) for reasons which will become clear. Autocorrelations and optical spectra were taken of the output pulses. There was no change to the spectrum of the pulses when the transmission fibre was altered but the autocorrelations varied greatly. Figure 4.11 shows the autocorrelations scaled to show the actual pulse widths assuming a $sech^2$ pulse shape for - (a) the input pulses, which were a good approximation to $sech^2$ in profile although the pulse had a pedestal. The pulse width was ~16ps. Figure 4.11 (b) - (d) show the pulses after propagation through 12, 25 and 32km of SIF respectively. It is clearly seen that after propagation through 12km of SIF there was a large distortion to the pulses. When the propagation distance was increased to 25km three peaks were seen in the autocorrelation due to the pulse beginning to split. After propagation through 32km of SIF the three peaks were well

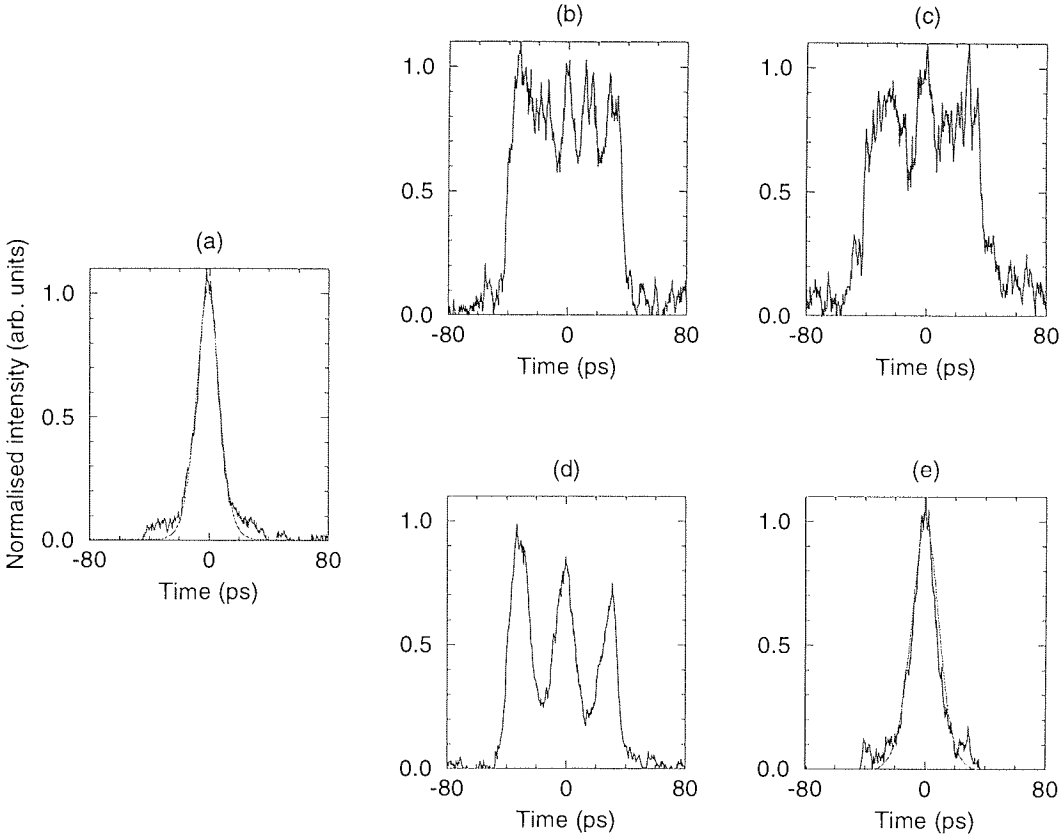

Figure 4.11: Pulse widths and shapes taken from autocorrelations of (a) the DFB input pulses and the pulse outputs after propagating these pulses through (b) 12km of SIF, (c) 25km of SIF and (d) 32km of SIF. (e) shows the pulses after propagating through 32km of SIF and 6.8km of DCF. $sech^2$ fits are also shown for cases (a) and (e).

resolved and the pulse had split into two distinct and separate pulses. Figure 4.11 (e) shows the autocorrelation of the pulses after propagation through 32km of SIF and 6.8km of DCF. This combination gave an average dispersion of 0.15ps/(nm km) and as can be seen the pulse splitting which occured after propagation through the SIF was reversed in the normally dispersive DCF and at the output of this fibre a single pulse was again seen, albeit with an increased width of ~21ps. The increase in the pulse width was due to the dispersion compensation not being complete – the average dispersion was not zero. It is possible that the interaction of the two pulses led to a shift in their relative temporal positions, the interaction is analogous to the interaction experienced by different channels in WDM systems where different wavelengths are used to carry different data channels. The experiment was repeated with the fibre ring laser described in Section 4.4 used as the source. The output spectrum of this laser (shown in Figure 4.6) indicated that the laser operated on a single transverse mode. Again there was no change to the spectrum of the pulses but the autocorrelation changed significantly as the transmission fibre was altered. Figure 4.12 (a) shows the autocorrelations of the input pulses. The pulse width was ~17ps and the spectral width was 0.18nm giving a time bandwidth product of 0.38

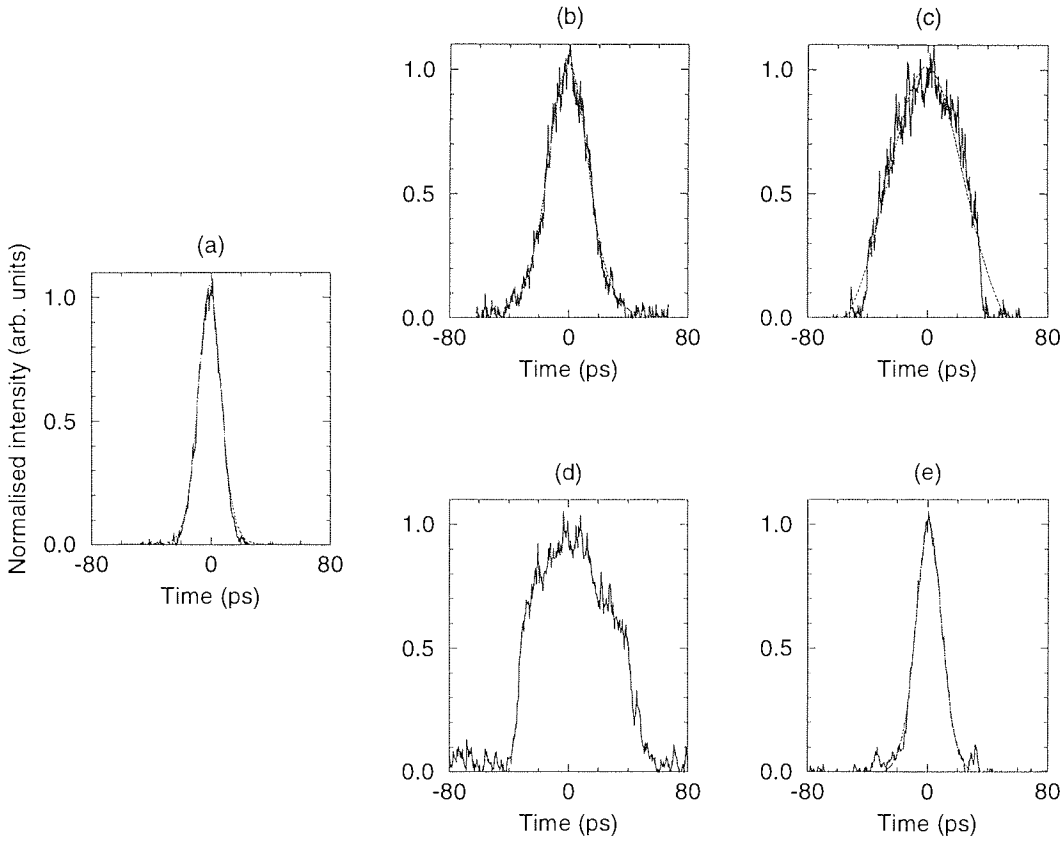

Figure 4.12: Pulse widths and shapes taken from autocorrelations of (a) the fibre laser input pulses, the pulse outputs after propagating these pulses through (b) 12km of SIF, (c) 25km of SIF and (d) 32km of SIF. (e) shows the pulses after propagating through 32km of SIF and 6.8km of DCF. $sech^2$ fits are also shown.

which indicates that the pulses were slightly chirped. Figure 4.12 (b) - (d) show the autocorrelations after propagation through 12, 25 and 32km of standard fibre. These results show that as the signal propagated there was an increase in the pulse width due to the dispersion but as expected there was no pulse splitting. Figure 4.12 (e) shows the autocorrelation after propagation through 323km of SIF and the same DCF as was used for the DFB laser. There was again a re-compression of the pulses in the DCF and the pulse width at the output of this fibre was ~20ps.

The pulse splitting which was seen with the DFB laser was a problem which was likely to severely reduce the performance which could have been achieved had a single transverse mode output been possible. Even if a single transverse mode DFB had been available there would still have been a problem with the output pulses being chirped but as has been shown above it is possible to compress chirped DFB pulses using appropriate fibre.

This section has shown that despite the undoubted advantages of stability, size and ease of operation, DFB lasers still present problems in that their output pulses are not ideal for use in soliton propagation experiments. The output power of the device tested here was also relatively low at $\sim 500\ \mu W$ and so large gain amplification would be required

for the laser output to achieve the required average power for propagation experiments. A further problem is that the tuning range was narrow and while this is not a problem in a real system where the wavelength of operation is fixed, increased tune-ability is advantageous in a research environment as different experiments may require different source wavelengths.

4.6 Conclusions

There are several factors which must be considered when choosing or developing a source for high speed soliton transmission experiments. At high data rates the source jitter must be low and the pulse width must be small. At a 10Gbit/s data rate a mark to space ratio of 1:5 (which is typically the lowest that can be used before soliton interactions severely limit the transmission length) requires 20ps pulses. This pulse width can be easily achieved using a broadband laser gain medium such as erbium but as data rates continue to increase the pulse width of the source must be reduced without degrading other source characteristics such as pulse shape, chirp and jitter. In order to achieve repetition rates above 10GHz the main problem which is encountered is that the high speed electronics required to give the necessary modulation of the gain medium, are not readily available. In order to achieve state of the art bit rates of 100Gbit/s or above it is therefore necessary to have a source working at a lower repetition rate and interleave the pulses to give the desired rate [13, 170, 172, 173, 174]. Although the base repetition rate of the source may only be 10 or 20GHz the pulse width must be as required at the final bit rate. The mark to space ratio of the source must therefore be high without the source jitter being significant.

In addition to working at the required repetition rate with low jitter and with the required pulse width the shape and chirp of the pulses is also important – particularly for use in dispersion managed systems. Unchirped $sech^2$ pulses are generally desired – if chirped pulses are required the chirp can be imposed on these transform limited pulses by propagating through a suitable fibre or grating. The laser must also be capable of providing the pulses for extended periods of time (several hours) with no drift in the characteristics. The output power of the source must also be considered. A pre-amplifier is generally needed in transmission experiments and if a source has lower power it requires higher gain amplification which introduces more noise.

Easy operation is not critical as long as the source remains stable for an extended

period of time – if the quality of the pulses is sufficiently high the extra effort to achieve this output is worthwhile. As an example the fibre laser and gain switched DFB laser described above can be compared. The fibre laser had to be interleaved to achieve a 10GHz rate. It also required polarisation and active cavity length control in order to achieve a stable output but for this effort a near transform limited $sech^2$ output which could be wavelength tuned over the entire erbium fluorescence spectrum was obtained. In contrast the gain switched DFB was extremely stable over extended periods of time and was simple to operate – an RF and DC bias had to be applied along with temperature control. However the output pulses were severely chirped, the tuning range was small and the spectrum was double peaked. In order to get close to transform limited pulses it was necessary to propagate the pulses through a suitable dispersive element. The dual wavelength operation caused problems in transmission as pulse splitting could occur because of the fibre dispersion. This problem can be solved by making the device lase on a single cavity mode but the problem of source chirp remains. In the experiments described in Chapter 7 the system performed better using the fibre laser than the DFB laser and therefore it was the worth the extra effort that was required to keep the laser stable to achieve the results. It should be stressed that this consideration only applies in a research scenario. In a real system the source must operate with the minimum amount of active control and must work over many years. For such applications fibre lasers are unsuitable.

It is also true that the required source characteristics vary from experiment to experiment and therefore flexibility is also an advantage. It also means that there is no single source which can be universally used and work will continue to be done on developing new sources for telecommunications applications.

Chapter 5

Soliton-like pulse propagation over ultra long distances close to the dispersion zero wavelength

5.1 Introduction

In order to increase the data rate and system lengths which can be achieved in soliton transmission experiments a low dispersion is required to increase the Gordon-Haus limit [47]. However the soliton power is proportional to the dispersion and so a limit is put on how low a dispersion can be used before the signal to noise ratio becomes too low to allow propagation over 1000s of km. This is one reason why there is interest in dispersion managed systems, which give an enhancement of the stable pulse power compared to the equivalent uniform dispersion system [98, 92]. This allows the dispersion of the system to be reduced further before SNR problems are encountered. As will be discussed in Chapter 7, there is currently a great deal of interest in using dispersion management to allow a low average dispersion value to be used [12],[86]-[98],[115, 116, 117] and work is also being done to compare the performance of RZ, soliton and NRZ systems where the average dispersion is low [12, 157, 175, 176]. This chapter investigates soliton-like RZ pulse propagation in a dispersion managed system where the average dispersion was at or close to zero. In order for conventional solitons to propagate the dispersion must be finite and anomalous, at the dispersion zero there will be no first order GVD effects and SPM can lead to break up of the pulse. At λ_0 a further nonlinear effect, four-wave mixing, can become significant as the required phase matching conditions can be met [6]. Four wave mixing leads to the generation of additional frequencies up-shifted and down-

shifted from the signal frequency leading to transfer of energy from the signal. Stable propagation of pulses at λ_0 therefore requires that these processes are counteracted by some pulse control technique before the perturbations to the pulse become too great. The experiments described here show how stable pulse propagation was achieved close to the zero dispersion wavelength over astonishingly long distances (greater than one million kilometres) without active control. It is not certain what the pulse control mechanism was but the saturable absorber effect of nonlinear polarisation rotation is a likely candidate and will be investigated.

5.2 Saturable absorption and nonlinear polarisation rotation

Saturable absorbers have been used as pulse shapers to generate ultra-short pulses in passively mode-locked of lasers for some time [177, 178, 179]. The principle of their operation is that the saturable absorber is opaque for low incident optical intensities but the device becomes bleached at some critical intensity and then becomes transparent. An important characteristic of a saturable absorber is the recovery time i.e. the time for which the device remains transparent after being bleached.

In laser cavities ultra-short pulses can be formed if a saturable absorber is included since the low intensity leading edge of the pulse will be absorbed up to the point where the device becomes transparent. Pulse shaping can also occur at the trailing edge of the pulse but this depends on the temporal width of the pulse and the recovery time of the saturable absorber. In order to generate pulses it the femtosecond regime it is therefore necessary to use a fast saturable absorber. In relation to transmission systems saturable absorbers can be used to discriminate between the low intensity noise and the high intensity signal. For such applications the recovery time of the saturable absorber must be shorter than the bit period (100ps at 10Gbit/s) and the switching power required to bleach the device must be comparable with the signal pulse power. Multiple quantum well saturable absorbers have been proposed to fulfil this role [78] but these devices suffer from a slow recovery time and a high switching power [79]. A second solution is to use nonlinear polarisation rotation in conjunction with a polarisation discriminating element.

As described in Section 2.6 two signals propagating in the same fibre with the same frequency but different polarisation states can interact with each other through the effect of cross phase modulation (XPM). Due to deviations from a perfect cylindrical geometry

optical fibre generally has a birefringence which leads to two orthogonal polarisation states which have different propagation constants and hence different group velocities. Due to this difference in the group velocities of the two polarisation axes they are referred to as the fast and slow axes. A signal which is launched into a fibre at an angle θ to the fast axis of the fibre will have electric field components

$$E_x = Ecos\theta \tag{5.1}$$

$$E_y = Esin\theta \tag{5.2}$$

along the fast and slow axes respectively. Through the effect of XPM these two components can interact leading to a nonlinear refractive index change given by (see Section 2.6)

$$\Delta n_x = n_2\left(|E_x|^2 + \frac{2}{3}|E_y|^2\right) \tag{5.3}$$

$$\Delta n_y = n_2\left(|E_y|^2 + \frac{2}{3}|E_x|^2\right). \tag{5.4}$$

This leads to coupling of the two polarisation states which can then be described by the two coupled Schrödinger equations

$$\frac{\partial A_x}{\partial Z} + \beta_{1x}\frac{\partial A_x}{\partial t} + \frac{i}{2}\beta_2\frac{\partial^2 A_x}{\partial t^2} + \frac{\alpha}{2}A_x = i\gamma\left[|A_x|^2 + \frac{2}{3}|A_y|^2\right]A_x \tag{5.5}$$

$$\frac{\partial A_y}{\partial Z} + \beta_{1y}\frac{\partial A_y}{\partial t} + \frac{i}{2}\beta_2\frac{\partial^2 A_y}{\partial t^2} + \frac{\alpha}{2}A_y = i\gamma\left[|A_y|^2 + \frac{2}{3}|A_x|^2\right]A_y \tag{5.6}$$

where it is assumed that the fibre is linearly birefringent and the effect of nonlinear mixing between the two polarisation states is neglected [6] pp179. The coupling of the two field components E_x and E_y causes a nonlinear birefringence which in turn causes the polarisation state of the input light to change as it propagates along the fibre. This effect is known as nonlinear polarisation rotation (NPR) since the rate of polarisation rotation depends on the intensities E_x and E_y. This also means that NPR depends on the angle that the light is launched into the fibre because for a fixed total field E, the components E_x and E_y vary as the launch angle θ is changed.

A saturable absorption effect can be achieved if a signal is propagated along a length of fibre followed by a polarisation discriminating element. The signal power, fibre length and/or polariser orientation can be altered so that the polarisation state of the high intensity signal is aligned with the polariser. Any noise in the system having lower intensity than the signal would not have undergone the same degree of polarisation rotation and

so would be absorbed at the polariser. In the case where the polariser was orthogonal to the input polarisation, the power after the polariser P_{out} is given by [180]

$$P_{out} = P_{in} sin^2(2\theta) sin^2(\frac{\Delta\phi}{2}) \tag{5.7}$$

where P_{in} is the power at the polariser input and $\Delta\phi$ is the phase difference between E_x and E_y given by

$$\Delta\phi = \frac{2\pi Z}{\lambda}\frac{n_2}{3}\left[|E_y^2| - |E_x^2|\right]. \tag{5.8}$$

The power out of the polariser therefore depends on the angle at which the signal is launched into the fibre and also on the length of fibre which is used, through the Z dependence of $\Delta\phi$. The dependence of P_{out} on P_{in} is more complicated than the simple linear dependence given in Equation 5.7 due to the dependence of E_x and E_y (which are contained in the expression for $\Delta\phi$) on P_{in}. Figure 5.1 shows P_{out} as the input power was varied in a numerical simulation for a 26km fibre length with a dispersion of 0.1ps/ (nm km) at the operating wavelength of 1.55μm. The value of n_2 was taken as $2.5x10^{-20}m^2W^{-1}$ and the signal was launched at $\theta = 35°$. For simplicity the effect of loss was neglected in this simulation and the polariser was taken to have 100% transmissivity for one polarisation state and 0% for the orthogonal state. This curve shows that switching

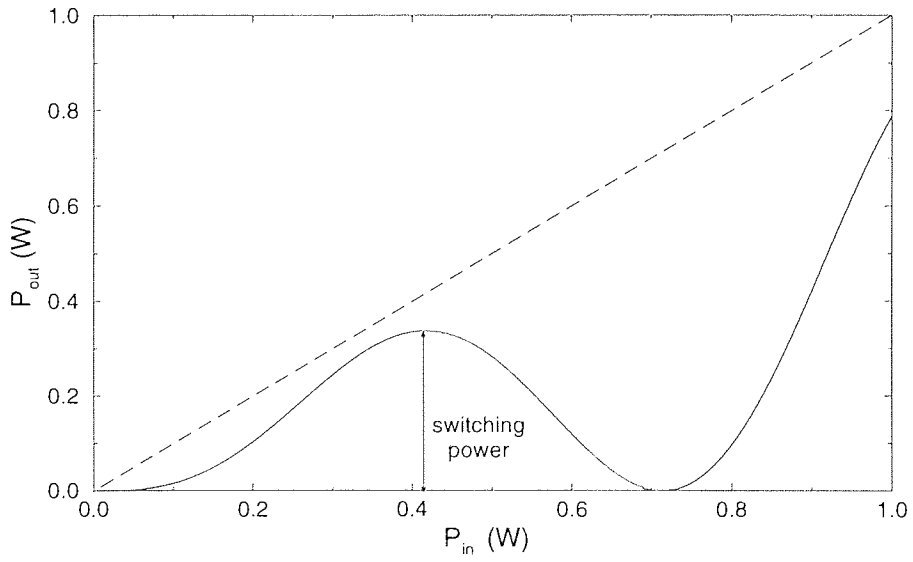

Figure 5.1: Switching curve for a NPR saturable absorber with the signal launched at 35° to the fibre axis. The fibre length was 26km.

is achieved at a power of $\sim$ 0.41W but this switching is not complete. The periodicity of the graph was determined by the $sin^2(\frac{\Delta\phi}{2})$ term in Equation 5.7. There was also a strong

dependence on the launch angle θ as this altered both the efficiency of the switching due to the $sin^2(2\theta)$ term and also the periodicity as θ alters E_x and E_y and hence $\Delta\phi$. By referring to Equation 5.7 it is seen that if the signal is launched along one of the axes of the fibre ($\theta = 0, 90^o$) then $P_{out} = 0$. This is because when light is launched along one of the axes of the fibre there is only one polarisation state and hence no XPM. A more interesting case is when the light is launched at 45^o to the axes. At first glance it appears from Equation 5.7 that this should give complete switching as the $sin^2(2\theta)$ term is equal to unity but for $\theta = 45^o$ $|E_x|$ and $|E_y|$ are equal and so the output power is equal to zero. In a real non-polarisation preserving fibre the orientation of the axes varies randomly along the fibre length and so it is highly unlikely that any of these three cases could be observed.

In relation to soliton transmission systems this effect can be used to reduce the noise level, leaving the soliton intact – a fundamental soliton undergoes NPR as a unit [44] and also has a uniform polarisation across the entire pulse [8] so there would be no pulse shape distortion at the polariser. In such a system fibre length would be fixed and so the switching power of the saturable absorber would have to be matched to the soliton power by altering the polarisation state of the light launched into the fibre

For pulses other than fundamental solitons there can also be a pulse shaping/spectral filtering effect. After a pulse is propagated along a fibre there will generally be a polarisation difference across the pulse when it reaches the polariser due to the intensity profile of the pulse giving different degrees of NPR. If the polariser is then set so as to allow the peak of the pulse to be transmitted with minimal attenuation then the leading and trailing edges of the pulses will suffer a greater loss at the polariser. In addition if the pulse is chirped on arrival at the polariser then the leading/trailing edge of the pulse will be red/blue shifted depending on the dispersion of the fibre and so there can also be a spectral filtering effect at the polariser.

5.3 76MHz Experiment

The experimental set-up is shown schematically in Figure 5.2. The transmission was performed using the recirculating loop which was described in Chapter 3. The pulse source used was the colour centre laser described in Section 4.2 operating at 76MHz. The width of the pulses from this laser was 9.5ps and as shown in Figure 5.3 (a) they were a good approximation to $sech^2(t)$ in profile. The spectral width of the FCL pulses

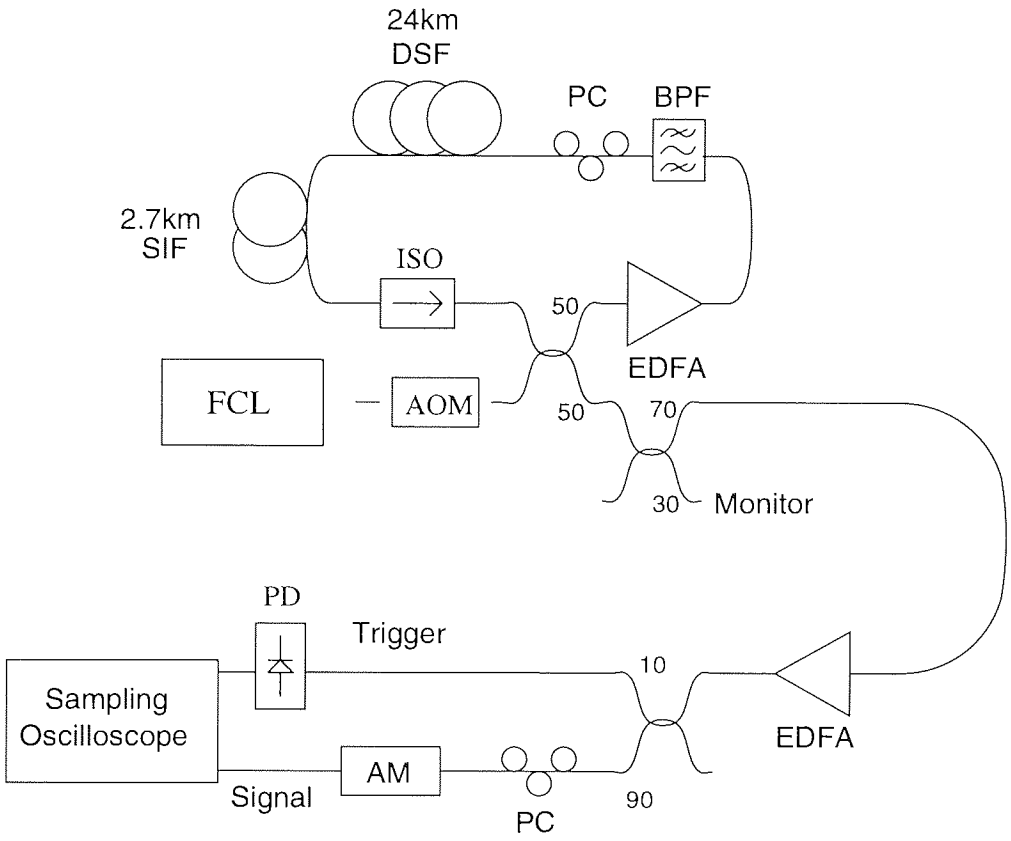

Figure 5.2: FCL pulses were propagated in the recirculating loop which contained an EDFA, a band-pass filter (BPF), a PC and an isolator (ISO). The transmission fibre was 23.7km of DSF and 2.7km of SIF. The loop output was gated by an amplitude modulator to allow jitter measurements to be taken.

was 0.27nm (see Figure 5.6 (a)) giving a time-bandwidth product $\delta\nu\delta\tau = 0.32$ which is the transform limited value for $sech^2(t)$ pulses indicating that the input pulses were not chirped. The pulses were gated into the loop using an AOM and a fibre coupler with a 50:50 splitting ratio. A tunable filter with a 3nm pass-band was included to give suppression on the ASE level, this filter also had a polarisation dependent loss of $\sim$ 2dB at the operating wavelength and was the main polarisation discriminating element in the loop. A polarisation controller (PC) was used to set the polarisation state of the signal launched into the transmission fibre. The loop output was split using a 70:30 fibre coupler to give a continuous monitor output before being amplified to give the output signal and trigger. The continuous monitor output was used to observe changes in the average power as the signal was propagating in the loop.

The transmission fibre in the loop was 23.7km of DSF with $\lambda_0 \sim$ 1560nm and 2.7km of SIF which was used to reduce λ_0. The dispersion of this fibre combination was measured using the technique described in Section 3.4.1 and as the result in Figure 5.4 shows, the dispersion zero was reduced to $\sim$1536nm by the inclusion of the SIF.

It was discovered that by carefully adjusting the tunable filter in the loop, altering the

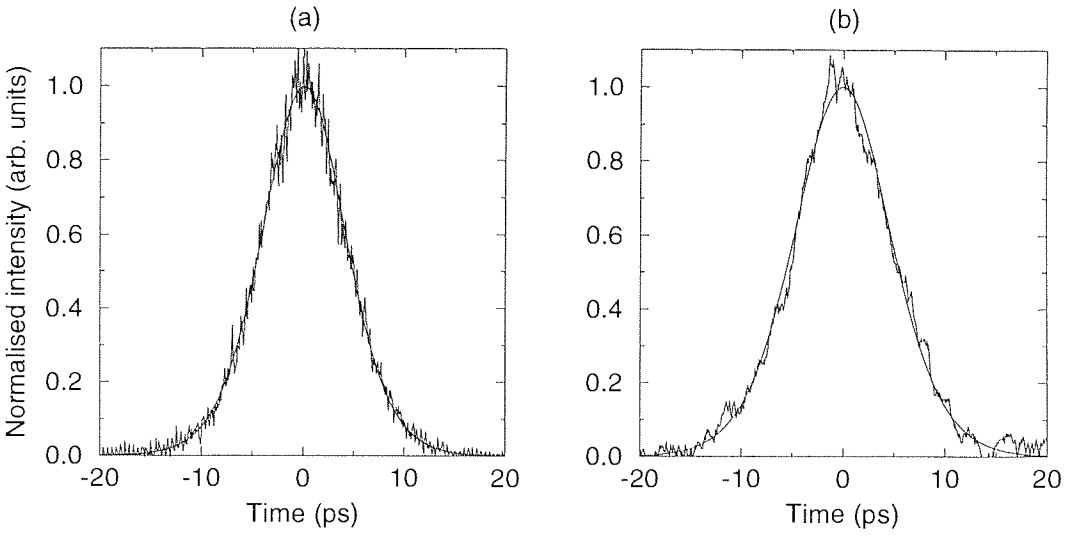

Figure 5.3: Autocorrelations and $sech^2(t)$ fits for (a) the FCL pulses and (b) pulses after propagation in the loop.

propagating signal power (which was adjusted by altering the pump power of the loop EDFA) and optimising the orientation of the polarisation controller it was possible to obtain stable pulse propagation with the ASE noise build up being suppressed for extremely long propagation distances (over one million kilometres) when the laser wavelength was tuned to 1537.6nm, which was very close to the zero dispersion wavelength. The noise level was observed by adjusting the timing electronics of the loop to leave a small section of the signal propagating in the loop free of pulses as described in Section 3.3.1. A photo-diode connected to the loop continuous monitor could then be used to measure the average power and noise levels as the loop was being run. A typical oscilloscope trace showing the average power and noise levels is shown in Figure 5.5 (a). The signal level (the upper line) was stable after an initial stabilisation and there was no build up in the the noise level (the lower line) over the entire 8000km propagation distance. Furthermore, when the loop timing controls were disabled allowing the signal to propagate in the loop for an extended period of time, there was no build up of the ASE level even over a period of up to half an hour. Comparing this trace with the one shown in Figure 5.5 (b) (which was taken during a soliton propagation experiment using the same fibre but with a net dispersion of 1ps/(nm km) and with the filter replaced by a low polarisation dependent loss FBG) shows that there was a large degree of ASE suppression.

Autocorrelations of the loop output with the ASE suppressed showed that there was a slight increase in pulse width from the initial value of 9.5ps shown in Figure 5.3 (a) to a stable width of 11ps shown in Figure 5.3 (b). The pulses maintained their $sech^2(t)$ profile

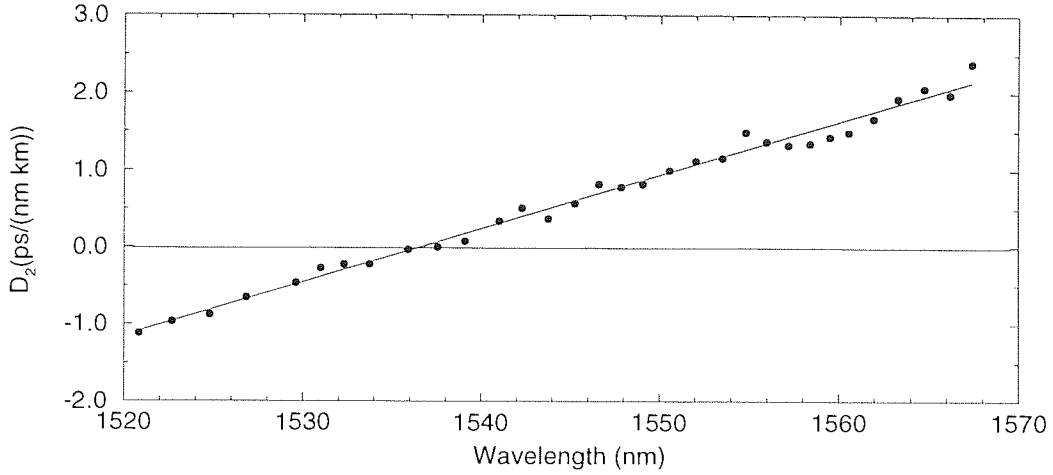

Figure 5.4: Net Dispersion of the combination of 24km of DSF and 3km of SIF The dispersion zero was reduced to ~1536nm by including the SIF.

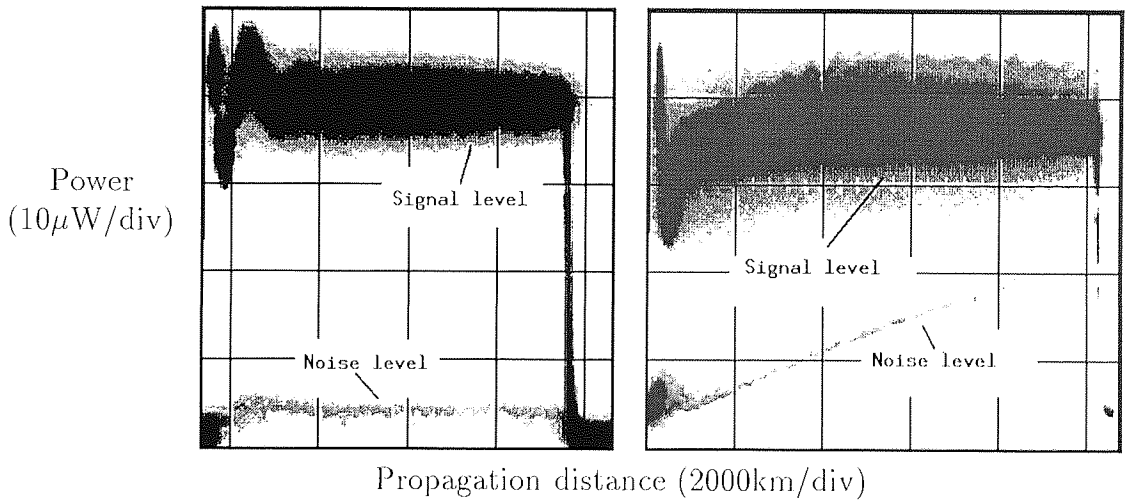

Figure 5.5: Photographs of oscilloscope traces showing the average power level and noise level for: (a) propagation over 8000km at λ_0 with the ASE level suppressed; (b) a 10 000km soliton propagation experiment which shows the normal rise in the ASE level.

but acquired a significant chirp as can be seen from the spectrum of the output pulses shown in Figure 5.6 (b). The spectral width of the stable pulses was 1.3nm which is far greater than the 0.47nm bandwidth of the transform limited input pulses. There was also a change in the wavelength of the stable pulses with the peak of the spectrum shifting to coincide with the peak in the super-fluorescence spectrum of the loop at 1537.8nm shown in Figure 5.6 (c). The two peaks in this super-fluorescence spectrum were due to two modes lasing. As can be seen by referring back to Figure 5.4 the dispersion at this wavelength was very close to zero but there was also some uncertainty in the actual value of λ_0.

As mentioned previously, it was necessary to very carefully adjust the wavelength,

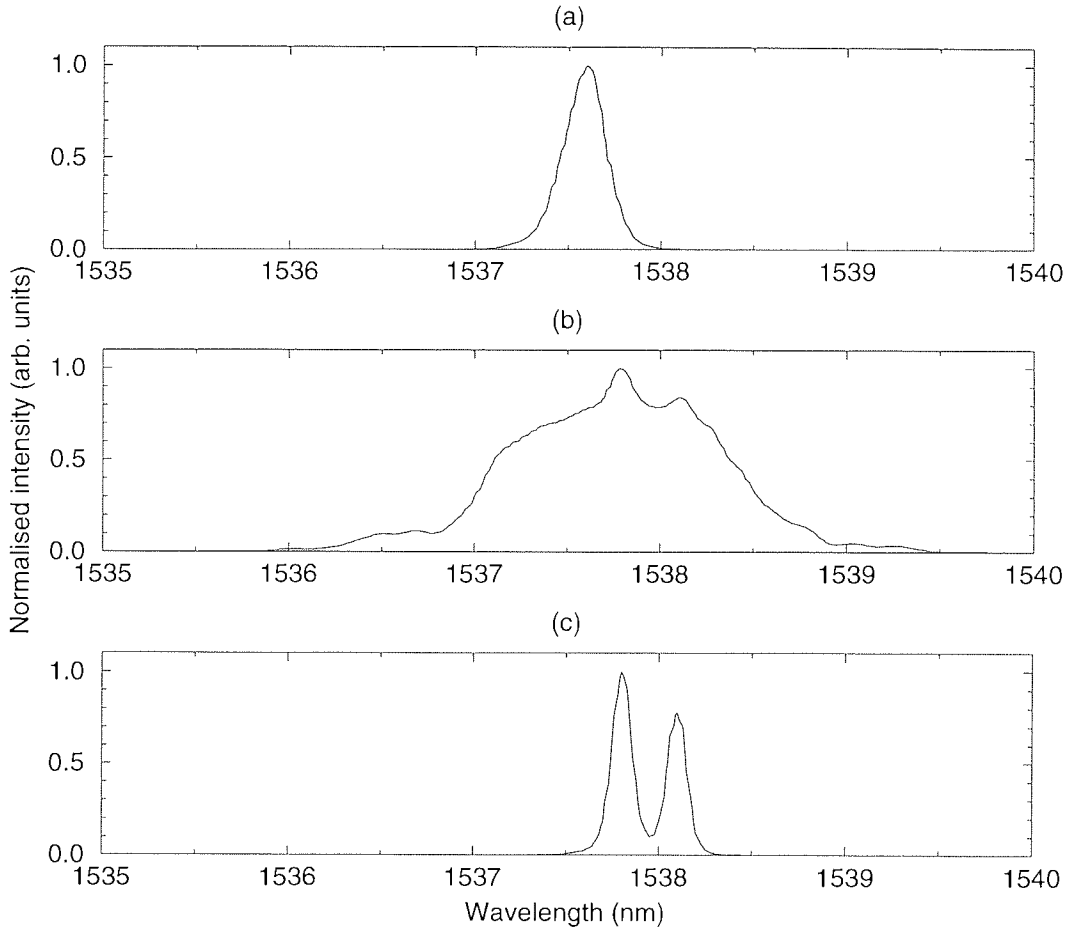

Figure 5.6: Spectra of (a) the input pulses (width =0.27nm) (b) the stable propagating pulses (width = 1.3nm) and (c) the super-fluorescence of the loop.

polarisation and power of the propagating signal in order to achieve a good suppression of the ASE. The power of the stable pulses was far in excess of the fundamental average soliton power. Taking a average dispersion value of +0.1ps/(nm km) and assuming a loss of 0.2dB/km gives the peak power for a fundamental average soliton to be 3mW using Equation 2.56. This assumes $\gamma = 2\ W^{-1}km^{-1}$ (the typical value for dispersion shifted fibre which made up the majority of the transmission fibre) and takes the FWHM pulse width to be 10ps. Taking the energy enhancement of the dispersion map into account increases the soliton power by a factor F = 1.7 using Equation 2.77 with $\beta_{2(DSF)} = 1.66$ and $\beta_{2(SIF)} = -20$. Therefore, the average power required to launch average solitons at the 76MHz data rate is give by Equation 2.74 to be $P_{(av)} = 4.4\ \mu$W. In the experiment the power launched into the transmission fibre could be estimated by measuring the average power out of the continuous monitor port and taking account of the losses of the preceding couplers, loop components and transmission fibre. This gave an estimated value of $P_{av} = 175 \pm 20\mu W$ the uncertainty in this value being due to the exact losses

involved not being known exactly. This average power corresponds to a peak power of $\sim$ 200mW which is roughly equivalent to an N = 8 soliton showing that it was not simply soliton propagation that was being observed. At such a high peak power nonlinear effects play an important role but the peak power was below the $\sim$300mW threshold power for Raman scattering. Numerical simulations of this experiment (see Ref. [180]) predict that for 10ps pulses a pulse energy of $\sim$1.5pJ is required for stable propagation. This energy corresponds to a peak power of 130mW which is in reasonable agreement with the value found experimentally considering that the simulations neglected fibre loss and took measurements at the unchirped points in the dispersion map.

For a peak power of $175\mu W$, a 10ps pulse has a dispersion length L_D = 264km and a nonlinear length $L_{NL} \sim$ 1km. SPM will therefore dominate the pulse evolution as described in Section 2.4 and it is SPM which is responsible for the spectral broadening seen in Figure 5.6 (b). The spectrum does not have the distinctive oscillatory nature of a typical SPM spectrum because of the inclusion of the filter but oscillations can be seen in the wings of the spectrum. The two peaks in the central region of this pulse simply corresponded to the peaks in the loop super-fluorescence spectrum shown in Figure 5.6 (c).

Ordinarily a pulse with such a high peak power would not propagate stably without some pulse shaping technique being used – the detrimental effects of SPM and four wave mixing would lead to break up of the pulse. In this experiment the process which was leading to the stability of the pulses and the suppression of the ASE may have been the saturable absorption effect of NPR described previously. In this experiment the polarisation discriminating element was the band-pass filter which was found to have a polarisation dependent loss of $\sim$2dB. Therefore after each round trip of the loop the signal was being spectrally filtered, separated from the noise and filtered by the polarisation dependent loss of the filter. Due to the position of the loop output coupler (see Figure 5.2) the optical spectrum of the pulses in Figure 5.6 (b) shows the pulses at their maximum spectral width before being filtered.

In addition to suppression of the noise level there was very little increase in the timing jitter of the pulses due to the low dispersion. Figure 5.7 (a) and (b) show the results of jitter measurements taken at various propagation distances using the technique described in Section 3.3.2. The data signal to the sampling oscilloscope was switched as required by a lithium niobate amplitude modulator controlled by the loop electronic delay generators and the trigger was a continuous electrical signal obtained using a photo-diode to convert

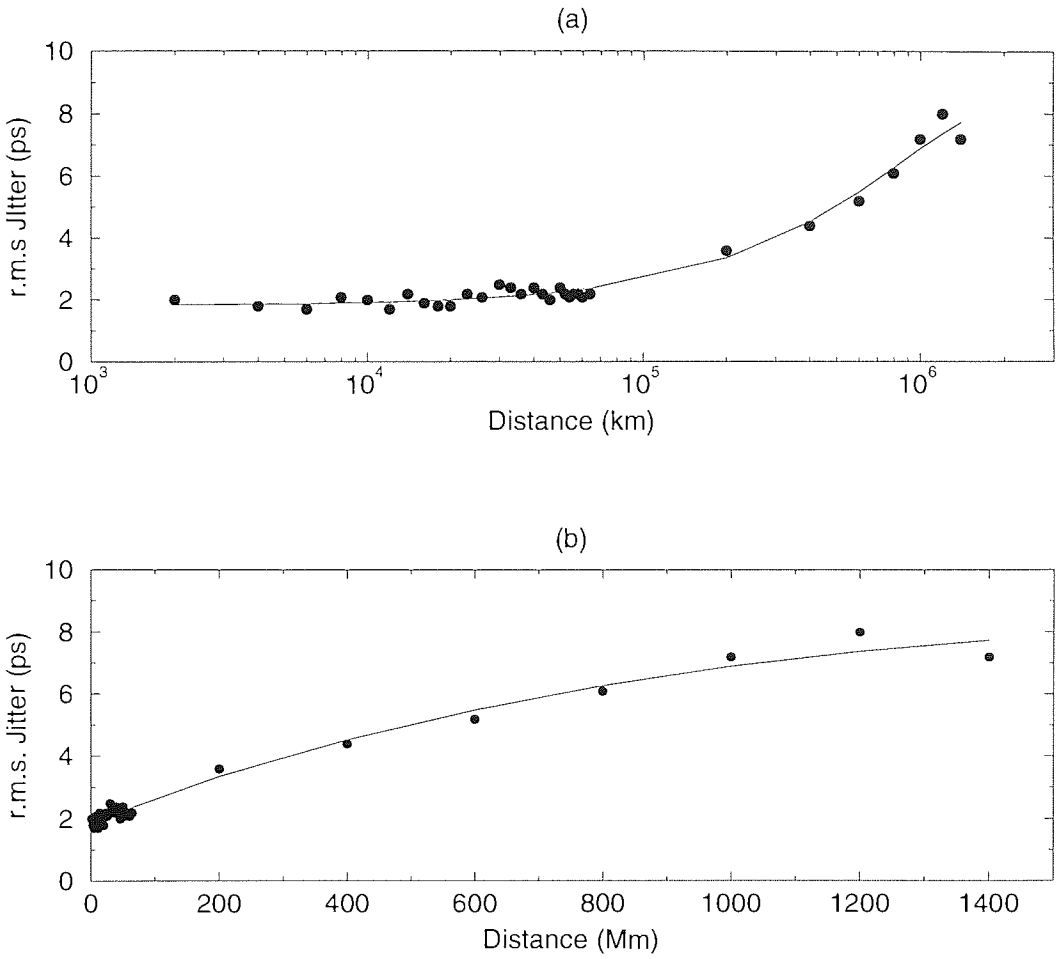

Figure 5.7: Results of jitter measurements for various propagation distances shown on (a)log and (b) linear scales. There was very little jitter increase over 60 000km but the jitter did increase with a further increase to the propagation distance.

the optical output of the loop. As a slight modification to this technique the loop output signal was sampled over a $5\mu s$ period (which corresponds to a propagation distance of $\sim$ 1000km)after the required propagation distance had been reached, as opposed to a single loop round trip period. This reduced the overall measurement time but meant that the measured jitter values were an average over a 1000km propagation distance. However the jitters were so low and slowly varying that this lead to insignificant errors.

The results are shown on both logarithmic and linear distance scales to emphasise different features. There was little increase in the jitter even after 60 000km which is well in excess of the the maximum length required for trans-oceanic systems. As the distance was further increased there was an increase in the jitter and the r.m.s. value had reached $\sim$8ps after 1450Mm. From Figure 5.7 (b) it looks as if the jitter increase was at worst linear with distance increase. In the equivalent soliton system, the maximum propagation length for a BER of 10^{-9}, (found using Equation 2.63) was $\sim$ 390Mm and

the equivalent r.m.s jitter at this propagation distance, found from Equation 2.63, was 720ps. This relatively large jitter could be tolerated because the bit interval was $\sim$ 13ns for the 76MHz bit rate. The r.m.s. jitter measured experimentally at this propagation distance was only 4.5ps and after a propagation distance of one million kilometres the r.m.s. jitter had only increased to 7ps which is still far below the maximum acceptable value for this system. This shows that in addition to maintaining the signal to noise ratio the suppression of the ASE build up also led to a reduction in the Gordon-Haus jitter. The low bit rate also meant that pulse interactions did not cause a problem – the mark to space ratio in this experiment was greater than 1:1300.

5.3.1 Discussion

While these results show that pulses can be propagated over ultra-long distances without significant jitter increase there is a second application, that of an all optical memory[84] which can store an optical data pattern for an extended period of time. The length of time that the pulses could be stored in the loop in this experiment was determined by the rate of jitter build up. From the experimental results shown in Figure 5.7 the jitter build up after 10^6 km which is equivalent to $\sim$5 seconds was only 8ps. As calculated above a jitter of 720ps could be tolerated in this system and by extrapolation of a linear fit to the experimental results in Figure 5.7 (b) it was estimated that a propagation distance of 10^8 km could be achieved before the jitter build up would begin to give errors. This is equivalent to over an hour of storage time in the loop and while this is a phenomenal distance for pulses to propagate unperturbed in an optical system, suppression of the ASE level has been observed for up to half an hour with this set-up. Jitter measurements could not be taken after this propagation distance because for jitters above $\sim$10ps the measurement technique became inaccurate due to the leading and trailing edges of the pulse becoming indistinguishable on the oscilloscope.

The experiment has been repeated with the relative positions of the two fibre reels interchanged and suppression of the ASE level and low jitter build up was again seen. This does not give any clear indication as to the effect of the dispersion map as the strength and average dispersion of the map remained unchanged. Further work is required in order to determine what, if any, effect the dispersion map has on the results.

One limitation of the experiment described above is that a pulse stream was used as opposed to a random data pattern. There is however a good indication that the effect could be used for a data stream. When the experiment was being performed the ASE

suppression was optimised by reducing the length of time that the AOM used to gate the signal into the loop was left "open". This meant that there was a gap in the pulse stream allowing the noise level to be observed in this gap as shown in Figures 5.5 (a) and (b). This gap was typically 2μs which corresponds to 152 bit intervals at the 76MHz bit rate used. Therefore the data pattern which was being propagated was essentially a long series of ones followed by 152 zeros. As Figures 5.5 (a) shows there was no increase in the noise level over 8000km with this "data pattern" being propagated. Furthermore, by disabling the loop control electronics it was possible to leave the signal propagating in the loop for an extended period of time. It was then possible to remove some of the pulses from the pulse stream in a random nature by reducing the pump power to the loop EDFA. After removal of pulses there was still no increase in the noise level even after several minutes of propagation. These observations can however only give an indication that a data pattern could be propagated/stored using this technique. When the actual experimental jitter measurements were being taken the loop was entirely filled with pulses and no gap was left in the pulse stream.

5.4 10GHz Experimental

The other major limitation of the experiment described above was that the data rate was far lower than would be used in any contemporary system. The experiment was therefore repeated at 10GHz although it again used only a pulse stream as opposed to a data pattern. The source used for this experiment was the fibre ring laser described in Section 4.4. The pulses from this laser were close to $sech^2(t)$ in profile and had a temporal (FWHM) width of 17ps. The spectral width of the laser pulses was 0.2nm giving a time-bandwidth product of 0.43 which indicates that the laser pulses were slightly chirped. The laser was mode-locked at 2.5GHz and the Mach-Zehnder inter-leaver described in Section 4.4.1 was used to achieve the desired 10GHz rate.

Again suppression of the ASE level was achieved by careful adjustment of the loop filter, PC and EDFA gain. In this experiment the average power which had to be launched into the transmission fibre for ASE suppression was $\sim 700\mu$W which is roughly seven times the power for the fundamental average solitons. This is much less than the factor of 80 power increase which was observed in the 76MHz experiment but the result is again in agreement with the numerical simulations of Ref. [180]. In these simulations two stable pulse energies, >2pJ and <0.1pJ were found for a 17ps pulse. These energies correspond

to average powers of 20mW and 1mW respectively. In the 10GHz experiment it was clearly the lower of these two energies which was used whilst the 76MHz experiment used the higher stable energy. In addition the pulse energy was lower in the 10GHz experiment as the pulse width was greater. It was not possible to attempt ASE suppression at the higher of the two stable pulse energies in the 10GHz experiment due to the high average power required.

Jitter measurements were taken as before but using a clock recovered trigger signal. The experimental results are shown in Figure 5.8 along with the results of the previous experiment. By comparison of these two sets of results it is immediately obvious that the

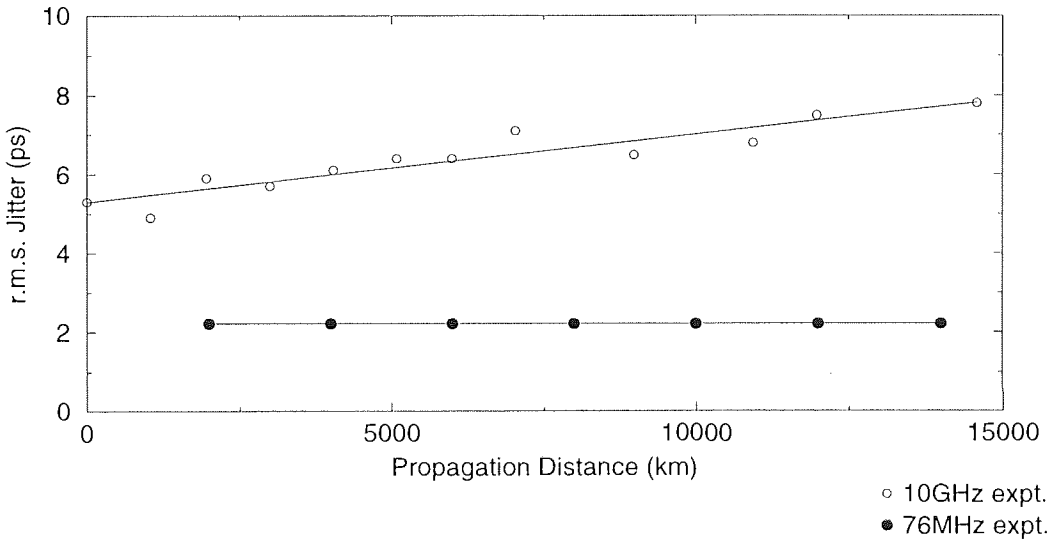

Figure 5.8: Results of jitter measurements at 10GHz (open circles) and 76MHz (solid circles). Linear fits to both sets of data are also shown.

rate of jitter increase was greater in the 10GHz experiment and also that the starting jitter was higher. The reason for the initial jitter being higher was not that the source laser had a significantly higher timing jitter but was due to the inter-leaving process introducing an additional jitter. This initial jitter put a severe limit on the system performance since Equation 2.64 allows a jitter of up to only 5.5ps before a BER of 10^{-9} is reached. The dramatic reduction in the maximum acceptable jitter from 720ps for the previous experiment is due to the data rate being increased by a factor of ~ 132 and the maximum jitter being inversely proportion to the data rate. There was therefore little chance of this system performing well as the initial jitter was 5.3ps.

The rate of increase of the jitter was higher in the 10GHz experiment for two reasons. The fact that the pulse energy was lower meant that the noise which was injected by the amplifier would have a greater effect on the pulse leading to greater frequency shifts and

hence temporal shifts as the pulses propagated. The relatively low peak power of the pulses also meant that there would be less of a difference in the nonlinear polarisation rotation rates for the signal and the noise and so the saturable absorption effect would be reduced. Despite this increase in the rate of jitter build up the r.m.s. value had only increased by 1.7ps after a propagation distance of 10 000km, which is an indication that if the initial jitter could be reduced, propagation over trans-oceanic distances could be achieved at 10Gbit/s using this technique. In the context of a storage ring or optical memory a propagation time of less than one second is anticipated before errors occured but it may be possible to increase the storage time/propagation distance if the higher stable pulse energy can be accessed.

5.5 Conclusions

A novel RZ pulse propagation scheme has been described. The likely control mechanism was the saturable absorption effect of nonlinear polarisation rotation which allowed suppression of the ASE noise level and propagation close to the zero dispersion wavelength. This noise suppression allowed a 76MHz pulse stream to be propagated over ultra-long distances without degradation of the SNR. A high SNR was also ensured as the peak power of the stable pulse was a factor of $\sim$ 80 higher than the soliton power at the equivalent dispersion. A possible reason for the stable pulse power being higher than the fundamental soliton was that in addition to the pulse spectrum being altered by the Fabry-Perot filter in the loop, there may also have been a spectral filtering effect of the NPR due to the pulses being chirped when they arrived at the polarising element – the low intensity wings would have undergone a lesser degree of polarisation rotation than the high intensity peak of the pulse and so would have suffered from greater attenuation at the polariser. However these wings of the chirped pulse would have been made up of the extreme blue and red ends of the pulses spectrum due to the dispersion of the propagating fibre and so the polariser would also have been wavelength selective. A higher stable pulse energy would therefore have been required to allow the pulse to recover from this strong filtering effect through SPM recreating the lost spectral components.

By working close to the zero dispersion wavelength the Gordon-Haus limit for the equivalent soliton system was exceptionally high at $\sim$ 390 Mm but it is estimated that an even greater propagation distance of $\sim 10^8$km could have be achieved before timing jitter began to cause errors in the experiment. These ultra-long distances correspond to

long propagation times leading to a further possible application as an optical storage ring or memory. Stable propagation without increase in the ASE level has been observed for up half an hour. When the experiment was repeated at 10GHz the system performance was compromised dramatically, the initial jitter before propagation had begun was close to the maximum acceptable value but even if this source jitter could be reduced to a similar level as that of the 76MHz experiment a propagation distance of only 30 000km is anticipated. This distance is greater than the length of trans-oceanic systems but corresponds to a propagation time of only $\sim$ 150ms and so this system would have been little use as an optical memory. It may be possible to increase the propagation time for a 10GHz data rate by using the higher of the two stable pulse powers which have been found in numerical simulations but it was not possible to investigate this experimentally without re-configuration of the loop amplifier.

In both the experiments a pulse stream as opposed to a random data pattern was used as the signal. There is therefore some doubt as to whether this technique would work with a data stream. The evidence of these experiments is that a data pattern could be used. Pulses could be removed from the pulse stream at random and a long series of zeros could be included in the pulse stream without the ASE suppression being compromised. There is no reason to expect the jitter to increase more rapidly with a data stream than with a pulse stream – the low dispersion and high mark to space ratio of these experiments meant that pulse interactions and acoustic interactions would not have much effect.

There is also some doubt whether this effect could be used in a real system. The experiments performed here were done using a single span recirculating loop and the pulse propagation is analogous to mode locking in a fibre laser. While a single span loop could be used as a storage ring/optical memory, a real transmission system would have variation of parameters such as fibre span, average dispersion per span and amplifier gain, all of which would lead to differing degrees of NPR for the different fibre spans. This would lead to difficulty in alignment of the polarisation discriminating elements along the system length and small polarisation changes due to environmental effects, which were responsible for the ultimate failure of the ASE suppression in the experiments, would cause misalignment of the signal polarisation and the minimum PDL of the polarisation discriminating element. It is also impractical to include polarisation controllers in a real system to set the polarisation state in each fibre span as was done in the experiments. The experiments were however complicated by the fact that the filter was used to provide both the spectral filtering and the polarisation discrimination. It should be possible to

use separate devices to provide these functions which would undoubtedly remove some of the sensitivity of the system to small fluctuations in polarisation and wavelength. It may also be possible to use a different saturable absorption mechanism such as a multiple quantum well device to separate the signal and noise but the saturable absorber must have a fast recovery time if it is to be used at high data rates and must also work at the correct power level.

Although the orientation of the PC and the filter had to be very carefully adjusted in order to get complete suppression of the ASE noise, repetition and verification of the experimental results was possible. Indeed, a considerable period of time (over a year) had elapsed between the initial discovery of this effect and the experiment at 76MHz being conducted and the experiment being repeated at 10GHz. In the time between the two experiments the recirculating loop had been reconfigured to allow other experiments to be conducted and several components had been replaced or changed although the transmission fibre remained the same. This indicates that the effects which were seen in the experiments were not related to one particular loop set-up and were not due to some stray effect such as a bad splice between fibres.

More experimental work is required to fully understand this phenomenon but these experimental results have demonstrated a new technique whereby soliton-like pulses can be propagated over ultra-long distances with a very low increase in the timing jitter of the pulses. Although the maximum propagation distance which is required for terrestrial communication systems is fixed, the data rate of these systems is not and at the very high bit rates ($\geq$ 100GHz) which future optical systems will employ the main limiting factor will be timing jitter. It may be possible to use this jitter suppression technique, which is entirely passive, to increase the propagation distance that can be achieved in such high speed transmission systems.

Chapter 6

Gordon-Haus jitter reduction using fibre Bragg gratings

6.1 Introduction

One of the main problems encountered in long-haul soliton transmission systems is Gordon - Haus jitter which is a result of noise introduced by each amplifier stage [47]. As described in Section 2.7.1, ASE noise from EDFAs (which must be included periodically to compensate for the loss in the system) can be included in the soliton spectrum leading to a random frequency shift which is translated into a random timing jitter through the effect of GVD. The r.m.s. timing jitter is proportional to the propagation distance to the power 3/2 but by including filters in the system the r.m.s jitter increase becomes proportional to the propagation distance at large distances [50, 51]. This enables the system length or data rate to be increased. If the central frequency of the filters is gradually changed along the transmission line the jitter can be further reduced[57].

To date, the majority of filtered soliton experiments have used bulk Fabry-Perot type filters to give suppression of the ASE noise and reduction in Gordon-Haus jitter. In this chapter the use of Fibre Bragg Gratings (FBGs) to perform these functions is investigated and the performance is compared with bulk Fabry-Perot filter experiments. The main advantages of FBGs are that they are in-fibre devices with the potential for low insertion loss and polarisation sensitivity[181]. The insertion loss must be kept low so that the EDFA gain can be kept to a minimum to reduce the noise in the system and a low polarisation dependent loss is important because ideally systems should have no polarisation sensitivity so that fluctuations in the polarisation state of the propagating signal do not impare the system performance. A further disadvantage of bulk devices is that they require the

signal to be coupled out of the fibre before it is passed through the filter and re-coupled into fibre. This makes them more susceptible to failure than in fibre devices and so makes them unattractive for use in real systems designed to have a lifetime of at least 25 years, particularly in the harsh environment of submarine systems. Although the simplicity of FBGs makes them attractive for use in all optical systems their aging characteristics are yet to be fully understood [182] but there is enough evidence from accelerated aging tests to allow the use of FBGs in real systems.

6.2 Fibre Bragg gratings

Having excited considerable interest in recent years fibre Bragg gratings have found a wide range of uses [183, 184] from temperature and strain sensors [185, 186] to optical communications applications[69, 187, 188, 189]. Obviously it is the uses of these devices in optical communications that will be of relevance to this thesis.

Fibre Bragg gratings are made by exposing photo-sensitive optical fibre to the fringe pattern created by the interference of two intense UV beams. There are two methods used to create the interference fringes. The first is to split a single UV beam into two, allow these two beams to follow different paths before recombining them to give the required interference pattern[190, 191]. The second method makes use of a surface relief grating phase mask. The beam is passed through this phase mask and the fringe pattern arises from interference between the diffraction orders [192, 193].

In both of these methods the exposure of the photo-refractive fibre core to the sinusoidally varying intensity pattern generated by the interference causes a sinusoidally varying modulation of the core refractive index given by [183]

$$n(z) = n_{core} + \delta n[cos(2\pi z/\Lambda)] \tag{6.1}$$

where

$$\Lambda = \frac{\lambda_{(uv)}}{sin\theta/2} \tag{6.2}$$

When an optical signal is incident on such a grating the modulation of the refractive index leads to a coupling of the forward propagating optical energy into a counter propagating mode since the grating appears as a series of partially reflecting boundaries. This reflection of the signal is maximised when the wavelength of the incident light equals the Bragg wavelength defined by

$$\lambda_B = 2n_{eff}\Lambda \tag{6.3}$$

where n_{eff} is the effective refractive index of the fibre. It is this in-fibre implementation of wavelength selective devices that has led to such great interest in FBGs. Potential applications for these devices in optical communications include Fabry-Perot type filters suitable for soliton control [69], demultiplexers for WDM systems [187, 189, 194, 195, 196] as well as pass-band filters [197]–[200].

In addition, it is possible to create chirped gratings which have a variation in grating period along the length of the device and so have a variation in reflected wavelength along their length [183, 191, 201]. Such devices have the potential to provide dispersion compensation (and dispersion slope compensation) in transmission systems [202]–[206] and pulse compression [207, 208, 209]. The use of FBGs for dispersion compensation in soliton systems will be investigated in Chapter 8.

The grating used in the experiments described in this chapter was fabricated using a slightly modified method to produce a narrow pass-band at the signal wavelength with the stop band extended to cover the whole of the erbium fluorescence band [210]. Initially a chirped grating was produced which reflected the required range of wavelengths. The pass-band was then created by re-exposing a section of the grating with an intense UV beam. When a grating is re-exposed it undergoes a further refractive index change which effectively removes part of the grating at the re-exposed position creating a pass-band. The pass-band central wavelength is determined by the position along the chirped grating where the re-exposure takes place and the bandwidth of the pass band depends on the bandwidth of the chirped grating used and the characteristics of the UV beam used. For a fixed grating length the wider the stop band then the wider the pass band will be given that the same UV beam is used to re-expose both gratings. This is because a given UV beam width will remove the same physical length of both gratings but the wider bandwidth chirped grating will reflect a larger wavelength range per unit length and hence a greater wavelength reflection range would be removed. Obviously the quality, particularly the beam width, of the UV beam will affect the pass band characteristics. Using this technique multiple pass band filters suitable for WDM experiments can easily be created in a single fibre device by repeatedly re-exposing the chirped grating at each position where a pass band is required. When a grating with a narrow pass-band is required with a large stop band (as in this experiment), the pass band can be created in a chirp grating with a relatively narrow stop band to give the required pass band position

and bandwidth before concatenating this structure with blocking FBG filters to extend the stop band as required.

6.3 Experimental results

A schematic of the experimental set-up is shown in Figure 6.1. The soliton pulse source

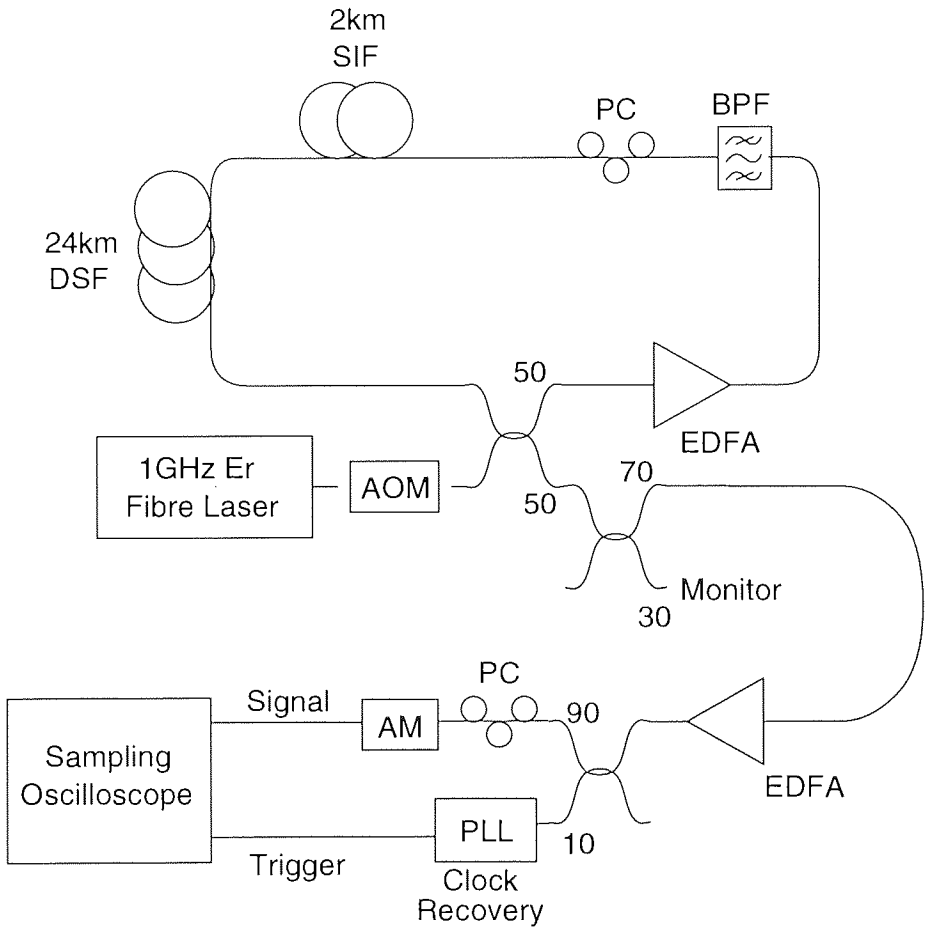

Figure 6.1: Schematic diagram of the re-circulating loop. AOM: Acousto-optic modulator, EDFA: erbium doped fibre amplifier, BPF: bandpass filter, PC: polarisation controller, SIF: Step index fibre, DSF: dispersion shifted fibre, PLL: phase locked loop, AM: amplitude modulator. Numbers beside fibre couplers denote the coupling ratios.

used was the actively mode-locked 1GHz fibre figure-8 laser (described in 4.3). The operating wavelength of this laser was tuned to 1554nm to coincide with the centre of the pass band of the filter. The pulse width of the laser was 10ps and the spectral width was 0.37nm giving a time-bandwidth product of 0.46 which shows that the input pulses were slightly chirped. The pulse stream from the laser was coupled into the single span recirculating loop as described in Section 3.2. The transmission fibre in the loop was 2.7km of standard fibre (SIF) with a dispersion of $\sim$ 16.5ps/(nm km) and 23.9km of dispersion

shifted fibre (DSF) which had a λ_0 of ~1560nm and a dispersion of -0.22 ps/(nm km) at the operating wavelength of 1554nm. Although the majority of fibre in the loop had a negative (normal) dispersion and so was not soliton supporting, the average dispersion per 26.6km amplifier span, measured using the technique described in Section 3.4.1, was anomalous with a value of $\sim$ 1.2ps/(nm km) allowing stable propagation of soliton-like pulses. The result of the dispersion measurement is shown in Figure 6.2. This average

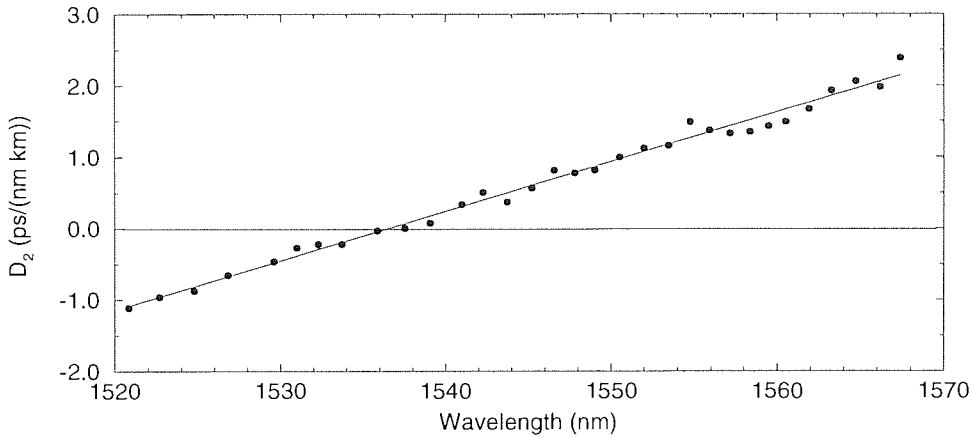

Figure 6.2: Dispersion measurement result for 24km of DSF and 2.7km of SIF. The dispersion at the operating wavelength of 1554.3nm was $\sim$ 1.2ps (nm km).

dispersion gave a soliton period $Z_0 \sim$ 34km and thus the average soliton requirement that $L_a \ll 8Z_0$ was met [36]. The peak power of a 10ps fundamental average soliton at this dispersion was calculated to be 39mW taking $\gamma \sim 2$ corresponding to DSF. For a 1GHz pulse stream the average launch power required was then ~450μW. The effect of the dispersion map would be to increase the stable pulse power compared to the average soliton power for the equivalent uniform dispersion system as discussed in 2.8. In this case the energy enhancement factor calculated from Equation 2.77 was 1.7. The actual average power launched into the fibre in the experiment was ~700μW. This value was calculated by measuring the power out of the 30% continuous monitor port and taking account of the preceding losses in the transmission path. This average power gives an actual energy enhancement of ~1.6 which is slightly lower than the predicted value but there is good agreement considering the approximations of the theory. Using Equation 2.76 the propagation distance which could be achieved before the signal to noise ratio would be degraded below that acceptable for a 10^{-9} BER was estimated to be $\sim$ 2000km. While this distance would be the limit of the system's error free performance, the jitter could be measured beyond this point. The Gordon-Haus limit for the system was calculated to be

$\sim$ 5500km which is far in excess of the SNR limit due to the low bit rate which was used.

In addition to the bandpass filter (BPF) a polarisation controller was included in the loop to allow adjustments to the polarisation state of the propagating signal. The coupler used to couple the signal in and out of the loop had a 50:50 splitting ratio which gave an additional 3dB loss per round trip of the loop. The total loss per round trip of the loop excluding the insertion loss of the filter was estimated to be 10dB.

Initially, a fibre Bragg grating (FBG) with the characteristics shown in Figure 6.3 was used in the loop at position BPF. The pass-band of this device was centred at 1554.3nm

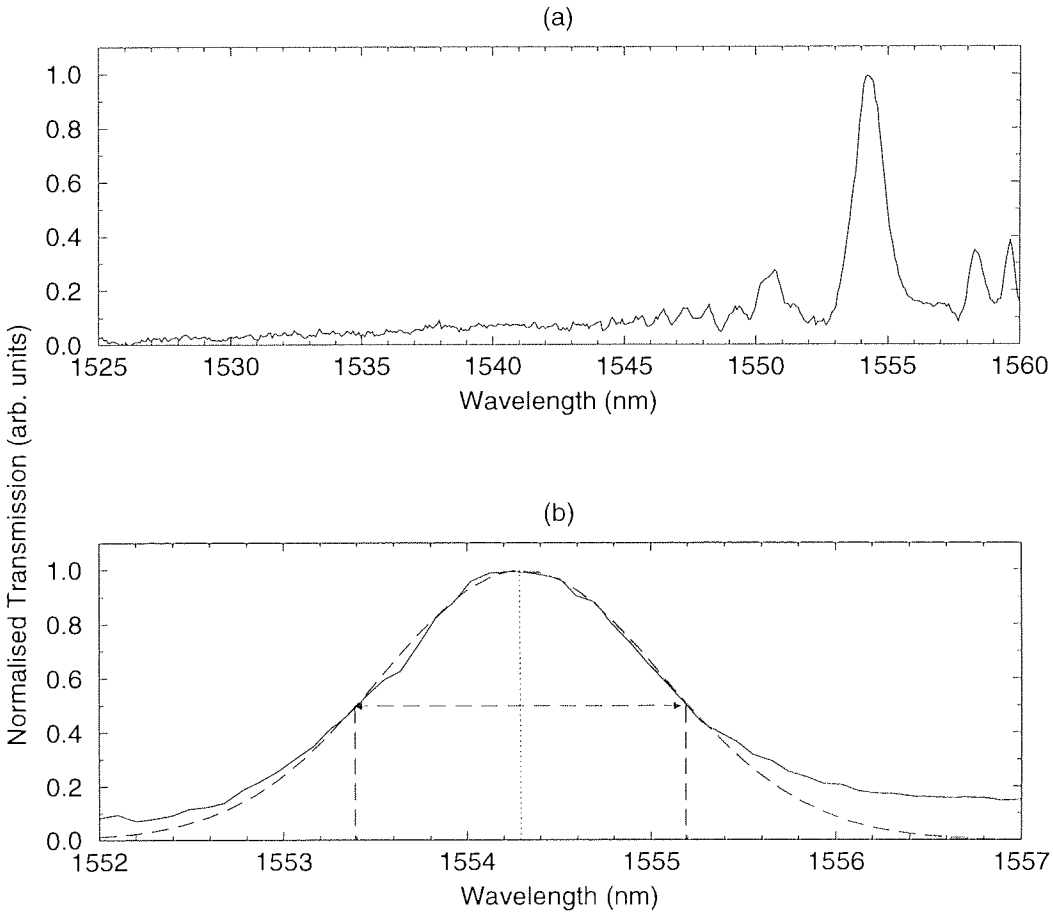

Figure 6.3: Transmission spectrum of the Fibre Bragg grating filter. (a) shows the FBG spectrum over the whole of the erbium fluorescence spectrum and (b) shows the spectrum around the 1.8nm pass-band centred at 1554.3nm. The dashed line is a Gaussian fit.

with a 3dB bandwidth of 1.8nm (see Fig 6.3 (b)). This bandwidth was much greater than the 0.27nm bandwidth of the soliton pulses and so strong soliton guiding effects due to this filter were not expected. The stop band of the FBG extended from 1525nm to 1560nm with an extinction of $\sim$ 10dB at 1530nm. Although this value is fairly low, the concatenation effect of successive round trips of the loop meant that a large extinction ratio was not required and using this bandwidth gave a reasonable suppression of ASE outside

the soliton bandwidth. The additional resonances in the transmission spectrum around the main transmission peak are associated with a beating effect which is a consequence of the manufacture process – removing a section of the initial chirped grating effectively produces two separate gratings. The wavelength overlap of these two gratings leads to resonant peaks in the transmission (and reflection) spectrum. These resonance peaks were $\sim$ 4dB down on the main peak and were expected to have little effect on the transmission. The insertion loss of this device was 2dB and although this value is relatively high for a FBG the device was a prototype and a much lower insertion loss should be possible. The actual PDL of the device was too low to be measured accurately but was <0.3dB.

The main results which were taken in this experiment were jitter measurements using the technique described in Section 3.3.2. As Figure 6.1 indicates the sampling oscilloscope received a continuous clock recovered trigger and the optical signal to the scope was switched using a lithium niobate amplitude modulator. This allowed the jitter to be measured only after the required propagation distance had been reached but limited the maximum jitter which could be measured accurately to $\sim$ 10ps. For a 1GHz system the bit interval is 1ns and so Equation 2.64 indicates that an r.m.s jitter of $\sim$ 55ps can be tolerated before a BER of less than 10^{-9} is detected. Thus the maximum measurable jitter was far less than the maximum jitter which the system could accept. However as stated above the SNR would have been degraded beyond the minimum acceptable value by the time a 54ps jitter was reached. The results in Figure 6.4 give a good indication of system performance and show that with the FBG positioned at BPF in the loop a propagation distance of 2700km was reached before an r.m.s jitter of 9.5ps was recorded. The solid line shown in Fig. 6.4 represents the theoretical values of Gordon-Haus jitter calculated for a filtered system using Equations 2.63 and 2.67 i.e.

$$\left\langle t_N^2 \right\rangle = f(\Delta\nu_f, \tau_0, L)\frac{2\pi n_2 N_{sp}|\beta_2|hc(G-1)L^3}{9\tau_0\lambda^2 A_{eff} L_a \Lambda_0^2}, \tag{6.4}$$

where $f(\Delta\nu_f, \tau_0, L)$ is the reduction to the Gordon-Haus jitter due to the filter. As discussed in Section 2.7.1 this reduction factor is a function of the filter bandwidth (in frequency space), $\delta\nu_f$, the pulse width, τ_0 and propagation distance, L. This function is, in general, also dependent on the spacing of the filters but in this experiment a single span loop was being used and so the filter spacing was determined by the span of the loop. The theoretical r.m.s. jitter is then given by $\sqrt{\langle t_N^2 \rangle}$. In the jitter calculation a fibre loss of 0.25dB/km, an effective cross sectional area of $30\mu m^2$ and a Gaussian filter function were

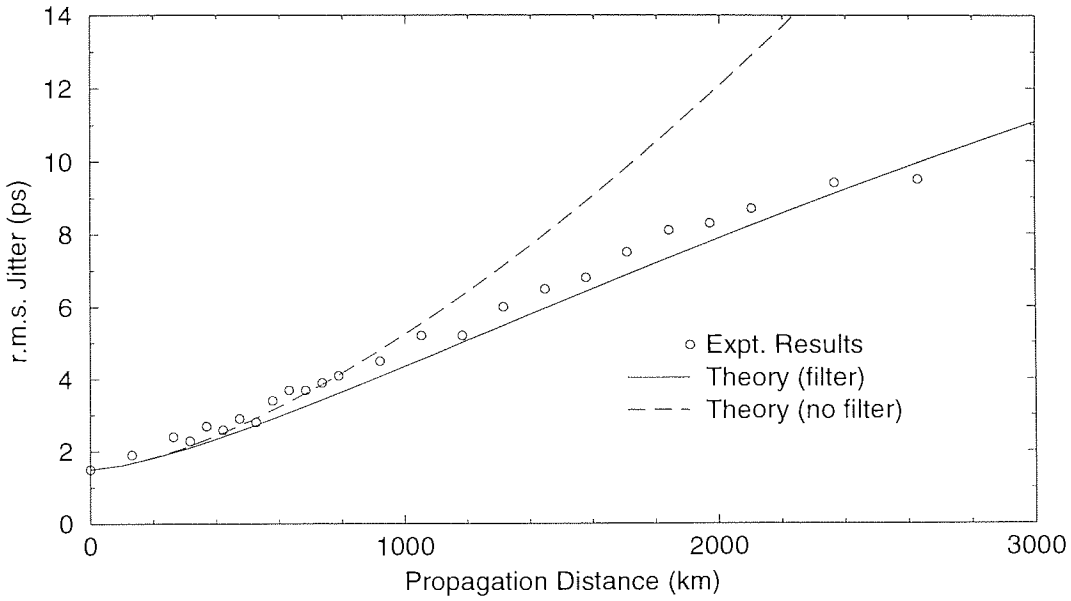

Figure 6.4: Jitter measurement results using the fibre Bragg grating filter. Circles represent the experimental results, the solid line is the theoretical prediction of Gordon-Haus jitter including the effect of the filter and the dashed line is the unfiltered theoretical case.

assumed. As Figure 6.3 (b) shows this is not an unreasonable approximation to the filter function for the FBG. Other parameters used in the calculation (pulse width, data rate, amplifier gain, span and noise figure, filter bandwidth and average dispersion) were as determined experimentally. The calculation was done with no source jitter but this effect was included by adding the experimental source jitter value to the theoretical results. As Figure 6.4 shows the theoretical curve was a good approximation to the experimental results. In both cases there was a linear increase of jitter with propagation distance and the gradient of this increase is the same for both experimental and theoretical results. However the experimental values were generally higher than the theoretical results but the difference between the two sets could be minimised by increasing the initial jitter in the theoretical case (which simply moves the curve up the y axis) to 1.8 which is slightly higher than the experimentally measured value but is within experimental error.

Other sources of difference between the theory and experiment are that the only source of jitter in the theoretical case was Gordon-Haus jitter and though this was likely to be the dominant source of jitter there may have been a small contribution from other sources (the high mark to space ratio and low dispersion ensured that soliton-soliton interactions and acoustic interactions would have been only small effects over this propagation distance). It should also be remembered that the theory assumed an average dispersion of 1.2ps/(nm km) which in practice was only known to $\pm$ 0.1ps/(nm km). The loss assumed

in the theory is also only an approximation as was the Gaussian filter function used in the calculation. By comparing the actual filter shape and the Gaussian fit shown in Figure 6.3 (b) it is clear that the assumption of a Gaussian filter function is a reasonable one but the difference in the wings of these two filter shapes (the actual filter has slightly higher transmission at long wavelengths) could lead to a larger jitter in the experiment than in theory since the noise suppression would not have been as great for the actual filter used. It addition, the Gaussian fit is only good over the main pass-band. The resonance peaks either side of the main transmission peak shown in Figure 6.3 (a) are a further feature which was not included in the theory. These are however $\sim$ 4nm away from the peak of the transmission and were unlikely to play any part in the soliton guiding but would allow extra noise to be injected into the system which could have degraded the signal to noise ratio.

As described in Section 2.8 there is some evidence that dispersion management leads to a reduction in the Gordon-Haus jitter since the stable pulse power is increased [96, 211]. There was no conclusive evidence that this was the case from these experimental results although the dispersion map used here led to only a modest energy enhancement factor of 1.6 and so the jitter reduction would have been small.

The effect of the filter in reducing the Gordon-Haus jitter can clearly be seen from Figure 6.4. In addition to the theoretical result for the filtered system (which is represented by the solid line) the jitter for the equivalent unfiltered system was calculated using Equation 2.63 and is shown as a dashed line. Numerically, the only difference between these two curves is that the filtered result contained the additional factor $f(x)$ given by Equation 2.67 which determined the effect of the filter. As can be seen from the results there was little difference between the filtered, unfiltered and experimental results over the first $\sim$800km but after this point the results diverged with the jitter increasing linearly in the filtered system but more rapidly in the unfiltered case. The experimental results clearly follow the linear increase of the filtered result showing that the FBG was giving the expected reduction in Gordon-Haus jitter.

Figure 6.5 shows the spectra of the input and the propagated pulses. The 3dB bandwidth of the fibre laser output was 0.37nm. On propagation in the loop the bandwidth decreased to 0.29nm and the stable width shown was reached within 250km of propagation. Autocorrelations could not be taken of the loop output as the output was only a burst of signal and so it is difficult to comment on the pulse shape of the output pulses. Assuming no change to the temporal pulse width gives a time-bandwidth product of the

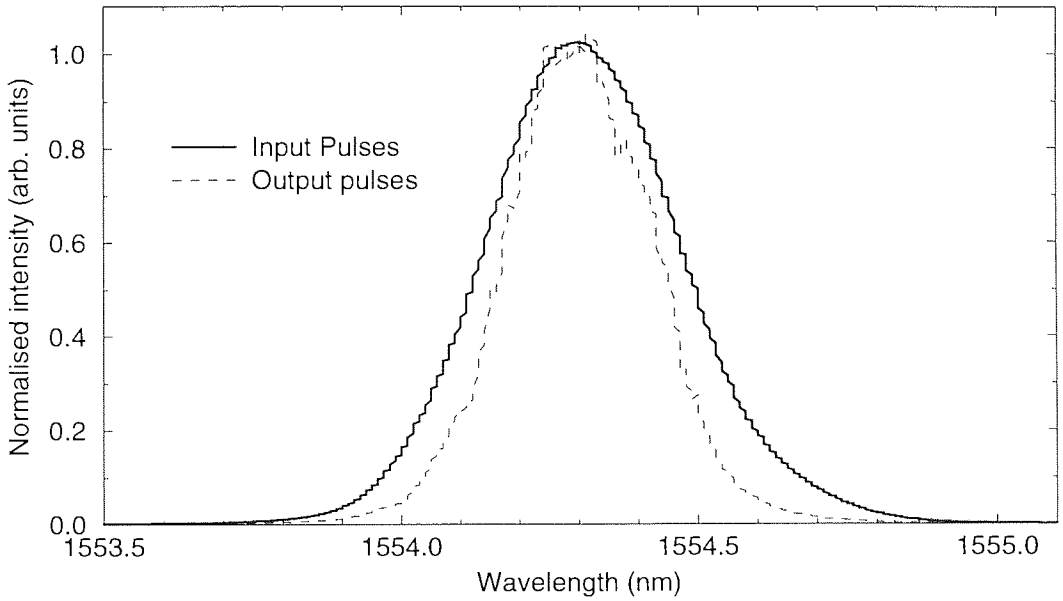

Figure 6.5: Optical Spectra for the input (solid line) and output pulses (dashed line). The input pulse width was 0.37nm and the stable pulse width was 0.29nm.

output pulses of $\Delta\nu\Delta t$ ~0.36 but an increase in pulse width to 12ps would have given $\Delta\nu\Delta t \sim 0.43$.

As discussed in Section 2.8 the points in a dispersion managed system where the pulses are transform limited are actually within the fibres whereas the experimental measurements were taken at the output of the DSF. It is therefore likely that the value of $\Delta\nu\Delta t$ estimated here is higher than the transform limited value of the output pulses. It is therefore likely that the stable pulses of this dispersion managed system were not far removed from $sech^2(t)$ in profile. It has been shown by simulations that the time-bandwidth product of the stable pulses in a lossless dispersion managed system increase towards the 0.44 value of Gaussian pulses as the strength of the dispersion map is increased [98] but when loss is included the increase in $\Delta\nu\Delta t$ may be reduced [117]. Only a small change from the ~0.32 value of $sech^2(t)$ pulses was estimated in this experiment due to the dispersion map being fairly weak.

When propagation of the signal was attempted with the FBG removed from the loop, the signal would propagate no further than 250km before the ASE noise level rose catastrophicaly. This indicates that in addition to giving a reduction in the Gordon-Haus jitter the FBG was successfully suppressing the accumulation of ASE noise outside the soliton spectrum despite having an extinction ratio of only 10dB.

In order to compare the performance of the FBG with a more traditional bulk device the experiment was repeated with a tunable air-gap Fabry-Perot (FP) filter used in place

of the FBG. Figure 6.6 shows the spectrum of this filter over (a) the whole of the erbium fluorescence spectrum and (b) a close up of the pass-band. The scales of these two graphs are the same as those of Figures 6.3 (a) and (b) to aid comparison. The most obvious difference between the two filters is in their bandwidths. The FP filter had a 3dB bandwidth of 2.7nm compared to the 1.8nm of the FBG. The extinction ratio of the FP

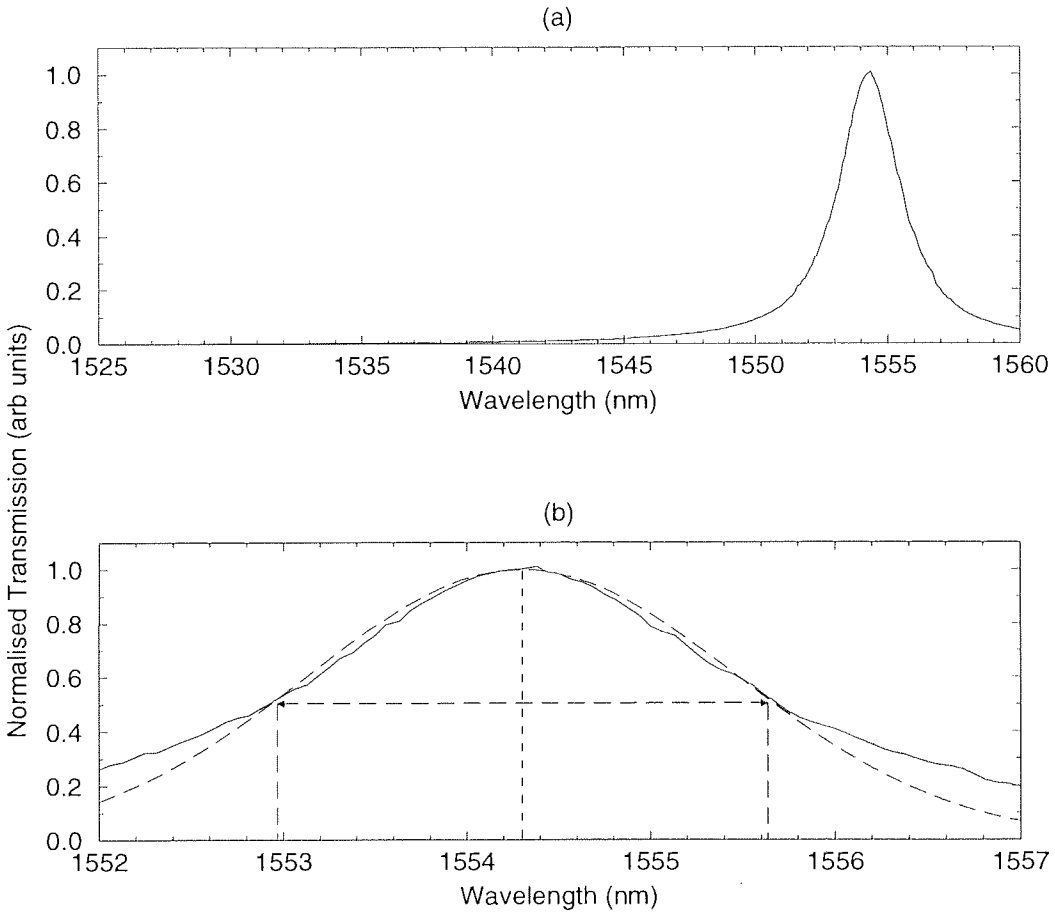

Figure 6.6: Transmission spectrum of the Fabry-Perot filter. (a) shows the spectrum over the whole of the erbium fluorescence spectrum and (b) shows a close-up of the 2.7nm pass-band. The dashed line is a Gaussian fit.

filter was ~25dB which was considerably higher than the FBG filter. This device had an insertion loss of 2.2dB and a PDL of 1.5dB.

Jitter measurements were again taken at various propagation distances and the experimental results of Figure 6.7 show that using this filter there was again a linear increase of the r.m.s. jitter with propagation distance which was in agreement with the theoretical calculation of jitter in the equivalent filtered system which is shown by the solid line. This calculation was exactly the same as for the FBG but with the filter bandwidth changed and the amplifier gain increased to take account of the additional 0.2dB insertion loss of the FP filter. There was again a discrepancy between the theoretical and experimental

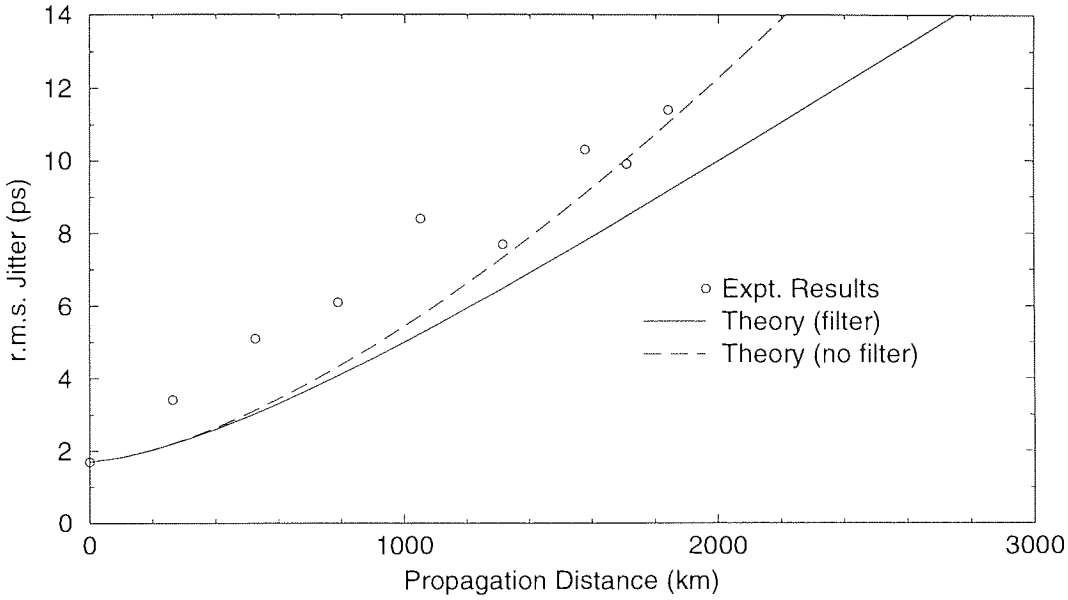

Figure 6.7: Jitter measurement results using the Fabry-Perot filter. Circles are the experimental data points, the solid line is the theoretical curve including a 2.7nm filter and the dashed curve is the unfiltered theoretical curve.

jitter values and for this filter the difference was greater than for the FBG. The probable reason for this is that there was a greater difference between the actual filter function and the Gaussian fit (which is assumed in the theory) for the FP filter than the FBG filter.

Direct comparison of the experimental results for the two filters shows that the rate of jitter increase was greater for the bulk Fabry-Perot device, a 9.5ps r.m.s jitter was reached after only 1700km in this case compared to 2700km when the FBG was used. The dashed line in Figure 6.7 shows the jitter in the unfiltered case using a 2.7nm filter and comparison of the theoretical results for both filters also shows that using the 2.7nm bandwidth filter gave less reduction in the jitter than the 1.8nm filter. This is simply due to the fact that the bandwidths of the two devices were different. The larger bandwidth of the FP filter meant that less of the ASE noise was filtered out on each pass of the amplifier and hence a larger portion of the noise was incorporated into the soliton, leading to a larger timing jitter. As there was less difference between the filtered and unfiltered results for the FP filter it is more difficult to determine how the experimental jitter values evolve with propagation distance. More data points are required at longer propagation distances, where there is more divergence of the two theoretical curves to give a better indication. These results could not be taken in this experiment as jitter values above $\sim$ 10ps could not be measured accurately. It does however appear that the increase in the experimental jitter values was linear as propagation distance was increased.

The experimental results presented here show that in terms of suppression of the ASE noise and reduction in the rate of Gordon-Haus jitter accumulation FBGs perform comparably with bulk FP devices. It should be pointed out that the bandwidth of the FBG used here was not picked to give optimal reduction in the Gordon-Haus jitter, the purpose of this experiment was to compare the performance of the FBG with the FP filter. The main limitations of this experiment were that it was restricted to pulse train measurements, as opposed to using real data, and the data rate was only 1GHz which is relatively low compared to the data rates of current and future long haul systems. Therefore the experimental results can only give an indication that FBGs could be used in real high bit rate long-haul systems. To give further proof a second experiment was conducted at a data rate of 10Gbit/s with a pseudo-random data pattern (PRBS) used as the signal.

In this experiment a 10GHz gain switched DFB laser was used as the pulse source. The operation of this laser is described in Chapter 4.5. The pulse width of the signal pulses was $\sim$ 12ps and the time-bandwidth product was 0.53 indicating that the output pulses were chirped. The output wavelength of the DFB laser was temperature tuned so that the output wavelength coincided with the centre of the filter pass-band. The experimental set up is shown in Figure 6.8. Using a 10GHz pattern generator and a 10GHz lithium niobate amplitude modulator a $2^{31} - 1$ PRBS was imposed on the DFB pulse stream. This 10Gbit/s data stream was then gated by an AOM and coupled into the loop through a 70:30 coupler. The transmission fibre used in this experiment was 32.1km of standard fibre with a dispersion of $\sim$ 16.5ps/(nm km) at the operating wavelength and 6.8km of dispersion compensating fibre with a total dispersion of -520ps/(nm/km). The average dispersion of this combination of fibres was measured to be 0.15ps/(nm km) using the technique described in Section 3.4.2.

The fibre was split into sections so that 25.6km of standard fibre and the dispersion compensating fibre were positioned before the amplifier with the remaining 6.5km of standard fibre positioned after the amplifier and filter. The advantages of this dispersion map and the associated advantages with regard to soliton propagation are investigated in Chapter 7. In this experiment the aim was to compare the fibre Bragg grating with the bulk device and the details of the propagating system were not crucial. The energy enhancement predicted by Equation 2.77 for this dispersion map was $\sim$9 which is slightly higher than the actual value of $\sim$6 which was used experimentally, the average power power launched into the transmission fibre being $\sim 630\mu$W. For this average power limit

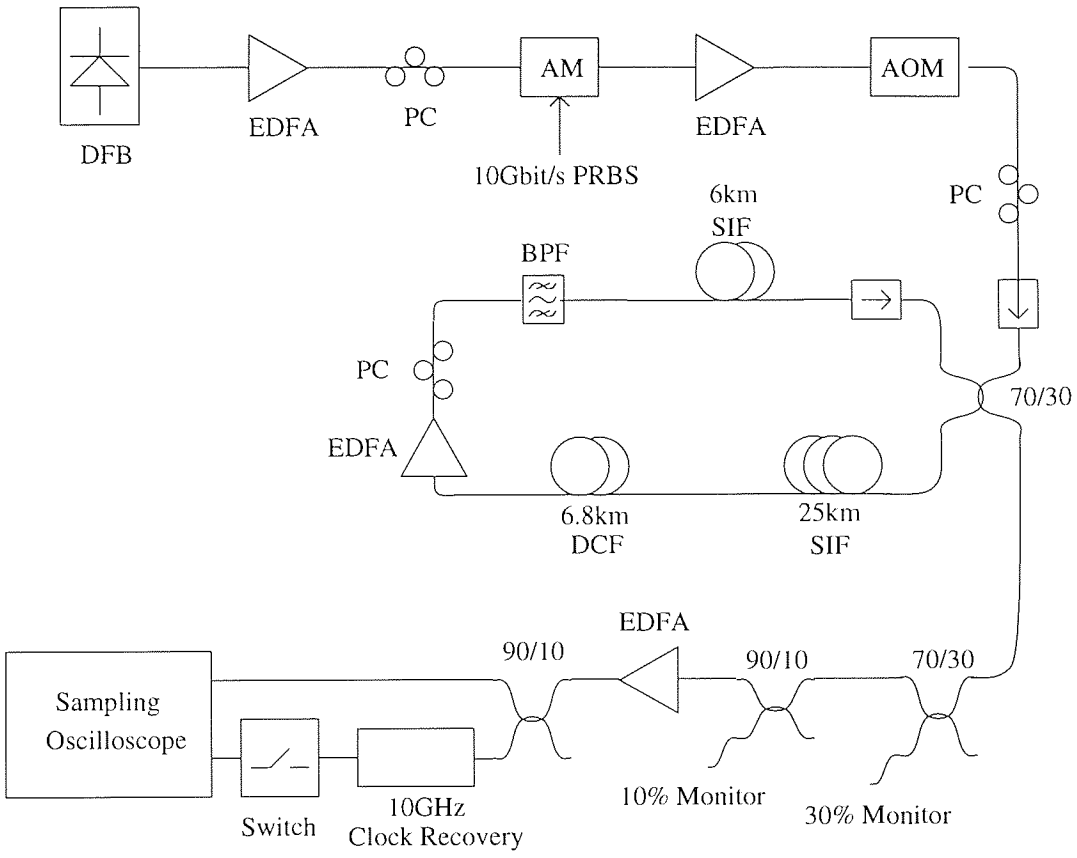

Figure 6.8: Schematic diagram of the recirculating loop set-up used for the 10Gbit/s FBG propagation experiment. A 10Gbit/s PRBS was propagated in the loop which contained 32km of SIF and 6.8km of DCF. Q measurements were taken on the sampling oscilloscope.

the maximum transmission distance expected before the SNR became too low to give a BER better than 10^{-9} was ~2000km. The effect of the soliton-soliton interaction was again expected to be small due to the high mark to space ratio and low dispersion. Theoretical values of the Gordon-Haus jitter were calculated for this system and the results are shown in Figure 6.9 (a). From Equation 2.64 the maximum jitter giving a BER less than 10^{-9} in a 10Gbit/s system is ~5.4ps and this value is represented by a solid line on the graph. From this maximum jitter value the Gordon-Haus limit for the unfiltered system was calculated to be ~2600km. With a 2.7nm filter this was increased to ~ 2900km and with a 1.8nm filter it was ~ 3500km. These values assume no source jitter and when the source jitter is included the Gordon-Haus limit is reduced – for a source jitter of 1.5ps the Gordon-Haus limit is reduced to ~2600km when using a 1.8nm filter and ~2100km in the unfiltered case. These values are similar in magnitude to the SNR limit and so both these constraints must be kept in mind when analysing the experimental results.

As before the signal was propagated round the loop until the required distance was

reached. However both the experimental results taken and the method of gating the loop output were different in this experiment. Instead of using a continuous trigger and switching the signal the opposite was done, a microwave switch was used to switch the continuous 10GHz clock recovered trigger and a continuous loop output was connected to the sampling oscilloscope. Since data was being used, as opposed to the previous pulse stream, Q measurements could be taken using the method described in Section 3.3.2.

Again the experiment was repeated with firstly the FBG and then the FP filter put in the loop at position BPF. Figure 6.9 (b) shows the Q value versus propagation distance results for both filters. It should be kept in mind that these results do not give a direct

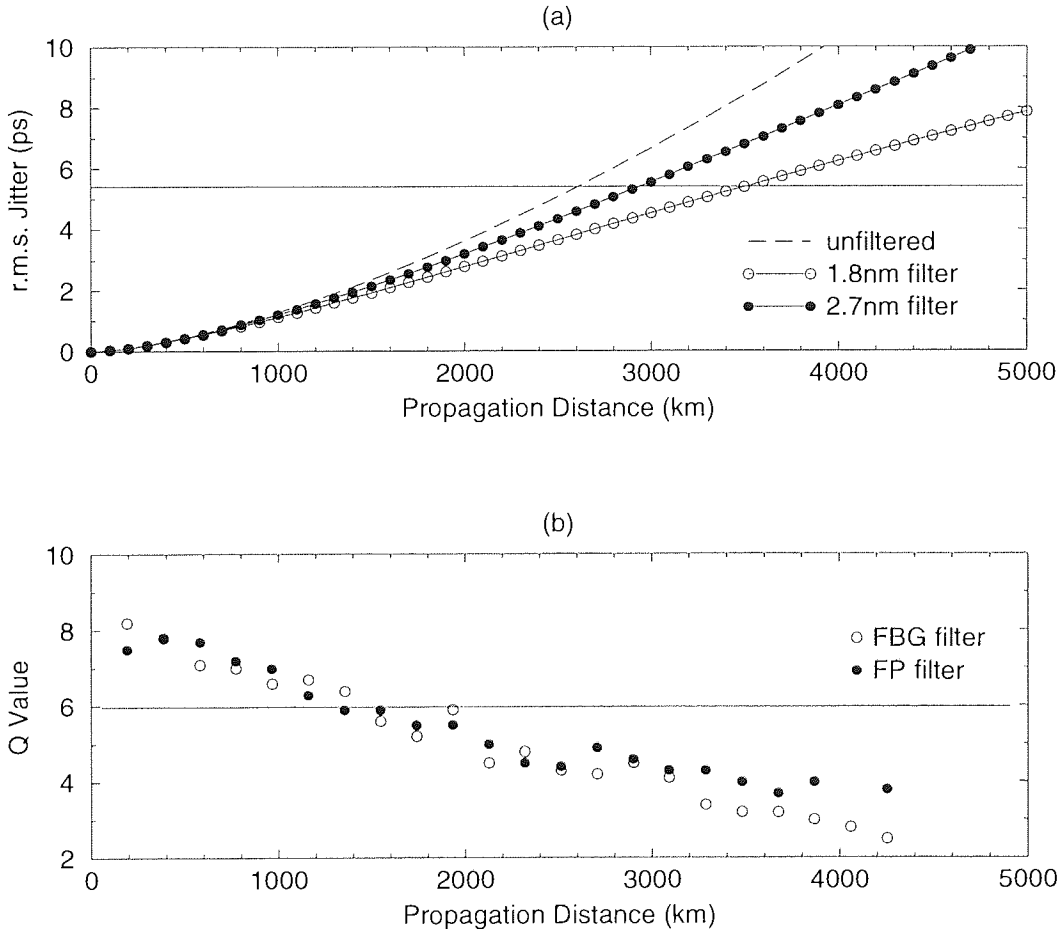

Figure 6.9: Q value versus propagation distance results for both the FBG filter (open circles) and FP filter(filled circles).

measurement of the Gordon-Haus timing jitter, other effects such as amplitude noise and ASE noise build up also affect the final Q value. Comparing the results for both filters shows that both sets were very similar. For both cases the maximum propagation distance achieved before the Q fell below 6 which corresponds to a BER of 10^{-9} was $\sim$ 1500km. At this propagation distance there is little difference between the theoretical jitter values

using both filter bandwidths and so it is not surprising that similar "error free" distances were achieved in both experiments. The 1500km distance achieved was shorter than the ~2000km SNR limit but this limit neglects the effect of Gordon-Haus jitter – when these two effects are combined it is reasonable to assume that there will be a reduction in the maximum propagation distance which can be achieved.

When the propagation distance was increased beyond the error free distance there was a slight divergence of the two sets of results with the FP filter appearing to give marginally improved Q values after ~3000km. This is contrary to what would be expected if Gordon-Haus jitter were the only effect degrading the system performance since the jitter reduction of the FBG would be less than that of the FP filter. However the Q would also have been reduced by SNR degradation and it is possible that the SNR would have been higher for the FP filter as it had a higher extinction ratio than the FBG. In any case the Q values were so low by this propagation distance that experimental error could account for the difference between the two sets of results. As the timing jitter alone was not measured in this experiment it is not possible to make any comment on whether or not the enhanced power of the stable pulses led to a reduction in the Gordon-Haus jitter.

6.4 Conclusions

The experimental results in this chapter show that it is possible to use fibre Bragg gratings as bandpass filters in high bit rate soliton communications to give a reduction in the rate of increase of Gordon-Haus jitter and suppression of the build up in ASE noise from successive amplifications along the transmission line. Although there was no advantage in terms of jitter reduction to be gained from using FBGs (both devices tested here gave close agreement with the theoretical results) there were other advantages. FBGs are inherently polarisation insensitive – the device used in these experiments had a PDL of <0.3 dB compared to 1.5dB for the bulk device. The PDL for the bulk filter was relatively high, a typical value for such a device is ~0.7dB but this value is still higher than that of the FBG. FBGs are also more attractive as they are compact in-fibre devices – device size is typically only a few centimetres and the in-fibre nature means that FBGs can be spliced directly into a system, there is no need to couple out and back into fibre as is the case with bulk devices. This should lead to a lower insertion loss for FBGs and this was the case. Of the two devices used in these experiments the insertion loss of the FBG was 2dB which was 0.2 dB lower than that of the bulk device. It should be pointed out that

the FBG used here was only a prototype and it should be possible to further reduce the insertion loss by more careful design and manufacture.

In the 1GHz experiment the rate of increase of the Gordon-Haus jitter was lower for the FBG than for the FP filter. The reason for this was simply that the bandwidths of the two devices were different, the experimental results for both filters were in good agreement with the theoretical predictions for filters of the relative strengths. For a real system more consideration would have to be given to filter bandwidth and the average dispersion of the system in order to optimise the performance. This is also true for the 10Gbit/s experiment. The propagation distance over which the signal Q value was above the required value of 6, which corresponds to a BER of 10^{-9}, was only 1500km. This is far short of trans-oceanic distances but is not much less than the SNR and Gordon-Haus limits for the system. The object of these experiments was not to achieve propagation over long distances – the intention was to compare the performance of FBGs with bulk FP filters at a data rate which is realistic in terms of the next generation of fibre links.

A further factor which must be taken into account when considering future systems is than wavelength division multiplexing may be used to increase the system capacity. If different wavelengths are to be used for different data channels then it is necessary to have a separate filter with the required pass-band for each channel. Due to the flexibility of the post-fabrication exposure technique which was used to make the grating used in these experiments, it is simple to fabricate a single FBG with multiple pass-bands positioned as required. As pass-bands can be positioned arbitrarily there is no problem making gratings for WDM schemes, even if unequal channel spacings are used to reduce the detrimental effect of four wave mixing. FBGs are also compatible with sliding guiding schemes where the central frequency of the filters is gradually changed along the length of the system.

Chapter 7

Soliton propagation over standard fibre using dispersion compensation

7.1 Introduction

Optical pulse propagation in standard fibre is a subject which has received a great deal of attention in recent years [9, 10, 11, 14, 15, 21, 121, 122, 123, 128],[212]–[223]. The main reason for this is that standard fibre makes up the majority of the >90 million kilometres of optical fibre which is installed worldwide and there is a desire to increase the capacity of these pre-installed fibre systems by increasing the data rate. Most of the existing links are currently operating at data rates far below the 5Gbit/s of the recently installed TAT12/13 trans-Atlantic cable[7]. The vast difference in the data rates of systems currently being deployed and older systems is that the older systems rely on electrical "3R" repeater stages to re-time, re-shape and re-generate the data signal with the optical fibre being used only as a transmission medium, whereas new systems are unrepeated systems which use optical amplifiers. In addition to being expensive and complicated electronic circuits 3R repeaters limit the data rates achievable as they require the optical signal to be converted into an electrical signal before it can be processed and re-converted into an optical signal.

The desire to increase the bit rate of transmission links led to research into methods of optical amplification, the idea being that if amplification could be achieved all optically without having to change from an optical to an electrical signal and back again, it would be possible to increase data rates dramatically. One method of optical amplification is to use the Raman gain of the optical fibre itself to boost the signal level [224]. This technique has achieved some success [103, 140],[225]–[228] but suffers from the need for a high pump power. It wasn't until the discovery and development of the erbium doped

fibre amplifier (EDFA) [22, 23] that all optical systems became a reality. In addition to being potentially faster than repeated systems, all optical systems are bit rate transparent and so have a great advantage when it comes to upgrading the system to a higher data rate: for a repeated system it is necessary to replace each of the electronic repeaters, as they can only operate at one fixed data rate whereas in an all optical system it is only necessary to upgrade the transmitter and receiver, the amplifiers will work at the new data rate. There is however a major drawback of the all optical system in that there is no re-timing or re-shaping of the data pulses between transmitter and receiver.

Unfortunately, the upgrade of existing standard fibre links from sub Gbit/s to 10Gbit/s is not simply a case of replacing the electronic repeaters with EDFAs; dispersion poses a major problem. Standard fibre is designed to have low dispersion in the 2nd telecommunications window as this is the operational wavelength of the original optical communications systems. EDFAs however operate in the 3rd telecommunications window at 1.5μm where the loss of optical fibre is minimal (early optical systems avoided 1.5μm as reliable, cost effective semiconductor devices for sources and detectors were not available at this wavelength at the time of implementation). This means that all optical standard fibre soliton systems have to overcome the prohibitively high dispersion of standard fibre at 1.5μm if they are to be viable - as mentioned in Section 2.7.1 Gordon-Haus jitter limits the length of 10Gbit/s SIF systems to ~1000km but in standard fibre the soliton period is only ~2.5km for 10ps pulses which are required for a 1:10 mark to space ratio. This restricts the system length to only a few hundred kilometres [128] as the amplifier span is higher than the soliton period and so the average soliton constraint is not met [36, 37]. Various methods of overcoming the dispersion limit have been suggested and tried: optical phase conjugation [229]-[237] is very effective but difficult to implement; pulse pre-chirping [212, 238, 239, 240] involves imposing a chirp, of the opposite sign to that which is acquired on propagation, on the pulses at the beginning of the transmission line. This pre-chirp is then undone as the signal propagates along the standard fibre. The propagation distance which can be achieved with this method is far short of real systems lengths as is the case with duobinary encoding of the signal [241]-[245].

This chapter considers the use of a technique which is showing a great deal of promise for increasing the propagation distance of high bit rate soliton data in standard fibre - dispersion compensation [89]-[94],[121, 128, 134, 246]. Using this technique a system suitable for upgrading existing standard fibre links to 10Gbit/s will be investigated experimentally. The extension from upgrading existing systems to developing new trans-oceanic

systems will also be considered. By using soliton-like pulses compatibility with all optical processing techniques [16, 18, 19] is ensured and the pulses can be used in optical time division multiplexed (OTDM) systems where pulses at a relatively low base data rate are interleaved to achieve a higher line rate [13]–[16],[150, 170, 172]. Both of these technologies require RZ pulse formats.

7.1.1 Dispersion compensated standard fibre systems – upgrade of existing links

Dispersion compensation is a technique which has been used extensively for NRZ systems to reduce the effect of dispersive pulse broadening and to reduce interactions between different channels in WDM systems [86, 118, 120]. The principle is that by including fibres/elements with opposing signs of dispersion in the transmission line the accumulated dispersion can be reduced. For a standard fibre soliton systems this means including a normal dispersive element to compensate for the high anomalous dispersion of the standard fibre. This section will concentrate on using fibre as the compensating elements but fibre Bragg gratings can also be used [247]–[250] as will be discussed in Chapter 8).

Early work showed that by including a single dispersion compensating element at the receiver timing jitter could be reduced [127], but if the dispersion compensation is carried out periodically along the transmission line system performance can be improved further and indeed such dispersion managed systems have advantages over uniform dispersion systems as described in Section 2.8.

Numerical simulations have shown that in a periodically dispersion compensated standard fibre system it is possible to propagate 10Gbit/s soliton data over 2000km [128] which is far in excess of the 200km uncompensated limit. Such a data rate and system length are typical of those required to upgrade existing European standard fibre systems. Here experimental results which go beyond this distance are presented and discussed.

7.2 Experiment

7.2.1 Experimental set-up

The experiment described in this section was designed to show that it is possible to propagate 10Gbit/s solitons over a few thousand km of standard fibre using periodic dispersion compensation. The experimental parameters were closely matched to those of

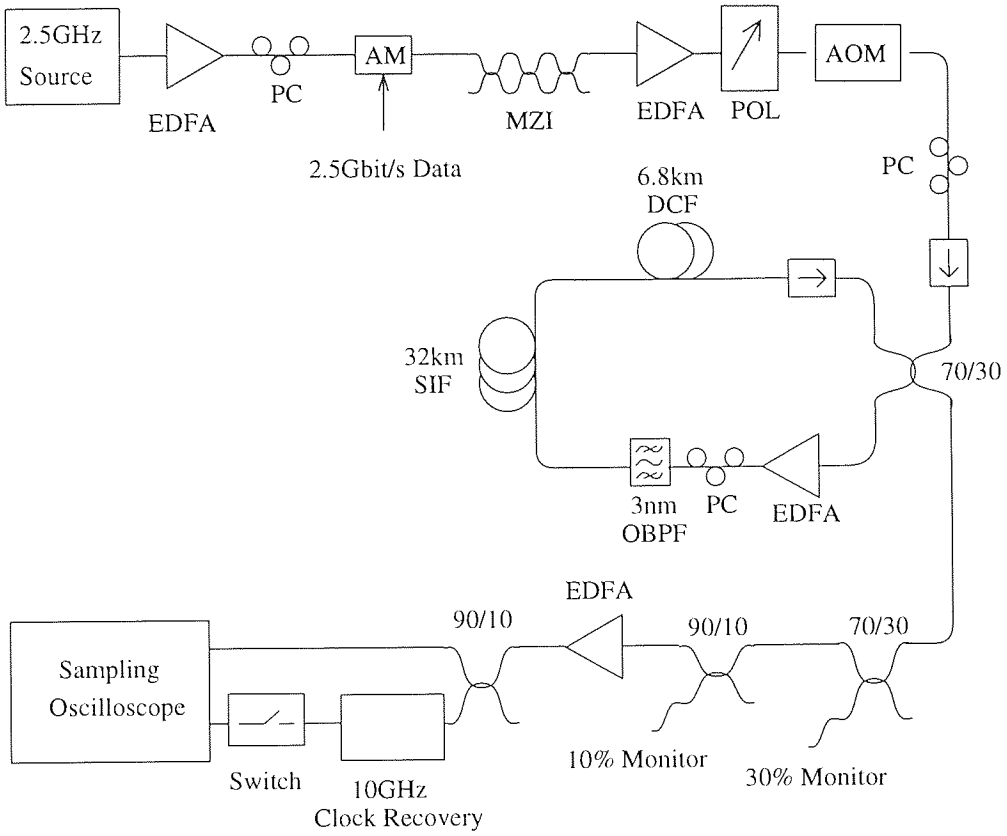

Figure 7.1: Schematic diagram of the standard fibre propagation experiment. An interleaved 10Gb/s PRBS was used as the signal and Q values were taken after propagation.

the previous numerical simulation described in Ref. [128]. The object was to show that existing standard fibre links could be upgraded to 10Gbit/s using a soliton system and replacing each of the electronic 3R repeaters with dispersion compensating fibre and an EDFA. The experimental set up is shown in Figure 7.1. The pulse source was a 2.5GHz actively mode locked erbium fibre ring laser (see Section 4.4 for details) and the 10Gbit/s data rate was achieved by interleaving as described in Section 4.4.1. In this experiment the operating wavelength was 1557nm, the pulse width was ~20ps and the time-bandwidth product was ~0.35 showing that the laser output pulses were a good approximation to transform limited and $sech^2(t)$ in profile.

The transmission system was the recirculating loop shown and as this was only a single span loop our experiment was limited to considering dispersion compensation and filtering every amplifier span. A schematic diagram of the transmission line is shown in Figure 7.2. After amplification, polarisation adjustment and filtering the signal passed through 31.6km of standard fibre (SIF), with a dispersion of 16.75ps/(nm km) at the operating wavelength, then through 6.8km of dispersion shifted fibre (DSF), with a total dispersion of -522ps/nm and loss of 4.2dB. A portion of the signal was coupled out of the loop after the DCF each round trip with this loop output giving the main output signal and two

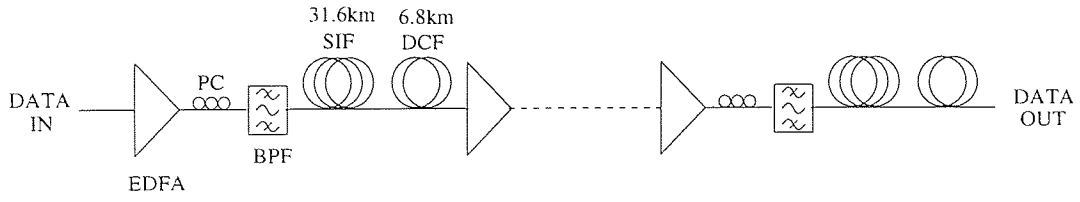

Figure 7.2: Schematic representation of the transmission line. Polarisation adjustment and filtering were done after each amplification. After propagation through 31.6km of standard fibre the average dispersion per amplifier span was reduced using 6.8km of standard fibre. This was repeated along the line until the required propagation distance was reached.

monitor outputs. The total round trip loss taking account of the fibre, the output coupler and all components was $\sim$ 15dB.

The average dispersion for the combined fibres was measured using the technique described in Section 3.4.2 and showed that at the operating wavelength the average dispersion was $\sim$0.15ps/nm/km. This dispersion gave an soliton period of $\sim$1100 km (taking the pulse width to be 20ps) which is far in excess of the 38.4km amplifier span indicating that the average soliton requirement that $L_a \ll 8Z_0$ was fulfilled. The low dispersion also meant that soliton soliton interactions would not be significant despite the mark to space ratio being relatively high at 1:5. Using Equation 2.69 gives a collapse length of 45000km which is far greater than even trans oceanic systems. The Gordon-Haus effect was more likely to put a restriction on the maximum possible transmission. Using Equation 2.63 and taking typical values for A_{eff} and n_2 gives the Gordon-Haus limit to be $\sim$ 6000km. This value does however assume a uniform average dispersion and takes no account of the effect of dispersion management which is known to extend the Gordon-Haus limit [96, 211]. For a data stream consisting of half ones and half zeros on average the power required to launch average solitons into the transmission fibre was $\sim$ 2.6mW which is in excess of the 1.4mW which was required to give a SNR corresponding to a BER of 10^{-9} after 10 000km.

7.2.2 Experimental results

Using the method described in Section 3.3.2, Q measurements were taken at various propagation distances, with the sampling oscilloscope trigger being a switched 10GHz clock recovered signal. The two loop output monitors were used to measure the average power and the power in the 10GHz component.

As the results in Figure 7.3 show the Q value decreased rapidly from the back-to back value of 11 reaching 7.2 after only 1100km. The Q then recovered and oscillated with a well defined period of $\sim$1400km. There was however an underlying decrease and a maxi-

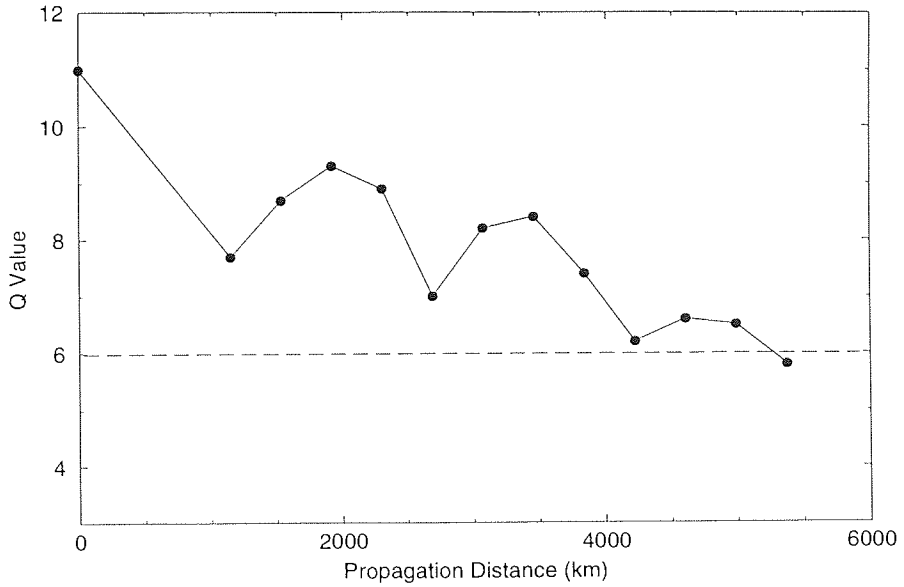

Figure 7.3: Q value versus propagation distance. The line indicates the minimum acceptable value of 6 which corresponds to error free transmission.

mum distance of 5275km was reached before the Q had fallen to the minimum acceptable value of 6. These oscillations in Q value were accompanied by oscillations in the pulse width. Measurements of the pulse width using autocorrelation could not be taken but eye diagrams from the sampling scope gave an indication of the pulse width fluctuations. Figure 7.4 shows scope traces corresponding to various propagation distances. From the

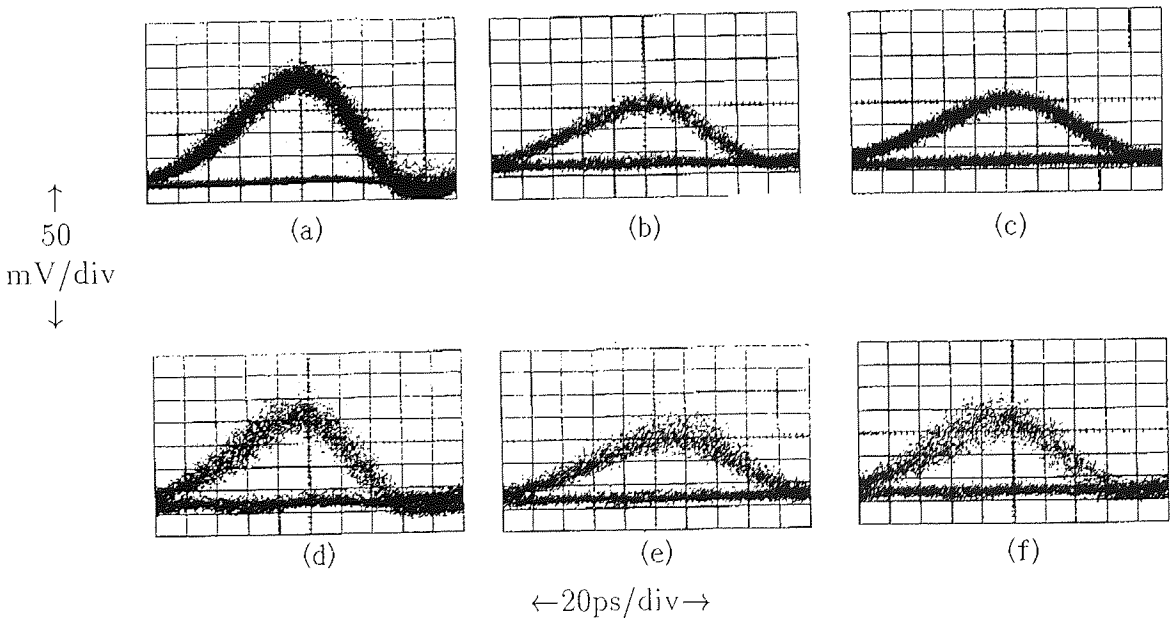

Figure 7.4: Eye diagrams of (a) the input pulses and after propagation distances of (b) 200km, (c) 400km, (d) 1750km, (e) 2500km and (f) 3500km. After an initial broadening of the pulse width the pulse width underwent a periodic compression and expansion.

initial width shown in Fig 7.4 (a) the pulses broadened rapidly with a corresponding de-

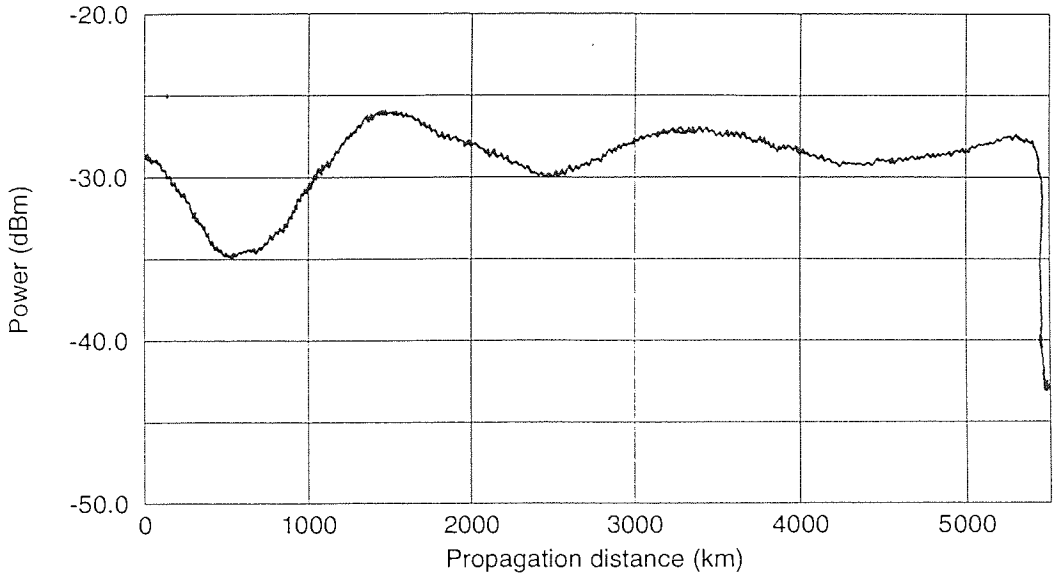

Figure 7.5: Power of the 10GHz electrical spectrum component of the propagating signal.

crease in Q value. By 1750km the original pulse width had been recovered (Figure 7.4 (d)) and the Q value had also improved to 9.2. This periodic broadening and compression of the pulse width continued in synchronisation with the Q value oscillations as the propagation distance increased. The power of the 10GHz electrical spectrum component of the propagating signal (shown in Fig. 7.5) also exhibited these oscillations with peaks in the spectrum corresponding to high Qs/narrow pulses and troughs corresponding to low Qs/broad pulses.

This long scale evolution of pulse width and Q, which should not be confused with the breathing of pulse width within the dispersion map, can be understood by considering the effect of dispersion management as described in Section 2.8. In this experiment a strong dispersion map was used where there were large fluctuations in the local dispersion and it is to be expected that the stable pulses varied significantly from the 20ps $sech^2(t)$ soliton input pulses. The degradation in the Q value over the first ~1000km was therefore due to the near $sech^2(t)$ input pulses changing shape and width to those most suitable for transmission in the strong dispersion map. The following oscillations in Q value were caused by a further complex evolution as the pulses settled to those with their time-bandwidth limited points at the required positions in the dispersion map.

These oscillations have also been reported in numerical simulations of dispersion compensated systems[92, 156] and a simulation was conducted for this experimental set-up. In this simulation the loss of the SIF was taken to be 0.22dB/km and the DCF loss was 0.62dB/km giving a total loss of 4.2dB. The loss of the DCF was taken as being uniformly distributed but in reality the actual loss of the fibre would have been lower than

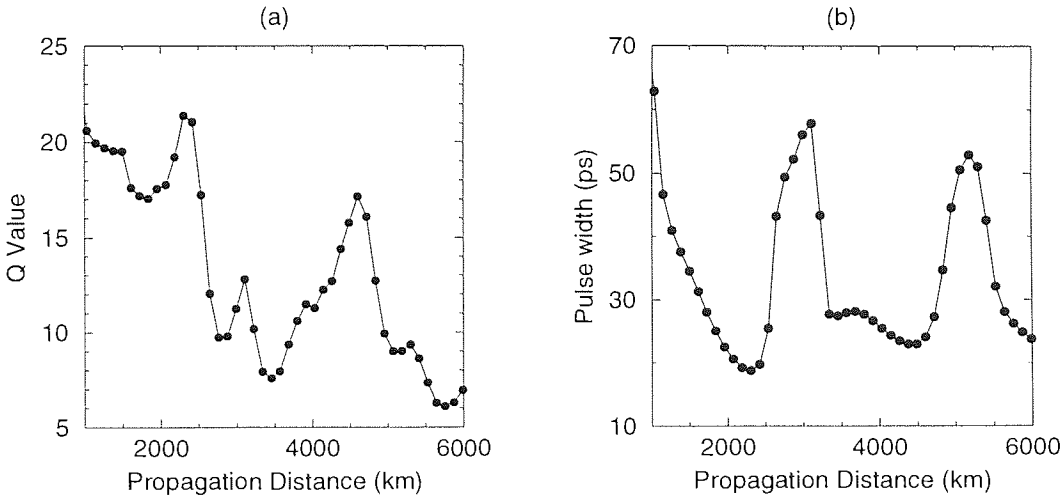

Figure 7.6: Numerical simulations of the standard fibre propagation experiment showing (a) Q values and (b) pulse widths versus propagation distance.

this value and there would have been a high slice loss due to mismatch of the core areas of the DCF and the SIF pigtails. The dispersion of the fibres and the average dispersion were as measured experimentally. Figure 7.6 (a) and (b) show the Q values and pulse widths versus propagation distance for this simulation. As for the experimental results, the simulation showed an initial degradation in the Q value and a subsequent oscillation. Oscillations in the pulse width were also seen with broad pulses corresponding to low Qs and vice versa. The periodicity of the oscillations and the exact values of Q differed for the numerical simulation and the experiment (the starting Q value was far higher in the simulations than could be achieved experimentally) but there is still a good qualitative agreement between the two sets of results.

An additional feature of dispersion managed systems is that there is an enhancement in the power of the stable pulses compared to those of the equivalent uniform dispersion system (see section 2.8). Using equation 2.77 to calculate the power enhancement for this experimental set up gives a theoretical value of F = ~9 for the lossless case. Experimentally, the optimum average power was found to be ~2.3mW which is ~ 10 times greater than the average power of the equivalent uniform dispersion system, which was calculated using Equations 2.46 and 2.74 for a data stream which has half ones and half zeros on average. Thus there is good agreement between the theoretical and experimental enhancement factors, even though the loss per amplifier span was 15dB in the experiment. This contradicts the findings of Ref. [117] which predicts a reduction of the enhancement factor when loss is included.

This enhanced power of the stable pulses in dispersion managed soliton systems has a major impact on system design as it allows lower dispersions to be used, which increases

the Gordon-Haus limit, without decreasing the SNR. As discussed in Section 2.5 the power of the solitons is proportional to the dispersion of the fibre so at low dispersion the signal power and hence the SNR is low. For propagation over 5500km (which was the distance achieved in this experiment) the average power required to give an acceptable SNR in this experiment was found (using Equation 2.73) to be ~0.8mW. Whilst this value was below the 2.3mW used experimentally it is greater than the average power of the equivalent uniform dispersion soliton which, as discussed above, was ~0.23mW. This indicates that in this experiment a lower average dispersion was used than could have been tolerated in an equivalent uniform dispersion system.

7.3 Discussion

This experiment has shown that it is possible to propagate 10Gbit/s soliton data over 5000km in a dispersion compensated standard fibre system. This distance is short of trans-oceanic distances but shows that such a system could be used to upgrade existing land based standard fibre links by replacing the electronic repeaters with an optical EDFA and the length of dispersion compensating fibre required to reduce the preceding amplifier span to the required average value. The inclusion of this additional fibre increases the loss per amplifier span and so increases the amplifier gain, which has the disadvantage of introducing more noise into the system. Despite this a standard fibre propagation distance of ~4700km was achieved with an amplifier span (standard fibre length) of 31.6km. A further point to note is that this experiment used a single span recirculating loop and so suffered from an additional loss of ~4dB per amplifier span, compared to an in-line system due to the loss of the fibre coupler, isolator, polarisation controller and filter each round trip of the loop. This additional 4dB could be taken up in an in-line system by increasing the amplifier span. Adding a further 15km of standard fibre and an appropriate additional length of DCF to the amplifier span would increase the loss by ~4dB per amplifier span and so an estimated amplifier span of almost 50km could be tolerated in a real system and further increases to amplifier span could be made at the cost of overall system length. Further advantages of using a dispersion managed soliton system are that there is an increase of the stable pulse power. In the experiment the soliton power was increased by a factor of 10 which increased the signal to noise ratio and would have had an associated reduction in G-H jitter. When upgrading existing links the effect of PMD may be considerable due to both the increase in data rate and the relatively high PMD

of the older standard fibre. By using soliton-like pulses the effects of PMD should be reduced [46] and also the system would be compatible with proposed all optical switching technologies[16]–[19]. It should also be possible to extend this system to a multi-channel WDM system and in relation to such systems dispersion management has the advantage of reducing the effects of collision induced jitter [138] and four wave mixing between different channels [137].

7.4 Reduction of pulse perturbations by optimisation of the dispersion map

The preceding section has shown that on a distance scale of 1000s of kilometres there was an evolution of the pulse width as the input pulses stabilised to those most suitable for propagation in the strong dispersion map. There was also an evolution of pulse width within the dispersion map and although this evolution could not be observed in the experiment because the pulses were only coupled out of the loop at the end of each recirculation, numerical simulations could be used to indicate what was happening within the fibres. Figure 7.7 (b), (c) and (d) show the evolution of the spectral width, pulse width and time-bandwidth product within the lossless dispersion map shown in (a). As discussed in Section 2.8 the unchirped and pulse width minima positions are at the mid point of the two fibres in the lossless case and the effect of loss is to move the unchirped position from the mid-point of the fibre [117]. It is therefore intuitive that the optimum launch position for a transform-limited source is not at the start of the fibre but at one of the transform limited points of the fibre. Launching at this position should lead to a reduction in the energy shed by the pulses and hence a minimum of corruption of the data. There will still be some evolution of the pulses though, as the pulse shape and width may not be ideal but by launching at the required point in the dispersion map stable propagation should be achieved sooner. When using a chirped source it would be necessary to alter the launch position so as to match the sign and chirp of the source. Alternatively, the pulses from a transform limited source could be pre-chirped so that on the input to the transmission fibre the pulse chirp matched that of the stable pulses [136, 251].

This purpose of this experiment was to examine how the dispersion map could be optimised to give stable pulse propagation in a dispersion compensated standard fibre system and to investigate what effect the alteration of the dispersion map had on the

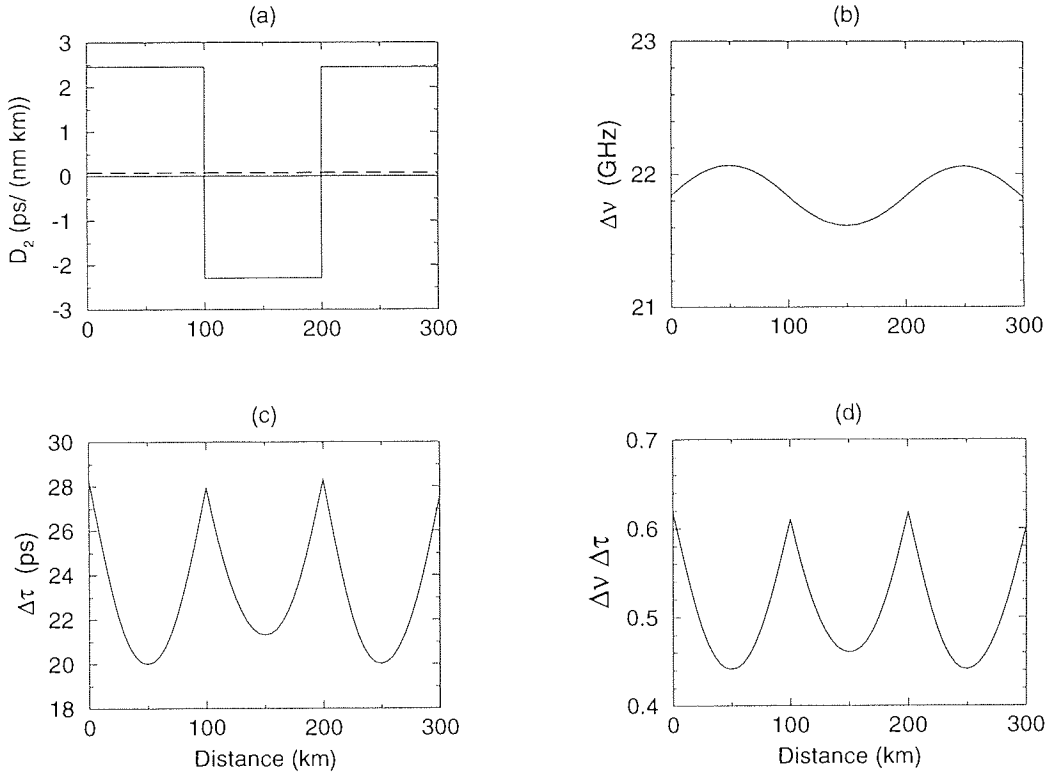

Figure 7.7: Evolution of (b) the spectral width, (c) the temporal width and (d) the time-bandwidth product of the stable pulses of the lossless dispersion map shown in (a).

transmission distance achievable. Both the launch position into the dispersion map and the position of the dispersion compensating fibre in the dispersion map were varied. Two sources with different chirps are also used and the effect of varying the input pulse power was investigated. The maximum transmission distances of the various set-ups will be compared and although unavoidable variations in the quality of the pulse from the source and in the back-to-back Q values make direct comparisons difficult, the stability of the propagation using the various dispersion maps can be compared.

7.4.1 Experiment

The basic loop set up of Figure 7.1 was changed as shown in Figure 7.8. The 10Gbit/s PRBS input data stream was derived as before and the loop output diagnostics were unchanged but after being coupled into the loop the pulses were propagated through an initial length of standard fibre (Fibre A) before being amplified. The DCF then followed the amplifier/PC/filter combination and the remainder of the standard fibre was positioned at B immediately before the output coupler.

To alter the relative launch position of the pulses within the dispersion map, the lengths of fibres A and B were varied but the total length of fibre in the loop was kept

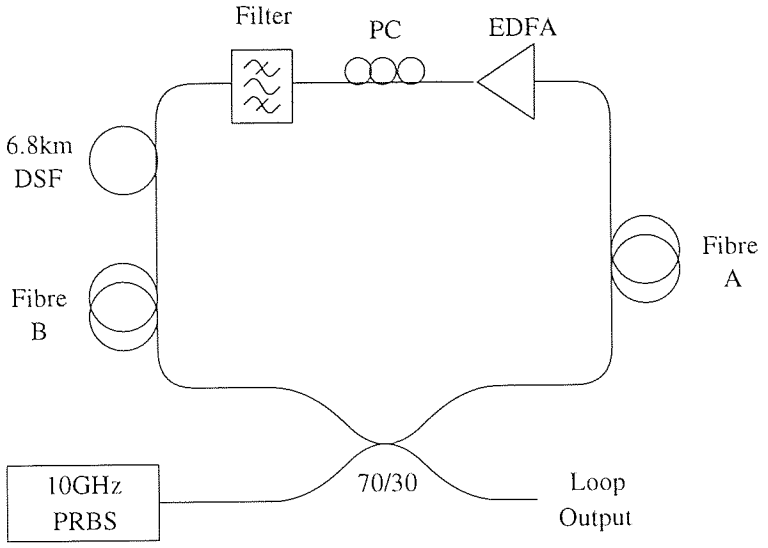

Figure 7.8: Schematic diagram showing the amended experimental set-up. The 10Gbit/s PRBS was coupled into the loop and passed through Fibre A before reaching the amplifier

fixed. Initial standard fibre lengths of 6km, 13km, 19km and 25km were used to give the transmission paths shown schematically in Figure 7.9. It is immediately obvious from this figure that for each set-up the dispersion map between amplifiers was identical and hence the amplifier span, the average dispersion per span and the loss per span were the same. It was therefore expected that the stable power and power enhancement factor would be roughly equal for each of the dispersion maps. The loop output coupler was however at a different position within the dispersion map for each set-up which meant that the additional ~1.5dB loss associated with the loop output coupler was encountered at a different relative position in the soliton power cycle. This was expected to have only a small effect on the average soliton dynamics but from a practical point of view it meant that the loop output power and loop monitor output powers were different for each set-up, even when the pulse power was the same.

Results were taken at different average power values for each set-up but for clarity the effect of varying the input power will be considered in Section 7.6. The results presented in this section were all taken with the an average power of ~2mW launched into the transmission fibre after each amplification. This corresponded to approximately the same average power and enhancement factor as was used in the previous experiment.

For each experimental set-up Q values and the 10GHz component of the electrical spectrum were measured against propagation distance. The 10GHz component of the electrical spectrum gives an indication of pulse intensity and timing jitter. To give an additional indication of pulse width variations the peak pulse heights were taken from the sampling oscilloscope. The peak pulse height taken as the position of the mean "one"

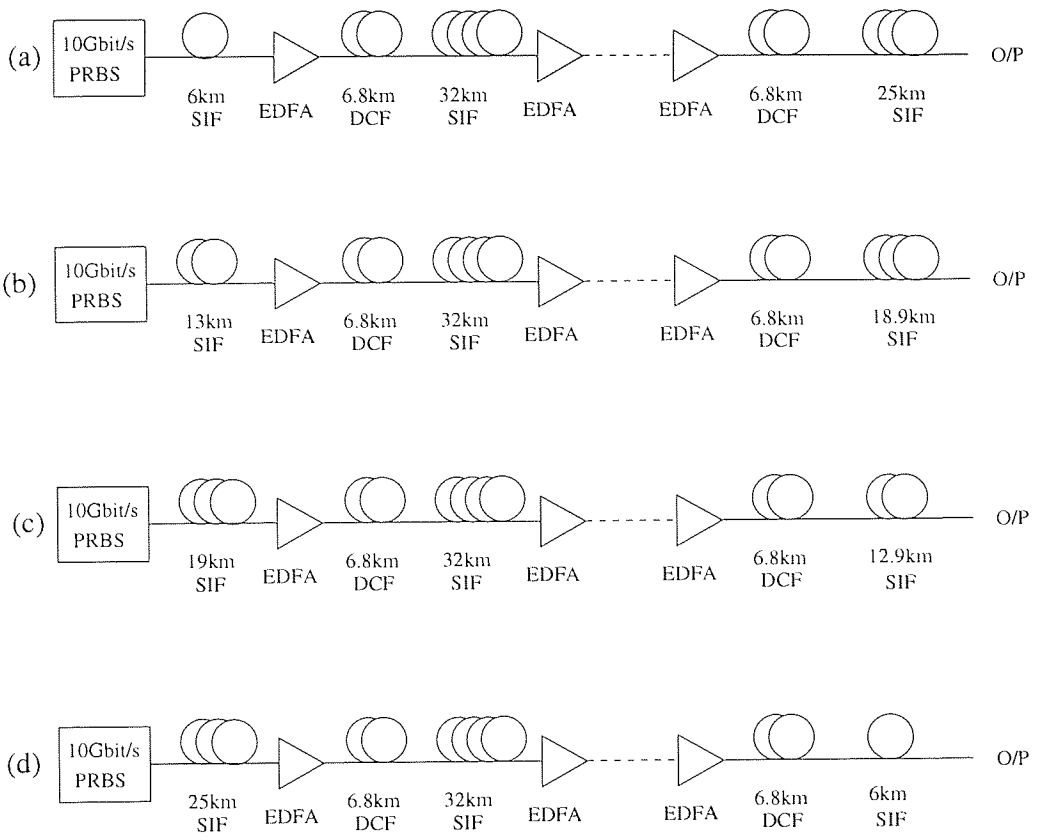

Figure 7.9: Schematic representation of the transmission lines. The fibre between amplifiers was the same but the initial length (and final length) of standard fibre was varied between set-ups.

level in the Q measurement eye diagram, was inversely related to the pulse width, with broader pulses having lower peak pulse heights. Thus, the pulse height could be used as an indicator of pulse width but it must be stressed that it only gives an *indication* of pulse width and does not give a direct measurement of pulse width.

The experimental results for each dispersion map are shown in Figures 7.10, 7.11 and 7.12 which show Q values, pulse height and power of the 10GHz electrical spectrum component respectively. Examining the results sequentially shows that for set-up (a) there was a rapid degradation of the Q and instability of the pulse width. There were however no oscillations in Q value as had been seen in the experiment in the previous section. When the initial standard fibre length was increased to 13km (set-up (b)) the pulse width became more stable, the electrical spectrum trace in particular showing no oscillations apart from the initial transient behaviour due to the circulating power stabilising. Again there was a steady decrease of the Q value but the rate of decrease was lower. With a further increase of the initial standard fibre length to 19km a slight ripple in the Q value was seen and there was a decrease in the stability of the pulse width. When the initial fibre length was increased to 25km clear oscillations in both the Q value and pulse width were seen. Comparing Figures 7.10,7.11,7.12 for set-up (d) shows that as before

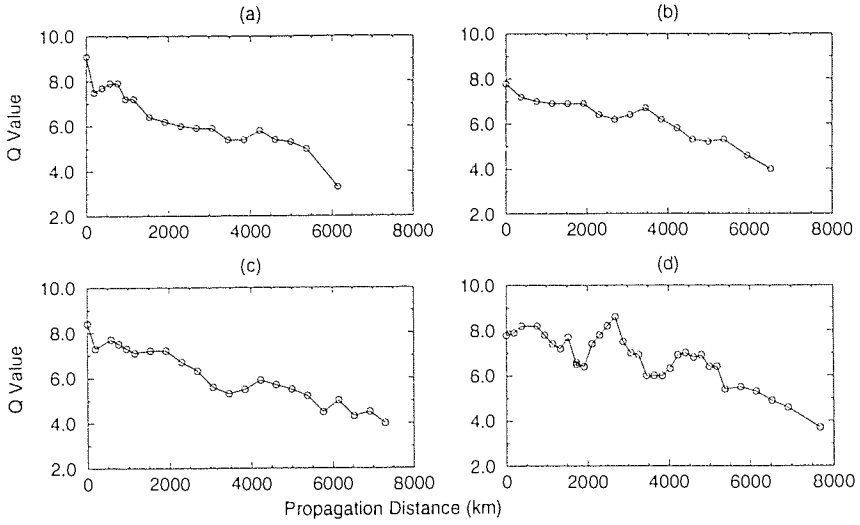

Figure 7.10: Q value versus propagation distance for propagation in standard fibre with initial SIF lengths of (a) 6km, (b) 13km, (c) 19km and (d) 25km.

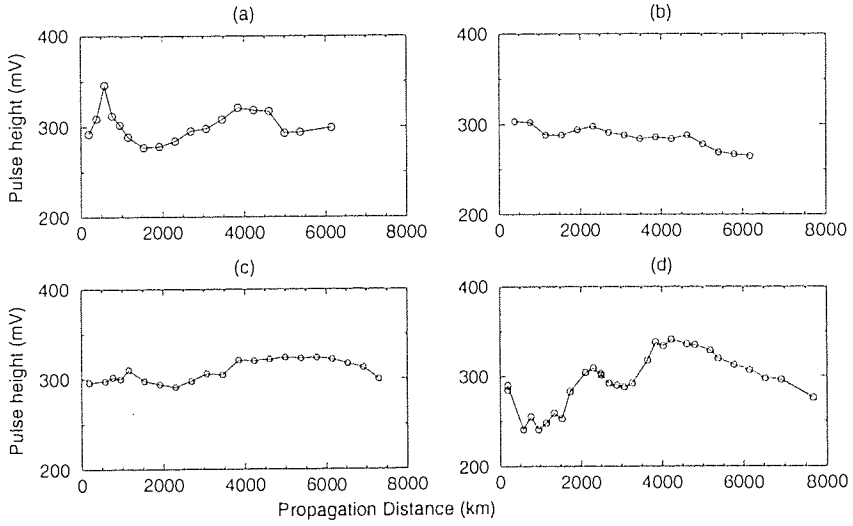

Figure 7.11: Pulse height versus propagation distance for the above experiment.

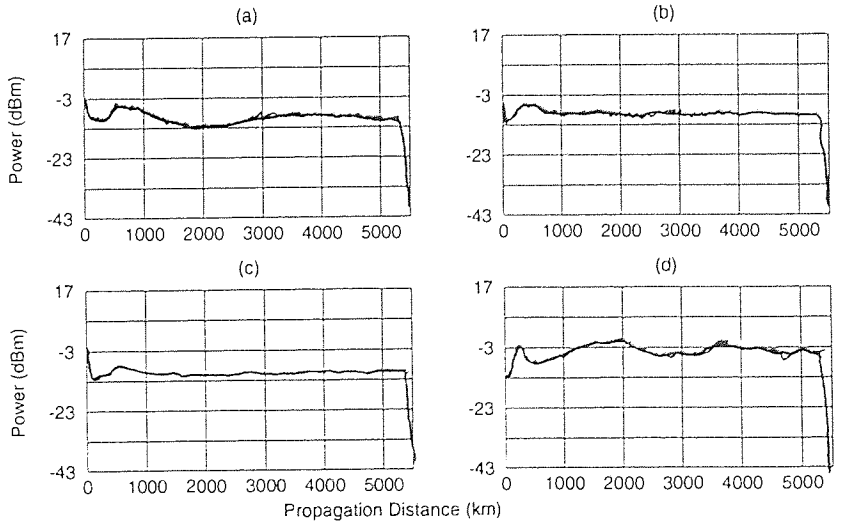

Figure 7.12: Power of the 10GHz electrical spectra versus propagation distance for the above experiment.

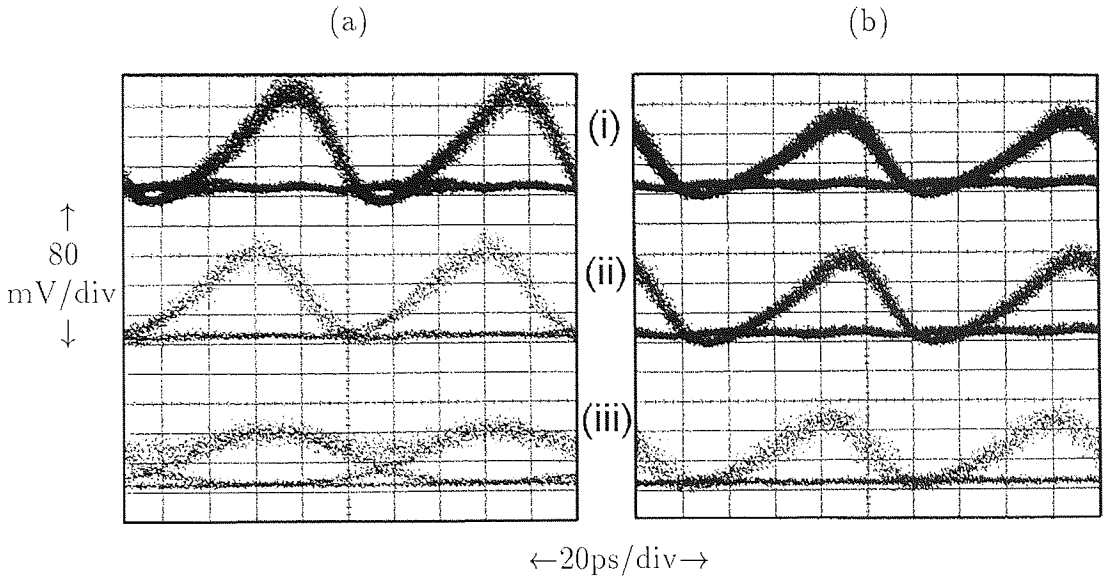

Figure 7.13: Eye diagrams for: (a) an initial SIF length of 6km at (i) 0km (input pulses), (ii) 1000km and (iii) 1900km; (b) an initial SIF length of 13km at (i) 0km (input pulses), (ii) 1000km and (iii) 3900km.

the oscillations in Q value follow those in pulse width with broader pulses corresponding to lower Qs.

These results show that in terms of pulse stability there is clearly an optimum launch position. For the source used here the pulse width variations were minimised for an initial standard fibre length of ~13km. A further indication of the pulse width stability is given in Figure 7.13.

Figure 7.13 (a) shows eye diagrams of (i) the input pulses and output pulses after (ii) 1000km and (iii) 1900km propagation in the loop for an initial standard fibre length of 6km (map (a)). There was little change in the pulse width within the first 1000km but after 1900km the pulses had broadened dramatically. For an initial standard fibre length of 13km (map (c)) there was little change to the input pulse width over 3800km of propagation. Figure 7.13 (b) shows eye diagrams for this map for (i) the input pulses, (ii) the output at 1000km and (iii) the output at 3800km.

Comparison of the maximum possible propagation distance for the four set-ups shows that set-up (b) which gave the most stable pulse evolution also gave the greatest transmission distance of 4000km before the Q value fell below 6. However for set-up (d) the Q recovered after falling below 6 at ~3500km and a maximum distance of ~5300km was achieved before the Q fell below 6 without recovery. This shows that the oscillations in pulse width were not having an adverse effect on the integrity of the data pulses which indicates that the pulses were not shedding a significant amount of dispersive radiation as they evolved – any dispersive radiation would have lead to a more rapid degradation of

the Q value. Whilst it is true that the oscillations in the Q value could have been masked out by using a saturated electrical amplifier and an appropriate filter at the receiver this would not have altered the fact that the pulse width was varying along the system length. In terms of upgrades to existing land based standard fibre systems, all four of the dispersion maps gave "error free" performance over 2000km at 10Gbit/s despite the rather poor back-to-back Q values of ~8. However the propagation distances achieved were short of trans-oceanic distances.

The experiment described above used a fibre ring laser as the source. As discussed in Chapter 4 such sources are used extensively for research purposes but in real systems semiconductor diode lasers are generally used due to their reliability, long life, ease of operation and small size. To give an indication of how such a device would perform with a dispersion compensated system the experiment was repeated using the 10GHz DFB laser described in Section 4.5 as the source in place of the fibre laser and inter-leaver. The time-bandwidth product of this laser was ~0.6 indicating that the output pulses were chirped and it was therefore expected that a different initial length of fibre would be required to give stable propagation.

The experimental results shown in Figures 7.14, 7.15 and 7.16 show that none of the four set-ups used gave particularly stable propagation and certainly the electrical spectrum trace could not be flattened to the same extent as could be achieved when the fibre laser source was used. Set-up (d) with a 25km initial fibre length was particularly unstable and the signal degraded rapidly.

Of the four set-ups (a) gave the greatest propagation distance of ~2800km which was considerably lower than the maximum distance which was achieved using the fibre laser source. In general, the system performed better when the fibre laser was used and the poor performance of the DFB was undoubtedly due to the dual wavelength operation of the DFB causing pulse splitting in the strong dispersion map.

7.5 Effect of re-positioning the DCF

The previous section showed how the launch position into the dispersion map could be optimised by varying the initial length of standard fibre. By referring back to Figure 7.7, which shows that there is one point in each of the fibres where the pulses are transform limited, it may also be possible to optimise the launch position by having an initial section of dispersion compensating fibre of the correct length and there is an indication

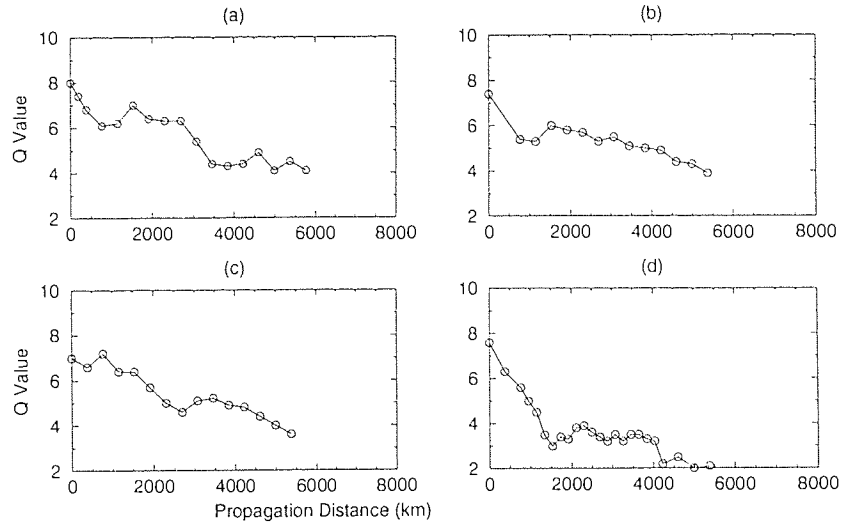

Figure 7.14: Q value versus propagation distance results for set-ups (a) - (d) using a DFB source laser.

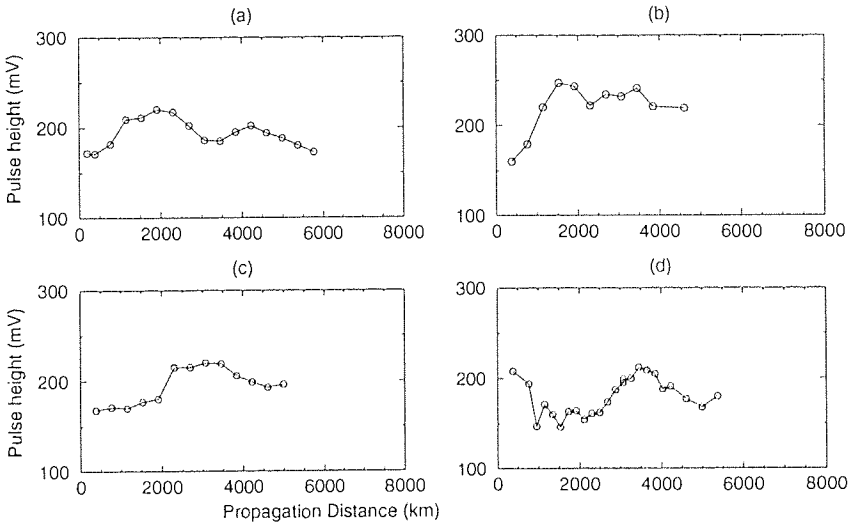

Figure 7.15: Pulse height versus propagation distance results for the above experiment.

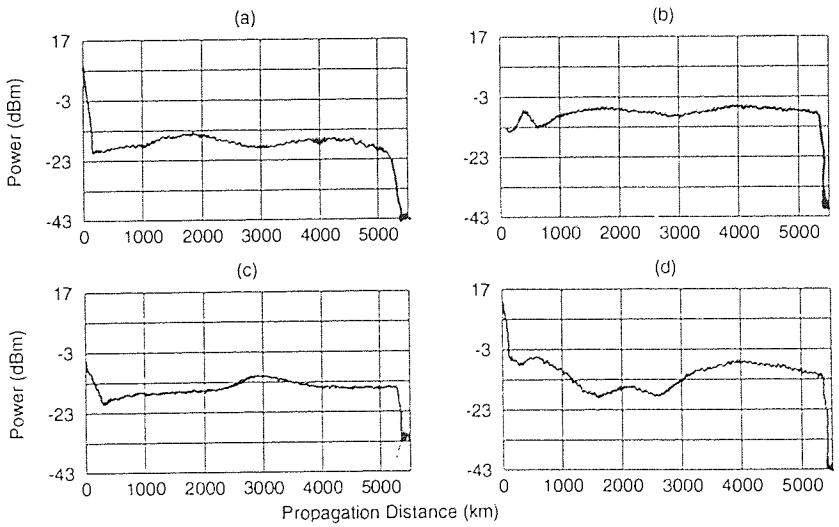

Figure 7.16: 10GHz electrical spectra for the above experiment.

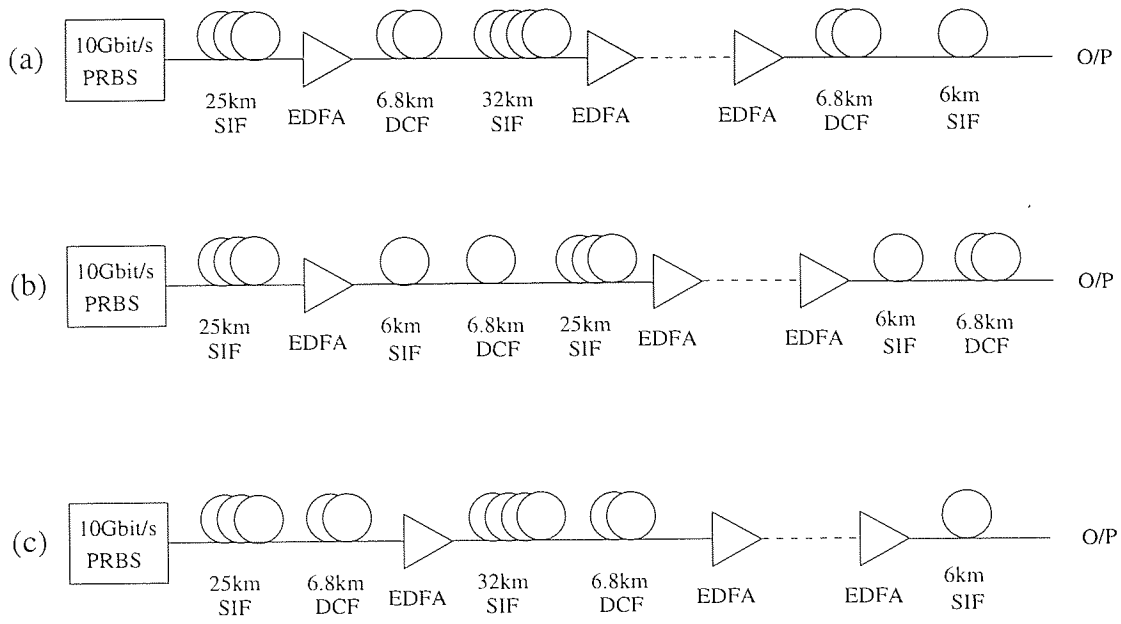

Figure 7.17: Schematic representation of the transmission lines with the DCF position was varied to give different dispersion maps.

from numerical simulations that this is the case [252]. Unfortunately, this could not be tested experimentally as the required lengths of dispersion compensating fibre were not available and splitting the 6.8km length was not possible. However the relative position of the entire 6.8km of DCF could be altered and as numerical simulations have shown the positioning of the dispersion compensating fibre within the map relative to the amplifier is important [94]. Here the effect of varying the DCF position is investigated experimentally and by numerical simulations.

Initially, three cases were considered as shown schematically in Figure 7.17. The source laser was the fibre ring laser and each of the three set-ups used the same fibres (6km and 25km of SIF and 6.8km of DCF) with only their relative positions altered. The first set-up was exactly the same as map (d) in the previous experiment with an initial standard fibre length of 25km. In set-up (b) the DCF was positioned in between the 6km and a 25km standard fibre lengths and in set-up (c) the initial length of fibre was both 25km of standard fibre and the DCF.

Experimental results are shown in Figures 7.18 and 7.19. For set-up (a) both Q value and pulse width showed oscillations as discussed in the previous section. With the DCF positioned between the two fibre lengths as shown in Figure 7.17 (b) the signal would not propagate over 1000km. The likely reason for this is that the standard fibre was split with the amplifier positioned between the two sections causing a significant departure from the average soliton model and leading to instability.

The only difference between set-ups (a) and (c) was that in (a) the DCF was positioned

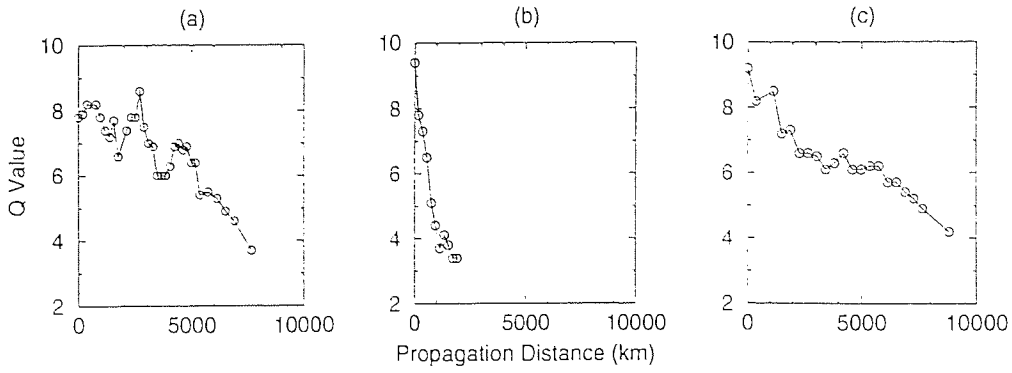

Figure 7.18: Q value versus propagation distance for three different DCF positions.

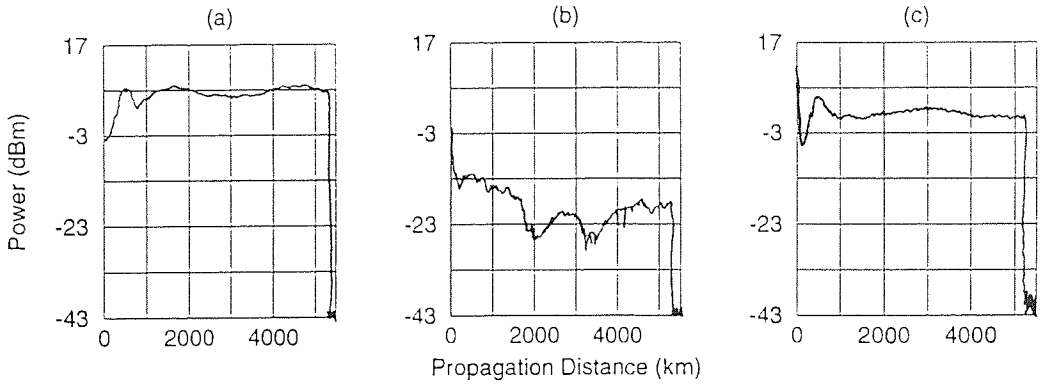

Figure 7.19: 10GHz Electrical spectrum for three different DCF positions.

after the amplifier whereas in (c) it was positioned before. The results show that this had a considerable effect on the stability of the system. With the DCF positioned before the amplifier there were no oscillations in either the Q value or pulse width. In addition there was no rapid degradation of the Q value within the first 1000km which is an indication that for this set-up the launch position and source were well matched and there was a minimal amount of pulse shaping required to achieve a stable pulse shape and width. A further reason for the instability of set-up (a) compared do set-up (c) is that for (a) the DCF was positioned after the amplifier where the pulse power (and hence nonlinearity) was highest. This could have an adverse effect on the pulse propagation since the DCF had normal dispersion and so was not soliton supporting. In case (c) the reverse was true and the SIF was positioned at the high power point where nonlinearity dominates and the DCF was positioned where the GVD was the dominating feature. However there is an indication from the results of Section 7.4 that the most important effect is the matching of the launch position with the source as it was possible to achieve stable propagation even with the dispersion compensating fibre positioned after the amplifier as long as the correct initial length of standard fibre is chosen. Despite the differences in the pulse evolutions for these two set ups similar error free distances were achieved. The error free distance

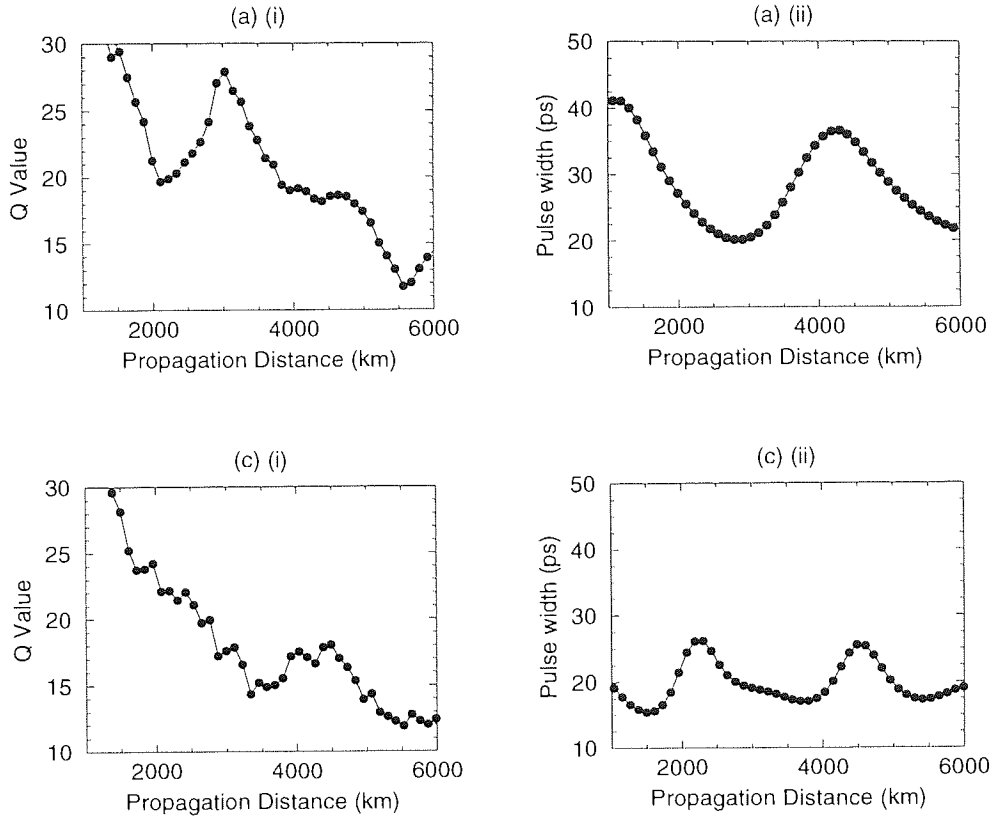

Figure 7.20: Numerical simulation results for set-ups (a) and (c) showing (i) Q values and (ii) pulse widths versus propagation distance.

with the DCF positioned before the amplifier was slightly higher at ~6000km but in this experiment the input Q was slightly higher.

Numerical simulations of Q value and pulse width versus propagation distance were performed for set-ups (a) and (c) using the same fibre paramenters as for the simulation in Section 7.2.2. The results of these simulations are shown in Figure 7.20.

There is a good qualitative agreement between the experimental results and the numerical simulations. The actual Q values are higher in the simulations but the starting Q value was far higher than could be achieved in the experiment. With the DCF positioned after the amplifier there was oscillation of the pulse width and instability in the Q value. With the DCF repositioned before the amplifier the pulse width oscillations were suppressed (though not completely removed) and the Q decrease in Q value was more stable. There was a good agreement between the Q values for the two numerical simulations beyond a propagation distance of 4000km.

As a further investigation the initial standard fibre length was varied with the DCF position maintained directly before the amplifier. The same fibres were used as before but with the maps shown schematically in Figure 7.21.

The experimental results are shown in Figures 7.22, 7.23 and 7.24 with the fibre laser

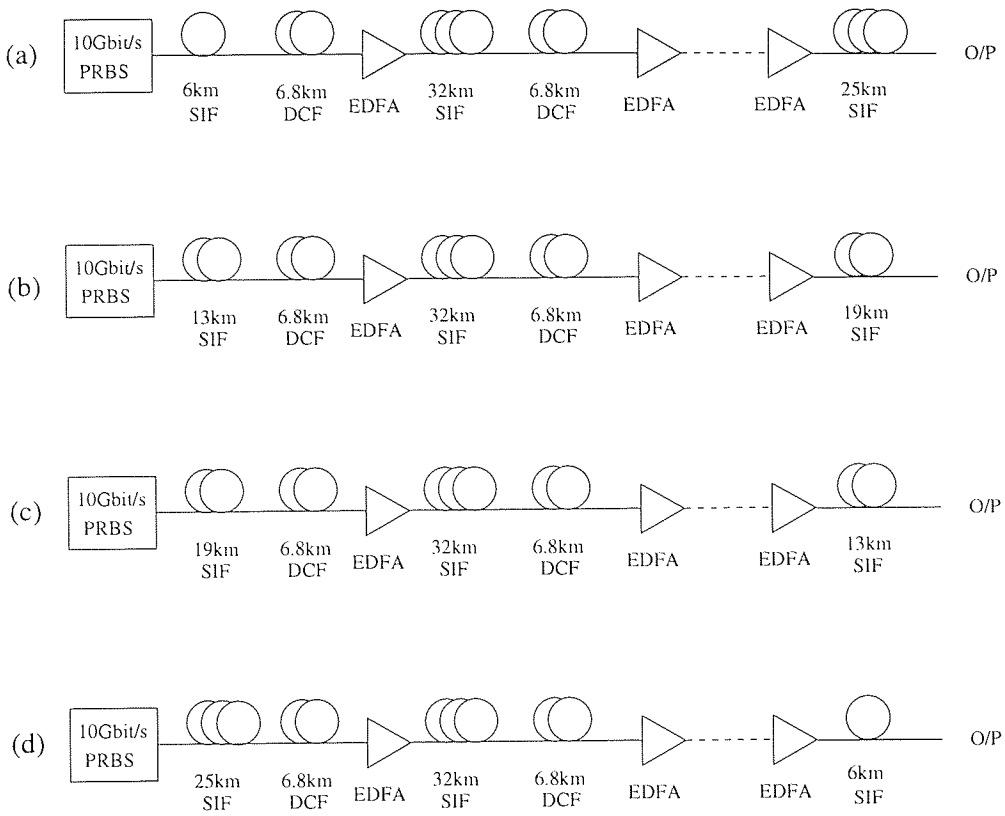

Figure 7.21: Schematic representation of the four experimental set-ups with the DCF positioned before the amplifier and the initial length of standard fibre was varied.

used as the pulse source. These results show that with the DCF positioned before the amplifier the optimum initial length of standard fibre was 25km (c.f. 13km with the DCF positioned after the amplifier). With this set-up the pulse width was stable after an initial adjustment of the pulses and the Q value showed no oscillations. The maximum propagation distance achieved was ~6000km and was roughly equal for set-ups (b),(c) and (d), which again shows that the oscillations in pulse width were not having a significant effect on system performance. For all four set-ups the maximum transmission which could be achieved was improved by positioning the DCF before the amplifier and the greatest distance which could be achieved with the DCF positioned before the amplifier was ~ 1000km greater than with the DCF after the amplifier.

Again the experiment was repeated using the 10GHz DFB laser as a source. The experimental results of Figures 7.25, 7.26 and 7.27 show that as expected the initial length of fibre which gave stable propagation was different for this source due to the different chirps of the two sources. For the DFB a 13km initial standard length gave the best stability. Once more, the system was not as stable when the DFB laser was used as the source due to the pulse splitting. The maximum propagation distance of ~3400km was less than when the fibre laser source was used but is an improvement on that achieved with the DCF positioned after the amplifier.

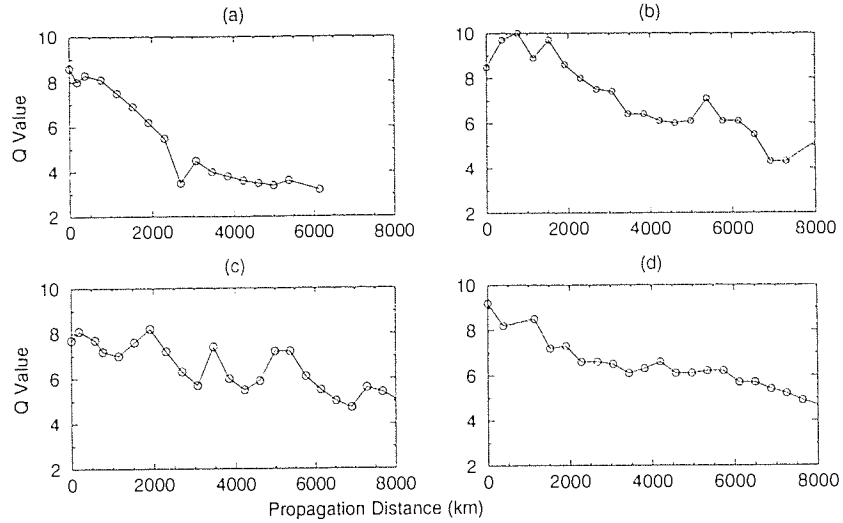

Figure 7.22: Q value versus propagation distance with DCF positioned before the amplifier

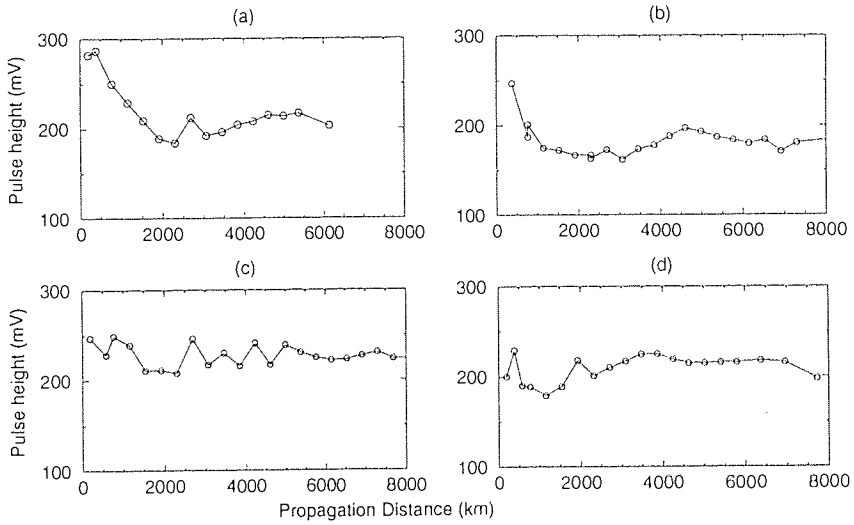

Figure 7.23: Pulse height versus propagation distance with DCF positioned before the amplifier.

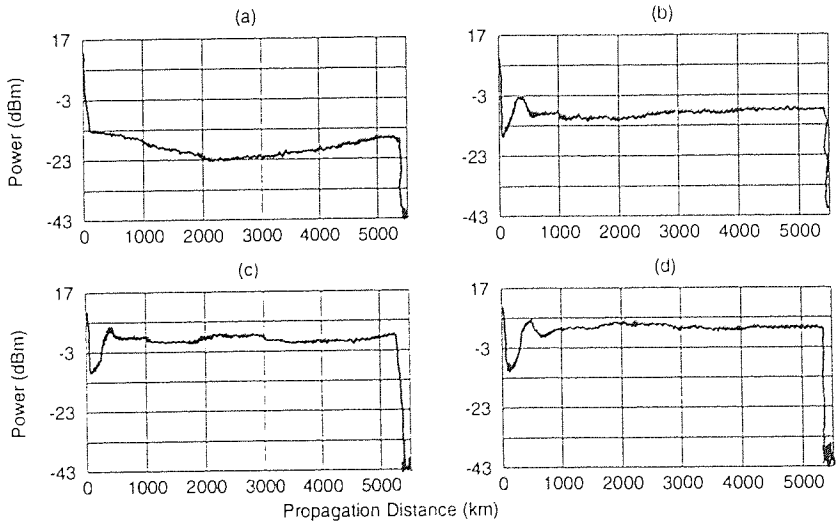

Figure 7.24: 10GHz Electrical Spectra with DCF positioned before the amplifier.

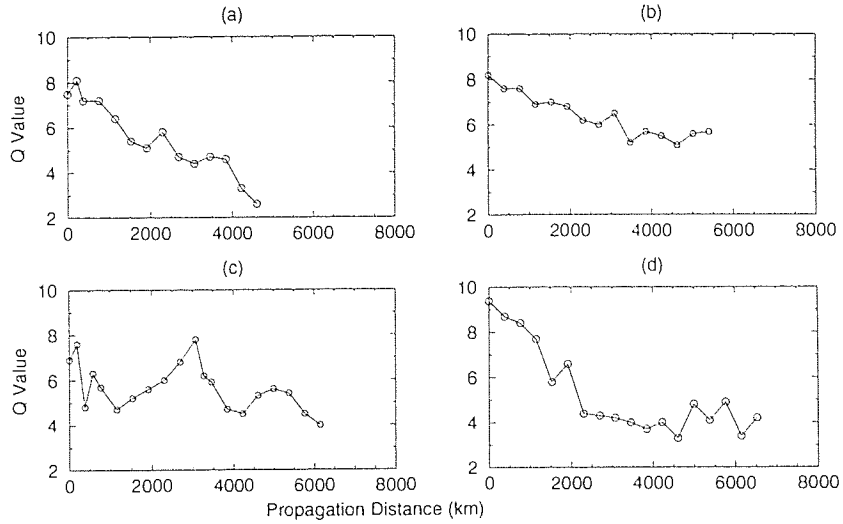

Figure 7.25: Q values using DFB source with DCF positioned before the amplifier.

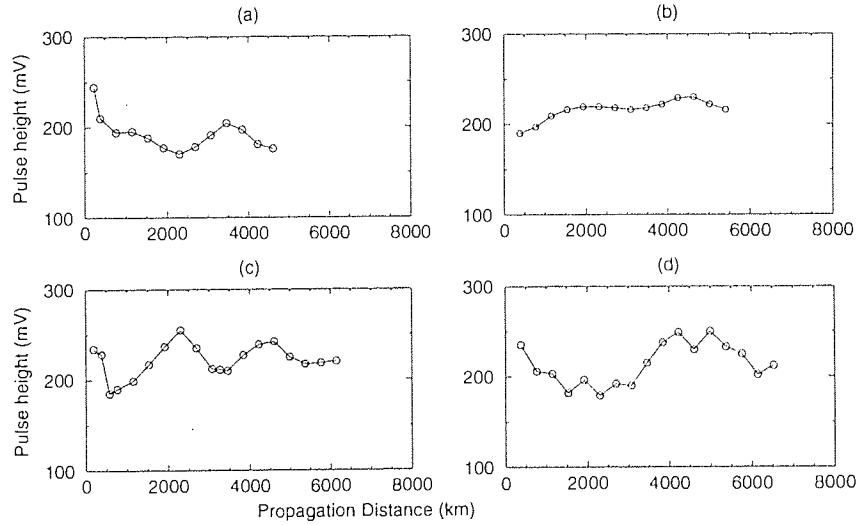

Figure 7.26: Pulse height versus propagation distance using DFB source with DCF positioned before the amplifier.

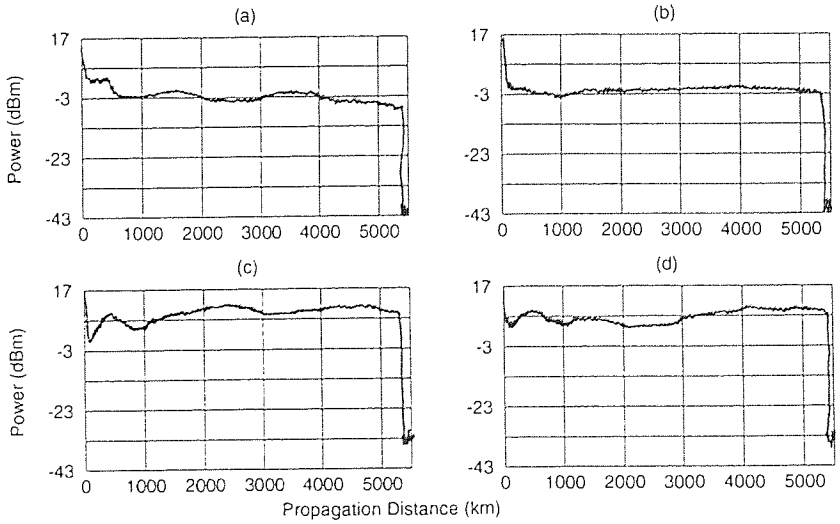

Figure 7.27: 10GHz electrical spectra using DFB source with DCF positioned before the amplifier.

7.6 Effect of varying the pulse power

By altering the gain of the loop amplifier as detailed in Section 3.2, the average power and hence energy of the pulses launched into the transmission fibre could be altered. This was done as a matter of course for each experimental set-up in order to determine the optimum power (i.e. the power at which the pulse evolution was most stable) and it was found that for different set-ups there was not a significant difference in the average power required for optimum transmission, the power required being more dependent on the strength of the dispersion map and the average dispersion of the system. Small variations in the pulse power ($\sim$ 1dBm or less) did not have a great deal of effect on the transmission with the pulses being resilient to small perturbations in their energy. This section looks at the effect on transmission when the pulse power deviated significantly from the optimum value.

Using the set-up shown in Figure 7.21 (b) (which had an initial length of fibre consisting of 13km of SIF and the 6.8km of DCF preceding the amplifier) and using the DFB laser gave the best illustration of the effect of varying the pulse power and so the results of this experiment will be used as an example. Figures 7.28, 7.29 and 7.30 show results of the experiment with the average powers of (a) 4.1mW, (b) 3.3mW, (c) 2.0mW and (d) 1.4mW launched into the transmission fibre.

At high pulse power the pulse width was unstable and oscillations were seen in the Q value. These oscillations decreased in amplitude as the propagation distance increased. As the average power was reduced the oscillations reduced and at $\sim$2mW the pulse width was stable and no oscillations of Q value were seen. With a further decrease in the pulse power there was a rapid increase in the pulse width accompanied by a decrease in Q. For the other dispersion maps used, which showed oscillations even when the input power was $\sim$2mW, a reduction in power did not give suppression of the oscillations but led to a rapid increase in pulse width. The reason why no suppression of the oscillations was seen was that these oscillations were due to a mismatch of the dispersion map and the launched pulses as opposed to power mismatch. The changes in pulse evolution as the pulse energy is changed is qualitatively analogous to that of solitons in uniform dispersion fibre. When the pulse energy was too high the pulses were unstable with the pulse width varying periodically. The instability in pulse width reduced as the pulse energy was reduced but after reaching a stable operating regime a further reduction in pulse energy led to broadening of the pulses without recovery. For an average power of 2mW a maximum

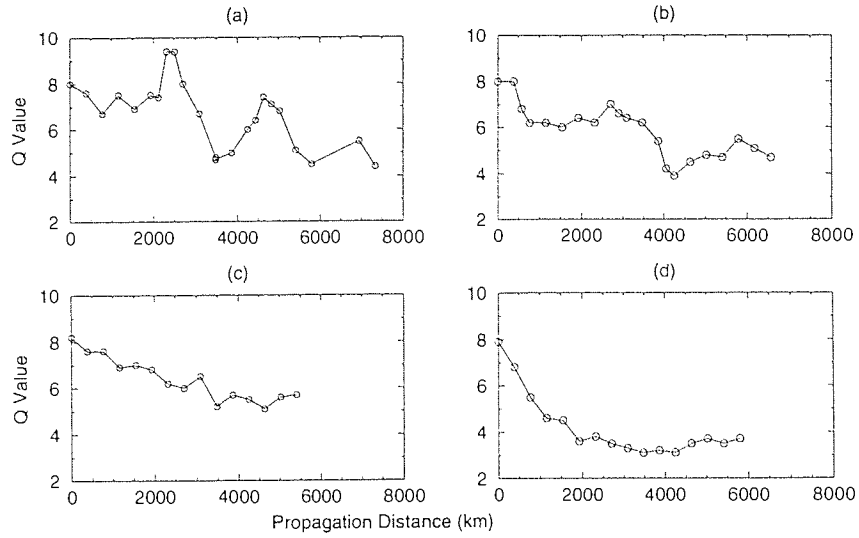

Figure 7.28: Q value versus propagation distance for four different pulse powers. Average powers were (a) 6.1dBm,4.1mW, (b) 5.2dBm,3.3mW, (c) 3.1dBm,2.0mW, (d) 1.6dBm,1.4mW

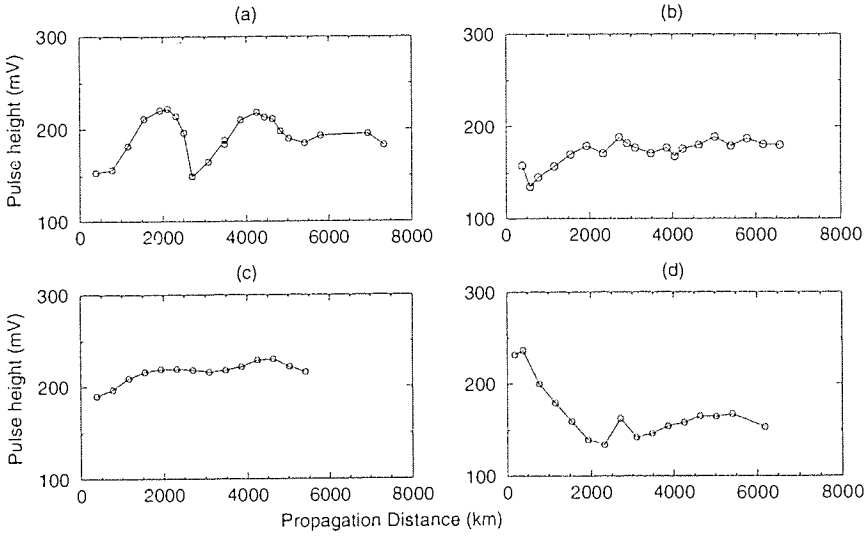

Figure 7.29: Pulse height versus propagation distance for the four pulse powers.

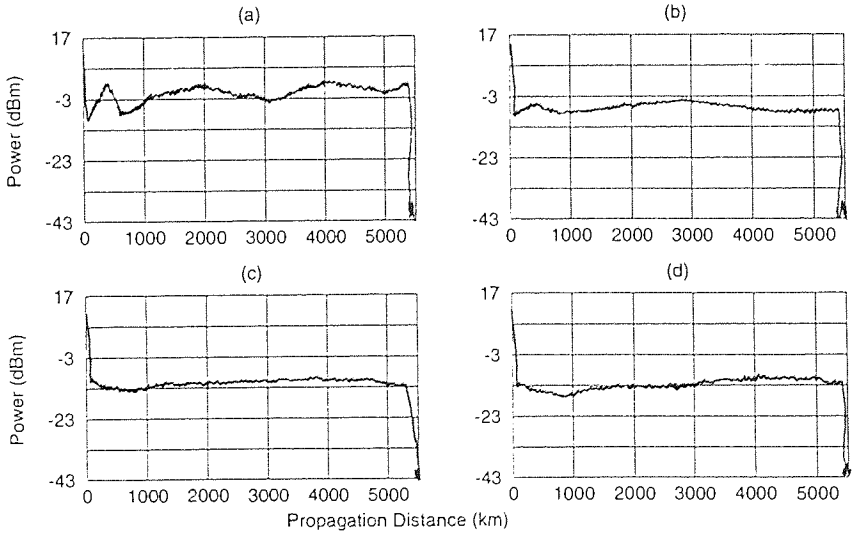

Figure 7.30: Electrical Spectra for the four pulse powers.

propagation distance of ~ 3200km was achieved before the Q fell below 6. A similar distance was achieved when the average power was increased to 4.1mW but in this case the Q value recovered and a maximum distance of 5100km was achieved.

7.7 Conclusions

In all of the experiments which have been conducted to try and determine the optimum launch position and pulse energy, oscillations in the pulse width have been observed when the dispersion map and the source are not well matched. These oscillations do not however appear to have a negative effect on the transmission of the data, indeed in many cases the propagation distance is increased when the oscillations in pulse width are present as the corresponding Q value oscillations allow the system to recover after initially falling below the minimum acceptable value of 6. Further work, both experimentally and numerically, is required in order to understand fully why these oscillations do not degrade the system performance and to ascertain what is causing the degradation of the Q value in the stable operating regime. It should be possible to damp out the oscillations in Q value by using an appropriate saturated RF amplifier and filter at the receiver

The maximum transmission distance which has been achieved with this single span recirculating loop is ~7600km. This value is short of the 10 000km required for a trans-Pacific system due mainly to the low back-to-back Q values and indeed "error free" transmission over this distance has been achieved with a similar dispersion map using a multi-span loop and an improved source [134]. Improvements in system performance may also be made by optimisation of the average dispersion of the system. The propagation distance achieved is however in excess of the maximum which has been reported in NRZ experiments [216, 253].

This chapter has shown experimentally that it is possible to upgrade existing standard fibre links to a 10Gbit/s data rate by simply replacing the electronic repeaters with a suitable length of dispersion compensating fibre and an erbium doped fibre amplifier. There are benefits of a more careful consideration of the dispersion map required and the stability of the pulse widths and the Q value of the propagating data depends on the position within the dispersion map that the pulses are launched and for different sources with different chirps this optimum launch position will vary. Matching the dispersion map to the source chirp is important in short-haul systems as mismatch can lead to a rapid degradation of the Q over ~1000km without recovery. The positioning of the

dispersion compensating fibre relative to the amplifier is also important – if a system is to be upgraded as detailed above, there is a clear advantage in positioning the DCF before the amplifier. By using solitons the upgraded system would be compatible with WDM and all optical processing techniques and should be resilient to PMD effects in the older pre-installed fibres. Due to the strong dispersion map of such a system a large power enhancement factor can be expected. In these experiments the stable pulse power was increased by a factor of 10 compared to the equivalent uniform dispersion system. This can allow a low dispersion to be used without encountering SNR problems leading to an increase in the Gordon-Haus limit. Although it is not clear from these experiments which process is causing the eventual failure of the system it seems likely that Gordon-Haus jitter was dominant – the Gordon-Haus limit for the equivalent uniform dispersion system is $\sim$ 6000km. There is evidence that the Gordon-Haus limit is increased for dispersion managed systems [96, 211] and this finding is backed up with these experimental results. Transmission has been achieved over $\sim$7600km which is in excess of the $\sim$ 6000km limit for the equivalent uniform dispersion system. WDM systems also benefit from using dispersion management as there is a reduction in the collision induced timing jitter [138] and in the efficiency of the four wave mixing process[137].

As is to be expected with a nonlinear propagating scheme the pulse power was critical to the operation of the system, too much power led to oscillations in the pulse width and Q and too little power led to rapid degradation of the signal. Whilst the system performance was not degraded (and may even be improved) by having excess power, too little power led to rapid degradation in system performance. The system was however resilient to small changes in the average power. For the various dispersion maps used there was little variation in the optimum power, the power enhancement factor being more dependent on the average dispersion and strength of the dispersion map than how the fibres were arranged in the dispersion map. It is therefore expected that the stable pulse width was similar for the various setups but unfortunately this could not be verified by autocorrelation.

Chapter 8

Dispersion compensation using fibre Bragg gratings

8.1 Introduction

As an alternative to using fibre in dispersion compensated systems, chirped fibre Bragg gratings (FBGs) can be used as the dispersion compensating elements [203, 208, 248, 249, 250],[254]-[257]. Fibre Bragg gratings are currently the subject of much interest and their use as dispersion compensating elements has been the focus of several recent experiments [188, 203, 204, 250, 257]. These experiments have not yet shown propagation over the same distances as has been achieved using DCF but this is an new technique and as the grating fabrication technology improves it is inevitable that the propagation distances achieved will increase and may even supersede DCF results. The reason for the interest in FBGs is that they have the advantages of being short compared to the equivalent length of dispersion compensating fibre and potentially have lower loss than DCF [181]. The small size is an advantage if existing standard fibre systems are to be upgraded to higher data rates by periodically including dispersion compensating elements – it is more practical to include a FBG at an amplifier stage than to include several km of DCF. FBGs unlike fibre are linear devices and this may lead to different propagation characteristics for example, it was seen in Section 7.5 that the position of the compensating fibre relative to the amplifier affected the pulse propagation. This may not be the case with FBGs.

Here the applicability of FBGs as dispersion compensating elements in 10Gbit/s soliton trans-oceanic systems is investigated. In principle the dispersion compensating scheme is simple but the main practical problem is that the gratings must have a relatively large physical size, typically being 10s of cm long in order to give the required delay over the

signal spectral bandwidth to compensate for the chromatic dispersion of several kilometres of SIF. This makes the gratings difficult to fabricate using existing technologies although the length of fibre gratings is steadily increasing, with the longest currently being over 1m in length [258].

A chirped grating, which reflects different wavelengths from different points along the length of the device, can give dispersion compensation for a length of standard fibre if the sign of the chirp is such that the blue end of the spectrum (which travels faster in standard fibre) is reflected from the far end of the grating whilst the red end of the spectrum is reflected by the near end. This creates a relative delay between the blue and red ends of the pulse spectrum and if the magnitude of the grating chirp is correct the temporal spreading of the pulse due to propagation in the fibre can be reversed. To compensate for a length of normal dispersion fibre the sign of the chirp of the grating must be reversed which can simply be done by turning the device around. In addition to having the required sign and magnitude of chirp the FBG must have a low insertion loss which means that a high reflectivity is required over the pass-band.

In order to give dispersion compensation for several km of standard fibre the required delay is large and hence the physical size of the required grating is large. In general, the length of a dispersion compensating grating is given by

$$L_G = \frac{c}{2n}\Delta\lambda(D_G) \tag{8.1}$$

where L_G is the grating length, c is the speed of light, n is the refractive index of the fibre, $\Delta\lambda$ is the grating bandwidth and D_G is the required dispersion of the grating. This equation shows that if a larger grating bandwidth or dispersion is required the grating length increases proportionally. In the case of a grating required to compensate for a 40km standard fibre span, the grating must have a total dispersion D_G = 660ps/nm assuming a dispersion of 16.5ps/(nm km) for standard fibre. The relative delay for a bandwidth $\Delta\lambda$ = 1nm is therefore 660ps. The physical size of the grating is then half the distance that light travels in fibre in 660ps (the factor of 1/2 being due to the reflected light making a double pass of the grating) giving a length of ~7cm taking n = 1.45 for optical fibre. While this length is very small compared to the ~ 7km of DCF which would be required to give the same dispersion, it is large on the scale of the wavelength of light and this makes fabrication difficult. Such gratings are typically fabricated using a phase mask of the required size and with the required characteristics. Phase masks are expensive and

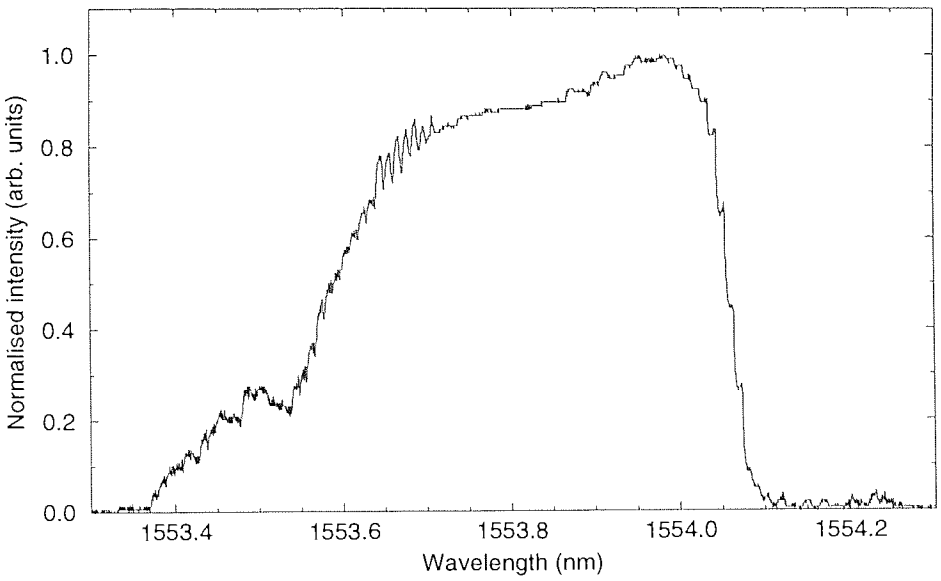

Figure 8.1: Reflection spectrum of the FBG. The peak of the spectrum was at 1554nm and the bandwidth was 0.47nm.

have the disadvantage of being inflexible – their characteristics are fixed at the time of fabrication and so only a limited range of gratings can be made with any phase mask. The grating characteristics can be varied slightly by stretching, heating or cooling the fibre before making the grating in order to alter the periodicity of the final device.

8.2 Propagation experiment

In determining the characteristics of the device which was to be used in the experiment restrictions were imposed by the fact that the longest phase mask available was ~5cm in length, fixing the length of grating which could be made. From Equation 8.1 it is seen that the grating bandwidth and fibre span are inversely proportional for a given grating length and for a 5cm grating with a 1nm passband the standard fibre length which can be compensated for is ~ 30km. In the experiment a longer fibre span was desired and so the bandwidth had to be reduced accordingly. The grating which was fabricated had the reflection spectrum shown in Figure 8.1. The peak of the reflection band was at 1554nm and the bandwidth of the grating was 0.47nm. The dispersion of the grating was measured using the technique described in Section 3.4.2 and the delay curve obtained is shown in Figure 8.2 (a) along with a linear fit to the data. From the fitted curve, the relative delay over the grating bandwidth was -435ps (the -ve indicating that the dispersion was normal) giving a total dispersion of -925ps/nm which shows that the grating could give total compensation for ~56km of standard fibre, assuming a dispersion of +16.5ps/(nm

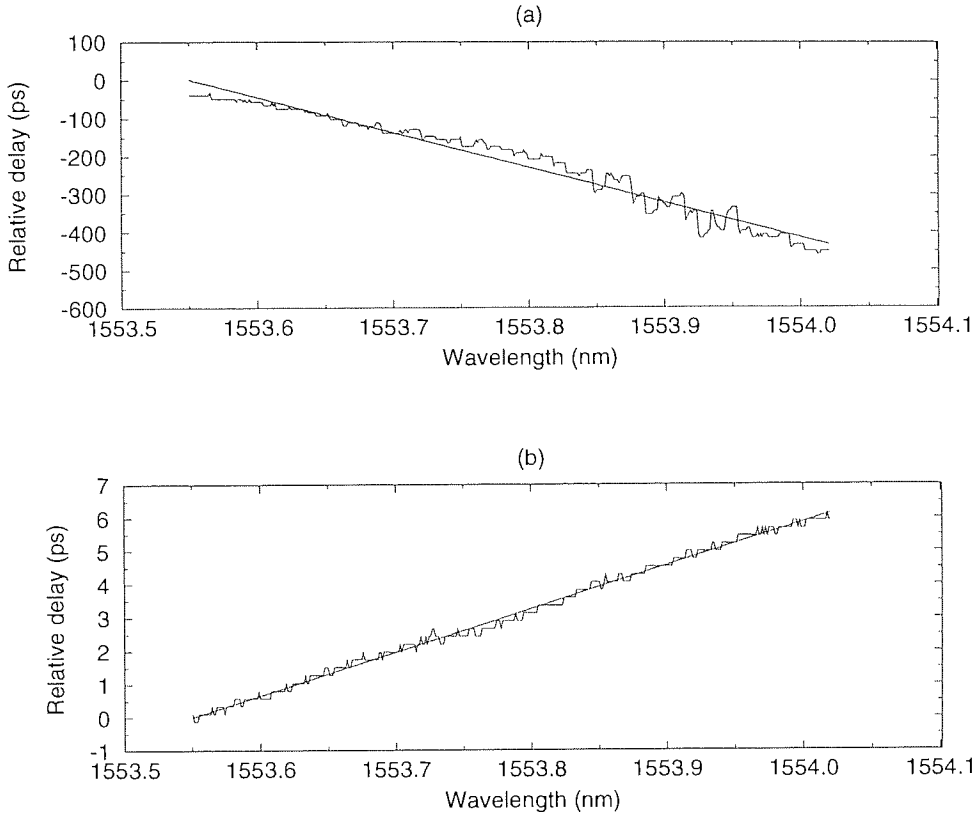

Figure 8.2: Relative delay versus wavelength for (a) the FBG and (b) the FBG and 57km of SIF.

km) for the standard fibre.

The experimental set-up used is shown schematically in Figure 8.3. The 10Gbit/s source used was the interleaved fibre laser described in Section 4.4.1 and with the wavelength tuned to 1554nm to coincide with the peak of the grating reflection band. A 3-port fibre circulator was used to couple the loop signal into the grating and then couple the reflected signal from the grating back into the loop. Fibre circulators are multi-fibre devices which use the Faraday rotation principle [259] to allow signals to be coupled through the ports of the device sequentially. Consider for example the path of the signal propagating through the loop. After passing through the transmission fibre the signal was coupled into the circulator (which in this case was a 3 port device) through port 1 and emerged on port 2 with a high isolation to port 3. This allowed the signal to be compressed by reflection in the FBG. After this reflection the signal was again coupled into the circulator with port 2 now being the input port. The light was coupled from this port onto port 3 where the signal emerged from the device. There was a high isolation between port 2 and port 1 to avoid back reflection into the loop. From this example it is easy to see that the ideal device characteristics are that there is lossless coupling between adjacent ports and infinite isolation between the input port and all other ports. High isolation between the final output port (port 3 in this case) and the other ports is also required

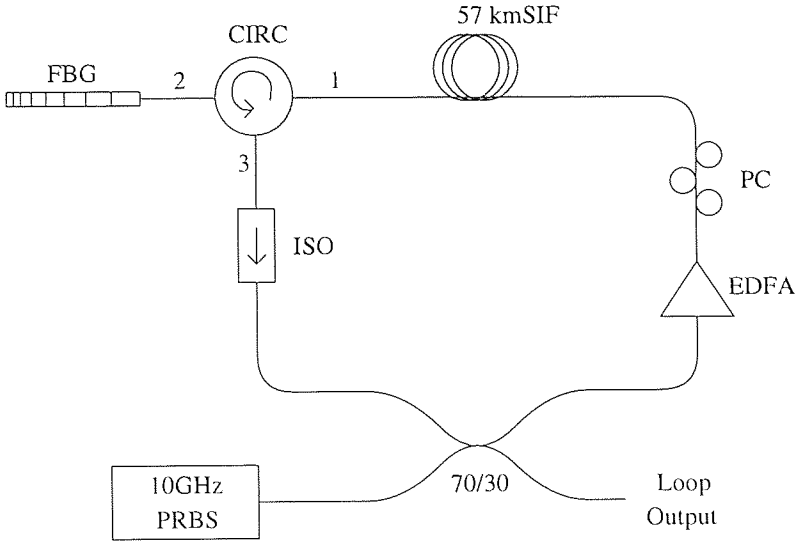

Figure 8.3: Schematic representation of the FBG dispersion compensation experiment. The propagating signal was coupled into the grating using a circulator. The reflected signal from the grating was then coupled back into the loop through the circulator

Ports	Forward Loss (dB)	Isolation (dB)
1-2	0.7	50
2-3	1	51
1-3	68	60

Table 8.1: Characteristics of the 3 port circulator

so that any stray light which enters the circulator through this port is highly attenuated. The characteristics of the circulator which was used here were measured and are shown in Table 8.1. The losses indicated include splice and connector losses and show that the total insertion loss of the circulator was $\sim$ 1.7dB. Since a circulator must always be used in such experiments it is important that the total insertion loss of the grating and the circulator is as low as possible. As these characteristics show the circulator gave high isolation in the reverse direction.

The transmission fibre used was 57km length of SIF to give a net anomalous dispersion in the loop. The dispersion of the fibre, circulator and grating was measured using the technique described in Section 3.4.2 and the delay curve obtained is shown in Figure 8.2 (b). As shown the dispersion was anomalous and the delay was $\sim$ 6ps giving an average dispersion of 0.22ps/(nm km). The graph also shows that the grating did not compensate for the dispersion slope of the fibre.

The combined insertion loss of the circulator and grating was 3.6dB which was $\sim$0.6dB less than the loss of the DCF module used in the experiments in Chapter 7. Of this 3.6dB,

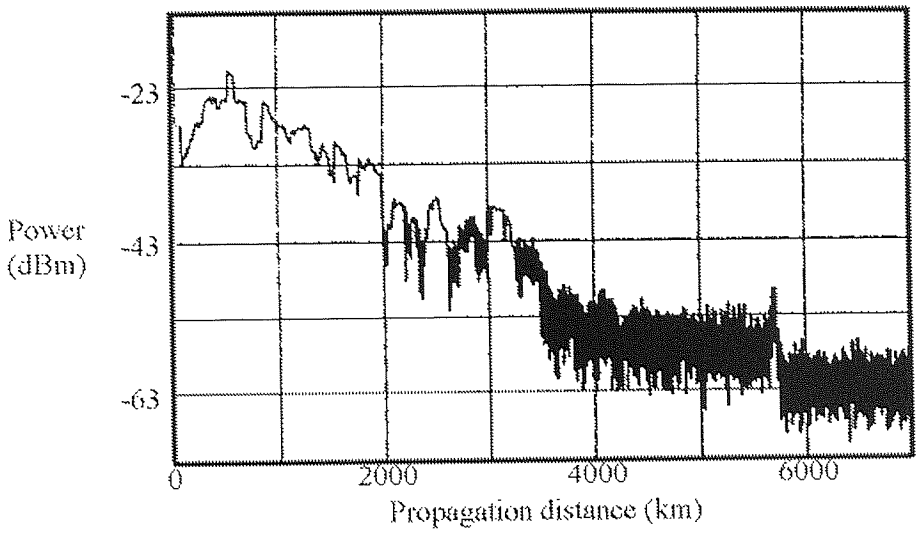

Figure 8.4: Electrical spectrum analyser trace for propagation with a FBG used to give dispersion compensation for 57km of SIF.

$\sim$ 1.7dB was due to the circulator as described in Table 8.1. In addition the loop round trip loss was reduced as the FBG was the only filter used in the loop saving another 2dB. This reduction in the round trip loss allowed a longer amplifier span to be used in this experiment, the amplifier span was increased to 57km from 38km when the dispersion compensated fibre was used with only a 1.2 dB increase in the loss per amplifier span.

8.2.1 Experimental results

The operation of the recirculating loop was exactly the same as in the DCF experiment described in Section 7.2. The two monitor outputs were used to check the average power level and the power in the 10GHz component of the electrical spectrum of the propagating signal, as the experiment was being performed. The average power was reasonably stable with time but the electrical spectrum was very unstable changing instantaneously in a random fashion. Figure 8.4 shows a typical electrical spectrum analyser trace with a rapid decrease in the power and an unstable power level. Q values were measured and from a back-to-back value of 9, the Q had fallen to 3 within the first 5 recirculations of the loop. There was no recovery of the Q value when propagation distance was increased.

The performance of the system was considerably poorer than was anticipated and in order to further study what was causing the pulse degradation the loop was split to allow an in-line experiment to be conducted using the set-up shown schematically in Figure 8.5. This allowed measurements to be taken after only a single pass of the grating.

The spectra of the input pulses and the grating output pulses were measured and are shown in Figure 8.6. There was no great difference between these two spectra but

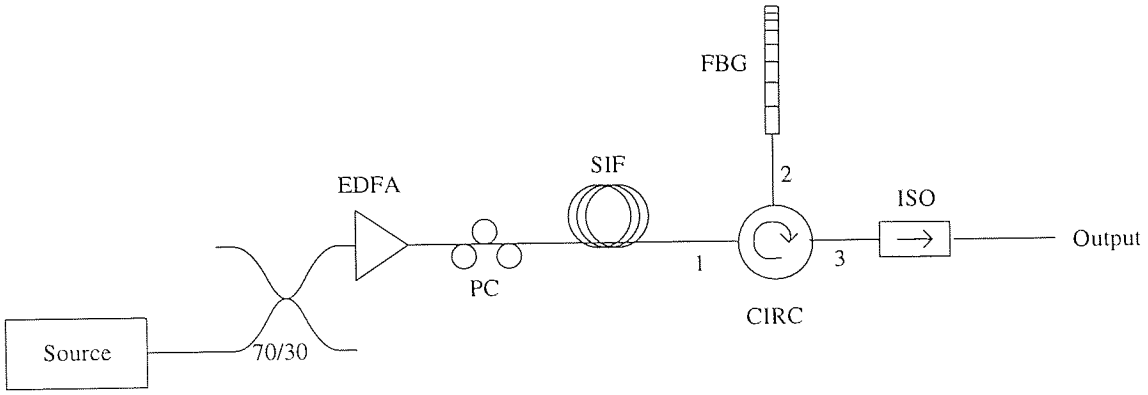

Figure 8.5: Schematic diagram of the in-line FBG dispersion compensation experiment. Measurements could be taken after a single pass of the circulator and grating. Including a PC allowed the input polarisation to be altered.

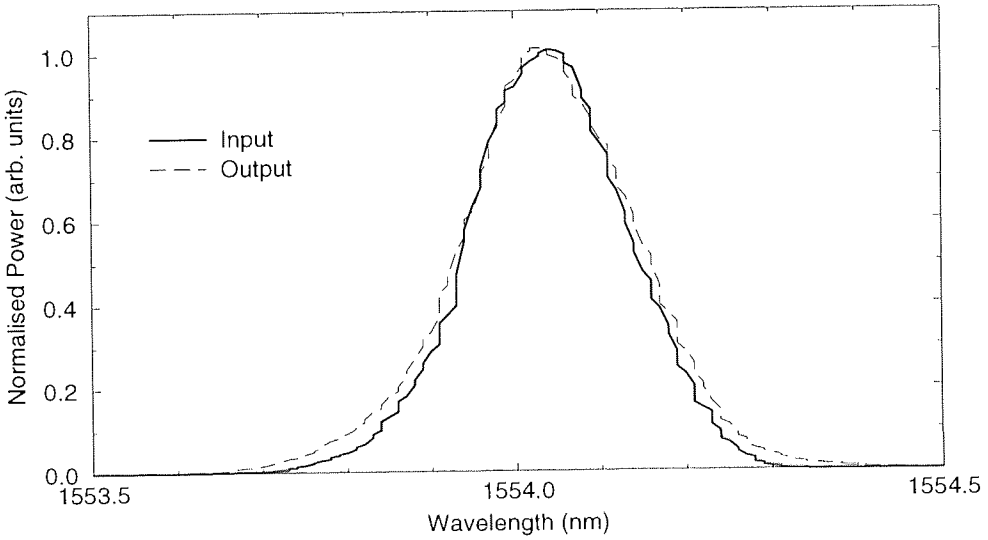

Figure 8.6: Spectra of the input (solid line) pulses and the pulses after a single pass of the FBG (dashed line).

the output pulses had a slightly broader spectral width of 0.24nm (compared to 0.21nm for the input pulses) which is approximately half the bandwidth of the grating. As the polarisation of the input signal was altered using the polarisation controller, no change was seen in the spectrum of the output pulses. Comparing the output data stream with the input as monitored on the sampling oscilloscope showed that there was a large increase in both the timing and amplitude jitter, as shown in Figure 8.7. The jitter was greater than expected for such a short propagation distance, so to investigate further the input signal was changed from a PRBS data stream to a continuous pulse stream. Observing the output pulse stream on the sampling oscilloscope, a large variation was seen with pulses dropping out randomly even when measured over only a few seconds. The four sampling scope outputs shown in Figure 8.8 give a good indication of this variation. These four traces were all taken within one minute of each other.

The fact that all pulses were not affected simultaneously indicated that the problem

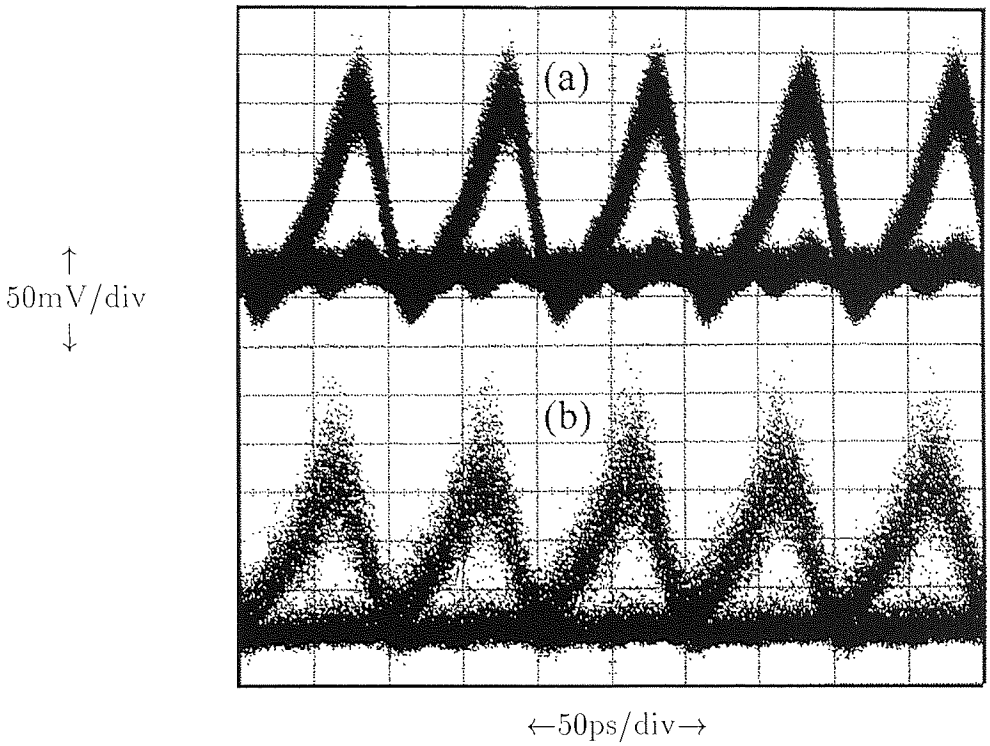

Figure 8.7: Sampling oscilloscope eye diagrams for (a) the input data stream and (b) output data stream after a single pass of the FBG.

was related to the signal polarisation – the pulse stream had been interleaved from 2.5GHz to 10GHz with adjacent pulses having travelled different paths through the inter-leaver. It was therefore expected that any small variation in polarisation of one set of pulses would not be matched by the others. This theory was backed-up by the fact that every fourth pulse in traces (b) - (d) of Figure 8.8 were similar.

In order to simplify the experiment the inter-leaver was removed and laser output pulse stream at 2.5GHz was used as the input. Comparison of the input and grating output pulses (see Figure 8.9 (a) and (b) respectively) showed that again there was a significant increase in the jitter and also that there was broadening of the pulses which is indicated by the reduction of the oscillations in the oscilloscope trace for the output pulses. These oscillations were caused by ringing in the photo-diode used to detect the optical signal and is more prominent the shorter the pulse width. The stability of the pulses had increased compared to the 10GHz experiment but when the polarisation of the input pulses was altered using the polarisation controller, there was a variation of the pulse position on the sampling scope screen. Figure 8.10 (a) and (b) show the grating output pulses for two different input polarisations and (c) shows a superposition of the output pulses as the input polarisation was varied. This variation in pulse position was attributed to high polarisation mode dispersion (PMD) in the system – one polarisation

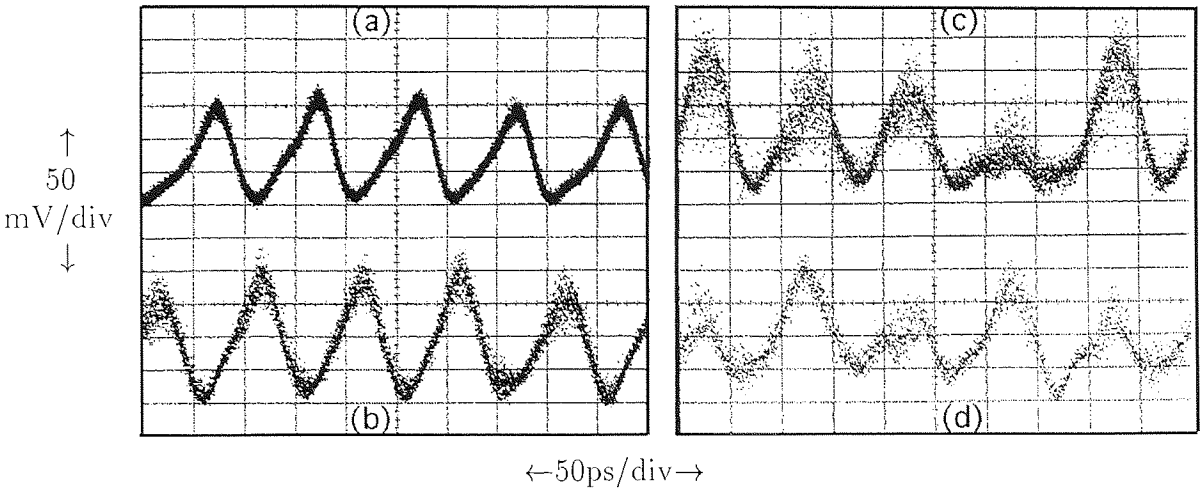

Figure 8.8: Sampling oscilloscope traces of (a) input interleaved 10GHz pulses and (b) - (d) grating outputs at three different times. The traces were all taken within one minute of each other.

state was being retarded relative to the other and the value of the PMD can be estimated at $\sim$ 10ps from the sampling oscilloscope traces in Figure 8.10 (c). The noise and missing pulses seen in the previous experiment (see Figure 8.8) were due to interference between pulses which had taken different paths through the inter-leaver. The random nature of the output being due to small random changes in polarisation being translated into random variations in temporal position due to the PMD.

When the DFB laser was used as a 10GHz pulse source the same effects were seen. There was still some broadening of the pulses after being passed through the grating, but a good output without much noise accumulation could be achieved with careful adjustment of the DFB input pulses. The stability of the grating output pulses was better than when the fibre ring laser was used but this was simply due to the increased stability of the DFB laser – any small change in the temperature or DC bias of the DFB (which changed the polarisation of the DFB output) caused a large change in the grating output pulses despite the change to the input pulses being un-noticeable.

In order to ascertain where the problem lay, the grating was removed and the circulator alone was tested, with the signal being reflected from the cleaved end of port 2. No polarisation dependent effects were seen and so the grating alone was then tested using the set-up shown in Figure 8.11. The source signal was amplified then split using a 50:50 coupler which had been checked and showed no polarisation dependent effects. One half of the signal was coupled into the unused port of the coupler which had an uncleaved end and a micro-bend to avoid back-reflections. The other half of the signal was reflected from the grating. This reflected signal returned to the coupler and was split with half the signal

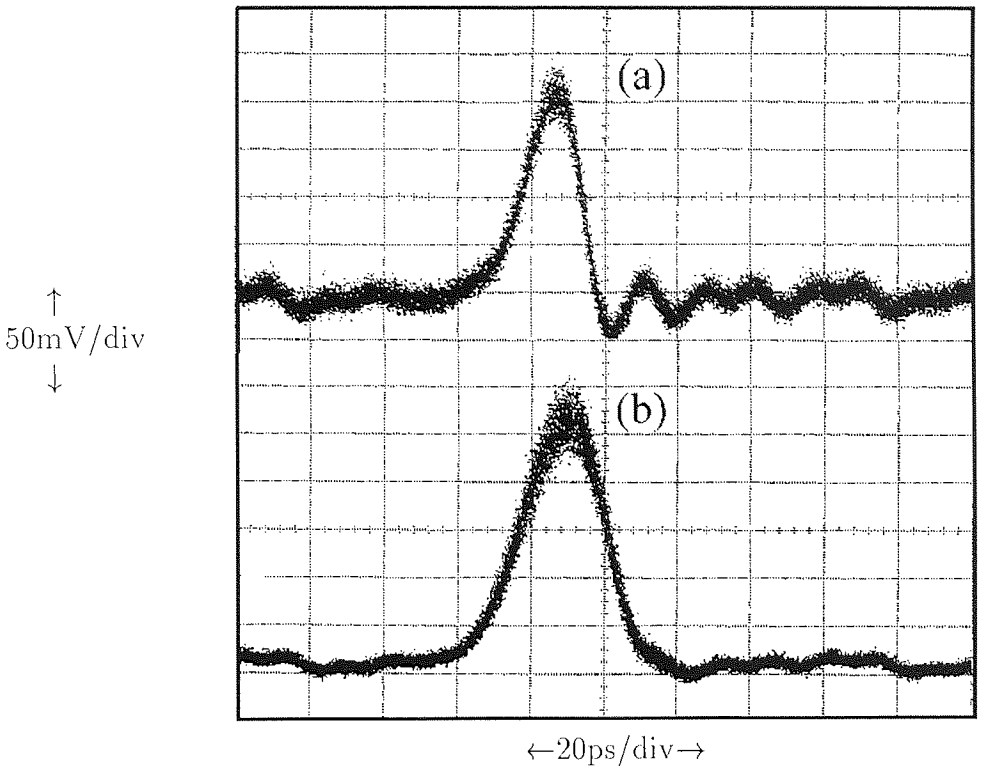

Figure 8.9: Sampling oscilloscope traces of (a) the 2.5GHz input pulses and (b) the FBG output pulses.

being coupled into the input arm, where it was absorbed by an isolator. The other half of the signal emerged from the output port allowing measurements to be taken. Using the DFB laser as the source, variations in the temporal position of the output pulses were again seen as the input polarisation was varied, indicating that the problem was due to the grating.

In order to accurately determine the PMD value of the grating the set-up shown schematically in Figure 8.12 was used. The measurement technique was similar to that used to measure the dispersion of the transmission fibres which was described in Section 3.4.2. The optical signal from a tunable laser tuned to the central wavelength of the grating was coupled into the grating through a fibre coupler and a PC. This light was then reflected by the grating with half the signal being detected by a photo-diode. By modulating the tunable laser output using a 1GHz modulator the phase difference between the photo-diode signal and a reference from the 1GHz modulator could be measured using a vector voltmeter. The change in the phase difference was then measured as the polarisation state of the signal was altered using a polarisation controller and from this the PMD could be calculated using the equation $\Delta t = \delta\phi/2\pi\nu$ where $\delta\phi$ is the phase change and ν is the frequency (1GHz in this case). The PMD was found to be 13.8ps which is in good agreement with the value previously estimated from the sampling

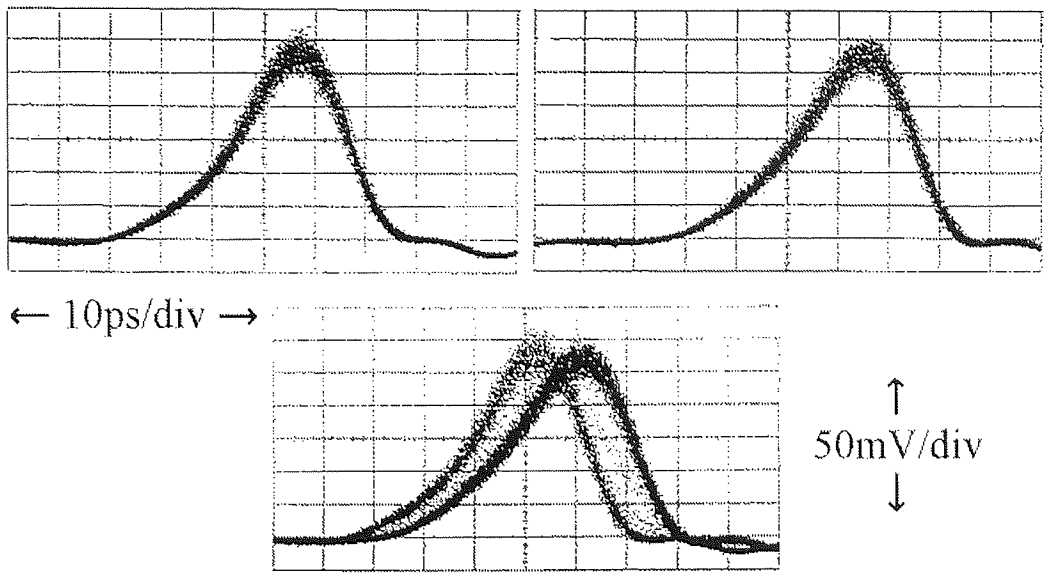

Figure 8.10: Sampling oscilloscope traces showing the grating output variation as the input polarisation was altered. The temporal position of the pulse varied by ~ 10ps as the input polarisation was altered.

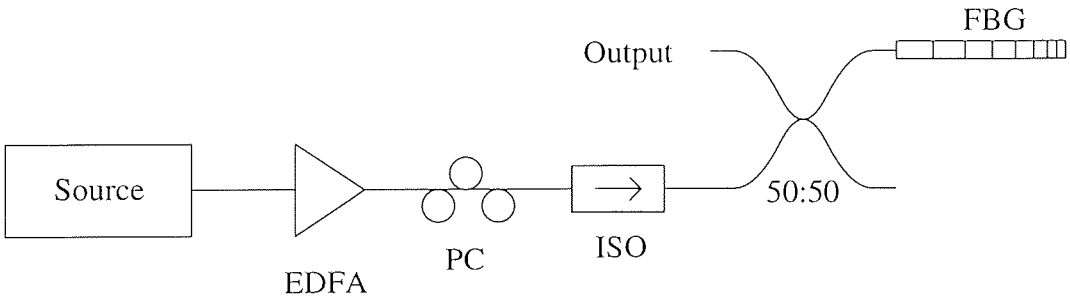

Figure 8.11: Schematic diagram of the experimental set-up used to test the FBG.

oscilloscope traces. This PMD value is very high and was undoubtedly the cause of the poor performance of the system. The problem of the high PMD was accentuated by using the same grating each amplifier span since a single span recirculating loop was used. In a larger loop or a straight line experiment which would use a greater number of compensating gratings there would be some variation in the polarisation mode dispersions of the gratings and the system performance should be improved. Indeed it has been shown that in an in-line experiment propagation over 1000km was possible despite the dispersion compensating gratings having ~8ps PMD [181] but the PMD value of FBGs must be reduced if propagation over trans-oceanic distances are to be achieved

8.3 Conclusions

The inconclusive experimental results of this chapter have highlighted what is undoubtedly a major problem with using fibre Bragg gratings as dispersion compensating elements in

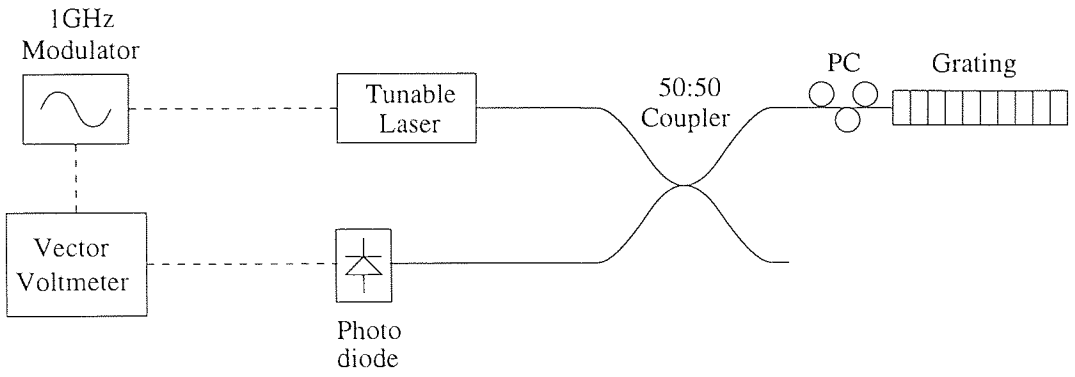

Figure 8.12: Schematic diagram of the PMD measurement set-up.

standard fibre systems - PMD. The grating used here had a high PMD which made it unsuitable for use in the recirculating loop propagation experiment. After an initial propagation experiment which was more unsuccessful than expected the grating was tested in an in-line configuration and the high PMD problem was discovered. At $\sim$ 14ps the dispersion between polarisation states was approximately equal to that of 1km of standard fibre over a 1nm bandwidth. Any small fluctuation in signal polarisation, which could be due to drift of the source, environmental effects or nonlinear effects, would therefore cause a large change in the dispersion of the grating and so alter the dispersion compensation and average dispersion of the system. This obviously had a disastrous effect on the system performance and propagation over even 500km was impossible. This problem will undoubtedly be overcome with improvements to the fabrication technique and gratings will remain attractive for use in dispersion compensating schemes due to their potentially low insertion loss. The insertion loss of this grating was only $\sim$ 2dB but a circulator with an insertion loss of $\sim$1.7dB was also required. However these two devices still had a 2.3dB lower loss than the $\sim$6dB of a 10km length of DCF which would be required to give the same dispersion compensation. The size of fibre Bragg gratings are also an advantage. The device used here was only 5cm long and yet could give dispersion compensation for almost 60km of SIF. If systems are to be upgraded by replacing existing electronic amplifiers by optical amplifiers and dispersion compensating elements it is obviously preferable to include a FBG which is a few centimetres long rather than several km of dispersion compensating fibre. For these reasons it is likely that research into the use of FBGs for use in dispersion compensated systems will continue to receive a great deal of attention and interest.

Chapter 9

Thesis conclusions

This thesis has investigated several aspects of soliton transmission in a dispersion managed recirculating loop with the emphasis on high bit rate long distance systems. The principles of operation of the recirculating loop and the design considerations have been discussed as have the advantages and disadvantages of the soliton laser sources which were used.

The first experimental investigation described a novel transmission scheme which allowed propagation of soliton-like pulses over ultra-long distances (> 1 million kilometres) with low timing jitter. The jitter was kept low by three factors: the operating wavelength was close to the dispersion zero wavelength and so Gordon-Haus jitter was low; the peak pulse power was far in excess of the average soliton power and the ASE noise level was suppressed. There are several unresolved questions concerning this experiment. Firstly, the reason for the noise suppression is not fully understood. A possible mechanism – a saturable absorption effect through nonlinear polarisation rotation with periodic polarisation discrimination has been proposed and discussed. Secondly, it is not clear why the stable pulse power was so far in excess of the soliton power although the high powers found do agree with those found from simulations of a nonlinear polarisation rotation–saturable absorber system. Thirdly it is not clear what effect of the dispersion map had. Changing the relative positions of the fibres in the dispersion map made no difference but further work is required to determine how the strength of the dispersion map affects the transmission. This new soliton control technique, which was entirely passive, may have a practical use in very high bit rate systems where the timing jitter poses a great problem.

A further area which is rapidly developing is the use of fibre Bragg gratings in optical systems. These devices have a range of uses and it has been shown here that they can be used in soliton systems to give both suppression of the ASE noise level outside the soliton bandwidth and jitter reduction. The performance of the FBG used here compared

favourably with that of a bulk device and the jitter reduction that it offered was in good agreement with the theoretical prediction for a Gaussian filter shape. The advantages of using FBGs are that they are compact in-fibre devices which potentially have lower insertion loss and polarisation sensitivity than bulk devices. The experiments conducted here used a device with a single passband but it is expected that a multiple wavelength device suitable for WDM applications would perform equally well. A further point of note is that the dispersion map used in this experiment consisted predominantly of normal dispersion fibre but through the use of dispersion management the average dispersion was anomalous. The use of a mostly normal dispersion map didn't cause any significant degradation of the transmitted signal.

The desire to upgrade existing systems to higher data rates to meet increasing bandwidth demands has led to interest in high bit rate standard fibre experiments. The initial investigation of soliton transmission in a dispersion compensated standard fibre system which was conducted showed that by replacing electrical regenerators with a length of DCF and an EDFA existing standard fibre systems could be upgraded to 10Gbit/s on a ~5000km length scale. This experiment did however show that the pulse width was not stable over this transmission distance and there was a transient oscillation in the pulse width and hence system Q. The reason for this oscillation was that the near transform limited launched pulses were stabilising in the strong dispersion map. A lossless numerical simulation showed that the stable pulses were transform limited in the centres of the fibre and therefore this would be the optimum launch position for a transform limited source. Experimentally, optimisation of the launch position led to a suppression of the pulse width oscillations but without any associated increase in the maximum propagation distance. It therefore seems likely that even when the pulse width was unstable, the pulses remained intact and there was no shedding of radiation as this would have led to a more rapid degradation in the Q. The effect of varying the position of the DCF relative to the fibre was also investigated and the performance was improved with the fibre preceding the amplifier. The maximum transmission distance which was achieved over standard fibre was 7600km.

Instead of using several kilometres of DCF, chirped fibre Bragg gratings have been proposed for use in standard fibre systems. Such a device was tested and performed very poorly in the recirculating loop. The main reason for this was that the FBG suffered from a high (~14ps) polarisation mode dispersion and the use of a single span recirculating loop highlighted the problem. Nonetheless FBGs are promising devices for this use as

they have lower loss than the equivalent length of standard fibre. The grating used compensated for 57km of SIF and had a total insertion loss (including the circulator) of 3.6dB. This compares to a loss of 4.2dB for the DCF used in the previous experiment which compensated for only 32km of SIF. FBGs are also far more convenient than DCF – the length of the grating and fibre pigtails was only a few meters compared to the 7km length of the DCF. These reasons should be sufficient to ensure that research continues into this application of FBGs.

As a result of using dispersion managements all of the experiments gave an enhancement of the stable pulse energy compared to the equivalent uniform dispersion system. This had the advantage of allowing the average dispersion to be kept low without degrading the signal to noise ratio and gave an associated reduction in the Gordon-Haus jitter. Using dispersion management also allowed the stable propagation of pulses through fibres with high dispersion as long as the average dispersion was low (lower than the local dispersion) and anomalous. It also allowed propagation through a dispersion map which had predominantly normal dispersion.

9.1 The future of optical communications

There is no doubt that the data rates of optical systems are going to increase for the foreseeable future through the use of both OTDM to increase the single channel data rate and WDM to increase the number of channels used. Using these techniques single channel bit rates of 400Gbit/s have been reported [260], 32 5Gbit/s channels have been propagated over trans-oceanic distances [20] and experimental demonstrations of terabit/s transmission have recently been reported using a combination of these techniques [170, 261, 262]. When these data rates are compared with the single channel 5Gbit/s rate of the recently installed trans Atlantic TAT12/13 systems it is easy to see that it is still possible to increase system data rates substantially. It is probable that both OTDM and WDM systems will be deployed in the future depending on the system requirements. The advantage of WDM systems are that they allow single channels to be added and dropped [189] leaving the other channels unaltered. Such systems are suitable where several system nodes are to be connected, communication between each pair of nodes can be assigned a particular wavelength. WDM systems do however require several sets of components - a sixteen channel system requires sixteen sources, sixteen filters and sixteen receivers which would add complication to a long haul point to point system and it is therefore

likely that such systems will use OTDM as far as possible before WDM is used. In dispersion compensated systems there is an additional problem for WDM in that only a single channel can be optimally compensated, the others will suffer some penalty which can only be partially reduced by post transmission dispersion compensation. The final problem is that the WDM channels will not all be amplified equally at each EDFA due to the gain profile of the amplifier. To reduce this effect gain flattened EDFAs have been developed [263] and the unequal gain can be compensated for by pre-emphasis or gain equalisation [264] leading to impressive results.

At these high bit rates RZ systems perform better than NRZ systems [12, 265] and it is therefore only a matter of time before RZ systems become a reality. New pulse formats are however being investigated one of these, the dispersion managed soliton which has been discussed in this thesis is achieving some success experimentally and amplitude or phase modulated NRZ experiments [120, 266] are in the early stage of development. This may allow NRZ system performance to be improved at higher bit rates to compete with RZ pulses. These new operating regimes shows some convergence of the traditional NRZ and RZ formats to an intermediate format and the distinction between RZ and NRZ may not be so clear cut in future systems.

As far as soliton systems are concerned, field trials have shown that solitons can be used in existing systems [267, 268] at 20Gbit/s and from recent experimental evidence it seems likely that if solitons are to be used that they will be used with dispersion management. As has been seen the stable pulses in dispersion managed systems are far removed from lossless fundamental solitons but they are periodically stable and owe their existence to a balance between nonlinearity and dispersion. These soliton-like pulses do not therefore suffer from the cumulative effect of nonlinearity along the transmission line as is the case for NRZ and RZ pulses. This is a good argument for the use of dispersion managed solitons as nonlinearity is a serious problem at high bit rates. A further area where dispersion managed solitons can be used is in the upgrade of existing standard fibre systems. The actual PMD values of the older installed fibres may be the deciding factor in these systems. Solitons are more resilient to PMD than NRZ/RZ pulses and it is expected that dispersion managed solitons will also show this resilience.

Work will therefore continue into the use of nonlinear soliton-like pulses for telecommunications and dispersion management will continue to be investigated as this is a promising and interesting technique which has brought the implementation of the first soliton based optical telecommunications system a step closer.

Bibliography

[1] M.J.N. Sibley. *Optical Communications 2nd Edition.* Macmillan, London, 1995.

[2] C.K. Kao and G.A. Hockman. Dielectric-fibre surface waveguides for optical frequencies. *Proc. of the IEE*, 133:1151–1158, 1966.

[3] F.P. Kapron, D.B. Keck, and R.D. Maurer. *Appl. Phys. Lett.*, 17(6):423–426, 1970.

[4] P-A. Bélanger. *Optical Fiber Theory.* World Scientific, Singapore, 1993.

[5] E. Saintdizier, E. Brandon, J-P. Blondel, and J-F. Vinchant. 2.5-Gbit/s unrepeated transmission with directly modulated laser and without dispersion compensating fiber over 385-km (412-km with FEC) of pure silica core fiber. *Electron. Lett.*, 32(15):1383–1384, 1996.

[6] G.P. Agrawal. *Nonlinear Fibre Optics.* Academic Press, San Diego, 1989.

[7] H. Taga, N. Edagawa, S. Yamamoto, and S. Akiba. Recent progress in amplified undersea systems. *IEEE J. Lightwave Technol.*, 13(5):829–840, 1995.

[8] S.G. Evangelides, L.F. Mollenaue, J.P. Gordon, and N.S. Bergano. Polarisation multiplexing with solitons. *IEEE J. Lightwave Technol.*, 10(1):28–35, 1992.

[9] K. Ennser and K. Petermann. Performance of RZ vs NRZ transmission on standard mode fibres. *IEEE Photon. Technol. Lett.*, 8(3):443–445, 1996.

[10] D. Breuer and K. Petermann. Comparison of NRZ and RZ modulation format for 40Gb/s TDM standard fibre systems. *IEEE Photon. Technol. Lett.*, 9(3):398–400, 1997.

[11] K. Ennser, R.I. Laming, and M.N. Zervas. Investigation of RZ and NRZ format 40Gbit/s transmission over non dispersion shifted fibre using chirped fibre grating dispersion management. In *Eur. Conf. on Netw. and Opt. Comm. (NOC'97) - Antwerp*, pages Vol2 40–46. IOS Press, 1997.

[12] J.M. Jacob, E.A. Golovchenko, A.N. Pilipetskii, G.M. Carter, and C.R. Menyuk. 10Gbit/s transmission of NRZ over 10 000km and solitons over 13 500km error-free in the same dispersion managed system. *IEEE Photon. Technol. Lett.*, 9(10):1412–1414, 1997.

[13] M.J. Guy, S.V. Chernikov, J.R. Taylor, D.G. Moodie, and R. Kashyap. Low repetition rate master source for optical-processing in ultrahigh-speed OTDM networks. *Electron. Lett.*, 31(20):1767–1769, 1995.

[14] R. Ludwig. Unrepeated 40Gbit/s RZ single channel transmission over 150km of standard fibre at 1.55μm. In *Opt. Fib. Comm. (OFC'97) - Dallas*, pages 245–246. OSA, 1997.

[15] W.S. Lee, D.Garthe, G.A. Petitt, and A. Hadjifotiou. 40Gbit/s TDM transmission over 160km (2x80km) of standard nondispersion-shifted fibre. In *Opt. Fib. Comm. (OFC'97) - Dallas*, pages 244–245. OSA.

[16] A.D. Ellis, T. Widdowson, X. Shan, and D.G. Moodie. Three node,40 Gbit/s OTDM network experiment using electro-optic switches. *Electron. Lett.*, 30(16):1333–1334, 1994.

[17] D. Cotter, J.K. Lucek, M. Shabeer, K. Smith, D.C. Rogers, D. Nesset, and P. Gunning. Self-routing of 100Gbit/s packets using 6 bit 'keyword' address recognition. *Electron. Lett.*, 31(17):1475–1476, 1995.

[18] I.D. Phillips, A. Gloag, P.N. Kean, N.J. Doran, and A.D. Ellis I. Bennion. Simultaneous demultiplexing, data regeneration and clock recovery with a single semiconductor optical amplifier-baser nonlinear-optical loop mirror. *Opt. Lett.*, 22(17):1326–1328, 1997.

[19] A.J. Poustie, K.J. Blow, and R.J. Manning. Amplitude restoration and storage threshold in an all-optical memory. In *Eur. Conf. on Opt. Comm. (ECOC'97) - Edinburgh*, pages Vol2 69–72. IEE, 1997.

[20] N.S. Bergano, C.R. Davidson, M.A. Mills, P.C. Corbet, S.G. Evangelides, B. Pedersen, R. Menges, J.L. Zyskind, J.W. Sulhoff, A.K. Srivastava, C. Wolf, and J. Judkins. Long-haul WDM transmission using optimum channel modulation: A 160Gb/s (32x5Gb/s) 9,300km demonstration. In *Opt. Fib. Comm. (OFC'97) - Dallas*, page PD16. OSA, 1997.

[21] K. Fukuchi, T. Ono, and Y. Yano. 10Gbit/s 120km standard fibre transmission employing a novel optical phase-encoded intensity modulation for signal spectrum compression. In *Opt. Fib. Comm. (OFC'97) - Dallas*, page ThH3. OSA, 1997.

[22] E. Desurvire, J.R. Simpson, and P.C. Becker. High gain erbium doped traveling-wave fibre amplifier. *Opt. Lett.*, 12(11):888–890, 1987.

[23] R.J. Mears, L. Reekie, I.M. Jauncey, and D.N. Payne. Low-noise erbium-doped fibre amplifier operating at $1.54\mu m$. *Electron. Lett.*, 23(19):1026–1028, 1987.

[24] A. Hasegawa and Y. Kodama. *Solitons in optical communications.* Clarendon Press, Oxford, 1995.

[25] G.P. Agrawal. *Nonlinear Fibre Optics 2nd Edition.* Academic Press, San Diego, 1995.

[26] A. Takada and M. Saruwatari. Picosecond optical pulse-compression from gain-switched 1.3 μm distributed-feedback laser diode through highly dispersive single-mode fiber. *Electron. Lett.*, 21(21):969–971, 1985.

[27] C.S. Gardener, J.M. Green, M.D. Kruskal, and R.M. Miura. Method for solving the Kortrweg-deVries equation. *Phys. Rev. Lett*, 19(19):1095, 1967.

[28] V.E. Zakarov and A.B. Shabat. Exact theory of two-dimensional self-focusing and one-dimensional self-modulation of waves in nonlinear media. *Sov. Phys. JEPT*, 34(1):62–69, 1972.

[29] C. Desem and P.L. Chu. Effect of chirping on solution propagation in single-mode fibres. *Opt. Lett.*, 11(4):248–251, 1986.

[30] D. Anderson, M. Lisak, and T. Relchel. Asymptotic propagation properties of pulses in a soliton-based optical fibre communication system. *J. Opt. Soc. Am. B*, 5(2):207–210, 1988.

[31] K.J. Blow, N.J. Doran, and D. Wood. Generation and stabalisation of short soliton pulses in the amplified nonlinear schrodringer equation. *J. Opt. Soc. Am. B*, 5(2):381–391, 1988.

[32] S.V. Chernikov, J.R. Taylor, and R. Kashyap. Experimental demonstration of step-like dispersion profiling in optical-fiber for soliton pulse generation and compression. *Electron. Lett.*, 30(5):433–435, 1994.

[33] C. Lester, K. Bertilsson, K. Rottwitt, P.A. Andrekson, M.A. Newhouse, and A.J. Antos. Soliton transmission over more than 90km using distributed erbium-doped fibers. *Electron. Lett.*, 31(3):219–220, 1995.

[34] A. Altunca, L Noel, W.A. Pender, A.S Siddiqui, T Widdowson, A.D Ellis, M.A Newhouse, A.J Antos, G Kar, and P.W. Chu. 40Gbit/s error free transmission over a 68km distributed erbium doped fibre amplifier. *Electron. Lett.*, 32(3):233–234, 1996.

[35] A. Altunca, A.S Siddiqui, A.D Ellis, M.A Newhouse, and A.J Antos. Gain and noise figure characterisation of a 68km long distributed erbium doped fibre amplifier. *Electron. Lett.*, 32(19):1800–1801, 1996.

[36] K.J. Blow and N.J. Doran. Average soliton dynamics and the operation of soliton systems with lumped amplifiers. *IEEE Photon. Technol. Lett.*, 3(4):369–371, 1991.

[37] A. Hasegawa and Y. Kodama. Guiding center soliton in optical fibres. *Opt. Lett.*, 15(24):1443–1445, 1990.

[38] A. Hasegawa and Y. Kodama. Guiding-center soliton. *Phys. Rev. Lett.*, 66(1):161–164, 1991.

[39] C. D. Poole and C. R. Giles. Polarisation-dependent pulse compression and broadening due to polarisation dispersion in dispertion-shifted fibre. *Opt. Lett.*, 13(2):155–157, 1988.

[40] J. Zhou and M.J. O'Mahony. Optical transmission system penalties due to fibre polarization mode dispersion. *IEEE Photon. Technol. Lett.*, 6(10):1265–1267, 1994.

[41] B. Clesca, J-P. Thiery, L. Pierre, V. Havard, and F. Bruyère. Impact of polarisation mode dispersion on 10Gbit/s terrestrial systems over non-dispersion shifted fibre. *Electron. Lett.*, 31(18):1594–1595, 1995.

[42] Pierre L. and Thiery J-P. Comparison of resistance to polarisation mode dispersion of NRZ and phase-shaped binary transmission formats at 10Gbit/s. *Electron. Lett.*, 33(5):402–403, 1997.

[43] T. Widdowson, A. Lord, and D.J. Maylon. Polarisation guiding in ultralong distance soliton transmission. *Electron. Lett.*, 30(11):879–880, 1994.

[44] M.N. Islam, C.E. Soccolich, J.P Gordon, and U.C. Paek. Soliton intensity-dependent polarisation rotation. *Opt. Lett.*, 15(1):21–23, 1990.

[45] R.P. Davey, N. Langford, and A.I. Ferguson. Role of polarisation rotation in an Er fibre laser. *Electron. Lett.*, 29(9):758–780, 1993.

[46] L.F. Mollenauer, K. Smith, and J.P. Gordon. Resistance of solitons to the effects of polarisation dispersion in optical fibres. *Opt. Lett.*, 14(21):1219–1221, 1989.

[47] J.P. Gordon and H.A. Haus. Random walk of coherently amplified solitons in optical fibre transmission. *Opt. Lett.*, 11(10):665–667, 1986.

[48] D. Marcuse. An alternative derivation of the Gordon-Haus effect. *IEEE J. Lightwave Technol.*, 10(2):273–278, 1992.

[49] A. F. Mitchell, J. V. Wright, S. F. Carter, A. D. Ellis, A. Lord, J. Lyle, and J. M. Scott. The future of optically amplified submarine systems. In *Techn. Digest of 2-nd Intern. Conf. on Optical Fibre Submarine Telecommun. Systems, Versailles, France*, pages 49–54, 1993.

[50] A. Mecozzi, J.D. Moores, H.A. Haus, and Y. Lai. Soliton transmission control. *Opt. Lett.*, 16(23):1841–1843, 1991.

[51] Y. Kodama and A. Hasegawa. Generation of asymptotically stable optical solitons and suppression of the Gordon-Haus effect. *Opt. Lett.*, 17(1):31–33, 1992.

[52] M. Ding and K. Kikuchi. Analysis of soliton transmission in optical fibers with the soliton self-frequency shift being compensated by distributed frequency-dependent gain. *IEEE Photon. Technol. Lett.*, 4(5):497–500, 1992.

[53] K.J. Blow, N.J. Doran, and D. Wood. Suppression of the soliton self-frequency shift by bandwidth-limited amplification. *J. Opt. Soc. Am. B*, 5(6):1301–1304, 1988.

[54] F.M. Mitschke and L.F. Mollenauer. Discovery of the soliton self-frequency shift. *Opt. Lett.*, 11(10):659–661, 1986.

[55] J.P. Gordon. Theory of the soliton self-frequency shift. *Opt. Lett.*, 11(10):662–664, 1986.

[56] L.F. Mollenauer, E. Lichtman, G.T. Harvey, M.J. Neubelt, and B.M. Nyman. Demonstration of error free soliton transmission over more than 15,000km at 5Gb/s,single channel and over 11,000km at 10Gb/s in two channel WDM. *Electron. Lett.*, 28(8):792–794, 1992.

[57] L.F. Mollenauer, J.P. Gordon, and S.G. Evangelides. The sliding-frequency guiding filter: An improved form of soliton jitter control. *Opt. Lett.*, 17(22):1575–1577, 1992.

[58] P.V. Mamyshev and L.F. Mollenauer. Stability of soliton propagation with sliding-frequency guiding filters. *Opt. Lett.*, 19(24):2083–2085, 1994.

[59] J.C. Dung, S. Chi, and S. Wen. Reduction of soliton-interactions by zigzag sliding-frequency guiding filters. 20(18):339–341, 1996.

[60] E.A. Golovchenko, A.N. Pilipetskii, C.R. Menyukm, J.P. Gordon, and L.F. Mollenauer. Soliton propagation with up and down sliding frequency guiding filters. *Opt. Lett.*, 20(6):539–541, 1995.

[61] A. Mecozzi, M. Midrio, and M. Romagnoli. Timing jitter in soliton transmission with sliding filters. *Opt. Lett.*, 21(6):402–404, 96.

[62] L.F. Mollenauer, E. Lichtman, M.J. Neubelt, and G.T. Harvey. Demonstration using sliding-frequency guiding filters, of error-free soliton transmission over more than 20Mm at 10Gb/s single channel and over more than 13Mm at 20Gb/s in a two-channel WDM. *Electron. Lett.*, 29(10):910–911, 1993.

[63] L.F. Mollenauer, P.V. Mamyshev, and M.J. Neubelt. Measurement of timing jitter in filter-guided soliton transmission at 10 Gbits/s and achievement of 375 Gbits/s-Mm error free at 12.5 and 15Gbit/s. *Opt. Lett.*, 19(10):704–706, 1994.

[64] F. Favre, D. Leguen, and M.L. Moulinard. Robustness of 20Gbit/s 63km span 6Mm sliding-filter controlled soliton transmission. *Electron. Lett.*, 31(18):1600–1601, 1995.

[65] D. Leguen, F. Favre, R. Boittin, J. Debeau, F. Devaux, M. Henry, C. Thebault, and T. Georges. Demonstration of sliding-filter-controlled soliton transmission at 20Gbit/s over 14Mm. *Electron. Lett.*, 31(4):301–302, 1995.

[66] S. Kawai, K. Iwatsuki, and S. Nishi. Demonstration of error-free optical soliton transmission over 30000 km at 10 Gbit/s with signal frequency sliding technique. *Electron. Lett.*, 31(17):1463–1464, 1995.

[67] Y. Kodama, M.Romagnoli, and S. Wabnitz. Stabilisation of optical solitons by an acousto-optic modulator and filter. *Electron. Lett.*, 30(3):261–262, 1994.

[68] G. Aubin, T. Montalant, J. Moulu, B.Nortier, F. Pirio, and J-B. Thomine. Demonstrantion of soliton transmission at 10Gbit/s up to 27Mm using signal frequency sliding technique. *Electron. Lett.*, 31(1):52–53, 1995.

[69] E. Kolltveit, B. Biotteau, I. Riant, F. Pitel, O. Audouin, P. Brindel, E. Brun, P. Sansonetti, and J.P. Hamaide. Soliton frequency-guiding by UV-written fiber Fabry-Perot filter in a 2x5 Gb/s wavelength-division multiplexing transmission over transoceanic distances. *IEEE Photon. Technol. Lett.*, 7(12):1498–1500, 1995.

[70] Y. Kodama, M. Romagnoli, and S. Wabnitz. Soliton stability and interactions in fibre lasers. *Electron. Lett.*, 28(21):1981–1983, 1992.

[71] H.P. Yuen. Reduction of quantum fluctuation and suppression of the Gordon-Haus effect with phase-sensitive linear amplifiers. *Opt. Lett.*, 17(1):73–75, 1992.

[72] J.N. Kutz, C.V. Hile, W.L. Kath, R.D. Li, and P. Kumar. Pulse-propagation in nonlinear-optical fiber lines that employ phase-sensitive parametric-amplifiers. *J. Opt. Soc. Am. B*, 11(10):2112–2123, 1994.

[73] M. Matsumoto, A. Hasegawa, and Y. Kodama. Adiabatic amplification of solitons by means of nonlinear amplifying loop mirrors. *Opt. Lett.*, 19(14):1019–1921, 1994.

[74] M. Matsumoto, H. Ikede, and A. Hasegawa. Suppresion of noise accumulation in bandwidth-limited soliton transmission by means of nonlinear loop mirrors. *Opt. Lett.*, 19(3):183–186, 1994.

[75] A. Mecozzi, W.L. Kath, P. Kumar, and C.G. Goedde. Long-term storage of a soliton bit stream by use of phase-sensitive amplification. *Opt. Lett.*, 19(24):2050–2052, 94.

[76] R.J. Essiambre and G.P. Agrawal. Ultrahigh-bit-rate soliton communication-systems using dispersion-decreasing fibers and parametric amplifiers. *Opt. Lett.*, 21(2):116–118, 1996.

[77] N.J. Smith and N.J. Doran. Picosecond soliton propagation using nonlinear optical loop mirrors as intensity filters. *Electron. Lett.*, 30(13):1084–1085, 1994.

[78] D. Atkinson, W.H. Loh, V.V. Afanajev, A.B. Grudinin, A.J. Seeds, and D.N. Payne. Increased amplifier spacing in a soliton system with quantum-well saturable absorbers and spectral filtering. *Opt. Lett.*, 19(19):1514–1516, 1994.

[79] A. Hirano, H. Tsuda, K. Hagimoto, R. Takahashi, Y. Kawamura, and H. Iwamura. 10ps pulse all-optical discrimination using a high-speed saturable absorber optical gate. *Electron. Lett.*, 31(9):736–737, 1995.

[80] F.M. Knox, P. Harper, P.N. Kean, N.J. Doran, and I. Bennion. Low jitter long distance pulse transmission near net fibre dispersion zero wavelength. *Electron. Lett.*, 31(17):1467–1468, 1995.

[81] M. Nakazawa, E. Yamada, H. Kubota, and K. Suzuki. 10Gbit/s soliton data transmission over one million kilometers. *Electron. Lett.*, 27(14):1270–1272, 1991.

[82] N.J. Smith, K.J. Blow, W.J. Firth, and K. Smith. Soliton dynamics in the presence of phase modulators. *Opt. Commun.*, 1993.

[83] N.J. Smith, W.J. Firth, K.J. Blow, and K. Smith. Suppression of soliton interactions by periodic phase modulation. *Opt. Lett.*, 19(1):16–18, 1994.

[84] S. Wabnitz. Suppression of interactions in a phase-locked soliton optical memory. *Opt. Lett.*, 18(8):601–603, 1993.

[85] N.J. Smith, N.J. Doran, K.J. Blow, and W.J. Firth. Gordon-Haus jitter suppression using a single phase modulator. *Electron. Lett.*, 30(12):987–988, 1994.

[86] C. Kurtzke. Suppression of fiber nonlinearities by appropriate dispersion management. *IEEE Photon. Technol. Lett.*, 5(10):1250–1253, 1993.

[87] N. Edagawa, I. Morita, M. Suzuki, S. Yamamoto, H. Taga, and S. Akiba. 20Gbit/s, 8100km straight line single channel soliton based RZ transmission experiment using periodic dispersion compensation. In *Eur. Conf. on Opt. Comm. (ECOC'95 - Brussels)*, pages 983–986, 1995.

[88] M. Suzuki, I. Morita, S. Yamamoto, N. Edagawa, H. Taga, and S. Akiba. Timing jitter reduction by periodic dispersion compensation in soliton transmission. In *Opt. Fib. Comm. (OFC'95) - Washington D.C.*, page PD20. OSA, 1995.

[89] M. Suzuki, I. Morita, N. Edagawa, S. Yamamoto, H. Taga, and S. Akiba. Reduction of Gordon-Haus timing jitter by periodic dispersion compensation. *Electron. Lett.*, 31(23):2027–2029, 1995.

[90] S. Wabnitz. Stabilization of sliding filtered soliton wavelength-division multiplexing transmissions by dispersion-compensating fibers. *Opt. Lett.*, 21(9):638–640, 1996.

[91] A. Naka, T. Matsuda, and S. Saito. Optical RZ signal straight line transmission experiments with dispersion compensation over 5520km at 20Gbit/s and 2160km at 2x20Gbit/s. *Electron. Lett.*, 32(18):1694–1696, 1996.

[92] M. Nakazawa, H. Kubota, A. Sahara, and K. Tamura. Marked increase in the power margin through the use of a dispersion-allocated soliton. *IEEE Photon. Technol. Lett.*, 8(8):1088–1090, 1996.

[93] M. Nakazawa, H. Kubota, and K. Tamura. Nonlinear pulse transmission through an optical fibre at zero average group velocity dispersion. *IEEE Photon. Technol. Lett.*, 8(3):452–454, 1996.

[94] S. Wabnitz, I. Uzunov, and F. Lederer. Soliton transmission with periodic dispersion compensation: Effects of radiation. *IEEE Photon. Technol. Lett.*, 8(8):1091–1093, 1996.

[95] N.J. Smith, N.J. Doran, F.M. Knox, and W. Forysiak. Energy-scaling characteristics of solitons in strongly dispersion managed fibres. *Opt. Lett.*, 21(24):1981–1983, 1996.

[96] N.J. Smith, W. Forysiak, and N.J. Doran. Reduced Gordon-Haus jitter due to enhanced power solitons in strongly dispersion managed systems. *Electron. Lett.*, 32(22):2085–2086, 1996.

[97] A Hasegawa, S. Kumar, and Y. Kodama. Reduction of collision-induced time jitters in dispersion- managed soliton transmission-systems. 21(1):39–41, 1996.

[98] N.J. Smith, F.M. Knox, N.J. Doran, K.J. Blow, and I. Bennion. Enhanced power solitons in optical fibres with periodic dispersion management. *Electron. Lett.*, 32(1):54–55, 1996.

[99] E.M. Dianov, A.V. Luchnikov, A.N. Pilipetskii, and A.N. Starodumov. Electrostriction mechanism of soliton interaction in optical fibres. *Opt. Lett.*, 15(6):314–316, 1990.

[100] E.M. Dianov, A.V. Luchnikov, A.N. Pilipetskii, and A.M. Prokhorov. Long-range interaction of solitons in ultra-long communication systems. *Soviet Lightwave Communications*, 1:235–246, 1991.

[101] E.M. Dianov, A.V. Luchnikov, A.N. Pilipetskii, and A.M. Prokhorov. Long-range interaction of picosecond solitons through excitation of acoustic waves in optical fibres. *Phys. Rev. B*, 54:175–180, 1992.

[102] E.A. Golovchenko and A.N. Pilipetskii. Acoustic effect and the polarisation of adjacent bits in soliton communication lines. *IEEE J. Lightwave Technol.*, 12(6):1052–1055, 1994.

[103] K. Smith and L.F. Mollenauer. Experimental observation of soliton interaction over long fibre paths: Discovery of a long-range interaction. *Opt. Lett.*, 14(22):1284–1286, 1989.

[104] J.P. Gordon. Interaction forces among solitons in optical fibres. *Opt. Lett.*, 8(11):596–598, 1983.

[105] F.M. Mitschke and L.F. Mollenauer. Experimental observation of interaction forces between solitons in optical fibres. *Opt. Lett.*, 12(5):355–357, 1987.

[106] C. Desem and P.L. Chu. Soliton interaction in the presence of loss and periodic amplification in optical fibres. *Opt. Lett.*, 12(5):349–351, 1987.

[107] P.L. Chu and C. Desem. Effect of 3rd-order dispersion of optical fiber on soliton interaction. *Electron. Lett.*, 21:228–230, 1985.

[108] Y. Kodama and K. Nozaki. Soliton interaction in optical fibres. *Opt. Lett.*, 12(12):1038–1040, 1987.

[109] M. Suzuki, N. Edagawa, H. Taga, H. Tanaka, S. Yamamoto, and S. Akiba. 10 Gbit/s over 12200-km soliton data-transmission with alternating-amplitude solitons. *IEEE Photon. Technol. Lett.*, 6(6):757–759, 1994.

[110] K. Suzuki, N. Edagawa, H. Taga, M. Takaya, S. Yamamoto, and S. Akiba. Feasibility demonstration of 20 Gbit/s single channel soliton transmission over 11500 km using alternating-amplitude solitons. *Electron. Lett.*, 30(13):1083–1084, 1994.

[111] M. Nakazawa, E. Yoshida, E. Yadama, K. Suzuki, T. Kitoh, and M. kawachi. 80 Gbit/s soliton data transmission over 500km with unequal amplitude solitons for timing clock extraction. *Electron. Lett.*, 30(21):1777–1778, 1994.

[112] P. Andrekson, N.A. Olsson, J.R. Simpson, T. Tanbunek, R.A. Logan, and K.W. Wecht. Observation of collision induced termporary soliton carrier frequency shifts in ultra-long fiber transmission systems. *IEEE J. Lightwave Technol.*, 9(9):1132–1135, 1991.

[113] Yariv. Signal to noise considerations in fiber links with periodic or distributed optical amplification. *Opt. Lett.*, 15(19):1064–1066, 1990.

[114] J.V. Wright and S.F. Carter. Constraints on the design of long-haul soliton systems. In *Conf. on Nonlinear Guided-Wave Phenomena, MA2-1*, pages 6–9, 1991.

[115] E.A. Golovchenko, A.N. Pilipetskii, and C.R. Menyuk. Periodic dispersion management in soliton WDM transmission with sliding filters. *Opt. Lett.*, 22(15):1156–1158, 1997.

[116] S. Kumar and A. Hasegawa. Quasi soliton propagation in dispersion managed fibres. *Opt. Lett.*, 22(6):372–374, 1997.

[117] M.K. Chin and X.Y. Tang. Quasi-stable soliton transmission in dispersion managed fibre links with lumped amplifiers. *IEEE Photon. Technol. Lett.*, 9(4):538–540, 1997.

[118] R.W. Tkach, A.R. Chraplyvy, F. Forghieri, A.H. Gnauck, and R.M. Derosier. Four-photon mixing and high-speed WDM systems. *IEEE J. Lightwave Technol.*, 13(5):841–849, 1995.

[119] L. Eskilden, P.B. Hansen, S.G. Grubb, A.M. Vengsarkar, S.K. Korotky, T.A. Strasser, J.J. Veselka, J.E.J. Alphonsus, D. Truxal, and D.J. Digiovanni. Single-fiber repeaterless transmission over 490 km at 2.488 Gbit/s using a remote preamplifier and dispersion compensation. *Electron. Lett.*, 32(18):1696–1697, 1996.

[120] N.S. Bergano and C.R. Davidson. Wavelength-division multiplexing in long-haul transmission-systems. *IEEE J. Lightwave Technol.*, 14(6):1299–1308, 1996.

[121] F. Favre, D. LeGuen, M.L. Moulinard, M. Henry, G. Michaud, F. Devaux, E. Legros, B. Charbonnier, and T.Georges. Demonstration of soliton transmission at 20Gbit/s over 2200km of standard fibre with dispersion compensation and pre-chirping. *Electron. Lett.*, 33(6):511–512, 1997.

[122] P. Harper, F.M. Knox, P.N. Kean, I. Bennion, and N.J. Doran. 10Gbit/s soliton propagation over 5250km in standard fibre with dispersion compensation. In *Opt. Fib. Comm. (OFC'97) - Dallas*, pages 304–305. OSA, 1997.

[123] P. Harper, F.M. Knox, D.S. Govan, P.N. Kean, I. Bennion, and N.J. Doran. Long distande 10Gbit/s soliton transmission over standard fibre with periodic dispersion compensation. In *Eur. Conf. on Netw. and Opt. Comm. (NOC'97) - Antwerp*, pages Vol2 18–24. IOS Press, 1997.

[124] K. Tajima. Compensation of soliton broadening in nonlinear optical fibres with loss. *Opt. Lett.*, 12(1):54–56, 1987.

[125] D.J. Richardson, R.P. Chamberlin, L. Dong, and D.N. Payne. High-quality soliton loss-compensation in 38km dispersion-decreasing fiber. *Electron. Lett.*, 32(19):1681–1682, 1995.

[126] W. Forysiak, F.M. Knox, and N.J. Doran. Stepwise dispersion profiling of periodically amplified soliton systems. *IEEE J. Lightwave Technol.*, 12(8):1330–1337, 1994.

[127] W. Forysiak, K.J. Blow, and N.J. Doran. Reduction of Gordon-Haus jitter by post-transmission dispersion compensation. *Electron. Lett.*, 29(13):1225–1226, 1993.

[128] F.M. Knox, W. Forysiak, and N.J. Doran. 10Gbit/s soliton communication system over standard fibre at 1.55μm and the use of dispersion compensation. *IEEE J. Lightwave Technol.*, 13(11):1955–1692, 1995.

[129] I.R. Gabitov and S.K. Turitsyn. Averaged pulse dynamics in a cascaded transmission system with passive dispersion compensation. *Opt. Lett.*, 21(5):327–329, 1996.

[130] A.B. Grudinin and I.A. Goncharenko. Increased amplifier spacing in soliton system with partial dispersion compensation. *Electron. Lett.*, 32(17):1602–1604, 1996.

[131] J.M. Jacob, E.A. Golovchenko, A.N. Pilipetskii, G.M. Carter, and C.R. Menyuk. Experimental demonstration of soliton transmission over 28Mm using mostly normal dispersion fibre. *IEEE Photon. Technol. Lett.*, 9(1):130–132, 1997.

[132] I. Morita, M. Suzuki, N. Edagawa, S. Yamamoto, and S. Akiba. Single-channel 40Gbit/s 5000km straight line soliton transmission experiment using periodic dispersion compensation. *Electron. Lett.*, 33(8):698–699, 1997.

[133] M. Suzuki, I. Morita, N. Edagawa, S. Yamamoto, and S. Akiba. 20Gbit/s-based soliton WDM transmission over transoceanic distances using periodic compensation of dispersion and it's slope. *Electron. Lett.*, 33(8):691–692, 1997.

[134] E. Yamada, H. Kubota T. Yamamoto, A. Sahara, and M. Nakazawa. 10Gbit/s, 10600km, dispersion-allocated soliton transmission using conventional 1.3μm singlemode fibres. *Electron. Lett.*, 33(7):602–603, 1997.

[135] H.A. Haus, K. Tamura nad L.E. Nelson, and E. P. Ippen. Stretched-pulse additive pulse mode-locking in fibre ring lasers: Theory and experiment. *IEEE J. Quantum Electron.*, 31(3):591–598, 1995.

[136] T. Georges. Pre-chirping and dispersion compensation for long-haul 20 Gbit/s soliton transmission at 1.55μm on non-dispersion-shifted fibres. In *Opt. Fib. Comm. (OFC'97) - Dallas*, pages 144–145. OSA, 1997.

[137] M.J. Ablowitz, G. Biondini, S. Chakravarty, R.B. Jenkins, and J.R. Sauer. Four-wave mixing in wavelength-division-multiplexed soliton systems: damping and amplification. *Opt. Lett.*, 21(20):1646–1648, 1996.

[138] L.F. Mollenauer, S.G. Evangelides, and J.P. Gordon. Wavelength division multiplexing with solitons in ultra-long distance transmission using lumped amplifiers. *IEEE J. Lightwave Technol.*, 9(3):362–367, 1991.

[139] T. Tanifuji and M. Ikeda. Pulse circulation measurement of transmission characteristics in long optical fibres. *Opt. Lett.*, 16(8), 1977.

[140] L.F. Mollenauer and K. Smith. Demonstration of soliton transmission over more than 4000km in fibre with loss periodically compensated by Raman gain. *Opt. Lett.*, 13(8):675–677, 1988.

[141] L.F. Mollenauer, J.P. Gordon, M.J. Neubelt, J.R. Simpson, S.G. Evangelides, and L.G. Cohen. Experimental study of soliton transmission over more than 10,000km in dispersion-shifted fibre. *Opt. Lett.*, 15(21):1203–1205, 1990.

[142] D.J. Malyon, T. Widdowson, E.G. Bryant, S.F. Carter, J.V. Wright, and W.A. Stallard. Demonstration of optical pulse propagation over 10000 km of fibre using recirculating loop. *Electron. Lett.*, 27(2):120–121, 1991.

[143] L.F. Mollenauer, B.M. Nyman, M.J. Neubelt, G. Raybon, and S.G. Evangelides. Demonstration of soliton transmission at 2.4 Gbit/s over 12,000km. *Electron. Lett.*, 27(2):178–179, 1991.

[144] L.F. Mollenauer, M.J. Neubelt, M. Haner, E. Lichtman, S.G. Evangelides, and B.M. Nyman. Demonstration of error free soliton transmission at 2.5 Gbit/s over more than 14 000km. *Electron. Lett.*, 27(22):2055–2056, 1991.

[145] N.A. Olsson, P.A. Andrekson, J.R. Simpson, T. Tanbun-ek, R.A. Logan, and K.W. Wecht. Bit-error-rate investigation of two-channel soliton propagation over more than 10,000km. *Electron. Lett.*, 27(9):695–696, 1991.

[146] S. Kawai, K. Iwatsuki, K. Suzuki, M. Saruwatari, K. Sato, K. Wakita, and S. Nishi. 10 Gbit/s optical soliton transmission over 7 200km by using a monolithically integrated MQW-DFB-LD/MQW EA modulator light source. *Electron. Lett.*, 30(3):251–252, 1994.

[147] H. Taga, M. Suzuki, N. Edagawa, H. Tanaka, Y. Yoshida, S. Yamamoto, S. Akiba, and H. Wakabayashi. Multi-thousand kilometer optical soliton data transmission experiments at 5Gbit/s using an electroabsorption modulator pulse generator. *IEEE J. Lightwave Technol.*, 12(2):231–236, 1994.

[148] T. Widdowson, D.J. Malyon, X. Shan, and P.J. Watkinson. Soliton propagation without transmission control using a phase-locked Er fibre ring laser. *Electron. Lett.*, 30(8):661–663, 1994.

[149] H. Toda, H. Yamagishi, and A. Hasegawa. 10GHz optical soliton transmission experiment in a sliding-frequency recirculating fibre loop. *Opt. Lett.*, 20(9):1002–1004, 1995.

[150] G. Aubin, T. Montalant, J. Moulu, F. Pirio, J-B. Thomine, and F. Devaux. 40Gbit/s OTDM soliton transmission over transoceanic distances. *Electron. Lett.*, 32(24):2188–2189, 1996.

[151] A.D. Ellis, T. Widdowson, and X. Shan. Wavelength dependence of 40Gbit/s solitonic transmission over distances greater than 2000km. *Electron. Lett.*, 32(4):381–382, 1996.

[152] L.F. Mollenauer, P.V. Mamyshev, and M.J. Neubelt. Demonstration of soliton WDM transmission at 6x10Gbit/s and 7x10Gbit/, error-free over transoceanic distances. 32(5):471–473, 1996.

[153] I. Morita, M. Suzuki, N. Edagawa, S. Yamamoto, H. Taga, and S. Akiba. 20Gb/s single-channel soliton transmission over 9000 km without in-line filters. *IEEE Photon. Technol. Lett.*, 8(11):1573–1574, 1996.

[154] M. Nakazawa, K. Suzuki, H. Kubota, and E. Yamada. 60GBit/s WDM (20 Gbit/s x3 unequally spaced channels) soliton transmission over 10000 km using in-line synchronous modulation and optical filtering. *Electron. Lett.*, 32(18):1686–1688, 1996.

[155] T. Matsuda, A. Naka, and S. Saito. 4x10Gbit/s RZ-signal transmission over 5,040km in anomalous regime with optimally dispersion compensated WDM channels. In *Eur. Conf. on Opt. Comm. (ECOC'97) - Edinburgh)*, pages Vol.2 5–8. IEE, 1997.

[156] E.A. Golovchenko, J.M. Jacob, A.N. Pilipetskii, C.R. Menyuk, and G.M. Carter. Dispersion-managed solitons in a fibre loop with in-line filtering. *Opt. Lett.*, 22(5):289–291, 1997.

[157] M. Nakazawa, E. Yamada, H. Kubota, T. Yamamoto, and A. Sahara. Numerical and experimental comparison of soliton, RZ pulse and NRZ pulses under two-step allocation. *Electron. Lett.*, 33(17):1480–1482, 1997.

[158] T. Terahara, T. Naito, N. Shimojoh, T. Chikama, and M. Suyama. 85Gbit/s WDM transmission of 16 5.3Gbit/s RZ data signals over 7931km using accurate gain equalisation and pre-compensation of group velocity dispersion. *Electron. Lett.*, 33(7):603–605, 1997.

[159] M.G. Taylor. Observation of new polarisation dependence effect in long haul optically amplified system. *IEEE Photon. Technol. Lett.*, 5(10):1244–1246, 1993.

[160] E. Lichtman. Performance degradation due to polarization-dependent gain and loss in lightwave systems with optical amplifiers. *Electron. Lett.*, 29(22):1967–1971, 1993.

[161] F. Bruyere. Measurement of polarization-dependent gain in EDFAs against input degree of polarization and gain compression. *Electron. Lett.*, 31(5):401–403, 1995.

[162] E.J. Greer, D.J. Lewis, and W.M. Macauley. Polarization-dependent gain in erbium-doped fiber amplifiers. *Electron. Lett.*, 30(1):46–47, 1994.

[163] V.J. Mazurczyk and J.L. Zyskind. Polarisation hole burning in erbium doped fibre amplifiers. In *CLEO'93*, page CPD26, 1993.

[164] H.K. Kim, C.H. Lee, and H.J. Lee. Suppression of polarization hole-burning in an EDFA using an unpolarized source. *Electron. Lett.*, 31(8):650–651, 1995.

[165] N.S. Bergano and C.R. Davidson. Circulating loop transmission experiments for the study of long-haul transmission system using erbium doped fibre amplifiers. *IEEE J. Lightwave Technol.*, 13(5):879–888, 1995.

[166] N.S. Bergano, J. Aspell, C.R. Davidson, P.R. Trischitta, B.M. Nyman, and F.W. Kerfoot. Bit error rate measurements of 14 000km 5Gbit/s fibre amplifier transmission system using circulating loop. *Electron. Lett.*, 27(21):1889–1890, 1991.

[167] N.A. Olsson. Lightwave systems with optical amplifiers. *IEEE J. Lightwave Technol.*, 7(7):1071–1082, 1989.

[168] C.J. Anderson and J.A. Lyle. Technique for evaluating system performance using Q in numerical simulations exhibiting intersymbol interference. *Electron. Lett.*, 30(1):71–72, 1994.

[169] D. Marcuse. Calculation of bit-error probability for a lightwave system with optical amplifiers and post-detection gaussian noise. *IEEE J. Lightwave Technol.*, 4(4):505–513, 1991.

[170] S. Kawanishi, H. Takara, K. Uchiyama, I Shake, O. Kamatani, and H. Takahashi. 14Tbit/s (200Gbit/s x 7ch) 50km optical transmission experiment. *Electron. Lett.*, 33(20):1716–1718, 1997.

[171] N.J. Doran and D. Wood. Nonlinear-optical loop mirror. *Opt. Lett.*, 13(1):56–58, 1988.

[172] D.G. Moodie, A.D. Ellis, A.R. Thurlow, M.J. Harlow, I.F. Lealman, S.D. Perrin, L.J. Rivers, and M.J. Robertson. Multiquantum-well electroabsorption modulators for 80Gbit/s OTDM systems. *Electron. Lett.*, 31(16):1370–1371, 1995.

[173] M.J. Guy, S.V. Chernikov, and J.R. Taylor. A duration-tunable, multiwavelength pulse source for OTDM and WDM communications systems. *IEEE Photon. Technol. Lett.*, 9(7):1017–1019, 1997.

[174] E Yamada, E. Yoshida, T. Kitoh, and M. Nakazawa. Generation of terabit per second optical-data pulse-train. *Electron. Lett.*, 31(16):1342–1344, 1995.

[175] J.H.B. Nijhof, N.J. Doran, W. Forysiak, and F.M. Knox. Stable soliton-like propagation managed systems with net anomalous, zero and normal dispersion. *Electron. Lett.*, 33(20):1726–1727, 1997.

[176] A. Sahara, H. Kubota, and M. Nakazawa. Optimum fibre dispersion for two-step dispersion-allocated optical soliton, RZ at zero GVD and NRZ systems. *IEEE Photon. Technol. Lett.*, 9(8):1179–1181, 1997.

[177] W. Sibbett and J.R. Taylor. Passive mode-locking in the green-yellow using the saturable absorber dasbti. *IEEE J. Quantum Electron.*, 18(12):1994–1996, 1982.

[178] T. Varghese. Passive mode-locking of a coumarin dye-laser from 505-520 nm using doci as the saturable absorber. *Opt. Commun.*, 44(5):353–356, 1983.

[179] D.J. Harter, Y.B. Band, and E.P. Ippen. Theory of mode-locked lasers containing a reverse saturable absorber. *IEEE J. Quantum Electron.*, 21(8):1219–1228, 1985.

[180] D.S. Govan, N.J. Smith, F.M. Knox, and N.J. Doran. Stable propagation of solitions with increased energy through the combined action of dispersion management and periodic saturable absorption. *J. Opt. Soc. Am. B*, 14(11), 1997.

[181] R.I. Laming and M.N. Zervas. Fibre Bragg gratings and their applications. In *Eur. Conf. on Opt. Comm. (ECOC'97) - Edinburgh)*, pages Vol.4 81–83. IEE, 1997.

[182] *Nonlinear Fibre Optics.* Academic Press, San Diego, 1989.

[183] I. Bennion, J.A.R Williams, L. Zhang, K. sugden, and N.J. Doran. UV-written in-fibre Bragg gratings. *Opt. and quant. elec.*, 28:93–135, 1996.

[184] C.R. Giles. Lightwave applications of fiber Bragg gratings. *IEEE J. Lightwave Technol.*, 15(8):1323–1328, 1997.

[185] A.D. Kersey, M.A. Davis, H.J. Patrick, M. LeBlanc, K.P. Koo, C.G. Askins, M.A. Putnam, and E.J. Friebele. Fiber grating sensors. *IEEE J. Lightwave Technol.*, 15(8):1442–1463, 1997.

[186] M.G. Xu, L. Dong, L. Reekie, J.A. Tucknott, and J.L. Cruz. Temperature-independent strain sensor using a chirped Bragg grating in a tapered optical-fiber. *Electron. Lett.*, 31(10):823–825, 1995.

[187] I. Baumann, J. Seifert, W. Nowak, and M. Sauer. Compact all-fiber add-drop-multiplexer using fiber Bragg gratings. *IEEE Photon. Technol. Lett.*, 8(10):1331–1333, 1997.

[188] W.H. Loh, R.I. Laming, N. Robinson, A. Cavaciuti, F. Vaninetti, C.J. Anderson, M.N. Zervas, and M.J. Cole. Dispersion compensation over distances in excess of 500 km for 10Gb/s systems using chirped fiber gratings. *IEEE Photon. Technol. Lett.*, 8(7):944–946, 1996.

[189] S.Y. Kim, S.B. Lee, J. Chung, I.J. Park, J. Jeong, and S.S. Choi. Highly stable optical add/drop multiplexer using polarization beam splitters and fiber Bragg gratings. *IEEE Photon. Technol. Lett.*, 9(8):1119–1121, 1997.

[190] G. Meltz, W. W. Morey, and W. H. Glenn. Formation of Bragg gratings in optical fibres by a transverse holographic method. *Opt. Lett.*, 14(15):823–825, 1989.

[191] K. Sugden, L. Zhang, J.A.R. Williams, and I. Bennion. Dissimilar wavefront technique for linear and quadratic chirps. In *OSA Topical meeting on photosensitivity and quadratic nonlinearity in Glass waveguides*, pages 136–139, 1995.

[192] K.O.Hill, B. Malo, F. Bilodeau, D.C. Johnson, and J. Albert. Bragg gratings fabricated in monomode photosensitive optical fiber by UV exposure through a phase mask. *Appl. Phys. Lett.*, 62(10):1035–1037, 1993.

[193] D.Z. Anderson, V. Mizrahi, T. Erdogan, and A.E. White. Production of in-fiber gratings using a diffractive optical-element. *Electron. Lett.*, 29(6):566–568, 1993.

[194] D.C. Johnson, K.O. Hill, F. Bilodeau, and S. Faucher. New design concept for a narrowband wavelength-selective optical tap and combiner. *Electron. Lett.*, 23(13):668–668, 1987.

[195] F. Bilodeau, D.C. Johnson, S. Theriault, B. Malo, J. Albert, and K.O. Hill. An all-fiber dense-wavelength-division multiplexer demultiplexer using photoimprinted Bragg gratings. *IEEE Photon. Technol. Lett.*, 7(4):388–390, 1995.

[196] L. Dong, P. Hua, T.A. Birks, L. Reekie, and P.S. Russell. Novel add/drop filters for wavelength division multiplexing optical fiber systems using a Bragg grating assisted mismatched coupler. *IEEE Photon. Technol. Lett.*, 8(12):1656–1658, 1996.

[197] F. Bilodeau, K.O. Hill, B. Malo, D.C. Johnson, and J. Albert. High-return-loss narrow-band all-fiber bandpass Bragg transmission filter. *IEEE Photon. Technol. Lett.*, 6(1):80–82, 1994.

[198] M.J. Guy, S.V. Chernikov, J.R. Taylor, and R. Kashyap. Low-loss fiber Bragg grating transmission filter based on a fiber polarization splitter. *Electron. Lett.*, 30(18):1512–1513, 1994.

[199] G.E. Town, K. Sugden, J.A.R. Williams, I. Bennion, and S.B. Poole. Wide-band Fabry-Perot-like filters in optical-fiber. *IEEE Photon. Technol. Lett.*, 7(1):78–80, 1995.

[200] L. Bakhti and P. Sansonetti. Wide bandwidth, low-loss and highly rejective doubly phase-shifted UV-written fiber bandpass filter. *Electron. Lett.*, 32(6):581–582, 1996.

[201] M.C. Farries, K. Sugden, D.C.J. Reid, I. Bennion, A. Molony, and M.J. Goodwin. Very broad reflection bandwidth (44nm) chirped fiber gratings and narrow bandpass-filters produced by the use of an amplitude mask. *Electron. Lett.*, 30(11):891–892, 1994.

[202] J.A.R. Williams, I. Bennion, K. Sugden, and N.J. Doran. Fiber dispersion compensation using a chirped in-fiber Bragg grating. *Electron. Lett.*, 30(12):985–987, 1994.

[203] P.A. Krug, T. Stephens, G.Yoffe, F. Ouellette, P. Hill, and G.Dhosi. Dispersion compensation over 270km at 10Gbit/s using an offset-sore chirped fibre Bragg grating. *Electron. Lett.*, 31(13):1091–1093, 1995.

[204] W.H. Loh, R.I. Laming, A.D. Ellis, and D. Atkinson. 10 Gb/s transmission over 700 km of standard single-mode fiber with 10-cm chirped fiber grating compensator and duobinary transmitter. *IEEE Photon. Technol. Lett.*, 8(9):1258–1260, 1996.

[205] B.J. Eggleton, T. Stephens, P.A. Krug, G. Dhosi, Z.Rodzeli, and F. Ouellette. Dispersion compensation using a fiber grating in transmission. *Electron. Lett.*, 32(17):1610–1611, 1996.

[206] J.A.R. Williams, L.A. Everall, I. Bennion, and N.J. Doran. Fiber Bragg grating fabrication for dispersion slope compensation. *IEEE Photon. Technol. Lett.*, 8(9):1187–1189, 1996.

[207] K.A. Ahmed, B.J. Eggletonand H-F Liu, P.A. Krug, and F. Ouellette. Simultaneous mode selection and pulse compression of gain switched pulses from a Fabry-Perot laser using a 40mm chirped optical fibre grating. *IEEE Photon. Technol. Lett.*, 7(2):158–160, 1995.

[208] J.A.R. Williams, I. Bennion, and L.Zhang. The compression of optical pulses using self phase modulation and linearly chirped Bragg gratings in fibres. *IEEE Photon. Technol. Lett.*, 7(5):491–493, 1995.

[209] B.J. Eggleton, K.A. Ahmed, F. Ouellette, P.A. Krug, and H.F. Liu. Recompression of pulses broadened by transmission through 10 km of non-dispersion-shifted fiber at 1.55μm using 40-mm-long optical-fiber Bragg gratings with tunable chirp and central wavelength. *IEEE Photon. Technol. Lett.*, 7(5):494–496, 1996.

[210] L.Zhang, K. Sugden, J.A.R. Williams, I. Bennion, D.C.J. Reid, and C.M. Ragdale. Postfabrication exposure of gap-type bandpass filters in broadly chirped fiber gratings. *Opt. Lett.*, 20(18):1927–1929, 1995.

[211] G.M. Carter, J.M. Jacob, C.R. Menyuk, E.A. Golovchenko, and A.N. Pilipetskii. Timing-jitter reduction for a dispersion-managed soliton system: Experimental evidence. *Opt. Lett.*, 22(8):513–515, 1997.

[212] A.D. Ellis, S.J. Pycock, D.A. Cleland, and C.H.F. Sturrock. Dispersion compensation in 450 km transmission system employing standard fibre. *Electron. Lett.*, 29(10):954–955, 1992.

[213] B. Christensen, G. Jacobsen, E. Bødteker, J. Mark, and I. Mito. 4Gb/s soliton communication on standarad non dispersion-shifted fibre. *IEEE Photon. Technol. Lett.*, 6(1):101–103, 1994.

[214] F. Matera, M. Romagnoli, and B. Daino. Alternate polarization soliton transmission in standard dispersion fiber links with no in-line controls. *Electron. Lett.*, 31(14):1172–1174, 1995.

[215] C. Das, U. Gaubatz, E. Gottwald, K. Kottenand C.J. Weiske, F. Kuppers, and A. Mattheus. Straight-line 20Gbit/s transmission over 617 km of standard single-mode fiber with dispersion compensation. *Electron. Lett.*, 31(4):305–307, 1995.

[216] N. Kikuchi, S.Sasaki, and K. Sekine. 10Gbit/s dispersion compensated transmission over 2245km conventional fibres in a recirculating loop. *Electron. Lett.*, 31(5):375–377, 1995.

[217] K. Morito, R. Sahara, K. Sato, and Y. Kotaki. Penalty-free 10Gbit/s NRZ transmission over 100km of standard fibre at 1.55μm with a blue-chirp modulator integrated DFB laser. *IEEE Photon. Technol. Lett.*, 8(3):431–433, 1996.

[218] R.J.S. Pedersen, B.F. Jørgensen, M. Nissov, and H. Yongqi. 10Gbit/s repeaterless transmission over 250km standard fibre. *Electron. Lett.*, 32(23):2155–2156, 1996.

[219] L. Pierre, J-P. Thiery, and D.Penninckx. 243km, 10Gbit/s transmission experiment through standard fibre and impact of self-phase modulation using partial response scheme. *Electron. Lett.*, 32(7):673–674.

[220] D. Breuer, F. Küppers, A. Mattheus, E.G. Shapiro, I. Gabitov, and S.K. Turitsyn. Symmetrical dispersion compensation for standard monomode fibre based communication systems with large amplifier spacing. *Opt. Lett.*, 22(13):1–3, 1997.

[221] F. Favre, D. LeGuen, and F. Devaux. 4x20Gbit/s soliton WDM transmission over 2000km with 100km dispersion-compensated spans of standard fibre. *Electron. Lett.*, 33(14):1234–1235, 1997.

[222] A.Shipulin, G. Onishchukov, P. Riedel, D. Michaelis, U. Peschel, and F. Lederer. 10Gbit/s signal transmission over 550km in standard fibre at 1300nm using semiconductor optical amplifiers. *Electron. Lett.*, 33(6):507–509, 1997.

[223] Y.K. Park, T.V. Nguyen, O. Mizuhara, C.D. Chen, L.D. Tzeng, P.D. Yeats, F. Heismann, Y.C. Chen, D.G. Ehrenberg, and J.C. Feggeler. Field demonstration of 10gb/s line-rate transmission on an installed transoceanic submarine lightwave cable. *IEEE Photon. Technol. Lett.*, 9(3):425–427, 1997.

[224] A. Hasegawa and Y. Kodama. Amplification and reshaping of optical solitons in a glass fibre (i). *Opt. Lett.*, 7(6):285–287, 1982.

[225] L.F. Mollenauer, J.P. Gordon, and M.N. Islam. Soliton propagation in long fibres with periodically compensated loss. *IEEE J. Quantum Electron.*, 22(1):157–173, 1986.

[226] K. Smith and L. F. Mollenauer. Experimental observation of adiabatic compression and expansion of soliton pulses over long fibre paths. *Opt. Lett.*, 14(14):751–753, 1989.

[227] A.B. Grudinin, S. Gray, and G.G. Vienne. Subpicosecond soliton transmission over 22km of dispersion-shifted fibre with loss compensated by Raman gain. *Electron. Lett.*, 32(6):573–575, 1996.

[228] K.M. Guild, S.M. Webb, and S.S. Sian. Unrepeated transmission over 415km at 2.5Gbit/s with Raman gain and +26.5dBm launch power. *Electron. Lett.*, 32(22):2087–2088, 1996.

[229] R.A. Fisher, B.R.Suydam, and D. Yevick. Optical phase conjugation for time-domain undoing of dispersive self-phase-modulation effects. *Opt. Lett.*, 8(12):611–613, 1983.

[230] S.F. Wen and S. Chi. Reduction of the soliton interaction and the Gordon-Haus effect by optical-phase conjugation. *Opt. Lett.*, 20(9):976–978, 1995.

[231] S. Watanabe, T. Naito, and T. Chikama. Compensation of chromatic dispersion in a single-mode fibre by optical phase conjugation. *IEEE Photon. Technol. Lett.*, 5(1):92–95, 1993.

[232] W. Forysiak and N.J. Doran. Conjugate solitons in amplified optical fibre transmission systems. *Electron. Lett.*, 30(2):154–155, 1994.

[233] S. Wan and S. Chi. Undoing of soliton interaction by optical phase conjugation. *Electron. Lett.*, 30(8):663–664, 1994.

[234] W. Forysiak, F.M. Knox, and N.J. Doran. Reduction of Gordon-Haus jitter in soliton transmission-systems by optical-phase conjugation. *IEEE J. Lightwave Technol.*, 13(5):850–855, 1995.

[235] X. Zhang and B.F. Jørgensen. Maximum transmission distance for a 10Gbit/s signal transmission over non dispersion shifter fibre using mid-span spectral inversion. *Electron. Lett.*, 32(8):752–754, 1996.

[236] R.J. Essiambre and G.P. Agrawal. Timing jitter of ultrashort solitons in high-speed communication systems ii. control of jitter by periodic optical phase conjugation. *J. Opt. Soc. Am. B*, 14(2):323–330, 1997.

[237] C. Lorattanasane and K. Kikuchi. Design theory of long-distance optical transmission systems using midway optical phase conjugation. *IEEE J. Lightwave Technol.*, 15(6):948–955, 1997.

[238] T. Saito, N. Henmi, S. Fujita, M. Yamaguchi, and M. Shikada. Prechirp technique for dispersion compensation for a high speed long span transmission. *IEEE Photon. Technol. Lett.*, 3(1):74–76, 1991.

[239] J.A.J. Fella, M.A. Gibbon, I.H. White, G.H.B. Thompson, R.V. Penty, C.J. Armistead, E.M. Kimber, D.J. Moule, and E.J. Thrush. Transmission beyond the dispersion limit using a negative chirp electroabsorption modulator. *Electron. Lett.*, 30(14):1168–1169, 1994.

[240] J-H. Jung, S-Y. Shin, and C-H. Lee. Effects of pre-chirping on the repeaterless dispersion-managed transmission system. *Electron. Lett.*, 32(9):831–833, 1996.

[241] G. May, A. Solheim, and J. Conradi. Extended 10Gb/s fibre transmission distance at 1538nm using a duobinary receiver. *IEEE Photon. Technol. Lett.*, 6(5):648–650, 1994.

[242] S. Kuwano, K. Yonenaga, and K. Iwashita. 10Gbit/s repeaterless transmission experiment of optical duobinary modulated signal. *Electron. Lett.*, 31(16):1359–1361, 1995.

[243] X. Gu, S.J. Pycock, D.M. Spirit, A.D. Ellis, and C.J. Anderson. 10Gbit/s, 138km uncompensated duobinary transmission over installed standard fiber. *Electron. Lett.*, 31(1):77, 1995.

[244] T.Takahashi and N. Ohkawa. 5Gbit/s unrepeated transmission over 360km of non-dispersion shifted fibre without dispersion compensation. *Electron. Lett.*, 32(19):1796–1797, 1996.

[245] K. Yonenaga and S. Kuwano. Dispersion-tolerant optical transmission system using duobinary transmitter and binary receiver. *IEEE J. Lightwave Technol.*, 15(8):1530–1537, 1997.

[246] I. Gabitov, E.G. Shapiro, and S.K. Turytsyn. Optical pulse dynamics in fibre links with dispersion compensation. 134(1):317–329, 1997.

[247] W.H. Loh, R.I. Laming, X. Gu, M.N. Zervas, M.J. Cole, and T. Widdowson. 10cm chirped fiber Bragg grating for dispersion compensation at 10 Gbit/s over 400km of non-dispersion shifted fiber. *Electron. Lett.*, 31(25):2203–2204, 1995.

[248] N.M. Litchinitser and D.B. Patterson. Analysis of fiber Bragg gratings for dispersion compensation in reflective and transmissive geometries. *IEEE J. Lightwave Technol.*, 15(8):1323–1328, 1997.

[249] N.M. Litchinitser, B.J. Eggleton, and D.B. Patterson. Fiber Bragg gratings for dispersion compensation in transmission: Theoretical model and design criteria for nearly ideal pulse recompression. *IEEE J. Lightwave Technol.*, 15(8):1303–1313, 1997.

[250] M.J. Cole, H. Geiger, R.I. Laming, S.Y. Set, M.N. Zervas, W.H. Loh, and V. Gusmeroli. Broadband dispersion-compensating chirped fibre Bragg gratings in a 10Gbit/s NRZ 110km non-dispersion-shifted fibre link operating at 1.55μm. *Electron. Lett.*, 33(1):70–71, 1997.

[251] T. Georges. Extended path-averaged soliton regime in highly dispersive fibres. *Opt. Lett.*, 22(10):679–681, 1997.

[252] X.Y. Tang, D. Breuer, and K. Peterman. Soliton WDM transmission in long-haul dispersion managed fibre systems. In *Eur. Conf. on Netw. and Opt. Comm. (NOC'97) - Antwerp*, pages Vol2 33–39. IOS Press, 1997.

[253] R.J. Nuyts, Y.K. Park, and P. Gallion. Dispersion equalisation of a 10Gb/s repeatered transmission system using dispersion compensating fibre. *IEEE J. Lightwave Technol.*, 15(1):31–42, 1997.

[254] K.O. Hill, S. Theriault, B. MAlo, F. Bilodeau, T. Kitagawa, D.C. Johnson, J. Albert, K. Takiguchi, T. Kataoka, and K. Hagimoto. Chirped in-fibre Bragg grating dispersion compensators: Linearisation of dispersion characteristics and demonstration in 100km, 10Gbit/s optical fibre link. *Electron. Lett.*, 30(21):1755–1756, 1994.

[255] K.O. Hill, F. Bilodeau, B. Malo T. Kitagawa, S. Theriault, D.C. Johnson, J. Albert, and T. Kitagawa. Chirped in-fibre Bragg gratings for compensation of optical fibre dispersion. *Opt. Lett.*, 19(17):1314–1316, 1994.

[256] D. Pastor, J. Capmany, D. Ortega, V. Tatay, and J. Marti. Design of apodized linearly chirped fiber gratings for dispersion compensation. *IEEE J. Lightwave Technol.*, 14(11):2581–2588, 1996.

[257] T. Stephens, P.A. Krug, Z. Bordzeli, G. Dhosti, F. Ouellette, and L. Poladian. 257km transmission at 10Gbit/s in non dispersion shifted fibre using an unchirped fibre Bragg grating dispersion compensator. *Electron. Lett.*, 32(17):1599–1600, 1996.

[258] R. Kashyap, H.G. Froehlich, A. Swanton, and D.J. Armes. 1.3m long super-step-chirped fiber Bragg grating with a continuous delay of 13.5ns and bandwidth 10nm for broad-band dispersion compensation. *Electron. Lett.*, 32(13):1807–1809, 1996.

[259] I. Yokohama, K. Okamoto, and J. Noda. Optical circulator consisting of a YIG spherical lens, panda-fibre polarizers and a fibre-optic polarizing beam splitter. *Electron. Lett.*, 21(17):746–748, 1985.

[260] S. Kawanishi, H. Takara, T. Morioka, O. Kamatani, K. Takiguchi, T. Kitoh, and M. Saruwatari. Single-channel 400Gbit/s time-division-multiplexed transmission of 0.98ps pulses over 40 km employing dispersion slope compensation. *Electron. Lett.*, 32(10):916–918, 1996.

[261] T. Morioka, H. Takara, S. Kawanishi, O. Kamatani, K. Takiguchi andK. Uchiyama, M. Saruwatari, H. Takahashi, M. Yamada, T. Kanamori, and H. Ono. 1Tbit/s (100Gbit/s x 10 channel) OTDM/WDM transmission using a single supercontinuum WDM source. *Electron. Lett.*, 32(10):906–907, 1996.

[262] A.R. Chraplyvy, A.H. Gnauck, J.L. Tkach, R.W.and Zyskind, J.W. Sulhoff, A.J. Lucero, Y. Sun, R.M. Jopson, F. Forghieri, R.M. Derosier, C. Wolf, and A.R. Mccormick. 1-Tb/s transmission experiment. *IEEE Photon. Technol. Lett.*, 8(9):1264–1266, 1996.

[263] H. Taga, T. Miyakawa, K. Murashige, N. Edagawa, M. Suzuki, H. Tanaka, K. Goto, and S. Yamamoto. A half Tbit/s (50 x 10.66Gbit/s over 1600km transmission experiment using widely gain flattened EDFA chain. In *Eur. Conf. on Opt. Comm. (ECOC'97) - Edinburgh)*, pages Vol.5 13–16. IEE, 1997.

[264] T. NAito, T. Treahara, and N. Shimojoh. 128Gbit/s WDM transmission of 24 5.3Gbit/s rz signals over 7828km using gain equalisation to compensate for asymmetry in EDFA gain characteristics. In *Opt. Fib. Comm. (OFC'97) - Dallas*, pages 44–45. OSA.

[265] M. Nakazawa, K. Suzuki, H. Kubota, A. Sahara, and E. Yamada. 100Gbit/s WDM (20Gbit/s x 5 channel) soliton transmission over 10000km using in-line synchronous modulation and optical filtering. In *Opt. Fib. Comm. (OFC'97) - Dallas*, page PD21. OSA, 1997.

[266] L. Dind, Golovchenko E.A., A.N. Pilipetskii, C.R. Menyuk, and P.K.A. Wai. Improvement of nrz signal transmission through phase modulation. In *Opt. Fib. Comm. (OFC'97) - Dallas*, pages 50–51. OSA, 1997.

[267] M. Nakazawa, Y. Kimura, K Suzuki, H. Kubota, T. Komukai, E. Yamada, T. Sugawa, E. Yoshida, T. Yamamoto, T Imai, A Sahara, H Nakazawa, O. Yamauchi, and M Umezawa. Field demonstration of soliton transmission at 10Gbit/s over 2000km in tokyo metropolitan optical loop network. *Electron. Lett.*, 31:992–994, 1995.

[268] M. Nakazawa, Y. Kimura, K. Suzuki, H. Kubota, T. Komukai, E. Yamada, T. Sugawa, E. Yoshida, T. Yamamoto, T. Imai, A. Sahara, O. Yamauchi, and M. Umezawa. Soliton transmission at 20 Gbit/s over 2000 km in Tokyo metropolitan optical network. *Electron. Lett.*, 31:1478–1479, 1995.

Appendix A

Publications

- F.M. Knox, P. Harper, P.N. Kean, N.J. Doran, and I. Bennion. Low jitter long distance pulse transmission of near net fibre dispersion zero wavelength. *Electron. Lett.*, 31(17):1467–1468, 1995.
- F. M. Knox, P. Harper, P. N. Kean, N. J. Doran, and I. Bennion. Stable 10ps pulse propagation near the average dispersion zero of a fibre loop. In *OSA Annual Meeting & exhibit program, paper ThKK4*, Portland, Oregon, Sept. 10-15 1995. OSA.
- P. Harper, F.M. Knox, D.S. Govan, P.N. Kean, I. Bennion, and N.J. Doran. Long distance 10Gbit/s soliton transmission over standard fibre with periodic dispersion compensation. In *Eur. Conf. on Netw. and Opt. Comm. Vol.2 18-24*, Antwerp, Belgium, 1997. IOS Press.
- P. Harper, F.M. Knox, P.N. Kean, I. Bennion, and N.J. Doran. 10Gbit/s soliton propagation over 5250km in standard fiber with dispersion compensation. In *Conference on Optical Fiber Communication p304-305*, Dallas, Texas, 1997. OSA.
- P.N. Kean, F.M. Knox, N.J. Smith, P. Harper, I. Bennion and N.J. Doran. Soliton transmission systems with dispersion profiling. In *URSI 25th General Assembly paper D-ICO3*, Lille, France, 1996.
- L. Zhang, P. Harper, K. Sugden, J.A.R. Williams, F.M. Knox, P.N. Kean, I. Bennion and N.J. Doran. Fabrication of high efficient grating bandpass filters and their applications in soliton propagation system. In *SPIE - 1996 International Photonics CHINA Symposium*, Bejing, China, 1996.
- F.M. Knox, P. Harper, P.N. Kean, I. Bennion and N.J. Doran. Soliton transmission at 10Gbit/s over 2022 km of standard fibre with dispersion compensation. In *Eur. Conf. on Opt. Comm. Vol,3 p101-104*, Oslo, Norway, 1996. IEE.
- P. Harper, F.M. Knox, P.N. Kean, L. Zhang, N.J. Doran and I. Bennion. Jitter suppression in a 2700km soliton propagation experiment using only a fibre Bragg grating filter. In *CLEO Europe CThF3*, Hamburg, Germany, 1996.
- F.M. Knox, N.J. Doran, P.N. Kean, I. Bennion and P Harper. 10 Gbit/s soliton transmission over standard fibre. In *Colloq. on Opt. Sol. Princ. and App. Tech Dig 1996/090 p13*, Birmingham, England, 1996. IEE.
- P. Harper, F.M. Knox, P.N. Kean, L. Zhang, N.J. Doran and I. Bennion. Soliton-transmission over 2700 km using an in-fibre Bragg grating filter to give Gordon-Haus jitter reduction. In *Colloq. on Opt. Sol. Princ. and App. Tech Dig 1996/090 p8*, Birmingham, England, 1996. IEE.